Confronting the R-parity-violating MSSM with Flavor Observables and Displaced Vertices

Dissertation
zur
Erlangung des Doktorgrades (Dr. rer. nat.)
der
Mathematisch-Naturwissenschaftlichen Fakultät
der
Rheinischen Friedrich-Wilhelms-Universität Bonn

von
Zeren Simon Wang
aus
Zhejiang, China

Bonn, März 2019

Dieser Forschungsbericht wurde als Dissertation von der Mathematisch-Naturwissenschaftlichen Fakultät der Universität Bonn angenommen und ist auf dem Hochschulschriftenserver der ULB Bonn http://hss.ulb.uni-bonn.de/diss_online elektronisch publiziert.

1. Gutachter:	Prof. Dr. Herbert K. Dreiner
2. Gutachter:	PD Dr. Bastian Kubis
Tag der Promotion:	03.06.2019
Erscheinungsjahr:	2019

Abstract

Supersymmetry (SUSY) was proposed as one of the solutions to the hierarchy problem. In addition, R-parity (R_p) is often imposed in such models in order to *e.g.* avoid proton decay. These R_p-conserving models also predict a stable candidate for cold dark matter. However, R_p-violating (RpV) SUSY models lead to a rich and distinctive phenomenology that should not be ignored.

While at the Large Hadron Collider (LHC), none of the new fundamental particles predicted by New-Physics (NP) theories have been discovered yet, both low-energy observables and direct-production searches at colliders can be exploited in order to constrain further NP theories. Among others, flavor observables that are already well explained by Standard-Model predictions could receive contributions from beyond-the-Standard-Model (BSM) physics. The experimental measurements therefore place limits on these contributions and through them on the NP parameters. In this thesis, we study the particular case of neutral meson oscillation phenomena, and present updated bounds on RpV couplings. At the LHC, small RpV couplings could produce displaced vertex signatures. Several new detectors such as `MATHUSLA`, `CODEX-b`, `FASER` and `AL3X` have been proposed for long-lived particle searches. We estimate sensitivity reach of these new components in the parameter space of several BSM frameworks including RpV-SUSY and heavy neutral leptons.

Acknowledgements

I am greatly indebted to many people who have helped me in one way or another during the past years of my PhD study in Bonn. My greatest gratitude goes to Herbi Dreiner. As my PhD supervisor, he has given me tremendous amount of freedom in deciding the direction of my research and career, and always supported me by all means to achieve my goals. Under his leadership, our group has an ideal environment where research works originate. I am very thankful to Bastian Kubis for spending time and effort reading and refereeing this thesis, and to Ian Brock and Tom McCann for joining the defense committee.

I am extremely lucky to have had the opportunity to visit Valencia, Spain to work with Martin Hirsch. I thank Martin not only for leading me into the world of collider search studies, but also for his care, respect and general guidance in various aspects.

It is absolutely a great honor to have spent these years with my colleagues at the BCTP. I am very grateful to our postdocs, Florian Domingo, Manuel Krauss, and Víctor Martín Lozano, for having answered innumerable questions of mine, worked closely with me and offered suggestions in different aspects of my life. In particular, I thank Florian and Víctor for patience and effort with proof-reading parts of this thesis. I also thank the other present and former group mates, Stefano Colucci, Kilian Nickel, Toby Opferkuch, Annika Buchholz, Max Berbig, Dominik Köhler, Saurabh Nangia, and Sebastian Belkner for either offering suggestions or sharing so many good memories. Thanks also go to Manuel Drees, Rahul Mehra, Zhongyi Zhang, Yong Xu, Andreas Trautner, Meng Shi and other colleagues in the department for all the enjoyable communications and happy moments that we had together. More importantly, the BCTP would be impossible to run well without the extraordinary help from the secretaries and other 'supporters'. Many thanks thus to Petra Weiss, Patricia Zündorf, Christa Börsch, Andreas Wißkirchen, Oliver Freyermuth, Peter Wienemann and Leni.

Collaborators from outside the BCTP have also been an important part of my PhD period. I owe an aweful lot to Jong Soo Kim who invited me to visit Johannesburg, South Africa to work on CheckMATE with him and offered many advices on my career. I am grateful to Daniel Dercks who has answered my various questions always promptly; without him some of our projects could not have been finished so fast. I also thank Oliver Fischer for inviting me to work together, for introducing me to his collaborators and for encouraging me to pursue my future career in Asia.

I sincerely acknowledge the financial support I received from the Bonn-Cologne Graduate School for attending summer schools and conferences in different parts of the world.

Outside the work environment, I have also been fortunate to have some good friends, Beatriz Arribas de Frutos, Veronika Kraus, Desiree Wilde, Bowen Jiang, Yifan Dai, Haoyang Xu, Xinyi Chen, etc., to have entered my life. The time we spent together shall never be forgotten.

I would like to thank my parents and grandparents, for always supporting me to pursue an academic career and for caring about my health, happiness and so on. Finally, I thank Jiajia for her love, care and support despite the long distance.

List of Publications

The projects presented in this thesis contain results that have been published in journals and preprint archives:

[1] D. Dercks, H. K. Dreiner, M. Hirsch, Z. S. Wang,
Long-Lived Fermions at AL3X,
Accepted by Phys. Rev. D, arXiv: 1811.01995 [hep-ph]

[2] F. Domingo, H. K.Dreiner, J. S. Kim, M. E. Krauss, V. Martín Lozano, Z. S. Wang,
Updating Bounds on R-parity Violating Supersymmetry from Meson Oscillation Data,
JHEP 1902 (2019) 066, arXiv: 1810.08228 [hep-ph]

[3] D. Dercks, J. de Vries, H. K. Dreiner, Z. S. Wang,
R-parity Violation and Light Neutralinos at CODEX-b, FASER, and MATHUSLA,
Submitted to Phys. Rev. D, arXiv: 1810.03617 [hep-ph]

[4] J. C. Helo, M. Hirsch, Z. S. Wang,
Heavy neutral fermions at the high-luminosity LHC,
JHEP 1807 (2018) 056, arXiv: 1803.02212 [hep-ph]

Contents

CHAPTER 1

Introduction

The modern understanding of the fundamental particles and their interactions was formulated in the 1960's, leading to the construction of what is known today as the Standard Model of particle physics (SM). This description results from the successful combination of several theoretical ingredients. The underlying framework is that of quantum field theory (QFT), which unites special relativity and quantum mechanics in a consistent way. In this context, the particles appear as the excitations of quantum fields, whose dynamics is encoded within a Lagrangian density. Another concept of 20th century particle physics is that of gauge interactions, which led to the successful development of quantum electrodynamics. In this picture, fundamental forces are carried by vector mediators whose interaction with matter is strictly determined by considerations of symmetries. The extension of this concept to the strong and weak interactions resulted in the formulation of the SM gauge group, $SU(3)_C \times SU(2)_L \times U(1)_Y$, where C, L, Y stand for color, left-chirality and hypercharge, respectively. Here, $SU(3)_C$ is associated to the strong interaction where the gauge mediator is called gluon, and leads to the confinement of the color-charged particles called quarks into hadrons. This specific strong dynamics is known as Quantum Chromodynamics (QCD) [1–3]. As for $SU(2)_L \times U(1)_Y$, the corresponding theory was introduced by Glashow, Weinberg and Salam [4–6] and mixes the electromagnetic and the weak interactions in terms of the so-called electroweak interactions. In the latter case, the evidence for massive mediators of the weak interactions first appeared in contradiction with the symmetry concept until the Brout-Englert-Higgs mechanism [7, 8] offered a solution in terms of spontaneously broken gauge theories. The simplest implementation of this mechanism to the SM gauge group, known as electroweak symmetry breaking (EWSB), involves a scalar $SU(2)$ doublet which takes a non-zero vacuum expectation value (VEV), explicitly breaking the gauge symmetry at the level of the ground state of the scalar potential. This EWSB generates mass terms that were originally forbidden by the gauge symmetry as in the case of the weak gauge bosons and the SM fermions. One generator of the electroweak gauge group remains unbroken, and corresponds to the electromagnetic interaction:

$$SU(3)_C \times SU(2)_L \times U(1)_Y \xrightarrow{\text{EWSB}} SU(3)_C \times U(1)_{\text{em}}, \tag{1.1}$$

Among the successful predictions of the SM, one finds the existence and mass of W- and Z-bosons [9–12], the existence of the massless $SU(3)_C$ gauge boson gluon [13–16] and of the Higgs boson [17, 18], as well as several fermions (charm and top quarks) [19–22], even though the matter content of the

model (such as the number of generation of leptons and quarks) was constructed in an empirical way. As a result of this construction, the SM involves in total 19 independent parameters: 3 lepton masses, 6 quark masses, 3 quark mixing angles, 1 CP-violating phase, 3 gauge couplings, the Higgs mass, the Higgs VEV, and the QCD vacuum angle. This standard structure has performed satisfactorily in view of most experimental tests (electroweak precision measurements, flavor transitions and CP properties, measured Higgs properties). In addition, colliders have not collected evidence so far for the existence of particles beyond the SM table.

However, the SM theory itself is confronted by both observations and theoretical flaws. From the observational side, the evidence for neutrino flavor oscillations [23, 24] points towards the existence of neutrino masses, giving a first hint of beyond-the-SM (BSM) physics, as such masses go beyond the SM predictions. Popular models of neutrino model building often employ the so-called seesaw mechanism [25–29] in order to explain the strong hierarchy between the neutrino masses and those of the charged leptons, postulating the existence of new (possibly very) massive fields. Another observational issue of the SM is the baryon asymmetry of the Universe [30–34], the fact that there appears to be much more matter than anti-matter in the Universe today. Although the SM satisfies all of the Sakharov conditions [35], the predicted baryon asymmetry proves insufficient as compared to the cosmological data [34, 36, 37]. Besides, there is bountiful evidence, based on astrophysical observations from the previous and the current century, for the existence of dark matter (DM) [38–46], pointing to further unexplored territory beyond the SM. We stress that these hints for the existence of DM only implicates its gravitational interaction, even though an estimate of the production of the current DM through thermal relics would point towards cross sections and masses of approximately electroweak size (the WIMP paradigm) [47–51]. A more conceptual problem is that of the status of gravitational interactions in the SM, since General Relativity cannot be simply embedded within a QFT framework. However, this problem does not matter up to energies comparable to the Planck scale $M_{Pl} \sim 10^{19}$ GeV, where gravitational effects would become large. Before this becomes relevant for collider experiments, one could instead worry about other flaws of the SM gauge group. There a first issue appears, known as the strong CP problem. Indeed, gauge and Lorentz symmetries would allow for the existence of a so-called 'θ term', $\bar{\theta}\tilde{F}^{\mu\nu}_{\alpha}F^{\alpha}_{\mu\nu}$, that breaks the CP-symmetry, where $\bar{\theta}$ is the QCD vacuum angle mentioned earlier, to which one would add radiative corrections of *e.g.* electroweak origins. However, the experimental measurement of the electric dipole moment of the neutron has set a very strict upper bound on the magnitude of $\bar{\theta}$: $\bar{\theta} < 10^{-10}$ [52, 53]. This smallness would arise as the unnatural tuning of contributions of various origins in the SM. The most well-known solution is Peccei-Quinn theory which involves new pseudoscalar particles called axions [54–57]. The structure of the SM gauge group itself also raises questions as to the cancellation of the gauge anomalies (necessary for the renormalizability of a gauge theory). This appears as a largely accidental fact in the SM. In addition, it is remarkable that the electric charges of fundamental particles always appear in rational proportions while the hypercharge would in principle allow for irrational numbers. All these curiosities suggest the existence of a more fundamental structure embedding the SM, and unifying its gauge groups. This branch of model building, known as Grand Unified Theories (GUT), motivates the existence of new matter field in close interaction with SM particles, in particular the Higgs field. Nevertheless, the interpretation of the SM as a low-energy effective theory instead of a fully fundamental model introduces a new issue: the hierarchy problem. Indeed the Higgs mass is unprotected with respect to radiative corrections from heavy New-Physics (NP) fields, receiving quadratic contributions that would push it towards high energies. This contradicts the observation of a SM-Higgs-like scalar with a mass of 125 GeV [17, 18] at the Large Hadron Collider (LHC)

in 2012, and previous hints in electroweak precision data [58, 59]. An accidental cancellation of the large radiative corrections of NP origins with the tree-level bare mass term would violate the principle of technical naturalness [60]. This argument motivates the extension of the SM in such a way that the Higgs mass is protected. Possible theoretical solutions include the use of symmetries such as supersymmetry (SUSY) [61–64], or a global symmetry from composite structure [65–71]. A further possibility is to resort to extra-dimensions, either flat and large [72, 73] or warped [74]. New constructions have emerged in recent years such as the 'clockwork' [75] and the 'relaxion' mechanisms [76].

Softly-broken supersymmetric extensions of the SM [77, 78] have long been regarded as a leading class of candidates for the resolution of the hierarchy problem [79–82], as well as a possible framework in view of understanding the nature of dark matter or the unification of gauge-couplings. SUSY theories have a symmetrical mapping between fermionic and bosonic representations of the Lorentz group, resulting in an equal number of fermionic and bosonic degrees of freedom. As long as the supersymmetry is unbroken, all the particles in the same super-multiplet are degenerate in mass. SUSY theories have a higher degree of regularity than usual QFT, which can be formulated in terms of non-renormalization theorems. This property suggested to particle physicists that a supersymmetrization of the SM could address the hierarchy problem. Indeed, by associating scalars and fermions, SUSY allows the chiral protection of fermion masses to extend to scalar masses as well. Technically, this protection takes the form of cancellations between the radiative corrections of partners of the same super-multiplet. The implementation of this recipe to the matter content of the SM led to the so-called 'supersymmetric extensions' of the SM, of which the realization with minimal field content is known as the Minimal Supersymmetric Standard Model (MSSM). This is the model on which we focus below.

1.1 MSSM

We introduce the MSSM in this section, starting with the field content of the theory. Each SM field is included in a super-multiplet of $\mathcal{N} = 1$ supersymmetry, in parallel with a superpartner field. The MSSM names the partners of charged leptons and neutrinos as sleptons and sneutrinos, those of quarks as squarks. In the Higgs sector, at least two Higgs doublets are needed in the model, as required by anomaly cancellation of the SM gauge group and the holomorphic property of the superpotential[1], in order to generate masses for both up- and down-type quarks. The superpartners of the Higgs bosons are called Higgsinos. The gauge fields of the SM, *i.e.* B-boson, W-bosons and gluons, are represented in gauge supermultiplets with spin-$1/2$ superpartners, namely bino, winos and gluinos. We list the chiral[2] super-multiplet fields of the MSSM in Table 1.1 and the gauge superfields in Table 1.2, where the fields are gauge eigenstates.

The superpotential of the (R_p-conserving) MSSM takes the following form

$$W_{\text{MSSM}} = \mu H_u \cdot H_d + Y^e_{ij} H_d \cdot L_i \bar{E}_j + Y^d_{ij} H_d \cdot Q_i \bar{D}_j - Y^u_{ij} H_u \cdot Q_i \bar{U}_j, \tag{1.2}$$

where μ is the Higgsino mass parameter, Y's are Yukawa matrices, Q, $\bar{U}$, $\bar{D}$, L, $\bar{E}$, H_u and H_d are the

[1] If we restrict ourselves to the renormalizable MSSM, the superpotential remains a polynomial of third degree of the superfields.

[2] A chiral super-multiplet consists of a complex scalar field and a fermionic field, transforming into one another through the SUSY symmetry.

Superfield	spin 0	spin 1/2	gen.	$SU(3)_C$	$SU(2)_L$	$U(1)_Y$
Q	$\left(\tilde{u}_L, \tilde{d}_L\right)$	$\left(u_L, d_L\right)$	3	$\mathbf{3}$	$\mathbf{2}$	$\frac{1}{3}$
$\bar{U}$	$\tilde{u}_R^*$	$u_R^\dagger$	3	$\bar{\mathbf{3}}$	$\mathbf{1}$	$-\frac{4}{3}$
$\bar{D}$	$\tilde{d}_R^*$	$d_R^\dagger$	3	$\bar{\mathbf{3}}$	$\mathbf{1}$	$\frac{2}{3}$
L	$\left(\tilde{\nu}_L, \tilde{e}_L\right)$	$\left(\nu_L, e_L\right)$	3	$\mathbf{1}$	$\mathbf{2}$	-1
$\bar{E}$	$\tilde{e}_R^*$	$e_R^\dagger$	3	$\bar{\mathbf{1}}$	$\mathbf{1}$	2
H_u	$\left(H^+, H^0\right)$	$\left(\tilde{H}^+, \tilde{H}^0\right)$	1	$\mathbf{1}$	$\mathbf{2}$	1
H_d	$\left(H^0, H^-\right)$	$\left(\tilde{H}^0, \tilde{H}^-\right)$	1	$\mathbf{1}$	$\mathbf{2}$	-1

Table 1.1: Chiral supermultiplets in the MSSM

Superfield	spin 1	spin 1/2	gen.	$SU(3)_C$	$SU(2)_L$	$U(1)_Y$
B	B	$\tilde{B}$	1	$\mathbf{1}$	$\mathbf{1}$	0
W^a	W^a	$\tilde{W}^a$	3	$\mathbf{1}$	$\mathbf{3}$	0
G^a	g^a	$\tilde{g}^a$	8	$\mathbf{8}$	$\mathbf{1}$	0

Table 1.2: Gauge supermultiplets in the MSSM

chiral superfields of Table 1.1, and $\cdot$ is the $SU(2)_L$ invariant product. The indices i, j, k refer to the three generations of flavor (the color indices are implicit). The MSSM superpotential recovers the Yukawa interactions that exist in the SM and includes a term, $\mu\, H_u \cdot H_d$, known as the μ-term, which is unique in the MSSM. The size of the free parameter μ is in principle undetermined and given that this parameter is SUSY-conserving, one would naively expect a large NP scale. A recent LHC search in ATLAS for electroweak SUSY production [83] excludes now values of μ, which sets the scale of the Higgsino masses, depending on other SUSY parameters, up to roughly $\mu \simeq 130$ GeV. On the other hand, if μ were very large, it would dominate the minimization conditions of the scalar potential and forbid the EWSB. In view of these considerations, μ should be comparable in size to the other scales entering the scalar potential (as we will discuss later, the SUSY soft-breaking scale and the EWSB scale.)

With the knowledge of the MSSM superpotential W_{MSSM}, one may derive the SUSY-conserving terms that appear in the interaction Lagrangian as follows:

$$\mathcal{L}_{\text{int}} = -\frac{1}{2}\frac{\partial^2 W_{\text{MSSM}}}{\partial\phi_i \partial\phi_j}\psi_i\psi_j - \left(\frac{\partial W_{\text{MSSM}}}{\partial\phi_i}\right)^2 + h.c., \tag{1.3}$$

where $\frac{\partial W_{\text{MSSM}}}{\partial\phi_k}$ means taking the derivative of W_{MSSM} with respect to the superfield ϕ_k and then replacing the superfields by their scalar components, and ψ_k is the fermionic component of the superfield ϕ_k.

Since no evidence of superpartners degenerate in mass with SM particles has been found, SUSY, if realized at all in Nature, should be broken at low energies (above the electroweak scale). Realistic SUSY-breaking mechanisms are notoriously difficult to design as sum rules forbid this breakdown to take place in the MSSM sector. Instead, SUSY-breaking effects should be mediated to the standard sector by some mediators, of which several scenarios have been proposed [74, 84–97]. On the

gauge eigenstates	mass eigenstates	name
$[\tilde{u},\tilde{c},\tilde{t}]_{L,R}$	$\tilde{u}_i,\ i=1\ldots6$	up-type squarks
$[\tilde{d},\tilde{s},\tilde{b}]_{L,R}$	$\tilde{d}_i,\ i=1\ldots6$	down-type squarks
$[\tilde{e},\tilde{\mu},\tilde{\tau}]_{L,R}$	$\tilde{e}_i,\ i=1\ldots6$	sleptons
$\tilde{\nu}_e,\tilde{\nu}_\mu,\tilde{\nu}_\tau$	$\tilde{\nu}_i,\ i=1\ldots3$	sneutrinos
$\tilde{H}_d^-,(\tilde{H}_u^+)^\dagger,\tilde{W}^-,(\tilde{W}^+)^\dagger$	$\tilde{\chi}_i^-,\ i=1,2$	charginos
$\tilde{H}_d^0,\tilde{H}_u^0,\tilde{W}^3,\tilde{B}$	$\tilde{\chi}_i^0,\ i=1,2,3,4$	neutralinos
H_u^0,H_d^0	$h,H,A^0(,G^0)$	neutral Higgs (,Goldstone)
$H_d^-,(H_u^+)^*$	$H^\pm(,G^\pm)$	charged Higgs (,Goldstone)
$\tilde{g}$	$\tilde{g}$	gluinos

Table 1.3: New gauge and mass eigenstates in the MSSM

other hand, it is possible to parametrize the effect of SUSY-breaking in the MSSM sector in a phenomenological way by adding so-called 'soft' terms to the Lagrangian. These terms are defined by the property of not spoiling the cancellation of quadratic radiative corrections to the scalar masses. Such terms are written as follows:

$$\begin{aligned}-\mathcal{L}_{\text{soft}} &= \tilde{Q}^\dagger m_q^2\tilde{Q}+\tilde{D}^\dagger m_d^2\tilde{D}+\tilde{U}^\dagger m_u^2\tilde{U}+\tilde{L}^\dagger m_l^2\tilde{L}+\tilde{E}^\dagger m_e^2\tilde{E}+m_{H_u}^2|H_d|^2+m_{H_d}^2|H_d|^2\\ &+ \frac{1}{2}\Big(M_1\tilde{B}\tilde{B}+M_2\tilde{W}^a\tilde{W}^a+M_3\tilde{g}^a\tilde{g}^a+h.c.\Big)\\ &+ \Big(A_u^{ij}\tilde{Q}_i\cdot H_u\tilde{U}_j+A_d^{ij}\tilde{Q}_i\cdot H_d\tilde{D}_j+A_e^{ij}\tilde{L}_i\cdot H_d\tilde{E}_j+bH_d\cdot H_u+h.c.\Big),\end{aligned}\tag{1.4}$$

where $\tilde{D}=\tilde{d}_R^*$, $\tilde{U}=\tilde{u}_R^*$, $\tilde{E}=\tilde{e}_R^*$. m_q^2, m_l^2, m_d^2, m_u^2, m_e^2, $m_{H_u}^2$ and $m_{H_d}^2$ correspond to quadratic parameters for the masses of the squarks, sleptons, and Higgs fields, while M_1, M_2, M_3 are respectively mass contributions to the masses of binos, winos and gluinos. A_u^{ij}, A_d^{ij}, A_e^{ij}, b define a holomorphic function of the scalar fields, hence reminiscent in form of the superpotential. The soft SUSY-breaking Lagrangian is essential for a successful low-energy phenomenology. Beyond lifting the degeneracy in mass between the SM particles and their superpartners, these terms are also needed in order to trigger the EWSB [98].

After the EWSB occurs, fields with the same quantum numbers mix and form mass eigenstates. We list the gauge eigenstates that are new in the MSSM in Table. 1.3, paired with the corresponding mass eigenstates. There are in total 6 mass eigenstates for each category among up-type squarks, down-type squarks, and sleptons. In the sneutrinos sector, there are 3 mass eigenstates. The charged Higgsinos and charged winos mix to form charginos $\tilde{\chi}_i^\pm,\ i=1,2$, while their neutral counterparts mix with one another as well as the bino to form neutralinos $\tilde{\chi}_i^0,\ i=1,2,3,4$. As the gauge group $SU(3)_C$ remains unbroken, the gluinos do not mix with other states. In the Higgs sector, five scalar particles remain as physical degrees of freedom (the other degrees of freedom are the electroweak Goldstone bosons) two CP-even[3] Higgs h and H, one CP-odd neutral pseudoscalar A, and two charged Higgs $H^\pm$.

At tree-level, the MSSM predicts an upper bound for the lighter CP-even Higgs boson mass:

$$m_h \leq M_Z|\cos 2\beta|,\tag{1.5}$$

[3] All the CP-conserving neutral components in the Higgs sector may mix if CP is broken

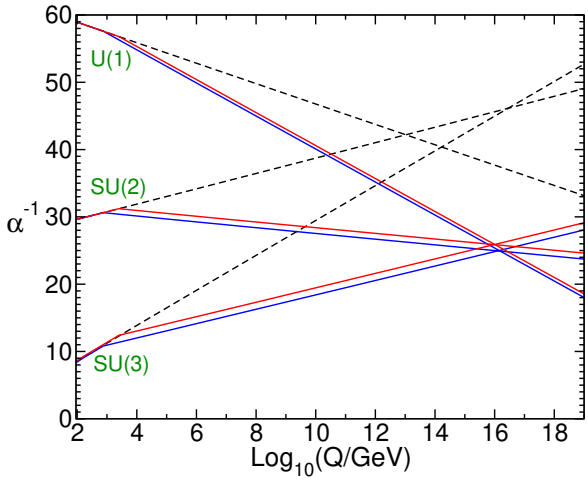

Figure 1.1: Two-loop RG evolution of inverse gauge couplings in the SM (dashed line) and the MSSM (solid lines). In the MSSM case, the sparticle masses are treated as a common threshold varied between 750 GeV and 2.5 TeV, and $\alpha_3(mZ)$ is varied between0.117 and 0.120 with $\alpha_3 = g_3^2/4\pi$. The plot is taken from [100].

where the angle β is defined from the ratio of the two Higgs doublet VEVs, and M_Z is the Z-boson mass. This upper bound is apparently in contradiction with the observed Higgs mass ($\sim$ 125 GeV). However, such a conclusion would be superficial since it overlooks the impact of the radiative corrections. The latter are actually known to be sizable due to the mass splitting between the SM particles and their superpartners. Previous to the Higgs discovery, an upper bound of about 140 GeV on the mass of the lightest Higgs state had been derived [99], which is in agreement with the measured value.

The running of the SM gauge couplings in the MSSM provides another interesting feature. In a quantum field theory, it is possible to re-sum the leading radiative corrections depending on the energy scale via the renormalization group equations. This applies in particular to the three gauge couplings of the SM, g_1, g_2 and g_3. It was observed that in the presence of the MSSM matter content, these couplings tend to converge towards a common high-energy limit at the scale of 10^{16} GeV, which would allow for a one-step unification as in $SU(5)$ GUT model building. This is illustrated in Fig. 1.1, which is taken from [100].

In the definition of the MSSM superpotential of Eq. 1.2 and its soft Lagrangian (Eq. 1.4), we have assumed an implicit ingredient which is R-parity (R_p). Indeed, renormalizability and gauge invariance alone would allow sets of terms that would break the lepton or the baryon numbers, leading to a possibly fast proton decay. R_p [101] is an additional discrete symmetry expressed in terms of the baryon B and the lepton L numbers as well as the spin s, defined for each field as

$$R_p = (-1)^{3(B-L)+2s}. \tag{1.6}$$

With this definition, all the SM fields are R_p-even while all the superpartners are R_p-odd. Therefore, the conservation of R_p implies that transition amplitudes with an odd number of external SUSY particles vanish. In particular, SUSY particles cannot decay into strict SM final states. Consequently, the lightest SUSY particle (LSP) is stable, and hence a possible candidate for weakly interacting DM [102]. This argument is often presented as an additional motivation for R_p. In the following section, we will see, however, why R-parity-violation should not be so easily dismissed as a framework of

collider physics.

1.2 RpV-MSSM

In the previous section, we presented R_p as a mean to prevent fast proton decay. However, imposing R_p does not completely solve the problem. In fact, if we view the R_p-conserving MSSM as an effective theory embedded in a more fundamental model at some higher energy scale, several R_p-conserving dim-5 operators could lead to proton decay [103]. This issue is more efficiently addressed by imposing other types of discrete symmetries such as proton hexality or baryon-triality [104–106]. Therefore, despite its attractive features, R_p conservation is perhaps not as fundamental as it appears at first. It is thus legitimate to consider the phenomenology associated with R_p violation (RpV) — see [107, 108] for reviews — which is not only viable but also opens new mechanisms at colliders.

On the high-energy frontier, the purpose of the LHC was not only the discovery of the SM Higgs boson, but also the investigation of new particles in the TeV mass range. Typical targets include the sparticles predicted by SUSY theories. Several years of operation of the LHC have (as yet) failed to reveal any conclusive evidence for BSM physics [109]. On the contrary, experimental searches keep placing ever stronger limits on hypothesized strongly [110–113] and even weakly-interacting [114] particles in the electroweak–TeV range. While this situation tends to leave the simpler models such as MSSM in an uncomfortable position, it also advocates for a deeper study of more complicated scenarios such as R-parity-violating MSSM (RpV-MSSM), satisfying the central motivations of the original paradigm but also requiring more elaborate experimental investigations for testing. In the traditional collider searches based on R-parity-conserving MSSM, the strategies focus on the detection of missing transverse energies associated with potential LSP's that would escape the detector. However, if a RpV scenario were realized in Nature, this strategy would need to be re-assessed. Indeed, not only are different signals expected, but there may be no long-lived LSP flying away without decaying (no missing energy). Collider limits then need to be revisited.

With an unstable LSP, RpV models do not provide an obvious DM candidate, except for the case where one particle has a lifetime comparable to the age of the Universe.

We now consider the most general RpV-model with minimal superfield content. The superpotential of the R_p-conserving MSSM is thus extended by the following terms [103]:

$$W_{RpV} = \mu_i\, H_u \cdot L_i + \frac{1}{2}\lambda_{ijk}\, L_i \cdot L_j \bar{E}_k + \lambda'_{ijk}\, L_i \cdot Q_j \bar{D}_k + \frac{1}{2}\lambda''_{ijk}\, \varepsilon_{abc}\, \bar{U}_i^a \bar{D}_j^b \bar{D}_k^c, \tag{1.7}$$

where ε_{abc} is the 3-dimensional Levi-Civita symbol and the indices a, b, c correspond to the color index. We note that symmetry-conditions may be imposed on the parameters λ_{ijk} and λ''_{ijk} without loss of generality: $\lambda_{ijk} = -\lambda_{jik}$, $\lambda''_{ijk} = -\lambda''_{ikj}$. This can be easily derived as follows (take $L_i \cdot L_j \bar{E}_k$ operators for example):

$$\lambda_{ijk} L_i \cdot L_j \bar{E}_k = \lambda_{ijk} \epsilon_{\alpha\beta} L_i^\alpha L_j^\beta \bar{E}_k = -\lambda_{jik} \epsilon_{\beta\alpha} L_j^\alpha L_i^\beta \bar{E}_k = -\lambda_{jik} L_i \cdot L_j \bar{E}_k, \tag{1.8}$$

where $\epsilon_{\alpha\beta}$ is the 2-dimensional Levi-Civita symbol.

The first three sets of terms of Eq. (1.7) violate lepton number and the last set of terms violate baryon number. Of course, allowing all the operators to be non-vanishing could lead to fast proton decay at the electroweak-SUSY scale. A predictive alternative to R_p at this level simply consists in

imposing conservation of either the baryon or the lepton number [104, 105, 115, 116].

With R_p discarded, new soft SUSY-breaking terms should be included, and can be expressed as follows:

$$\mathcal{L}_{\text{RpV, soft}} = m^2_{H_{di}} H_d^\dagger \tilde{L}_i + b_i H_u \tilde{L}_i + \frac{1}{2} A_{ijk} \tilde{L}_i \tilde{L}_j \tilde{E}_k + A'_{ijk} \tilde{L}_i \tilde{Q}_j \tilde{D}_k + \frac{1}{2} A''_{ijk} \tilde{U}_i \tilde{D}_j \tilde{D}_k + h.c.. \quad (1.9)$$

Again, only the last set of terms violate baryon number (in the squark sector) while the others violate lepton number.

With R_p broken, L_i and H_d superfields carry the same quantum numbers so that there is an ambiguity as to the definition of these fields, and the distribution of the electroweak VEV. This is made obvious by the first term of Eq. 1.7 as well as the first two terms of Eq. 1.9. In the most general case, the mixing matrices of MSSM and SM particles can take a relatively complicated form which is simply a consequence of this ambiguity. In practice, it is convenient to work in the basis of fields where the sneutrino fields have a vanishing VEV, and in this thesis we work in this basis indeed.

We stress that the first set of operators in the RpV superpotential (Eq. 1.7) and the first two sets of terms in the RpV soft Lagrangian (Eq. 1.9) are sources of several mixings between MSSM and SM fields: neutrinos-neutralinos, charged leptons-charginos, sneutrinos-neutral Higgs, sleptons-charged Higgs mixings. While in the R_p-conserving MSSM, there exist already slepton, sneutrino and squark flavor mixings, these new effects induced by the bilinear operators from the RpV superpotential add further complexities into the theory, and should be taken into account if one intends to consider the full RpV-MSSM model. As a side remark, the mixing between the neutrinos and the neutralinos yields a single massive neutrino state at tree level, and the trilinear RpV couplings can generate massive neutrinos at one-loop order by themselve or together with bilinear RpV couplings. See *e.g.* [108] for a review.

1.3 Phenomenological studies

RpV affects the phenomenology of the MSSM on the whole spectrum of particle physics ranging from direct searches of NP at *e.g.* the LHC [117, 118], flavor transitions in the lepton or quark sectors, to astrophysics and cosmology. In the following subsections, we briefly review limits applying to RpV-SUSY and originating either indirectly (in SM to SM transitions) or directly in the production and decays of SUSY particles. We restrict ourselves to a brief discussion here and refer the reader to Ref. [108] for further details.

1.3.1 Indirect bounds on RpV superpotential couplings

The violation of R_p could generate new interactions between the superfields and the SM fields, giving contributions to various processes for which the SM itself is already in good agreement with the experimental measurement. The experimental precision along with the SM and NP theoretical uncertainties then limit the amount of NP contributions that may enter the process and thus put indirect bounds on BSM parameters such as the RpV couplings. This class of limits include many possible processes.

RpV couplings potentially produce new sources of flavor violation both in the lepton and the quark sectors. Corresponding observables have been studied for a long time as potential probes of

NP, resulting in relatively strong constraints. In the lepton flavor sector, processes such as $\mu \to e\gamma$ and $\mu \to 3e$ constrain lepton-flavor-violating (LFV) RpV couplings of the $L \cdot L\bar{E}$ type [119–143]. Neutrinoless double beta decay is responsible for the so far strongest bound applying on a single RpV coupling, λ'_{111} [144]. In the quark flavor sector, rare decays of mesons, either into leptonic [119, 145–150], semileptonic [146, 151–153], or hadronic final states [154–156], placed severe bounds. Another example of flavor transition in the quark sector is that of the neutral meson systems including its CP-conserving and -violating observables [146, 157–165]. We investigate this specific case in Chapter 2 of this thesis. In addition, some experimental anomalies were observed in recent years including the so-called B-anomalies with observables $R_{K^{(*)}/D^{(*)}}$. The global deviation of the two types of B-anomalies [166–176] is almost 4σ. This can be accounted for by RpV-SUSY theories [177–182]. Finally, baryon-number-violating observables such as the nucleon decays and the neutron oscillation have been studied in the context of RpV [108, 145, 154, 183–189].

Here we extract from the literature a selected list of bounds on single RpV couplings and on RpV coupling products that are relevant to the studies presented in this thesis. It is indeed customary to assume the dominance of a single RpV coupling or coupling pair when studying the limits derived from a specific observable. While predictive, this hypothesis, known as the Single Coupling Dominance, could be simplistic in that it favors a particular base in flavor space at the level of the high-energy RpV couplings which have no specific reason to be determined by the low-energy consideration. The couplings λ'_{ijk} of the operator $L_i \cdot Q_j \bar{D}_k$ receive limits from different sources, though the bounds are substantially weakened for heavy sfermion masses above 1 TeV. For simplicity, we only show the limits for sfermion masses at 100 GeV. For reviews, see Refs. [108, 190–193]. We list the relevant bounds on single λ'_{ijk} couplings, reproduced from Ref. [193]:

$$|\lambda'_{112}| < 0.03\,, \qquad |\lambda'_{122}| < 0.2\,, \qquad |\lambda'_{131}| < 0.03\,. \tag{1.10}$$

As for the relevant RpV coupling product bounds, we reproduce the numbers from Ref. [159, 160, 164, 190] for sfermion masses at 100 GeV:

$$\begin{aligned}
&|\lambda'_{i21}\lambda'_{i12}| < 1.0\times10^{-9}\,, && |\lambda'_{i31}\lambda'_{i13}| < 3\times10^{-8}\,, && |\lambda'_{i32}\lambda'_{i23}| < 7.36\times10^{-7}\,,\\
&|\lambda'_{i21}\lambda'_{i23}| < 1.4\times10^{-3}\,, && |\lambda'_{i12}\lambda'_{i13}| < 2.52\times10^{-2}\,, && |\lambda'_{i31}\lambda'_{i33}| < 1.3\times10^{-3}\,,\\
&|\lambda'_{i32}\lambda'_{i33}| < 2.5\times10^{-3}\,, && |\lambda'_{i32}\lambda'_{i33}| < 2.5\times10^{-3}\,, && |\lambda'_{i21}\lambda'_{i22}| < 1.4\times10^{-6}\,,\\
&|\lambda'_{i31}\lambda'_{i12}| < 2.4\times10^{-5}\,, && |\lambda'_{i12}\lambda'_{i22}| < 2.2\times10^{-5}\,, && |\lambda''_{i13}\lambda''_{i23}| < 4.8\times10^{-4}\,,\\
&|\lambda''_{i12}\lambda''_{i23}| < 7.6\times10^{-3}\,, && |\lambda''_{i12}\lambda''_{i13}| < 6.2\times10^{-3}\,.
\end{aligned} \tag{1.11}$$

1.3.2 Constraining RpV from Collider Searches

Non-vanishing RpV couplings imply more instability of sparticles and would result in distinctive signals at the colliders. In particular, the decay of the LSP via RpV couplings would lead to decay topologies considerably different from those predicted by the existing searches based on R_p-conserving SUSY theories. Needless to say, this impact on collider phenomenology has elicited (and is likely to

keep eliciting) many searches at the high-energy frontier.

With RpV couplings larger than $\sim O(10^{-5} - 10^{-4})$, sparticles are expected to be short-lived and their decays lead to signals that may be detected at the colliders. The first types of signals that are searched for are direct decays of sfermions via trilinear RpV couplings to a pair of SM particles [194, 195] and those of neutralinos and charginos into three SM fermions with an off-shell sfermion exchange [196, 197]. Another possibility is that a cascade of sparticle decays happens first, before the LSP decays via a RpV coupling. Signals of different characteristics may arise depending on whether the sfermion and the gauginos-Higgsinos are produced singly or in pair, and on the collider type (proton-proton, electron-positron or electron-proton).

On the other hand, if RpV couplings are of a smaller size, the LSP (such as the lightest neutralino) becomes long-lived. In recent years, several detectors remote from the beam ($O(10^{1} - 10^{2})$ m) have been proposed to be built as new components of the LHC experiments, designed specifically for discovering long-lived particles (LLPs) [198–201]. In this context, it seems interesting to assess the sensitivity reach of these detectors in the parameter space of RpV-SUSY theories among other extensions of the SM. Works in this direction study the possibility of constraining RpV couplings with displaced vertex signatures in the near future at the LHC [202–205]. Chapter 3 of this thesis presents our studies in this research direction.

This thesis is organized as follows. In Chapter 2, we present the analytical calculation of the full RpV contributions to the observable ΔM's, show the numerical results in a set of benchmark scenarios, and provide new bounds on the RpV parameters in terms of sfermion masses. In Appendix A the details of loop calculation results are listed including the definition of loop functions and the analytical expressions of Wilson coefficients. In Chapter 3, we first introduce the simulation procedure of LLP signals and the basic setup of future detectors at the LHC including geometries and projected luminosities of data. Then we estimate the sensitivity reach of these new detectors in the parameter space of RpV-SUSY and heavy neutral leptons (HNL) theories; experimental searches in this direction may lead to either discovery of such LLPs or exclusion of larger regions in the parameter space.

CHAPTER 2

R-parity Violation & Meson Oscillation

One of the possibilities to test the RpV-MSSM is to exploit the many low-energy (LFV/QFV) flavor observables that are very sensitive to BSM physics. As discussed in the previous chapter, the neutral meson systems including $K^0 - \bar{K}^0$ and $B_{d/s} - \bar{B}_{d/s}$, provide several low-energy observables that can tightly constrain NP contributions. In this chapter, we present our studies in this direction.

This chapter is based on Ref. [165]. In the first section of this chapter, we briefly discuss the current experimental status of the observables that we consider, and introduce the calculation procedure. In the second section, we present the general ingredients of the full one-loop analytical calculation of the Wilson coefficients of the $\Delta F = 2$ EFT (effective field theory) in the RpV-MSSM, referring to the appendices where the exact expressions are provided. In Section 2.3, we discuss the implementation of these results employing the public tools `SPheno` [206–208], `SARAH` [209–214], `FlavorKit` [215] and `Flavio` [216]. Finally, numerical limits on the RpV-couplings are presented in a few simple scenarios, before a short conclusion.

2.1 The Current Experimental Status

The superpotential of Eq. (1.7) contains several sources of flavor-violation, in both the lepton and the quark sectors. Such effects are steadily searched for in experiments, placing severe bounds on the parameter space of the model. The impact of lepton-flavor violating observables on the RpV-MSSM has been discussed extensively in the literature, see *e.g.* [119–143]. In the quark sector, observables such as leptonic B-decays or radiative $b \to s$ transitions [147, 158, 217] have been considered. Here, we wish to focus on neutral-meson mixing observables, ΔM_K, ΔM_d, ΔM_s, for K^0, B_d^0 and B_s^0 mesons, respectively. They represent the mass difference between the two mass eigenstates of each of these meson systems. Such observables have been discussed in the R-parity conserving [218, 219] as well as in an RpV context in the past [146, 157–164]. Yet, diagrams beyond the tree-level and box contributions as well as sfermion or RpV-induced mixings have been routinely ignored. The purpose of this chapter consists in addressing these deficiencies and proposing a full one-loop analysis of the meson-mixing observables in the RpV-MSSM.

Experimental investigations of the neutral meson systems at the modern experiments usually proceed via an explicit measurement of the time dependence of the flavor oscillations, performed in a particular collider environment where the dominant production mode of kaons (B-mesons) goes through $s\bar{s}$ ($b\bar{b}$) pair production. The principle of these experiments exploits the difference between

the flavor eigenstates, determined at the production and decay vertices, and the mass eigenstates, determining the free evolution of the quantum state between the two vertices. The measurement hence essentially consists of two ingredients: the decay-time measurement and flavor tagging. Given the significant boost and the relatively large lifetime of the neutral kaons and B-mesons, there is a macroscopic distance between the production vertex and the decay vertex, which is sufficiently large for modern detectors with high-precision silicon tracking systems to discern. Conventionally, the hemisphere where one valence quark is reconstructed with the decay vertex is known as the vertex side, and the other is called the opposide side. The energy of the mesons deposits as they move in the detector chamber and it is hence possible to measure the momentum of the mesons, which, combined with the distance between the vertices, allows for the determination of the proper time lived by the mesons. Complementarily, flavor tagging has to be performed on the mesons at the production and decay vertices, in order to determine the charge of the valence quark (bottom and strange) and hence whether the oscillation has taken place or not. Depending on the collider environment and the meson type, different strategies are employed for such purposes. When the neutral kaon system is under consideration, an absorber is often placed at the position of flavor tagging. As K^0 and $\bar{K}^0$ interact strongly with the nuclei of the material of the absorber, measurement of the strangeness of the outgoing particles allows for determination of the kaon flavor. As for the B-meson systems, depending on the collider type, different methods for the flavor tagging are used. In an e^+e^- environment, a combination of determining the charge of a lepton produced from a semileptonic B decay and the charge of a kaon produced in the decay chain $b \to c \to s$ offers information from the two different sources. On the other hand, in a hadron collider setup, the flavor tagging is much more difficult because of the many more complicated background events. Two strategies are applied there, characterized as 'same-side' and 'opposite-side' techniques. The same-side tagging technique [220, 221] extracts charge-correlation information from the additional particles produced during the fragmentation processes for the B-mesons of interest. The opposite-side algorithms [222, 223] use the strategies similar to what is applied in an e^+e^- collider. They look for decay products of the B-meson from the opposide side.

From the experimental perspective, the measurements of B-meson oscillations by the ALEPH, DELPHI, L3, OPAL, CDF, D0, BABAR, Belle, ARGUS, CLEO and LHCb collaborations have been combined by the Heavy-Flavor Averaging Group [224], leading to the averages:

$$\Delta M_d^{exp} = 0.5065 \pm 0.0019 \text{ ps}^{-1}, \tag{2.1a}$$

$$\Delta M_s^{exp} = 17.757 \pm 0.021 \text{ ps}^{-1}. \tag{2.1b}$$

These values are in excellent agreement with the SM computations [225–227], resulting in tight constraints on new physics contributions. However, we note that the latest SM evaluation of ΔM_s [228] is in tension with Eq. (2.1). This largely appears as a consequence of the new lattice evaluation of the non-perturbative parameter $f_{B_s}^2 B_{B_s}$ by Ref. [229], with reduced uncertainties. While this situation interestingly favors effects beyond the SM, we prefer to remain conservative as long as the new value of $f_{B_s}^2 B_{B_s}$ is not confirmed by other studies. We thus assume that the uncertainties on the SM prediction are still of the order of the older computations.

For the $K^0 - \bar{K}^0$ system, the Particle Data Group [230] combines the experimental measurements as:

$$\Delta M_K^{exp} = (0.5293 \pm 0.0009) \cdot 10^{-2} \text{ ps}^{-1}. \tag{2.2}$$

Despite the precision of this result, constraints from $K^0 - \bar{K}^0$ mixing on high-energy contributions are considerably relaxed by the large theoretical uncertainties due to long-distance effects. Historically, estimates of the latter have been performed using the techniques of large N QCD — see *e.g.* Ref. [231] — while lattice QCD collaborations such as [232] are now considering the possibility of evaluating these effects in realistic kinematical configurations. Ref. [233] settles for a long-distance contribution at the level of $(20 \pm 10)\%$ of the experimental value, and we follow this estimate below. Concerning short-distance contributions, Ref. [234] performed a NNLO study of the charm-quark loops, resulting in a SM estimate of $\Delta M_K^{\text{SM, Short Dist.}} = (0.47 \pm 0.18) \cdot 10^{-2}\ \text{ps}^{-1}$.

Beyond the mass differences, CP-violating observables are also available in the meson-mixing system. Although our study is valid for these as well, we will not discuss them in the following, since we do not wish to pay much attention to the new-physics phases.

The computation of the meson oscillation parameters is usually performed in a low-energy effective field theory (EFT), where short-distance effects intervene via the Wilson coefficients of dimension 6 flavor-changing ($\Delta F = 2$) operators [235]. This procedure ensures a resummation of large logarithms via the application of the renormalization group equations (RGE) from the matching high-energy (*e.g.* electroweak) scale down to the low-energy (meson-mass) scale where hadronic matrix elements should be computed [236]. In this work, we calculate the contributions to the Wilson coefficients arising in the RpV-MSSM up to one-loop order. The λ' couplings of Eq.(1.7) already generate a tree-level diagram. Going beyond this, at one-loop order, diagrams contributing to the meson mixings involve both R-parity conserving and R-parity violating couplings. These are furthermore intertwined via RpV-mixing effects stemming for example from the bilinear term $\mu_i H_u \cdot L_i$. Our analysis goes beyond the approximations that are frequently encountered in the literature. We also find occasional differences with published results, which we point out accordingly.

2.2 Matching conditions for the $\Delta F = 2$ EFT of the RpV-MSSM

We consider the $\Delta F = 2$ EFT relevant for the mixing of $(\bar{d}_i d_j)$-$(\bar{d}_j d_i)$ mesons — d_i corresponds to the down-type quark of ith generation (d, s or b). The EFT Lagrangian is written as

$$\mathcal{L}_{EFT} = \sum_{i=1}^{5} C_i O_i + \sum_{i=1}^{3} \tilde{C}_i \tilde{O}_i, \tag{2.3}$$

where we employ the following basis of dimension 6 operators:

$$\begin{aligned}
O_1 &= (\bar{d}_j \gamma^\mu P_L d_i)(\bar{d}_j \gamma_\mu P_L d_i), & \tilde{O}_1 &= (\bar{d}_j \gamma^\mu P_R d_i)(\bar{d}_j \gamma_\mu P_R d_i), \\
O_2 &= (\bar{d}_j P_L d_i)(\bar{d}_j P_L d_i), & \tilde{O}_2 &= (\bar{d}_j P_R d_i)(\bar{d}_j P_R d_i), \\
O_3 &= (\bar{d}_j^a P_L d_i^b)(\bar{d}_j^b P_L d_i^a), & \tilde{O}_3 &= (\bar{d}_j^a P_R d_i^b)(\bar{d}_j^b P_R d_i^a), \\
O_4 &= (\bar{d}_j P_L d_i)(\bar{d}_j P_R d_i), & O_5 &= (\bar{d}_j^a P_L d_i^b)(\bar{d}_j^b P_R d_i^a).
\end{aligned} \tag{2.4}$$

The superscripts $(a, b = 1, 2, 3)$ refer to the color indices when the sum is not trivially contracted within the fermion product. We have employed the usual four-component spinor notations above, with $P_{L,R}$ denoting the left- and right-handed projectors.

The Wilson coefficients C_i, $\tilde{C}_i$ associated with the operators of Eq.(2.4) in the Lagrangian of the

EFT — Eq.(2.3) — are obtained at high-energy by matching the $d_i\bar{d}_j \to d_j\bar{d}_i$ amplitudes in the EFT and in the full RpV-MSSM. We restrict ourselves to the leading-order coefficients (in a QCD/QED expansion) on the EFT-side. On the side of the RpV-MSSM, we consider only short-distance effects, *i.e.* we discard QCD or QED loops. Indeed, the photon and gluon are active fields in the EFT, so that a proper processing of the corresponding effects would require a NLO matching procedure. Furthermore, both tree-level and one-loop contributions are considered in the RpV-MSSM: we stress that this does not induce a problem in power-counting, as the tree-level contribution is a strict RpV-effect, so that R_p-conserving (or violating) one-loop amplitudes are not (all) of higher QED order. Numerically speaking, one possibility is that the tree-level is dominant in the Wilson coefficients, in which case, the presence of the one-loop corrections does not matter. This case is essentially excluded if we consider the experimental limits on the meson-oscillation parameters. If, on the contrary, the tree-level contribution is of comparable (or subdominant) magnitude with the one-loop amplitudes, then the electroweak power-counting is still satisfied. Yet, one-loop contributions that are aligned with the tree-level always remain subdominant.

For our calculations in the RpV-MSSM, we employ the Feynman 't Hooft gauge [237] and dimensional regularization [238, 239]. For reasons of consistency with the tools that we employ for the numerical implementation, $\overline{DR}$-renormalization conditions will be applied. However, in the results that we collect in the Appendix, the counterterms are kept in a generic form, which allows for other choices of renormalization scheme. We apply the conventions where the sneutrino fields do not take vacuum expectation values.[1] Moreover, the λ' couplings of Eq.(1.7) are defined in the basis of down-type mass-states, *i.e.* a CKM matrix appears when the second index of λ' connects with an up-type field, but not when it connects to a down-type field [157]. Mixing among fields are considered to their full extent, including left/right and flavor squark mixings, charged-Higgs/slepton mixing, neutral-Higgs/sneutrino mixing, chargino/lepton mixing and neutralino/neutrino mixing. The details of our notation and the Feynman rules employed can be found in Appendix A.1. As a crosscheck, we performed the calculation using two different approaches for the fermions: the usual four-component spinor description and the two-component description [242].

On the side of the EFT, the operators of Eq.(2.4) each contribute four tree-level Feynman diagrams to the $d_i\bar{d}_j \to d_j\bar{d}_i$ amplitude. Half of these contributions are obtained from the other two by an exchange of the particles in the initial and final states: as the dimension 6 operators are symmetrical over the simultaneous exchange of both d_i's and both d_j's, we may simply consider two diagrams and double the amplitude. The two remaining diagrams correspond to an $(s \leftrightarrow t)$-channel exchange. We exploit these considerations to reduce the number of diagrams that we consider on the side of the RpV-MSSM to only one of the s/t-channels.

The tree-level contribution to the $d_i\bar{d}_j \to d_j\bar{d}_i$ amplitudes is due to the λ' couplings of Eq.(1.7). It involves a sneutrino exchange where, however, sneutrino-flavor and sneutrino-Higgs mixing could occur. The appearance of RpV contributions at tree-level complicates somewhat a full one-loop analysis: one-loop contributions indeed depend on the renormalization of the $d_i\bar{d}_j$-sneutrino vertex (and of its external legs). In principle, one could define this vertex 'on-shell', *i.e.* impose that one-loop corrections vanish for on-shell d_i, d_j external legs — while the counterterm for the sneutrino field is set at momentum $p^2 = M^2_{K,B} \simeq 0$. In such a case, one could restrict oneself to calculating the box-diagram contributions to $d_i\bar{d}_j \to d_j\bar{d}_i$. However, in any other renormalization scheme, self-energy

[1] For the general rotation to this basis see Ref. [240]. See also Ref. [241] for a discussion of this in terms of physics at the unification scale.

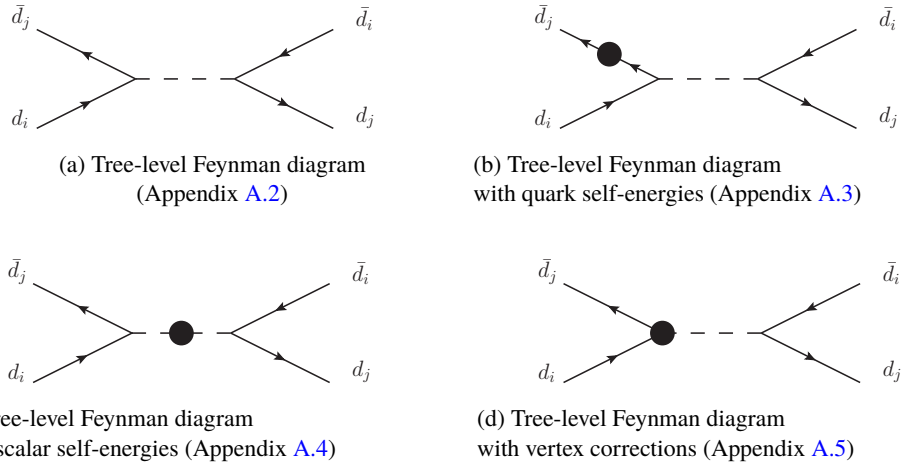

(a) Tree-level Feynman diagram (Appendix A.2)

(b) Tree-level Feynman diagram with quark self-energies (Appendix A.3)

(c) Tree-level Feynman diagram with scalar self-energies (Appendix A.4)

(d) Tree-level Feynman diagram with vertex corrections (Appendix A.5)

Figure 2.1: The tree level diagram and its one-loop corrections.

and vertex-correction diagrams should be considered. Yet, if the λ' couplings contributing at tree-level are small, the impact of the vertex and self-energy corrections is expected to be limited, since these contributions retain a (at least) linear dependence on the tree-level λ'. These contributions are symbolically depicted in Fig.2.1.

One-loop diagrams contributing to $d_i\bar{d}_j \to d_j\bar{d}_i$ include SM-like contributions (box diagrams with internal u, c, t quarks, W and Goldstone bosons), 2-Higgs-doublet-model-like contributions (box diagrams with internal u, c, t quarks, charged-Higgs bosons and possibly W or Goldstone bosons), R_p-conserving SUSY contributions (box diagrams with chargino/scalar-up, neutralino/sdown or gluino/sdown particles in the loop) and RpV-contributions (self-energy and vertex corrections, box diagrams with sneutrino/quark, slepton/quark, lepton/squarks, neutrino/squark or quark/squark internal lines). The RpV-driven mixing further intertwines these contributions, so that the distinction among *e.g.* the R_p-conserving chargino/scalar-up and RpV lepton/scalar-up boxes becomes largely superfluous. For all these contributions, with exception of the self-energy diagrams on the external legs, we neglect the external momentum, as it controls effects of order $m_{d_{i,j}}$, which are subdominant when compared to the momentum-independent pieces of order M_W or M_{SUSY}. Yet, when a SM-fermion f appears in the loop, some pieces that are momentum-independent still come with a suppression of order $m_f/M_{W,\text{SUSY}}$. We keep such pieces even though they could be discarded in view of the previous argument.

The diagrams of Fig.2.1 are calculated in Appendix A.2 (tree-level contribution), Appendix A.3 (d_i-quark self-energies), Appendix A.4 (scalar self-energy) and Appendix A.5 (vertex corrections). Fig.2.2 lists the various relevant topologies involved in box diagrams. The corresponding contributions are presented in Appendix A.6. The relevant loop functions are provided in Appendix A.1.3.

While we go beyond the usual assumptions employed to study the $\Delta F = 2$ Wilson coefficients in the RpV-MSSM, it is possible to compare the outcome of our calculation to partial results available in the literature. First, in the limit of vanishing RpV-parameters, we recover the well-known results in the R_p-conserving MSSM, which are summarized in *e.g.* the appendix of Ref. [218]. Then, RpV-contributions from the tree-level and box-diagram topologies have been presented in Ref. [158]

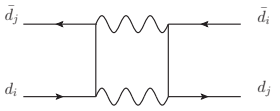

(a) Vector/fermion/vector/fermion "straight" box (Appendix A.6.1)

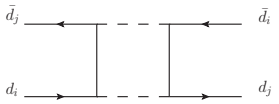

(b) Scalar/fermion/scalar/fermion "straight" box (Appendix A.6.1)

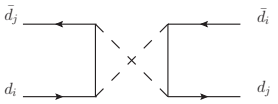

(c) Scalar/fermion/scalar/fermion "scalar-cross" box (Appendix A.6.3)

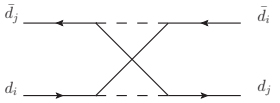

(d) Scalar/fermion/scalar/fermion "fermion-cross" box (Appendix A.6.4)

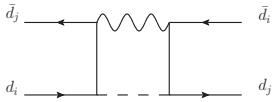

(e) Vector/fermion/scalar/fermion "straight" box (Appendix A.6.1)

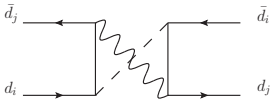

(f) Vector/fermion/scalar/fermion "cross" boxes (Appendix A.6.6)

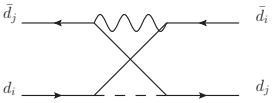

(g) Vector/fermion/scalar/fermion "fermion-cross" box (Appendix A.6.4)

Figure 2.2: The topologies of box diagrams that appear in the neutral mesons mixing with the RpV-MSSM.

in the no-mixing approximation. Taking this limit and neglecting further terms that are not considered by this reference, we checked that our results coincided, with the exception of the coefficient $c'^{\lambda'}_{LR}$ of Ref. [158] (a piece of the contribution to C_5). Transcripted to our notations, the result of Ref. [158] reads:

$$\begin{aligned} c'^{\lambda'}_{LR} &= -\frac{1}{64\pi^2}\lambda'^{*}_{i1k}\lambda'_{j2k}\lambda'_{im1}\lambda'^{*}_{jm2}D_2(m^2_{N_i}, m^2_{N_j}, m^2_{d_k}, m^2_{d_m}) \\ &\quad -\frac{1}{64\pi^2}\lambda'^{*}_{i1k}\lambda'_{j2k}\lambda'_{im1}\lambda'^{*}_{jm2}D_2(m^2_{\nu_i}, m^2_{\nu_j}, m^2_{\bar{D}^k_R}, m^2_{\bar{D}^m_R}), \end{aligned} \tag{2.5}$$

while we obtain:

$$\begin{aligned} c'^{\lambda'}_{LR} &= \frac{1}{32\pi^2}\lambda'^{*}_{i1k}\lambda'_{j2k}\lambda'_{im1}\lambda'^{*}_{jm2}D_2(m^2_{N_i}, m^2_{N_j}, m^2_{d_k}, m^2_{d_m}) \\ &\quad + \frac{1}{32\pi^2}\lambda'^{*}_{i1k}\lambda'_{j2k}\lambda'_{im1}\lambda'^{*}_{jm2}D_2(m^2_{\nu_i}, m^2_{\nu_j}, m^2_{D^k_R}, m^2_{D^m_L}). \end{aligned} \tag{2.6}$$

The mismatch lies in the prefactor and the sfermion chiralities. Another class of λ' boxes involving an electroweak charged current has been considered in the no-mixing limit in Ref. [159]. There, we find agreement with our results. As self-energy and vertex corrections have not been considered before, the opportunities for comparison are more limited. Still, we checked that the scalar self-energies were consistent with the results of Ref. [243]. Finally, our results can be controlled in another fashion, using

the automatically generated results of public tools: we detail this in the following section.

2.3 Numerical implementation and tools

In order to determine limits from the meson oscillation measurements on the parameter space of the RpV-MSSM, we establish a numerical tool implementing the one-loop contributions to the $\Delta F = 2$ Wilson coefficients and deriving the corresponding theoretical predictions for $\Delta M_{K,d,s}$. To this end, we make use of the Mathematica package SARAH [209–214] to produce a customized spectrum generator based on SPheno [206–208]. SPheno calculates the complete supersymmetric particle spectrum at the one-loop order and includes all important two-loop corrections to the neutral scalar masses [244].

The routines performing the calculation of flavor observables are generated through the link to FlavorKit [215]. FlavorKit makes use of FeynArts/FormCalc [245–247] to calculate the leading diagrams to quark and lepton flavor violating observables. For the meson mass differences, the tree-level and box diagrams as well as the double-penguin contributions are included per default. However, as parameters within SPheno are defined in the $\overline{DR}$ scheme, it is in principle necessary to implement the self-energy and vertex corrections. We added the vertex corrections via PreSARAH [215], which enables the implementation of new operators into FlavorKit within certain limits. As the scalar self-energies cannot be generated in this fashion, we incorporated these by hand.

The Wilson coefficients computed by FlavorKit and PreSARAH at the electroweak matching scale are stored in analytical form in the Fortran output of FlavorKit. We compared these expressions with our results of the previous section; we found explicit agreement in almost all cases — and adapted the code to match our results in the few cases where it proved necessary.[2]

After the Wilson coefficients at the electroweak matching scale are computed, further steps are necessary in order to relate them to the observables $\Delta M_{K,d,s}$. The FlavorKit output includes a theoretical prediction for these observables, however the hadronic input parameters are more up-to-date in the more recently-developed code Flavio [216], which shares an interface with FlavorKit using the FLHA standards [248]. We hence use Flavio to process the Wilson coefficients as calculated by FlavorKit. First, the Wilson coefficients must be run to a low-energy scale using the QCD RGE's of the EFT [236]. In the case of the $K^0 - \bar{K}^0$ system, the impact of the charm loop is sizable [234]: we upgraded the NLO coefficient η_{cc} coded within Flavio to the NNLO value 1.87(76) [234] and $\eta_{ct} = 0.496(47)$ [249]. For consistency, the charm mass in the loop functions is set to the $\overline{\text{MS}}$ value $m_c(m_c) \simeq 1.28$ GeV. Then, the hadronic dynamics encoded in the dimension 6 operators must be interpreted at low-energy in the form of hadronic mixing elements: this step gives rise to "bag-parameters", which are evaluated in lattice QCD. Here, Flavio employs the bag parameters of Ref. [250] for the $K^0 - \bar{K}^0$ system and of Ref. [229] for the $B_d^0 - \bar{B}_d^0$ and $B_s^0 - \bar{B}_s^0$ systems. In addition, the CKM matrix elements within Flavio are derived from the four inputs $|V_{us}|$, $|V_{ub}|$, $|V_{cb}|$ and γ. We set these to the fit-results of Ref. [230]: $|V_{us}| \simeq 0.22506$, $|V_{ub}| \simeq 3.485 \cdot 10^{-3}$, $|V_{cb}| \simeq 4.108 \cdot 10^{-2}$ and $\gamma \simeq 1.236$. Moreover, we changed the B_d^0 decay constant to a numerical value of 186 MeV [251]. Finally, we added the observable ΔM_K to Flavio (based on pre-included material) and made sure that

[2] In rare cases, we identified seemingly minor — but numerically important — differences between our computation and the FlavorKit code, namely in a few tree-level contributions to C_5 (which should be absent), as well as in $\tilde{C}_{2,3}$ and $C_{2,3}$ for a few one-loop box diagrams. We fixed those appearances in the code as well as the relative sign between tree and one-loop contributions after correspondence and cross-checking with the FlavorKit authors.

the predicted SM short-distance prediction was consistent with the theoretical SM estimate given by Ref. [234].

A quantitative comparison of the predicted $\Delta M_{K,d,s}$ with the experimental results of Eqs.(2.1) and (2.2) requires an estimate of the theoretical uncertainties. The Wilson coefficients have been obtained at leading order, which implies higher-order corrections of QCD-size. In the case of the SM-contributions, large QCD logarithms are resummed in the evolution of the RGEs between the matching electroweak scale and the low-energy scale. However, for the new-physics contributions, further logarithms between the new-physics and the electroweak scale could intervene — FlavorKit computes the new-physics contributions to the Wilson coefficients at the electroweak scale, hence missing such logarithms. Therefore, the higher-order uncertainty is larger for contributions beyond the SM and can be loosely estimated as $O\left(\frac{\alpha_S}{\pi}\log\frac{\mu_{NP}^2}{\mu_{EW}^2}\right)$, where μ_{NP} and μ_{EW} represent the new-physics and electroweak scales, respectively. Further sources of uncertainty are the RGE evolution in the EFT and the evaluation of hadronic matrix elements. For the SM matrix elements, the uncertainties on η_{cc}, η_{ct} and η_{tt} are of order 30% [234], 10% [249] and 1% [252], respectively, leading to a large SM uncertainty in ΔM_K and a smaller one in $\Delta M_{d,s}$. For the $K^0 - \bar{K}^0$ system, the bag-parameters are known with a precision of $\sim 3\%$ in the case of $B_K^{(1)}$ and $\sim 7\%$ for the other operators [250]. For the $B_d^0 - \bar{B}_d^0$ system, the uncertainty is of order 10% [229] — and even 20% for $B_{B_d}^{(3)}$. For the $B_s^0 - \bar{B}_s^0$, the bag parameters are known at about 7% accuracy [229] — 14% for $B_{B_s}^{(3)}$. Finally, CKM matrix elements contribute to the uncertainty at the level of a few percent. To summarize, we decided to estimate the theoretical uncertainties of our predictions for the meson oscillation parameters in the RpV-MSSM as follows:

- $40\% \times \left[|\Delta M_K^{\text{SM, Short. Dist.}}| + |\Delta M_K^{\text{RpV-MSSM, Short. Dist.}} - \Delta M_K^{\text{SM, Short. Dist.}}|\right]$ for the short-distance contribution to ΔM_K. As explained above, we will employ the estimate of Ref. [233] for the long-distance contribution: $\Delta M_K^{\text{SM, Long Dist.}} \simeq (20 \pm 10)\% \times \Delta M_K^{exp}$.
- $15\% \times |\Delta M_{d,s}^{\text{SM}}| + 30\% \times |\Delta M_{d,s}^{\text{RpV-MSSM}} - \Delta M_{d,s}^{\text{SM}}|$ for the evaluation of $\Delta M_{d,s}$.

These uncertainty estimates restore the magnitude of the SM uncertainties [225–227, 234]. Concerning the new-physics part, we stress that the calculation employs a (QCD/QED) LO matching and misses running effects between the SUSY and the matching scales, which motivates conservative estimates.

Finally, we note that our calculation of the Wilson coefficients for the $\Delta F = 2$ transition also provides access to CP-violating observables such as ϵ_K. These would grant complementary constraints on the parameter space, in particular when the RpV-parameters of Eq.(1.7) are considered as complex degrees of freedom. Obviously, in the presence of e.g. a large RpV tree-level contribution to the $d_i\bar{d}_j \to d_j\bar{d}_i$ amplitude, it is always possible to choose the phases of the λ'-parameters such that, amongst others, ϵ_K is in agreement with the experimental measurement (within uncertainties that are dominated by the theoretical evaluation [234]). On the other hand, it is less trivial whether such an adjustment would be possible within the magnitude of the NP contributions that is compatible with ΔM's. For simplicity — keeping in mind that our numerical studies are strictly illustrative in purpose and do not aim at conveying an exhaustive picture of possible RpV-effects associated to the meson-oscillation parameters —, we restrict ourselves to real values of the RpV-parameters and do not consider the CP-violating observables below. In practice, the R_p-conserving contributions beyond the SM in the scenarios that we consider in the following section are always subleading to RpV effects,

so that any deviation of the CP-violating observables from the SM predictions (caused by the CKM phase) is proportional to the RpV parameters and could be compensated via the corresponding RpV phases. Of course, if one chooses not to exploit this degree of freedom, the scenario with real RpV parameters itself would be subject to stronger limits when the CP-violating observables are also taken into account.

2.4 Numerical results

We are now in a position to study the limits on RpV-parameters that are set by the meson-oscillation parameters. However, it makes limited sense to scan blindly over the RpV-MSSM parameter space imposing only constraints from the ΔM's. Comparable analyses of all the relevant observables for which experimental data is available would be necessary. We will thus restrict ourselves to a discussion of the bounds over a restricted number of parameters and in a few scenarios. The input parameters that we mention below correspond to the `SPheno` input defined at the M_Z scale.

We first consider the case where no explicit source of flavor violation appears in the R_p-conserving parameters. The flavor transition is thus strictly associated to the CKM matrix or to the RpV-effects. The latter can intervene in several fashions:

- Flavor violation in the λ' couplings could lead to tree-level contributions to the ΔM's. The relevant combinations — in the absence of sneutrino mixing — are of the form $\lambda'_{fIJ}\lambda'^{*}_{fJI}$, where (I, J) are the indices of the valence quarks of the considered meson — *i.e.* $(1,2)$, $(1,3)$ and $(2,3)$ for ΔM_K, ΔM_d and ΔM_s respectively — and f is the flavor of the sneutrino mediator.

- Flavor violation in the λ' couplings could also intervene at the loop-level only. This happens when, for instance, one product of the form $\lambda'_{mnI}\lambda'^{*}_{mnJ}$ or $\lambda'_{mIn}\lambda'^{*}_{mJn}$ is non-zero — again, (I, J) corresponds to the valence quarks of the meson; m and n are internal to the loop.

- Finally, the flavor transition can be conveyed by the λ'' couplings, in which case it appears only at the loop level in the ΔM's. Possible coupling combinations include $\lambda''_{m12}\lambda''_{m23}$, $\lambda''_{m12}\lambda''_{m13}$ or $\lambda''_{m13}\lambda''_{m23}$.

Below, we first consider these three cases separately, before we investigate possible interferences between tree- and loop-level generated diagrams for several non-zero λ' couplings. However, we avoid considering simultaneously non-zero $LQ\bar{D}$ and $\bar{U}\bar{D}\bar{D}$ couplings: then, discrete symmetries no longer protect the proton from decay, so that the phenomenology would rapidly come into conflict with associated bounds. Still, we note that some diagrams contributing to the meson mixing parameters would combine both types of couplings: these are also provided in the appendix.

Then, flavor transitions can also be mediated by R_p-conserving effects. In this case, flavor violation could originate either in the CKM matrix, as in the Minimal Flavor Violation scenario [253], or in new-physics parameters, such as the soft squark bilinear and trilinear terms. We briefly discuss possible interferences with RpV-contributions.

For simplicity, we consider only the case of real $\lambda'^{(\prime)}$ and disregard the bilinear R-parity violating terms (though they are included in our analytical results in the appendix).

Scenario	M_A/TeV	μ/TeV	$\tan\beta$	$m_{\tilde{q}}$/TeV	$M_{1,2}$/TeV	M_3/TeV
SM-like	3.5	2	10	2	2	2
2HDM	0.8	2	10	2	2	2
SUSY-RpV(a)	1.2	0.6	10	$\simeq 2$	0.5	2
SUSY-RpV(b)	1.2	0.3	10	$\simeq 2\&1_{\tilde{t},\tilde{b}}$	0.5	2

Table 2.1: Input parameters for various scenarios under consideration. With $2\&1_{\tilde{t},\tilde{b}}$ we imply $m_{\tilde{q}_{1,2}} = 2\,\text{TeV}$ while keeping a lighter third generation, $m_{\tilde{q}_3} = 1\,\text{TeV}$.

2.4.1 Bounds on a pair of simultaneously non-zero $LQ\bar{D}$ couplings

Tree Level Contributions

Let us begin with the case where only two $LQ\bar{D}$ couplings are simultaneously non-vanishing and contribute to the ΔM's at tree-level. For doing so, we choose a spectrum of the form of an effective SM at low mass, where we have fixed the squark, higgsino and gaugino masses to 2 TeV, while varying all the slepton masses simultaneously in the range $0.2 - 2$ TeV. The important parameter values are listed in the first line of Table 2.1. In addition, the stop trilinear coupling A_t, of order 3 TeV (without endangering (meta)stability of the potential however[3]), is adjusted so that the lighter Higgs mass satisfies $m_h \approx 125$ GeV (within 3 GeV). We also considered several other scenarios, listed in Table 2.1, *e.g.* involving lighter charged Higgs or lighter squarks of the third generation, but the general properties of the constraints remained qualitatively unchanged. In fact, the predicted values of ΔM's in the R_p-conserving limit only differ at the percent level (a barely noticeable variation in view of the uncertainties) between these four scenarios, which can be placed into the perspective of the systematic suppression of the SUSY R_p-conserving loops due to the high squark masses. As the R_p-conserving contributions do not depend on the parameters that we vary in this subsection, the $n\,\sigma$-boundaries ($n = 0, \cdots, 3$) are only shifted by an imperceptible amount in parameter space when comparing the various scenarios of Table 2.1. Therefore, we only present the results in the SM-like scenario here. All the input is defined at the electroweak scale, so that we can discuss the various classes of RpV-contributions to the ΔM's without the blurring effect due to the propagation of flavor-violation via RGE's between a high-energy scale and the electroweak scale.

In Fig. 2.3, we present the limits set by ΔM_d, ΔM_s and ΔM_K on the tree-level flavor violating contributions. The plots in the first column are obtained for a positive product $\lambda' \cdot \lambda'$, while those in the second column correspond to negative $\lambda' \cdot \lambda'$. For each observable, the most relevant $\lambda' \cdot \lambda'$ combination, leading to a tree-level contribution, was selected. The individual sub-figures depict the extension of the $0, 1, 2, 3\,\sigma$ regions in the plane defined by the corresponding flavor-violating $\lambda' \cdot \lambda'$ product and the slepton mass. The colors in Fig. 2.3 are chosen such that purple regions are excluded at three standard deviations or more; red regions are excluded at $\geq 2\,\sigma$ — which is the limit that we apply later on, in order to decide whether a point in parameter space is excluded or allowed experimentally; the orange regions correspond to a prediction of the ΔM within 1 and $2\,\sigma$; finally, the green areas are consistent with the experimental measurement within $1\,\sigma$, while the black curves reproduce the

[3] The stability of the electroweak minimum was tested for individual points. To this end, we generated a model file allowing for non-vanishing squark VEVs with SARAH and tested it through the numerical code Vevacious [254], interfaced with CosmoTransitions [255]. A parameter point is deemed unstable on cosmological time-scales, and therefore ruled out, if the mean tunnelling time is smaller than 21.7% of the age of the Universe.

central values exactly. Experimental and theoretical uncertainties are added in quadrature to define the total uncertainty $U_{tot} = \sqrt{U_{theo}^2 + U_{exp}^2}$. In the case of ΔM_K, the theoretical uncertainties from long-distance and short-distance contributions are also combined quadratically. Since experimentally one cannot tell apart the two mass eigenstates of $B^0_{d/s}$, we simply consider the absolute value of $\Delta M_{d/s}$ in our evaluation. When we plot $\Delta M_{d,s}$, this feature may result in a doubling of the solutions for the central value or of the 1 σ-allowed regions, such as in the upper-left and middle-left plots of Fig. 2.3. For K^0, instead, the mass ordering, and hence the sign of ΔM_K is known.

The limits that we obtain on the λ' couplings contributing at tree-level are relatively tight. In the scenarios of Fig.2.3, the 2σ bounds read approximately:

$$\begin{cases} \lambda'_{i13}\lambda'_{i31} \lesssim 1.6\times10^{-6}\left(\frac{m_{\tilde{\nu}_i}}{1\,\text{TeV}}\right)^2, & -\lambda'_{i13}\lambda'_{i31} \lesssim 4\times10^{-7}\left(\frac{m_{\tilde{\nu}_i}}{1\,\text{TeV}}\right)^2, \\ \lambda'_{i23}\lambda'_{i32} \lesssim 3.6\times10^{-5}\left(\frac{m_{\tilde{\nu}_i}}{1\,\text{TeV}}\right)^2, & -\lambda'_{i23}\lambda'_{i32} \lesssim 8\times10^{-6}\left(\frac{m_{\tilde{\nu}_i}}{1\,\text{TeV}}\right)^2, \\ |\lambda'_{i12}\lambda'_{i21}| \lesssim 2.2\times10^{-8}\left(\frac{m_{\tilde{\nu}_i}}{1\,\text{TeV}}\right)^2, \end{cases} \tag{2.7}$$

where we assume that only one lepton flavor, namely i, has non-vanishing RpV-couplings — therefore the bounds only depend on the mass of the corresponding sneutrino $\tilde{\nu}_i$. Alternatively, with degenerate sneutrinos, we could sum over the index i on the left-hand side of Eq. (2.7). Limits on these products of couplings have been presented in Ref. [190] for a SUSY mass of 100 GeV and in [164] for a mass of 500 GeV – as explained above, our limits can be confronted to the bounds applying on $\sum_i \lambda'_{i13}\lambda'_{i31}$, *etc.*, in these references. In comparison, the bounds that we obtain in Fig.2.3 are somewhat stronger, at least by a factor ~ 3. This result should be put mainly in the perspective of the reduction of the experimental uncertainty in the recent years.

1-Loop Contributions to Flavor Transition

Next, we turn to the case where a pair of $LQ\bar{D}$ couplings mediate the flavor transition only at the loop-level and we focus on coupling combinations of the form $\lambda'_{mnI}\lambda'^{*}_{mnJ}$ or $\lambda'_{mIn}\lambda'^{*}_{mJn}$ (with I, J the valence quarks of the meson). In principle we could consider other combinations, such as $\lambda'_{mnI}\lambda'^{*}_{\tilde{m}nJ}$, $\lambda'_{mnI}\lambda'^{*}_{m\tilde{n}J}$, $\lambda'_{mIn}\lambda'^{*}_{\tilde{m}Jn}$ or $\lambda'_{mIn}\lambda'_{mJ\tilde{n}}$ (with $m \neq \tilde{m}, n \neq \tilde{n}$). However, either the associated contributions are CKM suppressed or they would require several $\lambda' \cdot \lambda'$ products to be simultaneously non-zero or non-degenerate scalar / pseudoscalar sneutrino fields. We thus restrict ourselves to the two types mentioned above. For these, we note that the limits are independent of the flavor m of the slepton field. In this context, RpV-effects in ΔM's are dominated by diagrams involving the comparatively light (charged or neutral) sleptons. We thus concentrate on these below. We can distinguish two types of contributions:

- If one of the pair of non-vanishing $LQ\bar{D}$ couplings is one of those involved for the tree-level exchange diagram — *i.e.* if it contains the two flavor indices of the valence quarks of the meson — we find that quark self-energy corrections on the tree-level diagram can be comparable to or even dominant over box contributions.

- If neither of the non-vanishing $LQ\bar{D}$ couplings participates in the tree-level diagrams, box diagrams are the main contributions.

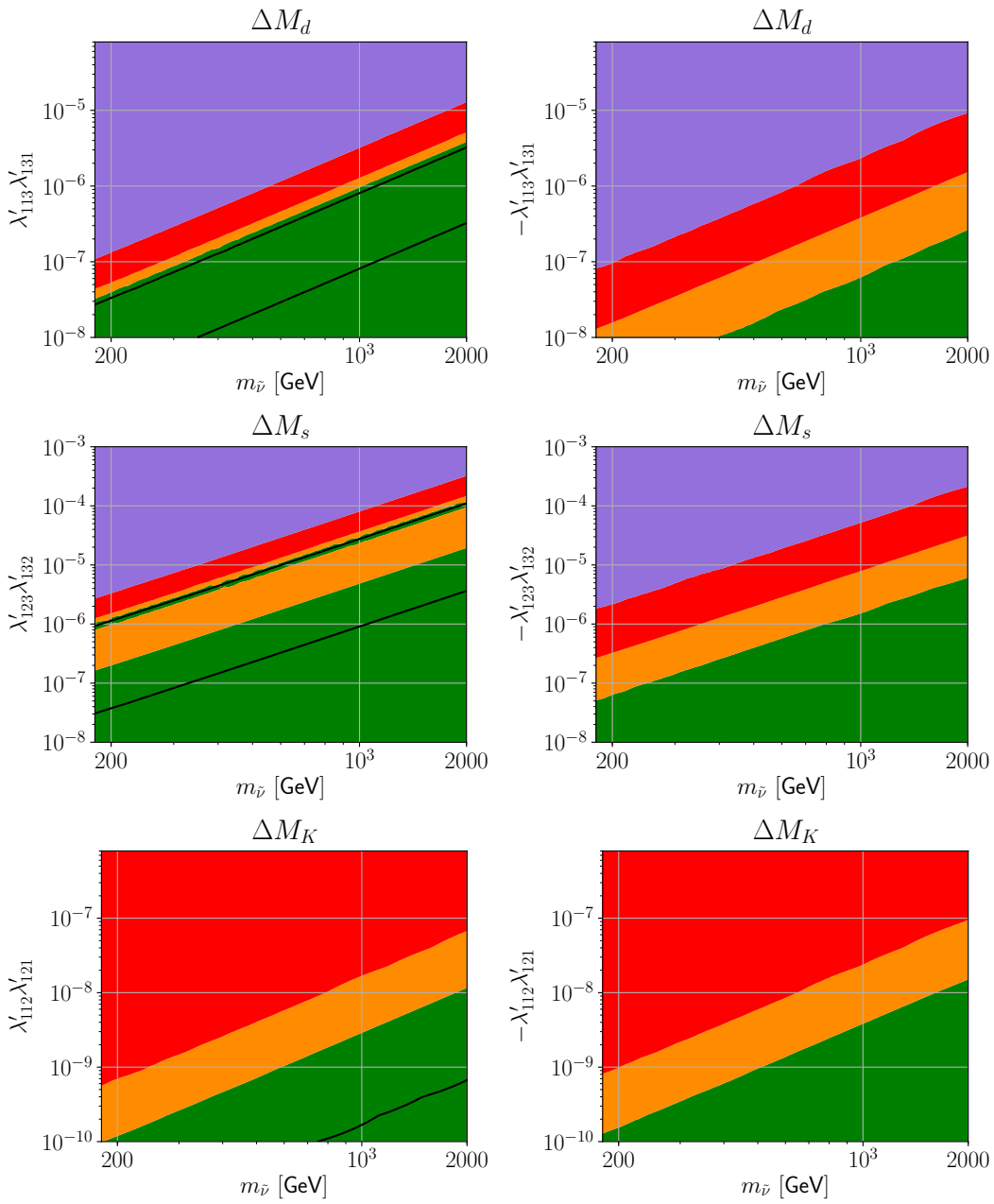

Figure 2.3: Constraints from the ΔM's on scenarios with RpV-mediated flavor violation contributing at tree-level, as a function of the sneutrino mass. The plots on the left correspond to the upper limit on positive $\lambda' \cdot \lambda'$; those on the right to lower limits on negative $\lambda' \cdot \lambda'$ combinations. The green, orange, red and purple colors represent regions within $[0, 1\sigma]$, $[1\sigma, 2\sigma]$, $[2\sigma, 3\sigma]$ and $> 3\sigma$ bounds, respectively. The experimental central value is exactly recovered on the black lines. For these plots, the parameter set of the scenario SM-like of Table 2.1 has been employed.

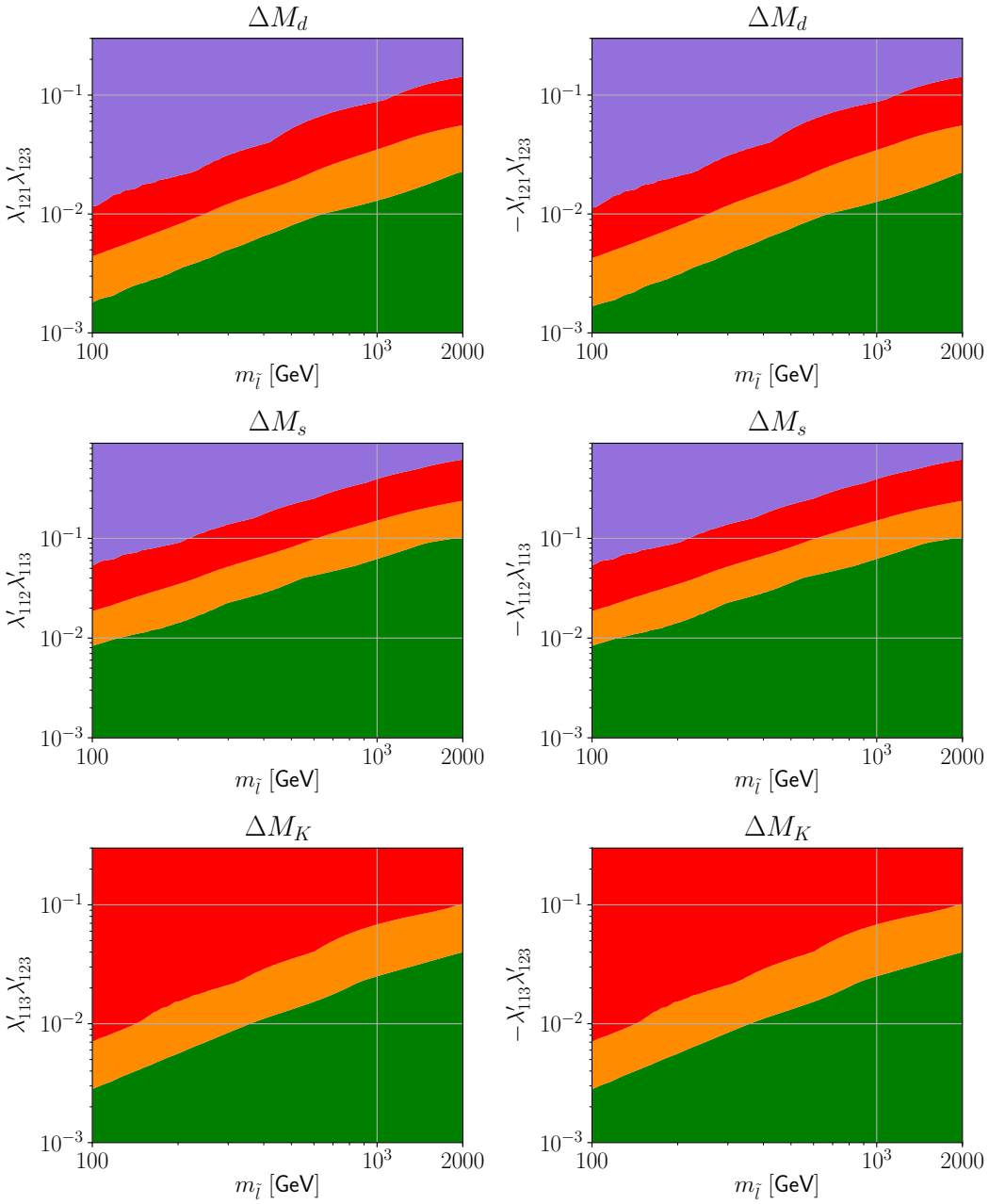

Figure 2.4: Constraints from the ΔM's on scenarios with RpV-mediated flavor violation of $LQ\bar{D}$-type, where the RpV-violating contribution is dominated by a box diagram. The limits are plotted against the slepton mass and follow the same color-code as Fig.2.3. For these plots, the parameter set of the scenario SUSY-RpV(a) of Table 2.1 has been employed.

This difference impacts both the magnitude of the resulting bounds and their dependence on the slepton mass, as we shall see below.

The spectrum that we focus on in this subsection (and later on) is described in the third row of Table 2.1. The choice of the scenario SUSY-RpV(a) instead of SM-like is motivated by the wish not to systematically suppress the loop diagrams associated with charginos/neutralinos. We will also comment on the mild differences that we obtain in the other scenarios of Table 2.1.

In Fig.2.4, we consider non-vanishing $\lambda'_{121}\lambda'_{123}$, $\lambda'_{112}\lambda'_{113}$ and, finally, $\lambda'_{113}\lambda'_{123}$. In these cases, the box diagrams dominate over the fermionic self-energy corrections. For each scenario, the limits from the ΔM's essentially originate in one of the three observables ΔM_d, ΔM_s or ΔM_K. The corresponding limits approximately read:

$$\begin{cases} |\lambda'_{i21}\lambda'_{i23}| \lesssim 3.4\times10^{-2}\left(\frac{m_{\tilde{\ell}_i}}{1\,\mathrm{TeV}}\right), \\ |\lambda'_{i12}\lambda'_{i13}| \lesssim 1.6\times10^{-1}\left(\frac{m_{\tilde{\ell}_i}}{1\,\mathrm{TeV}}\right), \\ |\lambda'_{i13}\lambda'_{i23}| \lesssim 6.3\times10^{-2}\left(\frac{m_{\tilde{\ell}_i}}{1\,\mathrm{TeV}}\right), \end{cases} \tag{2.8}$$

where $m_{\tilde{\ell}_i}$ denotes the mass of the degenerate sneutrinos and charged sleptons. Here, we note that the mass dependence of the form $(\lambda'\cdot\lambda')^2 < c\cdot m^2_{\tilde{\ell}}$ differs from that appearing when the RpV-contribution intervenes at tree-level. It is characteristic of the leading RpV-diagrams in the considered set-up, corresponding to the box formed out of two charged sleptons and two up-type quarks in the internal lines and to the box consisting of two sneutrinos and two down-type quarks: these diagrams roughly scale as $(\lambda'\cdot\lambda')^2/m^2_{\tilde{\ell}}$. As a consequence, the limits for positive and negative $\lambda'\cdot\lambda'$ products are comparable. In addition, the bounds on $\lambda'\cdot\lambda'$ now scale about linearly with the sparticle mass.

Expectedly, the limits are much weaker in these box-dominated scenarios than in the case where the flavor transition appears at tree-level. Refs. [159, 160, 164] presented limits on the corresponding coupling-combinations for a sfermion mass of 100 or 500 GeV. The bounds that we derive are of the same order. Similarly to the case where the RpV-contribution to the flavor transition is mediated at tree-level, the investigation of the various scenarios of Table 2.1 results in very little variations.

Finally, we turn to the case where one of the non-vanishing λ' involves both flavors of the valence quarks of the K^0, $B^0_{d,s}$ meson while the other is flavor-diagonal (and contains only one of the valence flavors). Then, the dominant diagrams are of the form of Fig. 2.1(b): one $\Delta F = 1$ transition is mediated by the non-vanishing λ' with both valence-flavor indices, while the second $\Delta F = 1$ transition appears at the loop level — typically through a SM loop (W/up-type quark), *i.e.* in association with the CKM matrix. We stress that such contributions were dismissed in previous analyses and are considered here for the first time.

Corresponding scenarios are displayed in Fig.2.5, where ΔM_{B_d}, ΔM_{B_s} and ΔM_K are plotted against $\lambda'_{131}\cdot\lambda'_{133}$, $\lambda'_{132}\cdot\lambda'_{133}$ and $\lambda'_{121}\cdot\lambda'_{122}$, respectively. The bounds have a comparable scaling to that appearing in the scenario with tree-level sneutrino exchange, but the constraints are far weaker. At $2\,\sigma$:

$$\begin{cases} \lambda'_{i31}\lambda'_{i33} \lesssim 6\times10^{-4}\left(\frac{m_{\tilde{\nu}_i}}{1\,\mathrm{TeV}}\right)^2, & -\lambda'_{i31}\lambda'_{i33} \lesssim 2.7\times10^{-3}\left(\frac{m_{\tilde{\nu}_i}}{1\,\mathrm{TeV}}\right)^2, \\ \lambda'_{i32}\lambda'_{i33} \lesssim 1.4\times10^{-2}\left(\frac{m_{\tilde{\nu}_i}}{1\,\mathrm{TeV}}\right)^2, & -\lambda'_{i32}\lambda'_{i33} \lesssim 3\times10^{-3}\left(\frac{m_{\tilde{\nu}_i}}{1\,\mathrm{TeV}}\right)^2, \\ |\lambda'_{i21}\lambda'_{i22}| \lesssim 1.5\times10^{-3}\left(\frac{m_{\tilde{\nu}_i}}{1\,\mathrm{TeV}}\right)^2, \end{cases} \tag{2.9}$$

where $-\lambda'_{i31}\lambda'_{i33}, -\lambda'_{i32}\lambda'_{i33} > 0$. Due to the inclusion of the missing and obviously relevant self-energy

$\Delta m_{B_d^0}$		$\Delta m_{B_s^0}$		Δm_{K^0}	
$\lvert\lambda'_{ijk}\cdot\lambda'_{imn}\rvert$	2σ bound	$\lvert\lambda'_{ijk}\cdot\lambda'_{imn}\rvert$	2σ bound	$\lvert\lambda'_{ijk}\cdot\lambda'_{imn}\rvert$	2σ bound
$(i31)(i13)^{(\mathrm{T})}$	1.6×10^{-6}	$(i32)(i23)^{(\mathrm{T})}$	3.6×10^{-5}	$(i12)(i21)^{(\mathrm{T})}$	2.2×10^{-8}
$(i11)(i13)^{(\mathrm{S})}$	1.8×10^{-3}	$(i22)(i23)^{(\mathrm{S})}$	9.5×10^{-3}	$(i12)(i11)^{(\mathrm{S})}$	1.5×10^{-3}
$(i21)(i13)^{(\mathrm{S})}$	$[2.8\times10^{-4}]$	$(i12)(i23)^{(\mathrm{S})}$	$[4.2\times10^{-2}]$	$(i22)(i21)^{(\mathrm{S})}$	1.5×10^{-3}
$(i31)(i23)^{(\mathrm{S})}$	0.15	$(i32)(i13)^{(\mathrm{S})}$	0.33	$(i12)(i31)^{(\mathrm{S})}$	9×10^{-6}
$(i31)(i33)^{(\mathrm{S})}$	2.7×10^{-3}	$(i32)(i33)^{(\mathrm{S})}$	1.4×10^{-2}	$(i32)(i21)^{(\mathrm{S})}$	4.2×10^{-5}
$(i21)(i23)^{(\mathrm{B})}$	3.4×10^{-2}	$(i12)(i13)^{(\mathrm{B})}$	0.16	$(i32)(i11)^{(\mathrm{B})}$	0.64
$(i21)(i33)^{(\mathrm{B})}$	0.64	$(i22)(i33)^{(\mathrm{B})}$	0.74	$(i22)(i31)^{(\mathrm{B})}$	0.24
$(i11)(i33)^{(\mathrm{B})}$	0.64	$(i12)(i33)^{(\mathrm{B})}$	4	$(i22)(i11)^{(\mathrm{B})}$	4
$(i11)(i23)^{(\mathrm{B})}$	N/A	$(i22)(i13)^{(\mathrm{B})}$	N/A	$(i32)(i31)^{(\mathrm{B})}$	0.01
$(i12)(i31)^{(\mathrm{S})}$	[0.012]	$(i23)(i31)^{(\mathrm{S})}$	N/A	$(i21)(i11)^{(\mathrm{S})}$	5×10^{-3}
$(i13)(i32)^{(\mathrm{S})}$	[0.73]	$(i22)(i32)^{(\mathrm{S})}$	0.23	$(i22)(i12)^{(\mathrm{S})}$	5.8×10^{-3}
$(i13)(i33)^{(\mathrm{B})}$	0.05	$(i23)(i33)^{(\mathrm{S})}$	0.24	$(i23)(i12)^{(\mathrm{S})}$	2.2×10^{-2}
$(i11)(i31)^{(\mathrm{B})}$	0.07	$(i21)(i32)^{(\mathrm{S})}$	[2.25]	$(i21)(i13)^{(\mathrm{S})}$	2.3×10^{-4}
$(i12)(i32)^{(\mathrm{B})}$	0.05	$(i21)(i31)^{(\mathrm{B})}$	0.21	$(i23)(i13)^{(\mathrm{B})}$	6.3×10^{-2}

Table 2.2: Compilation of the latest bounds on relevant couplings of $LQ\bar{D}$ operators, coming from the considered meson oscillation observables. These limits were established with the spectrum defined in the row SUSY-RpV(a) of Table 2.1, with slepton and sneutrino masses of 1 TeV. The precise $2\,\sigma$ boundary obviously depends on the sign of the non-vanishing $\lambda'\cdot\lambda'$ product: we always apply the most conservative (weakest) limit. In the list of couplings, the comment "(T)/(S)/(B)" indicates that the coupling product is dominated by a tree-level/quark self-energy/box contribution. "N/A" means that we did not identify upper-limits on the couplings below 4π (a rough limit from perturbativity considerations). Above the horizontal line, the non-vanishing coupling combinations select right-handed external quarks. Below this line, the external quarks are left-handed. The scaling with the sneutrino/slepton mass is roughly quadratic for all $\lambda'\cdot\lambda'$ products that contain both valence flavors in (at least) one of the non-vanishing λ', linear otherwise: see more precise explanation in the main body of the text. Some combinations contribute to two observables, such as $\lambda'_{i13}\lambda'_{i32}$, relevant for both ΔM_d and ΔM_s. In such a case, the square brackets identify the weaker limit.

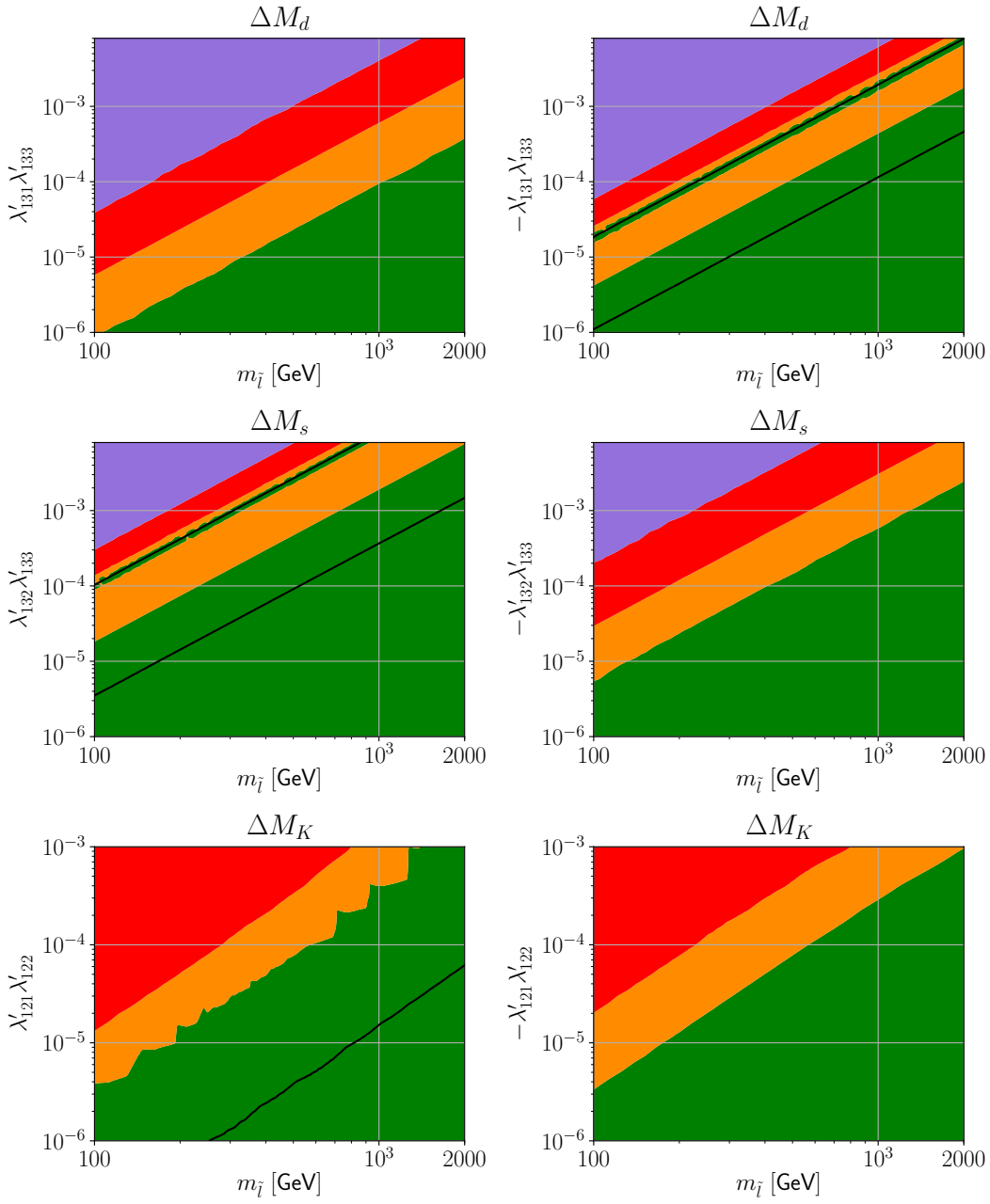

Figure 2.5: Constraints from the ΔM's on scenarios with RpV-mediated flavor violation of $LQ\bar{D}$-type, where the dominant RpV-diagram involves a one-loop quark self-energy. The limits are plotted against the sneutrino mass and follow the color code of Fig. 2.3. For these plots, the parameter set of the scenario SUSY-RpV(a) of Table 2.1 has been employed.

diagrams, the bounds that we report are accordingly tighter than in the literature[159, 160, 164]. If we compare the various scenarios of Table 2.1, we again observe little change at the qualitative level. However, the exact position of the $n\,\sigma$ ($n = 0, \cdots, 3$) boundaries is shifted by a numerical prefactor of order unity, homogeneous in the whole range of scanned parameters of Fig. 2.5. This prefactor is characteristic of the magnitude R_p-conserving loop entering the off-diagonal quark self-energy. For example, the upper-bounds on $\lambda'_{131}\lambda'_{133}$ are stronger by a factor ~ 2 in the SM-like scenario, as compared to the scenario SUSY-RPV(a) (shown in the plots), by a factor ~ 1.3 in the scenario 2HDM and by a factor ~ 1.6 in the scenario SUSY-RPV(b). Other numbers (of the same order) intervene for the two other considered sets of $\lambda' \cdot \lambda'$.

In Table 2.2, we compile the $2\,\sigma$ bounds on $\lambda' \cdot \lambda'$ products that we derive for 1 TeV sleptons in the scenario SUSY-RpV(a) of Table 2.1 (the limits depend only weakly on the chosen scenario). In this list, the pairs $\lambda' \cdot \lambda'$ are taken non-zero only one at a time and, in particular, for a unique (s)lepton flavor i. As explained above, the scaling with the slepton/sneutrino mass depends on the choice of non-vanishing λ': essentially quadratic if at least one of the non-vanishing λ' contains both valence-flavors of the decaying meson, linear otherwise. One of the ΔM's is usually more sensitive to a specific $\lambda' \cdot \lambda'$ product than the other two. etc.

2.4.2 Bounds on a pair of simultaneously non-zero $\bar{U}\bar{D}\bar{D}$ couplings

We proceed with our analysis and now consider baryonic RpV, *i.e.* non-zero $\bar{U}\bar{D}\bar{D}$ couplings. The corresponding RpV-effects appear only at the radiative level and are dominated by box diagrams. Contrarily to existing analyses [158], we always consider heavy gluinos (as indicated by the current status of LHC searches), so that the associated diagrams generally remain subdominant. In this setup, three classes of diagrams compete: (1) boxes including two squarks and two quarks in internal lines, which scale like $(\lambda'' \cdot \lambda'')^2$, (2) boxes including two quarks, one squark and a W-boson, which scale like $\lambda'' \cdot \lambda''$ but involve a CKM-suppression and a quark-chirality flip, and (3) similarly boxes with two squarks, one quark and a chargino, which scale like $\lambda'' \cdot \lambda''$. The matter of the chirality flip can be easily understood as only right-handed quarks couple via λ'' but only left-handed quarks couple to a W. Therefore, such diagrams with an internal W line are mostly relevant when the internal quark line involves a top-quark. As to the boxes with an internal chargino line, we also find that such contributions are mainly relevant for an internal stop line: indeed, the higgsino contribution scales with the Yukawa coupling, hence is suppressed for squarks of first or second generation. In addition, the gaugino contribution relies on left-right squark mixing, which we keep negligible for squarks of the first and second generation — making the assumption that the trilinear soft terms are proportional to the Yukawa couplings [77].

From now on, all the parameters are set to the values of the scenario SUSY-RpV(a) of Table 2.1, except for those that are explicitly scanned over (e.g. the squark masses). In Fig. 2.6, we present the 1, 2 and $3\,\sigma$ limits on coupling combinations allowing for internal (s)top lines. The relevant right-handed squarks are assumed to be mass-degenerate. The regime with small λ'' couplings is dominated by the box diagrams involving W bosons and top quarks in the internal lines. We find that, for low mass values, this contribution scales with the squark mass in an intermediate fashion between linear and quadratic, because of the finite top mass effects. These effects largely vanish for squark masses above $O(1\ \text{TeV})$ and we then recover the scaling with $\frac{\lambda''\cdot\lambda''}{m^2_{\tilde{q}}}$. The supersymmetrized version of the W boxes, *i.e.* boxes with internal charginos, are also contributing with a scaling of $\frac{\lambda''\cdot\lambda''}{m^2_{\tilde{q}}}$. However

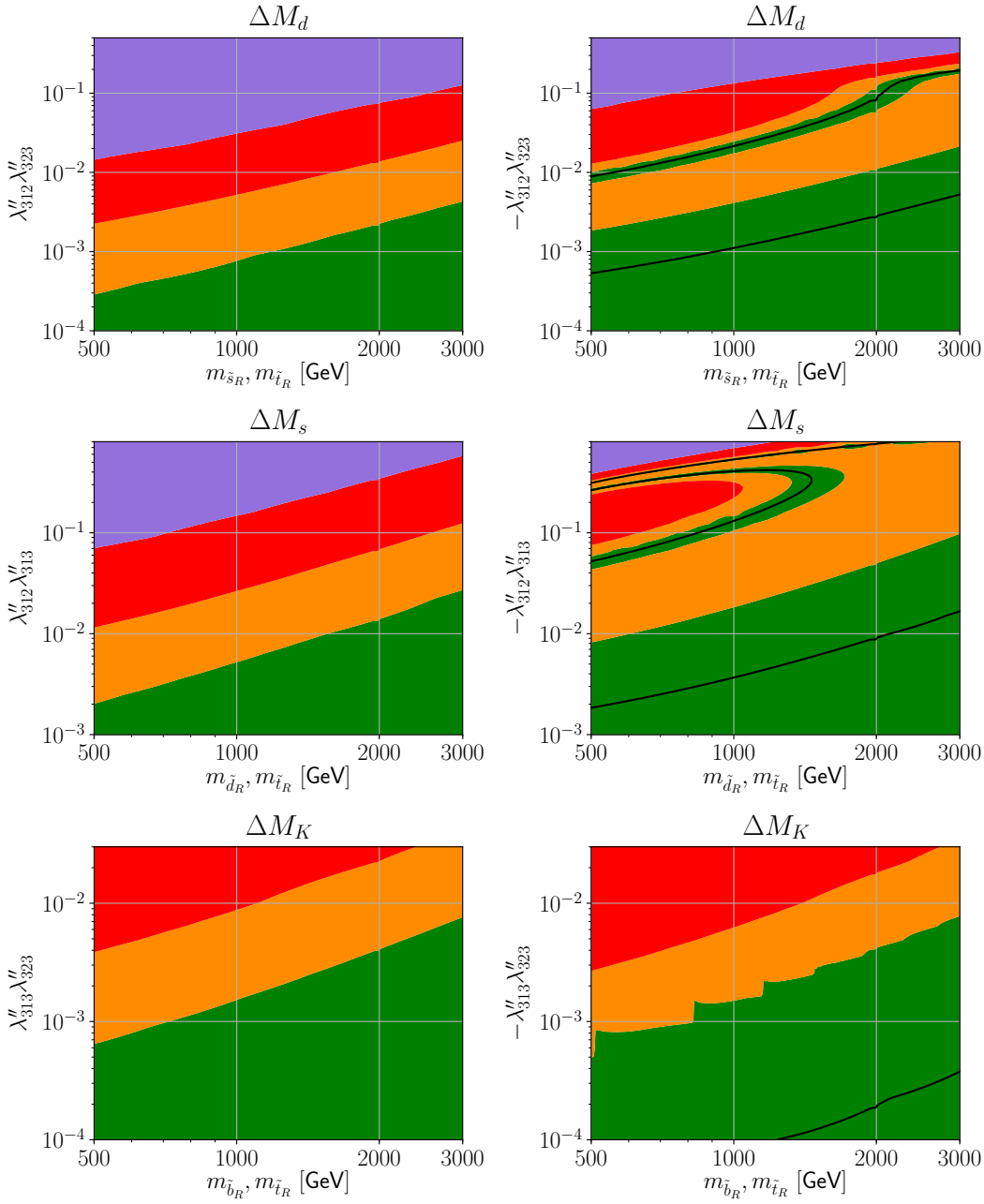

Figure 2.6: Limits on $\bar{U}_3\bar{D}_i\bar{D}_j$ couplings from the meson oscillation parameters. Internal (s)top lines are allowed by such couplings. The color code is similar to that of the previous plots. For these plots, the parameter set of the scenario SUSY-RpV(a) of Table 2.1 has been employed except for the squark masses that are scanned over.

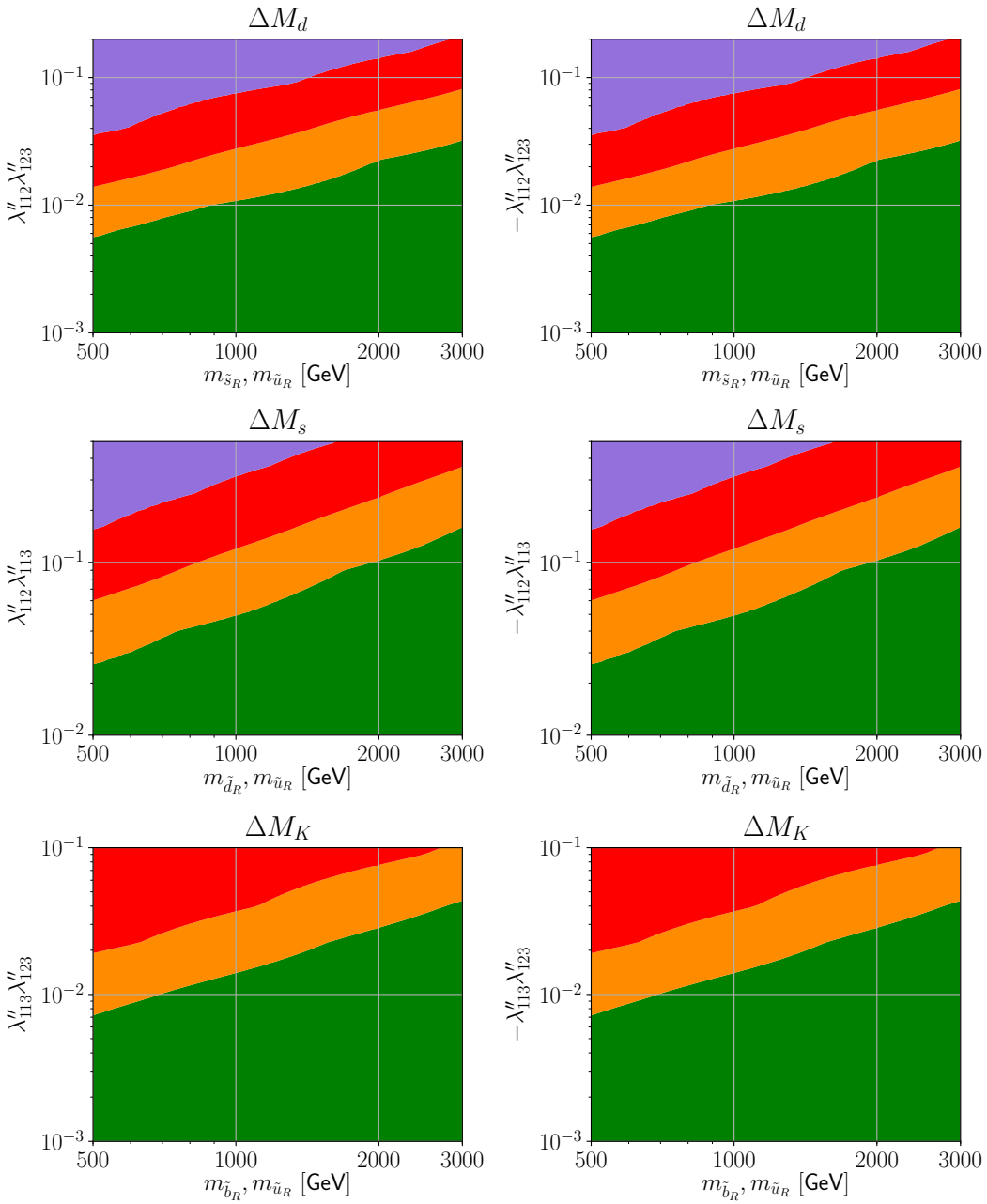

Figure 2.7: Limits on $\bar{U}_1\bar{D}_i\bar{D}_j$ couplings from the meson oscillation parameters. In this case, amplitudes with internal top lines vanish. The color code is similar to that of the previous plots. For these plots, the parameter set of the scenario SUSY-RpV(a) of Table 2.1 has been employed except for the squark masses that are scanned over.

their impact w.r.t. the W boxes is always reduced. At large values of the couplings and for light squarks, the purely $\bar{U}\bar{D}\bar{D}$-mediated diagrams appear to be the most relevant, scaling with $\frac{(\lambda''\cdot\lambda'')^2}{m_{\tilde{q}}^2}$ — in analogy to the slepton box-diagrams with non-vanishing $LQ\bar{D}$ coupling — so that the bounds on $\lambda''\cdot\lambda''$ show a roughly linear dependence with the squark mass. Then, for both large $|\lambda''\cdot\lambda''|$ and heavier quarks, the W-mediated diagrams and these purely $\bar{U}\bar{D}\bar{D}$ boxes can be of comparable magnitude, hence lead to interference structures. This interplay between various contributions brings about a non-trivial mass dependence of the bounds on the λ'' couplings, with both constructive as well as destructive effects between the individual amplitudes. The plots for negative $\lambda''\cdot\lambda''$ couplings perfectly illustrate this fact, in particular in the case of ΔM_s. Beyond this interference regime, at sufficiently large squark masses, the contribution from the UDD box with an internal W-line eventually supersedes the pure UDD amplitude.

Since the bounds on the individual coupling combinations do not scale with a simple power law in $m_{\tilde{q}_R}$, we refrain from showing approximate expressions as we did in the scenarios with flavor-violation of $LQ\bar{D}$-type.

In Fig. 2.7, by contrast, the choice of non-vanishing λ'' couplings does not allow for internal (s)top lines. Thus the RpV-diagrams with mixed W/squark or chargino/quark internal lines are suppressed, and the scaling of the limits from meson-oscillation parameters is closer to linear. In addition, the $2\,\sigma$ bounds are somewhat milder than in the previous case and roughly symmetrical for positive and negative $\lambda''\cdot\lambda''$ products. Thus, in this case, we extract the approximate bounds on $\bar{U}_1\bar{D}_i\bar{D}_j$ coupling pairs:

$$\begin{cases} |\lambda''_{112}\lambda''_{123}| \lesssim 2.8\times10^{-2}\left(\frac{m_{\tilde{s}_R,\tilde{u}_R}}{1\,\text{TeV}}\right), \\ |\lambda''_{112}\lambda''_{113}| \lesssim 1.2\times10^{-1}\left(\frac{m_{\tilde{d}_R,\tilde{u}_R}}{1\,\text{TeV}}\right), \\ |\lambda''_{113}\lambda''_{123}| \lesssim 3.6\times10^{-2}\left(\frac{m_{\tilde{b}_R,\tilde{u}_R}}{1\,\text{TeV}}\right), \end{cases} \tag{2.10}$$

Given that the scaling of the bounds on $\lambda''\cdot\lambda''$ pairs decidedly depends on the specific choice of couplings, we refrain from showing a compilation table as Table 2.2 for the $LQ\bar{D}$ couplings, since it would only be representative of a specific SUSY spectrum.

2.4.3 Competition among $LQ\bar{D}$-driven contributions

Bounds on individual RpV-coupling products may be misleading, in the sense that several RpV-effects could cancel one another. In fact, the decomposition along the line of the low-energy flavors provides likely-undue attention to these specific directions of RpV, while the latter have no deep specificity from the high-energy perspective. In particular, RGE's are expected to mix the various flavor-directions of non-vanishing RpV-couplings, while the boundary condition at, say, the GUT scale, has no particular reason for alignment with the low-energy flavor directions [241, 256]. Obviously however, the relevant directions in flavor space are highly model-dependent and we have no particular suggestion to make from the low-energy perspective of this work. Instead, we simply wish to illustrate the possibility of allowed directions with large RpV-couplings. To this end, we allow for two non-vanishing $\lambda'\cdot\lambda'$ coupling products and investigate the limits originating in the ΔM measurements.

If we consider Figs. 2.3 and 2.5, the tree-level diagram for $\lambda'_{i31}\cdot\lambda'_{i13} = O(10^{-6})$ and the RpV-box for $\lambda'_{i31}\cdot\lambda'_{i33} = O(10^{-4})$ — implying a hierarchy $\lambda'_{i13}/\lambda'_{i33} = O(10^{-2})$ – naively contribute to ΔM_d by amplitudes of comparable magnitude. Whether these contributions can interfere destructively clearly

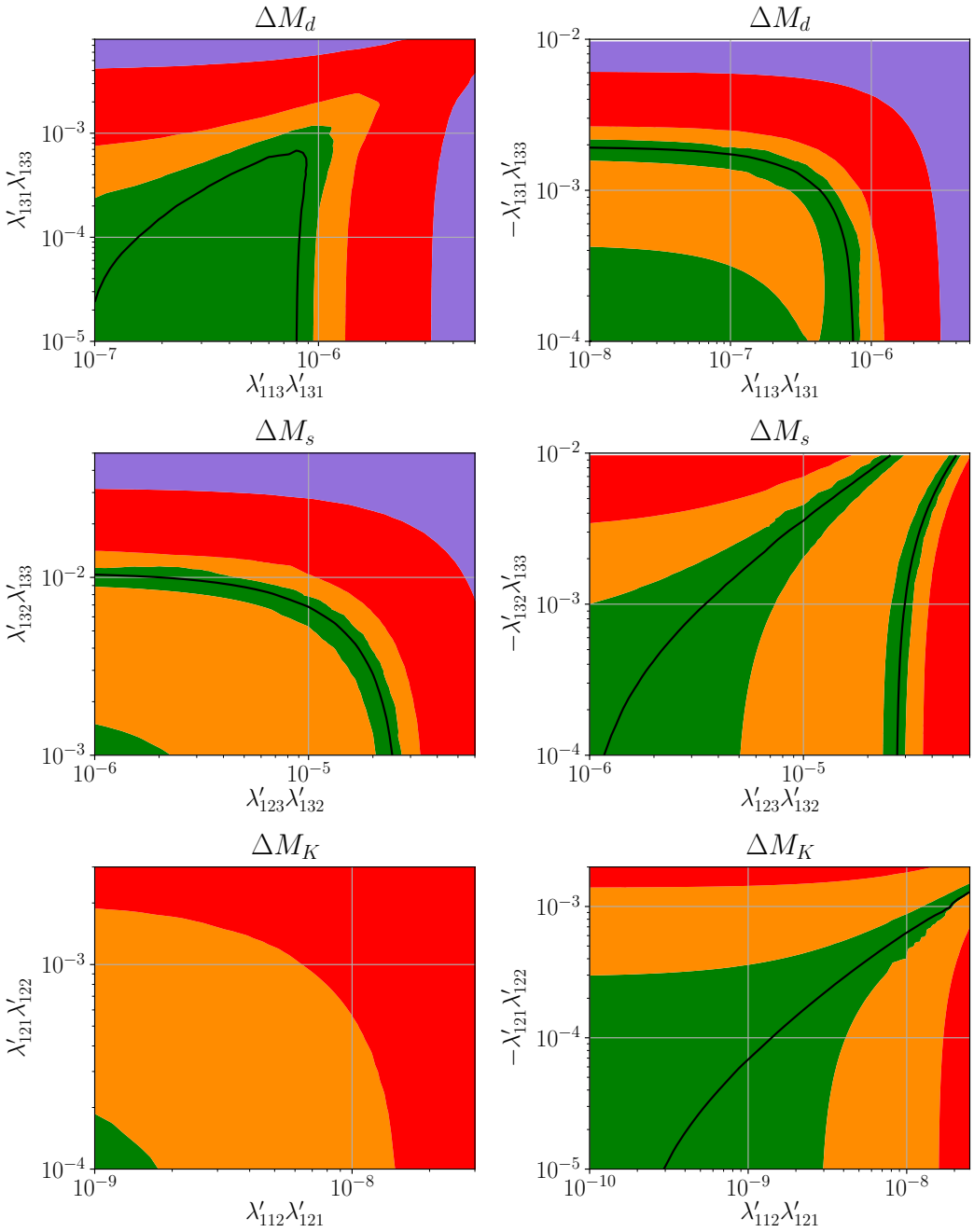

Figure 2.8: Limits from the meson-oscillation parameters on two RpV-directions of $LQ\bar{D}$-type. The parameters are set to the values in the third row of Table 2.1, with slepton/sneutrinos of 1 TeV. As in the previous plots, the color code reflects the level of tension between our predictions and the experimental measurements.

depends on the form of the amplitudes but also on the sign of the non-vanishing couplings. In Fig. 2.8, we complete the results from Figs. 2.3 and 2.5 by now allowing for three non-vanishing couplings. In practice, we set the slepton/sneutrino mass to 1 TeV and keep one $LQ\bar{D}$ coupling to a constant value: $\lambda'_{131} = 0.01$, $\lambda'_{132} = 0.1$, or $\lambda'_{121} = 0.1$. Then, we vary two independent λ', our choice depending again on the valence quarks of the considered ΔM. However, we stress that this procedure in fact opens three non-trivial $\lambda' \cdot \lambda'$ directions, so that the game is somewhat more complex than just playing one contribution versus the other.

As expected, in the plots of Fig. 2.8, the interplay of various RpV-contributions opens funnel-shaped allowed regions for comparatively large values of the $LQ\bar{D}$ couplings, highlighting the possibility of destructive interferences. We note that, considering that the tree-level and radiative contributions do not necessarily have the same scaling with respect to the slepton/sneutrino mass, the 'allowed angle' depends on the sfermion spectrum. Of course, the choice of parameters falling within the allowed funnels appears to be fine-tuned from the perspective of this work, but might be justified from a high-energy approach. On the other hand, constructive interferences lead to the 'rounded edges' observed in some of the plots.

As mentioned earlier, we will not consider the interplay of $LQ\bar{D}$- and $\bar{U}\bar{D}\bar{D}$-couplings, since such scenarios are of limited relevance without a quantitative analysis of the proton decay rate. On the other hand, our discussion in this subsection points to the relevance of considering a full evaluation of the ΔM's (and other observables), when considering RpV-scenarios beyond the simplistic one-coupling-dominance approach.

2.4.4 Competition between flavor violation in the R-parity conserving and R-parity violating sectors

RpV-couplings are not the only new sources of flavor violation in SUSY-inspired models. In fact, the large number of possible flavor-violating parameters of the R_p-conserving soft-SUSY-breaking Lagrangian is often perceived as a weakness for this class of model, known as the SUSY Flavor Problem. In particular, the soft quadratic mass-terms in the squark sector $m^2_{Q,\bar{U},\bar{D}}$ and the trilinear soft terms $A_{U,D}$ are matrices in flavor-space that are not necessarily aligned with the flavor-structure of the Yukawa/CKM matrices. In this case, flavor-violation is generated in $L-L$, $R-R$ (for $\tilde{m}^2$) or $L-R$ (for A) squark mixing. Correspondingly, flavor-changing-neutral gluinos or neutralinos, as well as new flavor-changing chargino couplings, could contribute to $\Delta M_{K,d,s}$ in *e.g.* diagrams of the form of Fig. 2.2, (b–d) — see *e.g.* Ref. [160]. Here, we wish to illustrate the potential interplay of R_p-conserving and RpV flavor violation. In particular, we note that the presence of flavor-violating effects in RpV-couplings would likely mediate flavor-violation in the squark sector via the RGE's [256].

We will focus on R_p-conserving flavor-violation in the quadratic squark mass parameters m^2_{ij}, where we assume the diagonal terms to be degenerate for squarks of left-handed and right-handed type (for simplicity): $m^2_{\bar{D}} = m^2_Q \equiv m^2$. Flavor-violation in the trilinear soft terms would lead to comparable effects at the level of the meson-oscillation parameters. However, large A-terms easily produce new (*e.g.* color- and charge-violating) minima in the scalar potential, that lead to instability of the usual vacuum, with possibly short-time tunnelling. In fact, we find that such stability considerations typically constrain the A-terms much more efficiently than the ΔM's.

In Fig. 2.9, we allow for non-vanishing m^2_{13}, m^2_{23} or m^2_{12}, simultaneously with non-zero $\lambda'_{113}\lambda'_{131}$, $\lambda'_{123}\lambda'_{132}$ and $\lambda'_{112}\lambda'_{121}$. The former induce contributions to ΔM_d, ΔM_s and ΔM_K through R_p-

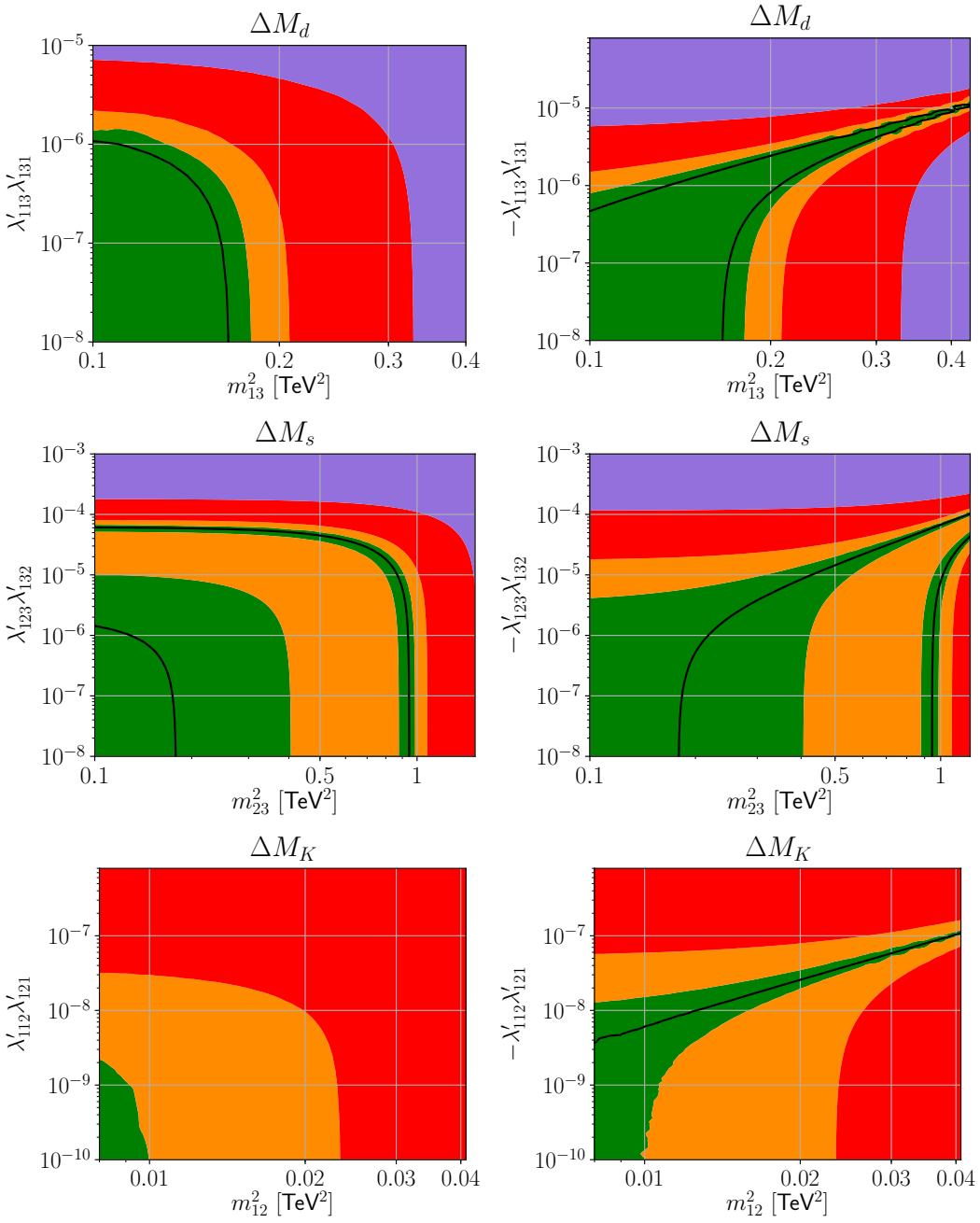

Figure 2.9: Constraints from the meson-oscillation parameters in the presence of both flavor-violating $LQ\bar{D}$-couplings and (R_p-conserving) flavor-violating mixing in the squark sector. The spectrum is set to the scenario SUSY-RpV(a) of Table 2.1, with the slepton/sneutrino mass at 1.5 TeV. The flavor-violating quadratic soft mass parameters in the squark sector, m^2_{ij}, are chosen to be degenerate for left-handed and right-handed squarks. The color code follows the same conventions as before.

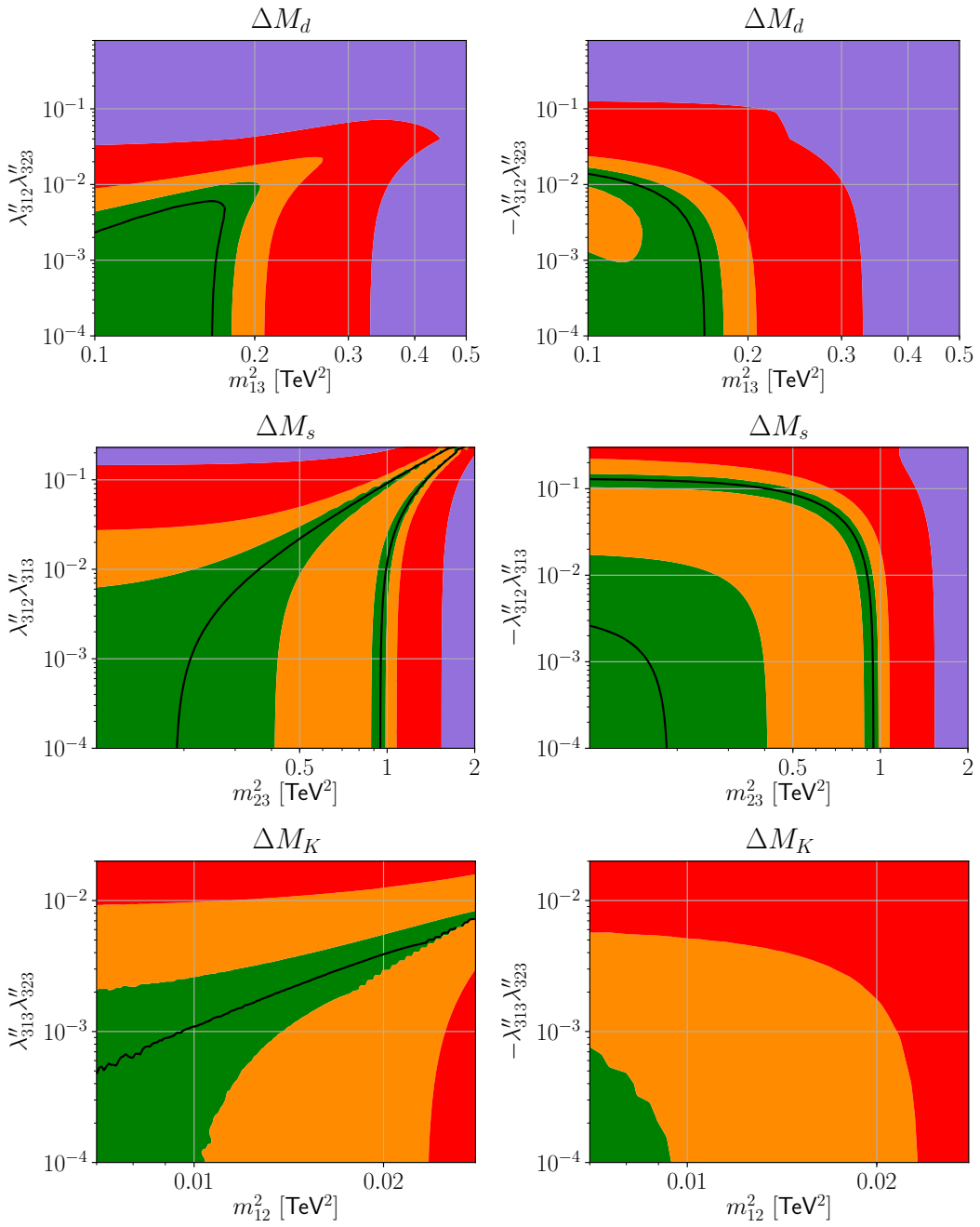

Figure 2.10: Constraints from the meson-oscillation parameters in the presence of both flavor-violating $\bar{U}\bar{D}\bar{D}$-couplings and flavor-violating squark mixing. The parameters are set to the scenario SUSY-RpV(a) from Table 2.1. The color code is unchanged compared to previous plots.

conserving squark mixing, while the latter provide RpV tree-level contributions to the same ΔM's. The parameters are set to the scenario SUSY-RpV(a) of Table 2.1, with the slepton/sneutrino mass at 1.5 TeV. In analogy with the results of section 2.4.3, we observe that R_p-conserving and RpV contributions may interfere destructively or constructively. Thus, allowed funnels with comparatively large values of the RpV-couplings open. In particular, we note that a tiny m_{12}^2 is sufficient for relaxing limits from ΔM_K, while the typical values of m_{13}^2 and m_{23}^2 affecting ΔM_d and ΔM_s are significantly larger.

A similar analysis can be performed with RpV of the $\bar{U}\bar{D}\bar{D}$-type. This is shown in Fig. 2.10.

In this subsection, we have stressed that the limits originating from meson-oscillation parameters are quite sensitive to the possible existence of flavor-violating sources beyond that of the RpV-couplings. A full analysis of these effects thus appears necessary when testing a complete model.

2.5 Conclusions

In this chapter, we have analyzed the meson-mixing parameters $\Delta M_{d,s}$ and ΔM_K at the full one-loop order in the RpV-MSSM. In particular, we have completed earlier calculations in the literature, in which only tree-level and box diagrams were usually considered. We also performed a numerical study based on our results and employing recent experimental and lattice data. The tighter limits that we derive — as compared to older works — illustrate the improvement of the precision in experimental measurements, but also the relevance of some of the new contributions that we consider. In particular, the interplay of SM-like and $LQ\bar{D}$-type flavor-violation modifies the scaling of the bounds with the sneutrino/slepton mass for a whole class of couplings. Finally, we have emphasized the possibility of interference effects amongst new sources of flavor violation, either exclusively in the RpV-sector or in association with R_p-conserving squark mixing. While the appearance of allowed directions with comparatively large couplings largely intervenes as a fine-tuned curiosity in the low-energy perspective of our work, it also stresses the relevance of a detailed analysis of the observables when considering a complete high-energy model, since accidental relations among parameters could affect the picture of low-energy limits.

CHAPTER 3

R-parity Violation & Displaced Vertex Signatures

There has recently been an increased interest in neutral long-lived particles (LLPs) which arise naturally in various models of dark matter or baryogenesis, for example[1]. In the past few years several experimental proposals with improved sensitivities to LLPs have been widely discussed. For instance, there are the planned fixed target experiment SHiP [258], the near detector of the future DUNE experiment [259], or also NA62 [260]. However, note that the primary goal of NA62 is to measure precisely $\mathrm{Br}(K^+ \to \pi^+ \nu\bar{\nu})$, while the main task of the near detector of DUNE is just monitoring the neutrino flux for the far detector [259]. Surprisingly, even though not designed for this purpose, the LHC detectors ATLAS and CMS, have a relevant sensitivity to LLPs [202, 261–263]. Nevertheless, there are significant gaps in sensitivity to these models at the LHC.

It is expected that the LHC will deliver up to $\mathcal{L} = 3000/\mathrm{fb}$ of luminosity over the next (15-20) years [264]. Perhaps unsurprisingly, a number of new proposals to search for LLPs have appeared, all based on the idea to exploit LHC's large luminosity: MATHUSLA [198], CODEX-b [199], FASER [200] and AL3X [201], which would be located at various positions with respect to the interaction points (IPs) of ATLAS, CMS, LHC-b or ALICE, using the LHC events. The physics potential of these experiments has so far not been fully discussed in the literature and it is the aim of the current chapter to estimate, and compare to each other and previous experiments, the sensitivity of these proposals for fermionic LLPs in the context of a class of BSM models. The discussion in this chapter collects the content of Refs. [203–205]

MATHUSLA [198] is a proposed very massive detector, possibly to be located above ground on top of the ATLAS/CMS experiment. The sizeable distance of MATHUSLA from the IP of the LHC beams implies that MATHUSLA is required to have a huge detection volume in order to possess a large coverage of polar angle. CODEX-b [199] is a proposal that takes advantage of a relatively large shielded empty space near the location of the LHCb experiment. Being closer to the IP, CODEX-b proposed size is much smaller than that of MATHUSLA. Since it is to be installed at LHCb instead of ATLAS or CMS, CODEX-b will have an expected luminosity of 300/fb, one order of magnitude smaller than the other two experiments, if LHCb runs until 2035 with upgrades to a Phases-II [265]. The authors of FASER [200] propose to construct a very modestly sized detector, situated in the very forward direction relative to either the ATLAS or the CMS IP. Recently a further experiment has been proposed, AL3X [201], which would be located at the ALICE site at the LHC. It differs from MATHUSLA, CODEX-b and FASER in that the center of the detector is located only 11.25 m from the ALICE IP, and furthermore the detector would have a

[1] For reviews and further models see Refs. [257, 258].

magnet. Due to the proximity to the IP the experiment would have a significantly higher geometric acceptance, even for a comparatively small detector, than the other three proposed new experiments. Such a small detector could be equipped with dense tracking instrumentation, which would be further improved by the magnetic field. We will summarize the experimental parameters of the different detectors in Sec. 3.1.

The CODEX-b physics proposal [199] examined two benchmark models, *i.e.* Higgs decay to dark photons, and B-meson decays via a Higgs mixing portal. Several FASER papers have respectively studied dark photons produced through light meson decays and photon bremsstrahlung [200], dark Higgs bosons produced through B- and K-mesons [266], heavy neutral leptons [267] and axion-like particles [268]. There are also studies investigating MATHUSLA with dark Higgs [269], exotic Higgs decays to LLPs [198, 270], and the Dynamical Dark Matter framework [271]. In a MATHUSLA white paper [272], the theory community presented detailed studies of MATHUSLA's potential of detecting LLPs in many different models. Ref. [273] investigated inelastic Dark Matter models at various existing and proposed LHC experiments including CODEX-b, FASER and MATHUSLA.

LLPs can be scalars, fermions or vectors. Neutral fermionic LLPs are also often called heavy neutral fermions (HNFs) in the literature. In this chapter we shall focus on two examples: (a) the lightest neutralino in SUSY, which can decay via RpV interactions. Somewhat surprisingly a light neutralino with a mass between 0.5 and 5 GeV, which we shall consider, is still consistent with all observations [274–277].[2] (b) heavy neutral leptons (HNLs). These are often also called sterile neutrinos in the literature. However we prefer the term HNL, because within the experimental neutrino oscillation community sterile neutrinos are usually identified with neutrinos with masses of order O(eV), whereas we shall focus on masses between 0.1 and 10 GeV. For the neutralinos we consider the single production from D- and B-mesons decays via a RpV coupling, and the direct pair production from Z-boson decays via the Higgsino component. For the HNLs we simulate the production from D-and B-mesons via the mixing of HNLs with $\nu_{e,\mu}$.

Before closing this introduction, we mention that there exist already many searches for HNLs (and other HNFs). For a review on constraints for sterile neutrino see, for example, Ref. [278]. Also the main LHC experiments, ATLAS and CMS, have searched for HNFs. ATLAS [279] published results of a search based on the final state $lljj$, giving only weak upper limits on the mixing of the HNLs $V^2_{\alpha N} \simeq (10^{-2} - 10^{-1})$ (with $\alpha = e, \mu$) for $m_N \sim (100 - 500)$ GeV. CMS searched for HNLs in trilepton final states and very recently published limits as low as $V^2_{\alpha N} \simeq 10^{-5}$ in the mass range $(10 - 100)$ GeV [280]. With these results [280], CMS now gives limits competitive with those derived by the DELPHI experiment at LEP [281].

Note that for small mixing angles $V^2_{\alpha N}$ below, say $V^2_{\alpha N} \sim 10^{-7}$, for $m_N \sim O(10)$ GeV, the decay lengths of HNLs become large enough to be detected experimentally and ATLAS/CMS could search for HNLs using the "displaced vertex" signal [282]. However, current displaced vertex search strategies, as used by CMS [283] for example, are not very well suited for light, say $m_N \lesssim 100$ GeV, HNLs [284].

We also mention in passing that our other HNF candidate, the neutralino, has been studied as an LLP candidate before. RpV-SUSY and neutralinos as LLPs are mentioned in the SHiP proposal [258] and the SHiP sensitivity for neutralinos has been studied in more details in [202, 285].

The outline of this chapter is as follows. In Sec. 3.1 we discuss the set-up of the proposed detectors and define the parameters for our analysis. We furthermore describe the details of our simulation of the long-lived HNFs. In Sec. 3.2 we present our results for the sensitivity of AL3X, CODEX-b, FASER

[2] In fact even a massless neutralino is consistent with all observations [277].

and MATHUSLA to long-lived light neutralinos. We consider separately the pair-production via Z^0 decays and the single production via rare heavy meson decays. In Sec. 3.3 we show our results for the sensitivity of the proposed detectors to long-lived HNLs. In Sec. 3.4 we summarize and reach our conclusions.

3.1 Simulation and Detectors

In this section we outline our simulation procedure and introduce the setup of the proposed detectors AL3X, CODEX-b, FASER, and MATHUSLA. Throughout this work we assume zero background events and 100% detector efficiency. See the relevant discussions about this matter in Refs. [198–201].

3.1.1 Simulation Procedure

In order to obtain the expected number of detectable decay events, we estimate the total number, N_M, of mother particles M produced at the LHC from existing experimental results. In our studies M can be a D- or a B-meson, or a Z-boson. We then calculate the branching ratio of the various Ms into the LLP(s), and compute the average decay probability of these LLPs inside the decay chamber of the detector. Since for $\mathrm{BR}(Z \to \tilde{\chi}_1^0 \tilde{\chi}_1^0)$ we have only an experimental upper limit, we will assume two different values of $\mathrm{BR}(Z \to \tilde{\chi}_1^0 \tilde{\chi}_1^0)$ in our numerical study for illustration.

Since the rare decays of charm and bottom mesons into HNLs lead to the strongest sensitivity reach in HNL mass m_N and mixing squared $|V_{\alpha N}|^2 (\alpha = e, \mu)$, defined in Sec. 3.3, we focus on these channels, discarding the complementary contributions from W-, Z- and Higgs bosons.[3] Similarly, in the case when an RpV $L \cdot Q\bar{D}$ coupling induces single production of a neutralino, we consider only rare decays of D- and B-mesons. From results published by the LHCb collaboration [286, 287], we estimate the number of produced mesons over a hemisphere for an integrated luminosity of $\mathcal{L} = 100/\mathrm{fb}$:

$$\begin{aligned} N_{D^\pm} &= 5.27 \times 10^{14},\ N_{D_s^\pm} = 1.70 \times 10^{14},\ N_{D_0} = 1.00 \times 10^{15}, \\ N_{B^\pm} &= 2.43 \times 10^{13},\ N_{B^0} = 2.43 \times 10^{13},\ N_{B_s^0} = 5.48 \times 10^{12}, \\ N_{B_c^\pm} &= 5.54 \times 10^{10}. \end{aligned} \tag{3.1}$$

Besides the LLPs produced from rare meson decays, we furthermore include the case of light neutralinos pair-produced from Z-boson decays. Experimentally viable light neutralinos must be dominantly bino-like [274, 275], with only a small higgsino component, which couples to the Z-boson. However, given the large cross section for Z-boson production at the LHC, we may still obtain good sensitivity reach in $L \cdot Q\bar{D}$ couplings up to a neutralino mass roughly half of the Z-boson mass. The ATLAS collaboration published the experimentally measured cross section of $Z \to \ell^+\ell^-$ ($\ell = e, \mu$) in pp collisions at $\sqrt{s} = 13$ TeV [288]. With the $\mathrm{BR}(Z \to \ell^+\ell^-)$ given by the PDG [289], we estimate the number of Z-bosons produced to be

$$N_Z = 2.94 \times 10^9, \tag{3.2}$$

over a hemisphere for $\mathcal{L} = 100/\mathrm{fb}$.

[3] The latter were, however, taken into account in Ref. [204].

We write the total number of LLPs produced, $N_{\text{LLP}}^{\text{prod}}$, as

$$N_{\text{LLP}}^{\text{prod}} = \sum_{M} N_M \cdot \text{BR}(M \to \text{LLP(s)} + X), \tag{3.3}$$

where M can be either a D-meson, a B-meson, or a Z-boson. To determine the average decay probability of the LLPs inside the "detectable region"("d.r."), $\langle P[\text{LLP in d.r.}]\rangle$, we perform a Monte Carlo (MC) simulation with `Pythia 8.205` [290, 291]. We implement the following formula:

$$\langle P[\text{LLP in d.r.}]\rangle = \frac{1}{N_{\text{LLP}}^{\text{MC}}} \sum_{i=1}^{N_{\text{LLP}}^{\text{MC}}} P[(\text{LLP})_i \text{ in d.r.}], \tag{3.4}$$

where $N_{\text{LLP}}^{\text{MC}}$ is the number of LLPs generated in the MC simulation sample. We generate the D- and B-mesons by making use of the matrix element calculators `HardQCD:hardccbar` and `HardQCD:hardbbbar`, respectively, of `Pythia`. Note that the differential cross section of producing heavy flavor mesons in the very forward direction, where `FASER` sits, is not validated in `Pythia`. In order to solve this problem, we reweigh the `Pythia` meson production cross section at different ranges of transverse momentum and pseudorapidity by the corresponding more reliable numbers calculated by using `FONLL` [292–295]. In order to extract the kinematics of pair-produced neutralinos from Z-boson decays, we resort to the "New-Gauge-Boson Processes" provided by `Pythia` to generate pure Z'-bosons with the same mass as the SM Z-boson and let it decay to a pair of new fermion particles. Finally, we calculate the number of observed decays of the LLPs in the detector,

$$N_{\text{LLP}}^{\text{obs}} = N_{\text{LLP}}^{\text{prod}} \cdot \langle P[\text{LLP in d.r.}]\rangle \cdot \text{BR}(\text{LLP} \to \text{visible only}), \tag{3.5}$$

where we also include BR(LLP $\to$ visible only), the branching ratio of the LLP into only visible states such that the event may be reconstructed by the detectors. In particular, for the `AL3X` detector, Ref. [201] points out that the LLP vertex is required, in order to point back to the IP, and thus be able to reduce the background.

With `Pythia` providing the kinematical information of each generated (LLP_i), we can easily derive its velocity β_i and Lorentz boost factor γ_i. We calculate the total decay width of the HNLs by using the formulas given in Ref. [278]. As for the decay width of the light neutralinos, we use the relevant expressions for neutralino two-body decays given in Ref. [202] for a neutralino mass below ~ 3.5 GeV, and take the three-body decay results given by `SPheno-4.0.3` [206, 207] for larger masses. Combining the total decay width $\Gamma_{\text{tot}}(\text{LLP})$ with the β_i and γ_i, we express the decay length, λ_i, of a given LLP, $(\text{LLP})_i$, in the laboratory frame:

$$\lambda_i = \beta_i \gamma_i / \Gamma_{\text{tot}}(\text{LLP}), \tag{3.6}$$

$$\lambda_i^z = \beta_i^z \gamma_i / \Gamma_{\text{tot}}(\text{LLP}), \tag{3.7}$$

where λ_i^z is the z-component of λ_i along the beam axis. The decay length is required in order to calculate the decay probability $P[(\text{LLP})_i \text{ in d.r.}]$.

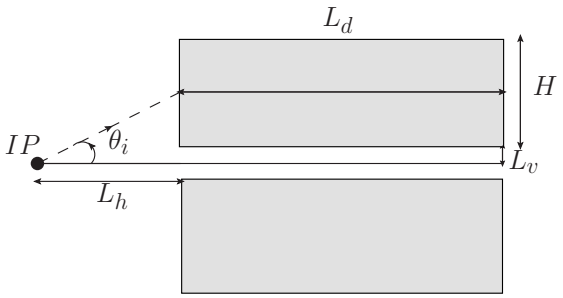

Figure 3.1: Side-view sketch of the AL3X detector with definition of distances and angles used in text. The detector is cylindrically symmetric around the beam axis. IP denotes the interaction point 2 at the LHC. The dashed line describes an example LLP track, with polar angle θ_i.

3.1.2 New Detectors

The AL3X Detector

AL3X ("A Laboratory for Long-Lived eXotics") [201] is proposed as an on-axis cylindrical detector situated several meters from IP2 in the ALICE/L3 cavern at the LHC. It has a length of $L_d = 12$ m and an inner/outer radius of 0.85/5 m. In virtue of its proximity to the IP, its pseudorapidity coverage of $\eta \in [0.9, 3.7]$ is large relative to other proposed future detectors such as MATHUSLA ($[0.9, 1.8]$) [272] and CODEX-b ($[0.2, 0.6]$) [199], and it has a full azimuthal coverage.[4] We calculate the probability of each individual LLP decaying inside the detector fiducial chamber $P[(\text{LLP})_i \text{ in d.r.}]$ as:

$$P[(\text{LLP})_i \text{ in d.r.}] = e^{-\frac{L_i}{\lambda_i^z}}\left(1 - e^{-\frac{L_i'}{\lambda_i^z}}\right), \tag{3.8}$$

$$L_i = \min\left(\max\left(L_h, \frac{L_v}{\tan\theta_i}\right), L_h + L_d\right), \tag{3.9}$$

$$L_i' = \min\left(\max\left(L_h, \frac{L_v + H}{\tan\theta_i}\right), L_h + L_d\right) - L_i\,, \tag{3.10}$$

where $L_h = 5.25$ m is the horizontal distance from the IP to the near end of the detector, $L_v = 0.85$ m and $H = 4.15$ m are respectively the inner radius and the transverse length of the detector, and θ_i is the polar angle of $(\text{LLP})_i$ with respect to the beam axis. In Ref. [201] the authors employed the benchmark integrated luminosities 100/fb and 250/fb, so that practical concerns such as moving the IP and beam quality, and constraints from backgrounds may be investigated. Here we follow their choice of luminosities. In Fig. 3.1 we show a profile sketch of AL3X.

The CODEX-b Detector

CODEX-b ("Compact detector for Exotics at LHCb") [199] was proposed as a cubic detector with dimension 10^3 m^3, sitting inside an underground cavity at a distance $L = 25$ m from the LHCb IP. The differential production distribution is flat in the azimuthal angle and the azimuthal coverage of the detector is about $0.4/2\pi \approx 6\%$. The polar angle range of the CODEX-b experiment at the

[4] FASER ($\eta \gtrsim 6.9$) covers a small angular region in the extreme forward direction.

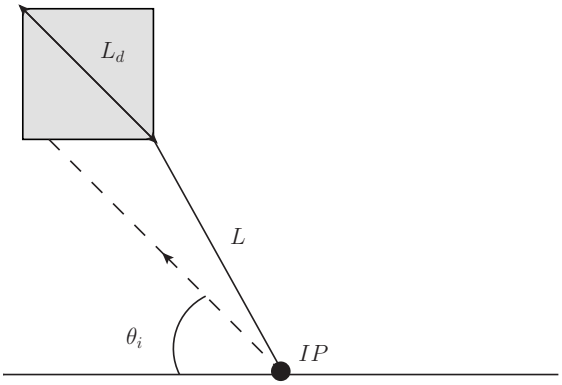

Figure 3.2: Side-view sketch of the CODEX-b detector with definition of distances and angles used in text. IP denotes the interaction point in LHCb. The dashed line describes an example LLP track.

appropriate azimuthal angle is between 11.4° and 32.5°. This corresponds to the pseudorapidity range $\eta \in [0.2, 0.6]$. For this narrow range, and at the precision of this analysis, we also treat the polar angle differential production distribution as flat. As we mentioned earlier, LHCb is expected to have a total integrated luminosity of 300/fb, smaller by one order of magnitude than ATLAS or CMS. We calculate $P[(\text{LLP})_i \text{ in d.r.}]$ with the following expression:

$$P[(\text{LLP})_i \text{ in d.r.}] = \begin{cases} \dfrac{0.4}{2\pi} \cdot e^{-\frac{L}{\lambda_i}}(1 - e^{-\frac{L_d}{\lambda_i}}), & \eta_i \in [0.2, 0.6], \\ 0, & \text{else}, \end{cases} \tag{3.11}$$

where we approximately treat the box detector as a spherical shell segment with the volume length $L_d = 10\text{m}$. η_i is the pseudorapidity of $(\text{LLP})_i$ and $\eta_i = -\ln[\tan\theta_i/2]$. A brief sketch of the setup of CODEX-b is shown in Fig. 3.2.

The FASER Detector

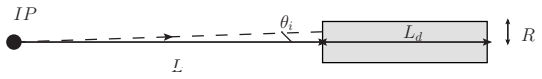

Figure 3.3: Side-view sketch of the FASER detector with definition of distances and angles used in text. The dashed line describes an example LLP track.

FASER ("ForwArd Search ExpeRiment") [200] proposes to build a small cylindrical detector placed a few hundred meters downstream of the ATLAS or CMS IP in the very forward region. In a series of papers [200, 266–268] several different variants of FASER have been proposed. In this chapter, we focus on a recent setup, which would sit at a particularly promising location in the side tunnel TI18 [268]. We denote the distance from the IP to the near end of the detector as $L = 470\text{m}$, the radius of FASER as $R = 1\text{m}$, and the detector length as $L_d = 10\text{m}$. Following is the expression for calculating

the probability for a given LLP_i to decay inside FASER:

$$P[(\text{LLP})_i \text{ in d.r.}] = e^{\frac{-L}{\lambda_i^z}}\left(1 - e^{-\frac{L_i}{\lambda_i^z}}\right), \tag{3.12}$$

$$L_i = \begin{cases} 0\,, & \tan\theta_i > \dfrac{R}{L}\,, \\ L_d\,, & \tan\theta_i < \dfrac{R}{L + L_d}\,, \\ \dfrac{R}{\tan\theta_i} - L\,, & \text{else}\,. \end{cases} \tag{3.13}$$

There is no azimuthal angle suppression because the FASER detector is cylindrical. Here the three cases correspond respectively to 1) the extended potential LLP trajectory misses the decay chamber, 2) the extended potential LLP trajectory passes through the entire length of the detector, and 3) the extended LLP trajectory exits through the side of the detector. In practice, we treat the third case as negligible. It corresponds to the very narrow angular range $\theta_i \in [0.1194^\circ, 0.1219^\circ]$. And furthermore the decay products of the LLPs may exit through the side and may thus miss the detector. These LLPs hence would not be detected. A sketch of the geometric configuration of FASER is shown in Fig. 3.3.

The MATHUSLA Detector

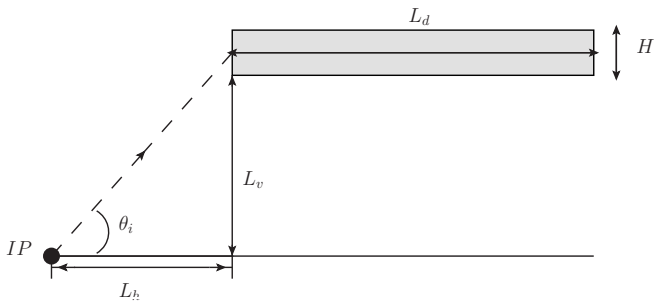

Figure 3.4: Side-view sketch of the MATHUSLA detector with definition of distances and angles used in text. The dashed line describes an example LLP track.

In Ref. [198] it has been proposed to construct a surface detector 100 m above the ATLAS/CMS IP called MATHUSLA ("MAssive Timing Hodoscope for Ultra Stable neutraL pArticles"). The detector should be horizontally offset by 100 m from the IP and with a massive dimension of 200m×200m×20m, MATHUSLA is expected to have excellent sensitivity for detecting LLPs. Below we show the formulæ

for calculating $P[(\text{LLP})_i \text{ in d.r.}]$ in MATHUSLA:

$$P[(\text{LLP})_i \text{ in d.r.}] = \frac{1}{4} \cdot e^{\frac{-L_i}{\lambda_i''}} \left(1 - e^{-\frac{L_i'}{\lambda_i''}}\right), \tag{3.14}$$

$$L_i = \min\left(\max\left(L_h, \frac{L_v}{\tan\theta_i}\right), L_h + L_d\right), \tag{3.15}$$

$$L_i' = \min\left(\max\left(L_h, \frac{L_v + H}{\tan\theta_i}\right), L_h + L_d\right) - L_i\,. \tag{3.16}$$

Here, L_h and L_v are the horizontal and vertical distance from the IP to the near end of MATHUSLA, and they both equal 100m. $L_d = 200$m is the horizontal length of MATHUSLA and $H = 20$m is its height. The factor $1/4$ comes from the azimuthal angle coverage. Both MATHUSLA and FASER expect to have 3/ab luminosity of data by ~ 2035. We show the schematic plot of MATHUSLA in Fig. 3.4.

3.2 Light Neutralinos Decaying via R-parity Violation

With R_p violated, the LSP is no longer stable and therefore there are no constraints on its nature from cosmology. Thus, even charged or coloured SUSY particles could be the LSP. Here, we are exclusively interested in the case where the lightest neutralino is the LSP.

In the so-called CMSSM the gaugino mass terms M_1 and M_2 follow the approximate relation $M_1 \simeq (1/2)M_2$. This leads to a lower limit on $m_{\chi_1^0}$ of roughly $m_{\chi_1^0} \gtrsim 46$ GeV [296]. However, in more general SUSY models, M_1 and M_2 are just free parameters and it is easy to show that for [277]

$$M_1 = \frac{M_2 M_Z^2 \sin(2\beta)\sin^2\theta_W}{\mu M_2 - M_Z^2 \sin(2\beta)\cos^2\theta_W}, \tag{3.17}$$

the lightest neutralino is massless at tree-level. In our numerical studies we will simply take the mass of the lightest neutralino, $m_{\chi_1^0}$ as a free parameter, without resorting to any underlying SUSY breaking model. Note, however, that this lightest neutralino necessarily has to be mostly bino, due to the lower mass limits on charginos that can be derived from LEP data [296].

In the RpV-MSSM superpotential (Eq. 1.7), the presence of the dimensionful parameters μ_i, and/or the Yukawa couplings λ_{ijk} and/or λ'_{ijk} leads to lepton-number violation, whilst a non-vanishing λ''_{ijk} violates baryon-number. In this subsection we only discuss the phenomenology of non-vanishing λ'. This choice conserves baryon number and hence does not lead to unobserved decays of the proton. See also Refs. [104, 118, 297–300] on the motivation for this choice of couplings and on the changes in phenomenology due to RpV. The $L \cdot Q\bar{D}$ operators predict, among others, the following effective operators between the neutralino, and the SM fermions u, d, ℓ and ν:

$$\begin{aligned}\mathcal{L} \supset\ & G^{S,\nu}_{iab}(\overline{\tilde{\chi}^0} P_L \nu_i)(\overline{d_b} P_L d_a) \\ & + G^{S,\ell}_{iab}(\overline{\tilde{\chi}^0} P_L \ell_i)(\overline{d_b} P_L u_a) + \text{h.c.}\,.\end{aligned} \tag{3.18}$$

The effective couplings G depend on several masses of the scalar supersymmetric partners $\tilde{f}$ of the SM fermions, the mixing within the neutralino sector and are linear in λ'. Formulæ for the partial widths of neutralino decays via $L \cdot Q\bar{D}$ couplings can be found in Refs. [202, 274, 277, 301]. If all $\tilde{f}$

are mass degenerate, G can be written as $O(1) \times \lambda'_{iab}/m^2_{\tilde{f}}$. Bounds on various combinations of λ'_{iab} and $m_{\tilde{f}}$ can be set from searches for exotic decays in the meson sector, see *e.g.* Ref. [165, 190, 193, 302]. In the special case of mass degenerate $\tilde{f}$ they can be compared to our sensitivity curves as we show below.

The absence of any R-parity violating terms predicts a stable $\tilde{\chi}_0$. In contrast, the terms in Eq. (3.18) directly imply a long-lived particle, which eventually decays into SM fermions.

3.2.1 Pair Production of $\tilde{\chi}^0_1$ from Z-Boson Decays

There are various possibilities to produce neutralinos at the LHC. One of them is the decay of on-shell Z-bosons into pairs of neutralinos if $m_{\tilde{\chi}^0_1} \lesssim m_Z/2$. The corresponding partial decay width $\Gamma(Z \to \tilde{\chi}^0_1 \tilde{\chi}^0_1)$ has been calculated in Ref. [303]. Important for us is the coupling between a Z-boson and two neutralinos:

$$g_{Z\chi^0_i\chi^0_j} = (N_{i3}N_{j3} - N_{i4}N_{j4})c_{2\beta} + (N_{i3}N_{j4} + N_{i4}N_{j3})s_{2\beta}. \tag{3.19}$$

Here, N_{ij} is the matrix that diagonalizes the neutralino mass matrix and $c_{2\beta}/s_{2\beta}$ are cosine and sine of β, with $\tan\beta$ being the usual ratio of the vacuum expectation values of the two Higgs doublets. Thus, the relevant coupling for the decay to neutralinos is proportional to the Higgsino content in χ^0_1 and is *not suppressed by small RpV parameters*. Different from the case of the single production of $\tilde{\chi}^0_1$ and HNLs, therefore for neutralinos production cross section and decay length *are not related*.

Importantly, there is an upper bound on $\Gamma(Z \to \chi^0_1 \chi^0_1)$ from the LEP measurement of the invisible width of the Z-boson. The PDG [296] gives for $\Gamma(Z \to \text{inv})$ a value in agreement with the standard model calculation with three generations of light neutrinos and the error bar on the measurement corresponds to an upper limit on the branching ratio into additional invisibly final states of roughly $\text{BR}(Z \to \tilde{\chi}^0_1 \tilde{\chi}^0_1) \lesssim 0.1$ % at 90 % c.l.

The Higgsino content in the lightest neutralino depends mostly on the parameter combination M_1/μ. LEP gives a lower limit of roughly $\mu \gtrsim 100$ GeV [296]. The limits from a ATLAS search [83] imply that μ should be larger than 130 GeV. For a cross check, we used the model *MSSMTriRpV* from the repository of SARAH-4.12.2 [209–214]. We perform numerical calculations with SPheno-4.0.3 [206–208]. For the choice

$$M_2 = 500 \text{ GeV}, \mu = 130 \text{ GeV}, \tan\beta = 10, \tag{3.20}$$

and a lightest neutralino mass $m_{\chi^0_1} \ll m_Z/2$, we find $\text{BR}(Z \to \tilde{\chi}^0_1 \tilde{\chi}^0_1) \simeq 0.06$ %. Thus, given current constraints on SUSY parameters, the Higgsino content in the lightest neutralino can still be large enough to (nearly) saturate the experimental bound on $\text{BR}(Z \to \tilde{\chi}^0_1 \tilde{\chi}^0_1)$. [5]

In our numerical calculations, we will not do a scan over the soft SUSY breaking parameters. Instead we will treat both, the mass of the lightest neutralino and $\text{BR}(Z \to \tilde{\chi}^0_1 \tilde{\chi}^0_1)$ as a free parameter in our numerical study. Note, however, that a future lower limit on μ larger than the numbers quoted above will consequently result in smaller values for the maximally achievable $\text{BR}(Z \to \tilde{\chi}^0_1 \tilde{\chi}^0_1)$. For our analysis we therefore choose $\text{BR}(Z \to 2\tilde{\chi}^0_1) = 10^{-3}$ and 10^{-5}, [6] as two representative and

[5] We have also checked that such a "largish" Higgsino content is not in disagreement with the experimental upper bound on the Higgs invisible width [304, 305].

[6] Here and elsewhere the values chosen for $\text{BR}(Z \to \tilde{\chi}^0_1 \tilde{\chi}^0_1)$ should be understood as the branching ratio of Z boson to a

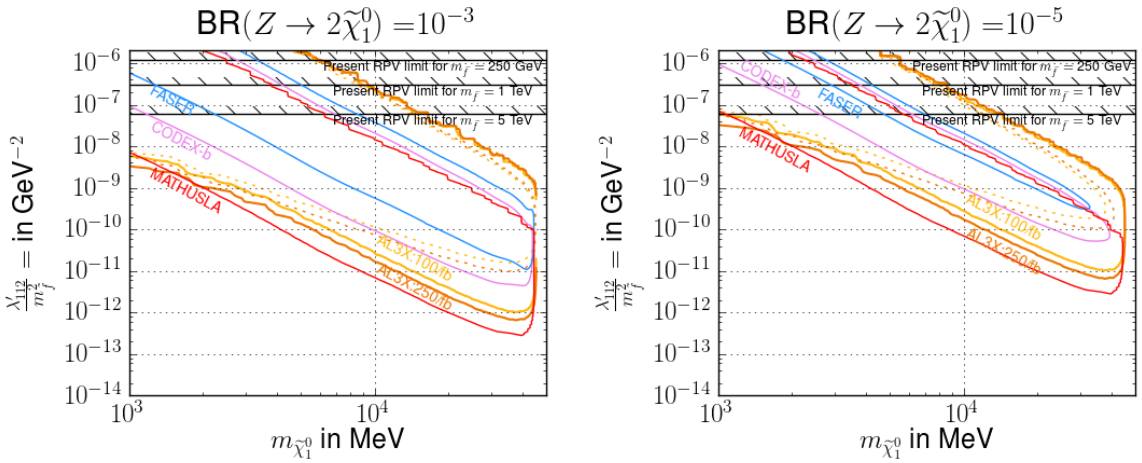

Figure 3.5: Sensitivity estimates shown in the plane spanned by the neutralino mass and the effective RpV coupling $\lambda'_{112}/m^2_{\tilde{f}}$ for two different assumptions of the Z branching ratio to neutralinos. Sensitivity curves denote the expected measurement of 3 visible events. Here we perform Monte-Carlo simulation for `AL3X` only; we extract the corresponding results for `CODEX-b`, `FASER` and `MATHUSLA` from Ref. [204] (where the hadronic corrections on the decay width of the neutralinos of mass O(GeV) were not included). Solid lines consider all hadronic final states while dashed lines — only evaluated for `AL3X` in this work — only consider the branching ratio into the charged $K^{\pm}e^{\mp}$ final state for observable neutralino decays. Overlaid current RpV limits on λ'_{112} are shown for comparison, using different assumptions on the degenerate sfermion mass $m_{\tilde{f}}$. The references are given in the text.

experimentally viable values for this invisible branching ratio. We would also like to mention that the lower limits on charged SUSY particles require that the lightest neutralino must be mostly bino, for the low mass we consider in Sec. 3.2.

For this benchmark analysis, we choose λ'_{112} to be the only non-vanishing RpV operator. In that case, the neutralino can decay into $u + \bar{s} + e^-$ and $d + \bar{s} + \nu_e$ final states, as well as their respective charge conjugates. We use these inclusive final states to calculate the total lifetime of the neutralino, see Ref. [204]. However, in practice it may only be feasible to detect charged final states with light mesons, $\tilde{\chi}_1^0 \to K^{\pm}e^{\mp}$. We also calculate the partial decay width into this particular final state according to Ref. [202] and multiply with the corresponding branching ratio. We determine results for both cases, *i.e.* if only the charged meson final state or if all hadronic final states can be observed. For simplicity, in the results for this scenario, shown in Fig. 3.5, we show both cases only for the `AL3X` detector, while for the other detectors we show only the case where all hadronic final stats can be observed.

Fig. 3.5 shows the results for both benchmark values of BR($Z \to \tilde{\chi}_1^0 \tilde{\chi}_1^0$). We choose the mass of the neutralino as one free parameter, which for kinematic reasons must be smaller than $m_Z/2$. As explained above, RpV-induced decays of the neutralino depend on the effective coupling $\lambda'/m^2_{\tilde{f}}$, which is why we choose this as our second free parameter. Current limits on the RpV operators $L_1 Q_1 \bar{D}_2$ are taken from Ref. [193] and compared to our results. Note, however, that such a comparison is only valid if all sfermions are mass degenerate. See the discussion in Ref. [202]. Here we perform MC simulation for `AL3X` only and overlap the results with those for `CODEX-b`, `FASER` and `MATHUSLA` from

pair of $\tilde{\chi}_1^0$'s for $m_{\tilde{\chi}_1^0} \ll m_Z$. With $m_{\tilde{\chi}_1^0}$ increased up to the threshold $m_Z/2$, phase space suppression effect becomes important and is correctly taken into account in our study.

Ref. [204]. In the latter, the hadronic corrections on the neutralinos decay width were not included for neutralino mass below ~ 4 GeV. If these effects were included, the reach of the corresponding detectors in $\lambda'_{112}/m^2_{\tilde{f}}$ would be extended by approximately one order of magnitude in the low mass regime.

Since the smallness of λ'_{112} controls only the decay length, but not the production cross section, in principle very small values of λ'_{112} are accessible in these searches. Note that the values of λ'_{112} shown can reach values several order of magnitudes smaller than the current upper limit on λ'_{112} [193].

We observe that for invisible branching ratios close to the current PDG limit, AL3X is sensitive to values of $\lambda'_{112}/m^2_{\tilde{f}}$ down to 10^{-12} GeV^{-2}, if all hadronic final states can be observed, while MATHUSLA may reach even the smallest values of $\lambda'_{112}/m^2_{\tilde{f}}$. This strongest sensitivity is reached for neutralino masses near the kinematic threshold, at $m_{\tilde{\chi}^0_1} \approx 40$ GeV. FASER is expected to be less sensitive than CODEX-b, while AL3X outperforms FASER and CODEX-b over the entire parameter range. From the AL3X isocurves, one observes that the sensitivity drops by nearly one order of magnitude, if only the charged final state $K^{\pm}e^{\mp}$ is taken into account. Note that all the experiments could reach $\lambda'_{112}/m^2_{\tilde{f}}$ several orders of magnitude smaller than the current limits on the λ'_{112} coupling. The lighter the neutralino, the lower the sensitivity on $\lambda'_{112}/m^2_{\tilde{f}}$. But even for O(GeV) masses AL3X and MATHUSLA may be expected to significantly improve on current limits. Note that smaller neutralino masses have a reduced accessible final state phase space and hence a reduced difference in sensitivity between the conservative "$K^{\pm}e^{\mp}$" and the optimistic "all hadronic final states".

As for BR$(Z \to \tilde{\chi}^0_1\tilde{\chi}^0_1) = 10^{-5}$, it is apparent to observe from the plot on the right of Fig. 3.5 that the overall sensitive regions in the parameter space shrinks dramatically, as a result of the reduced number of produced neutralinos. FASER now has its sensitive coverage of a very small size, while AL3X and MATHUSLA may still reach values of $\lambda'_{112}/m^2_{\tilde{f}}$ several orders of magnitude smaller than the current limits.

Note that too large values of λ' render the neutralino too short-lived to reach the detector which leads to upper bounds on the sensitivity to λ' for all LLP experiments. In comparison to FASER, MATHUSLA and CODEX-b, AL3X covers the largest region of parameter space here, due to its proximity to IP2. However, for masses above 10 GeV, sizable RpV couplings may still evade both current detection limits and even the limits from AL3X@250/fb.

In summary, if the lightest neutralino has a mass in the range (few) GeV to $m_Z/2$, LLP searches at AL3X, FASER, CODEX-b and MATHUSLA can probe part of RpV-SUSY parameter space not accesible in any other experiment.

3.2.2 Single Production of $\tilde{\chi}^0_1$ from Rare D and B-Meson Decays

In this subsection, we estimate the sensitivity reach of the proposed detectors for discovering singly produced light neutralinos from D- and B-mesons via RpV $L \cdot Q\bar{D}$ operators, and compare them with each other. We also interpret our studies in a model independent way, independently of the RpV couplings. Instead we set bounds on the product of the branching ratios of the production of an LLP from a meson decay and the decay of the LLP to a meson and charged lepton in terms of the neutralino decay length $c\tau$. This can be applied to any potential LLP. As mentioned above, neutralinos that are produced from charm and bottom meson decays are necessarily lighter than 10 GeV and are dominantly bino-like to avoid existing bounds, see Ref. [277]. Formulæ for the partial widths of heavy meson decays and for the partial widths of neutralino decays via $L \cdot Q\bar{D}$ couplings can be found in

Refs. [202, 274, 277, 301].

In principle, one single $L \cdot Q\bar{D}$ coupling introduces several effective SM operators and hence may simultaneously induce both meson decays to neutralinos and neutralino decays to lighter mesons. However, as Ref. [202] points out, due to kinematic constraints only the coupling λ'_{112} may lead to such a complete decay chain:

$$K^0_{L/S} \to \tilde{\chi}^0_1 \nu, \; \tilde{\chi}^0_1 \to K^{\pm} l^{\mp}. \tag{3.21}$$

Moreover, since the mass difference between $K^0_{L/S}$ and $K^{\pm}$ is only 4 MeV, the kinematically allowed neutralino mass range is very small and this case is not worth studying. Therefore, we only consider scenarios with two distinct non-vanishing RpV operators, one for the production of the neutralinos and the other for the decay.

In Sec. 1 we have shown upper limits on the couplings λ'_{ijk} for the operator $L_i Q_j \bar{D}_k$ and their products that are relevant to our studies. Therefore, here we refrain from repeating them.

Throughout this subsection, we assume that all sfermions have degenerate masses $m_{\tilde{f}}$. This allows us to directly compare the λ'_{ijk} bounds to our results even though the respectively relevant operators depend on the masses of possibly different SUSY particles. Note that results for significantly non-degenerate SUSY spectra may therefore differ significantly and can change the relative importance of bounds from different sources.

We calculate the relativistic kinematical variables β_i and γ_i of a neutralino $\tilde{\chi}^0_1$ by the following formulas:

$$\gamma_i = E_i / m_{\tilde{\chi}^0_1}, \tag{3.22}$$

$$\beta_i = \sqrt{1 - \gamma_i^{-2}}. \tag{3.23}$$

The z-component of β_i is obtained as:

$$\beta_i^z = p_i^z / E_i. \tag{3.24}$$

Results

In Ref. [202] a series of benchmark scenarios representative of $L \cdot Q\bar{D}$ couplings were investigated. In these scenarios, both the light lepton flavor (electron/muon) and the heavy tau flavor are considered, as the τ lepton leads to large phase space suppression effects. Also, different neutral or charged D- and B-mesons which would decay to the neutralino are considered; this is important because the cross sections of producing these mesons substantially differ, *cf.* Eq. (3.1). In this subsection, we exemplarily choose two benchmark scenarios with different choices for the non-vanishing λ', summarized in Table 3.1. We choose these two scenarios because they are representative for a class of $L \cdot Q\bar{D}$ couplings combinations. For more details, see the discussion below. For each scenario we have a different initial meson flavor, which produces the neutralinos via decays. This is important as these differ in their LHC production yields, see Eq. (3.1), as well as the different final states the neutralinos decay into. Due to the simultaneous presence of several operators from one λ' coupling, see Eq. (3.18), we often expect both charged and neutral final states. We call the former "visible", as only those can be experimentally measured by an LLP experiment. We need to consider all possible final states for the total lifetime of the lightest neutralino, $\tau_{\tilde{\chi}^0_1}$, but multiply the final number with the

	Scenario 1	Scenario 2
λ'_{prod} for production	λ'_{122}	λ'_{131}
λ'_{dec} for decay	λ'_{112}	λ'_{112}
produced meson(s)	D_s	$B^0, \bar{B}^0$
visible final state(s)	$K^{\pm}e^{\mp}, K^{*\pm}e^{\mp}$	$K^{\pm}e^{\mp}, K^{*\pm}e^{\mp}$
invisible final state(s) via λ'_{prod}	$(\eta, \eta', \phi) + (\nu_e, \bar{\nu}_e)$	none
invisible final state(s) via λ'_{dec}	$(K_L^0, K_S^0, K^*) + (\nu_e, \bar{\nu}_e)$	$(K_L^0, K_S^0, K^*) + (\nu, \bar{\nu})$

Table 3.1: Features of the R-parity violating benchmark scenarios studied in this section.

"visible branching ratio", *i.e.* the fraction of decays into a charged final state. More details on these benchmarks, including formulae for the respective decay widths and branching ratios can be found in Ref. [202].

Since the operators for production and decay scale with $\lambda'/m_{\tilde{f}}^2$, we have three free parameters in the theory, after assuming that all SUSY fermions $\tilde{f}$ have degenerate masses, namely: $\lambda'_P/m_{\tilde{f}}^2$, $\lambda'_D/m_{\tilde{f}}^2$, and $m_{\tilde{\chi}_1^0}$. Here $\lambda'_{P/D}$ is the $LQ\bar{D}$ coupling giving rise to the production/decay of the $\tilde{\chi}_1^0$, and $m_{\tilde{f}}^2$ is the sfermion mass relevant for the production/decay process, respectively.[7] We therefore show model-dependent plots in two separate planes for the aforementioned benchmark scenarios: $m_{\tilde{\chi}_1^0}$ vs. $(\lambda'_P/m_{\tilde{f}}^2 = \lambda'_D/m_{\tilde{f}}^2)$ and $\lambda'_P/m_{\tilde{f}}^2$ vs. $\lambda'_D/m_{\tilde{f}}^2$. For the latter plane, we present results for three different values of $m_{\tilde{\chi}_1^0}$.

In addition, we present model-independent results in the plane BR vs. $c\tau$ for a generic LLP. Here $c\tau$ is the decay length of the LLP, and BR is the product of the branching ratios of the respective meson decaying to the LLP and of the LLP decaying to a charged meson and a charged lepton. These results can be interpreted in terms of any LLP which has the same or similar reaction chain.

For the two benchmark scenarios, we choose to show all three types of plots. Depending on the exact construction of the detectors, they can possibly also track neutral mesons. We thus show sensitivity estimates for two cases: 1) only charged final states can be tracked, and 2) both neutral and charged ones.

Benchmark Scenario 1

We begin with the RpV scenario with D_s-mesons produced at the LHC, which decay to a neutralino, which in turn travels for a macroscopic distance before decaying to a kaon and a lepton. In this scenario we assume λ'_{122} and λ'_{112} are the only non-vanishing $L \cdot Q\bar{D}$ couplings. λ'_{122} gives rise to the production of $\tilde{\chi}_1^0$ via

$$D_s \to \tilde{\chi}_1^0 + e^{\pm}\,, \qquad \text{(production)} \tag{3.25}$$

and to the invisible neutralino decay

$$\tilde{\chi}_1^0 \to (\eta/\eta'/\phi) + \nu_e\,, \qquad \text{(decay via } \lambda'_{122}) \tag{3.26}$$

[7] The explicit formulae including the dependence on the relevant sfermion masses are given in Ref. [202].

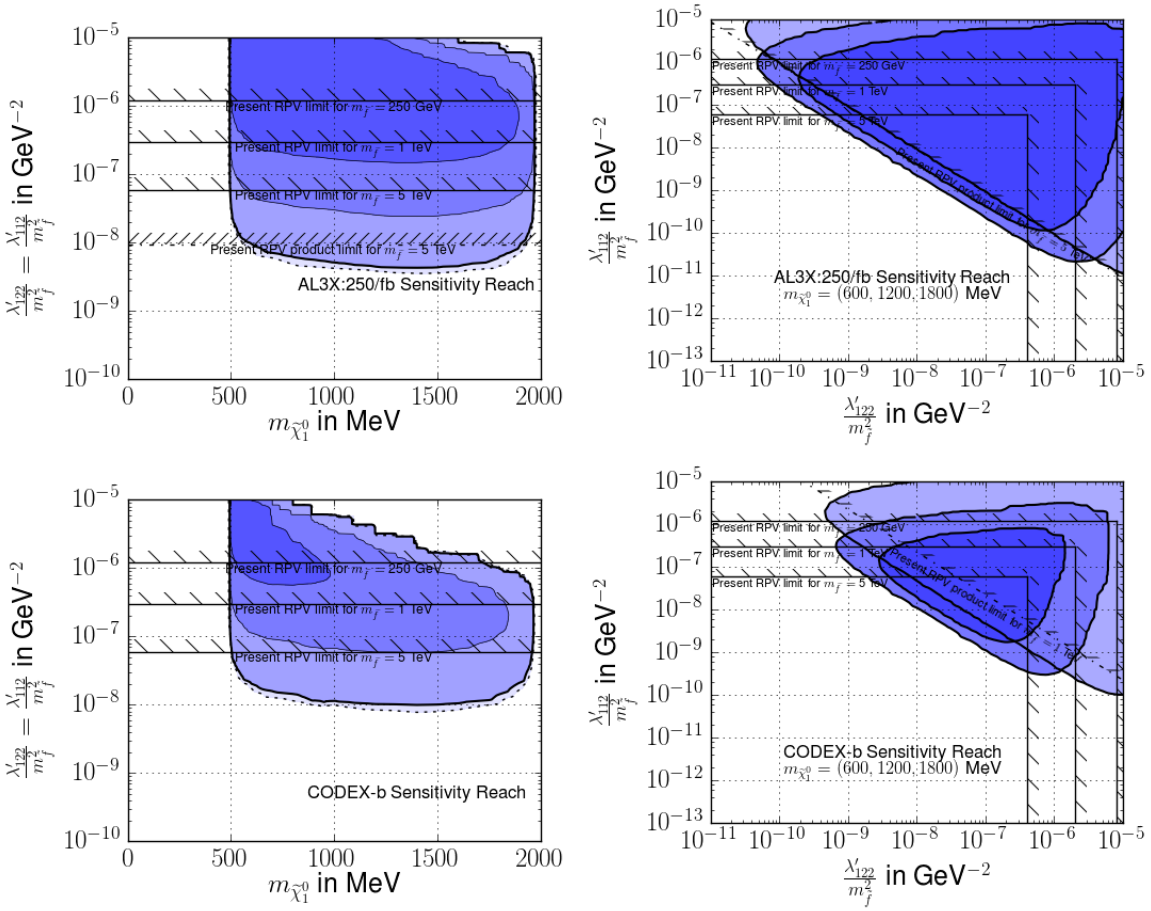

Figure 3.6: Sensitivity estimate of `AL3X:250/fb` and `CODEX-b` for Benchmark Scenario 1. On the left, we show the reach in terms of $m_{\tilde{\chi}_1^0}$ and $\lambda'_P/m^2_{\tilde{f}} = \lambda'_D/m^2_{\tilde{f}}$. The light blue/blue/dark blue regions enclosed by the solid black lines correspond to $\geq 3/3 \times 10^3/3 \times 10^6$ events. The light blue region is extended only slightly below by a dashed curve, representing the extended sensitivity reach if we assume our detectors can also detect neutral decays of the neutralino. The hashed solid lines correspond to the single RpV couplings' limit for different sfermion masses. On the right, the two couplings are not required to be identical and plots in the plane $\lambda'_P/m^2_{\tilde{f}}$ vs. $\lambda'_D/m^2_{\tilde{f}}$ are shown for the detectors. We consider three choices of $m_{\tilde{\chi}_1^0}$: 600 MeV (light blue), 1200 MeV (blue), 1800 MeV (dark blue). The solid hashed lines again represent the individual coupling bounds and the hashed dot-dashed line is the upper bound derived from the limit on the product of the two $LQ\bar{D}$ couplings for $m_{\tilde{f}} = 1$ TeV.

On the other hand, λ'_{112} leads to both visible and invisible decays

$$\tilde{\chi}_1^0 \to \begin{cases} K^{(*)\pm} + e^{\mp}, \\ K^0_{S,L} + \nu_e \,. \end{cases} \qquad \text{(decay via } \lambda'_{112}) \tag{3.27}$$

The invisible decays are important to take into account in the evaluation because they affect the total width of $\tilde{\chi}_1^0$. We summarize this scenario in Table 3.1.

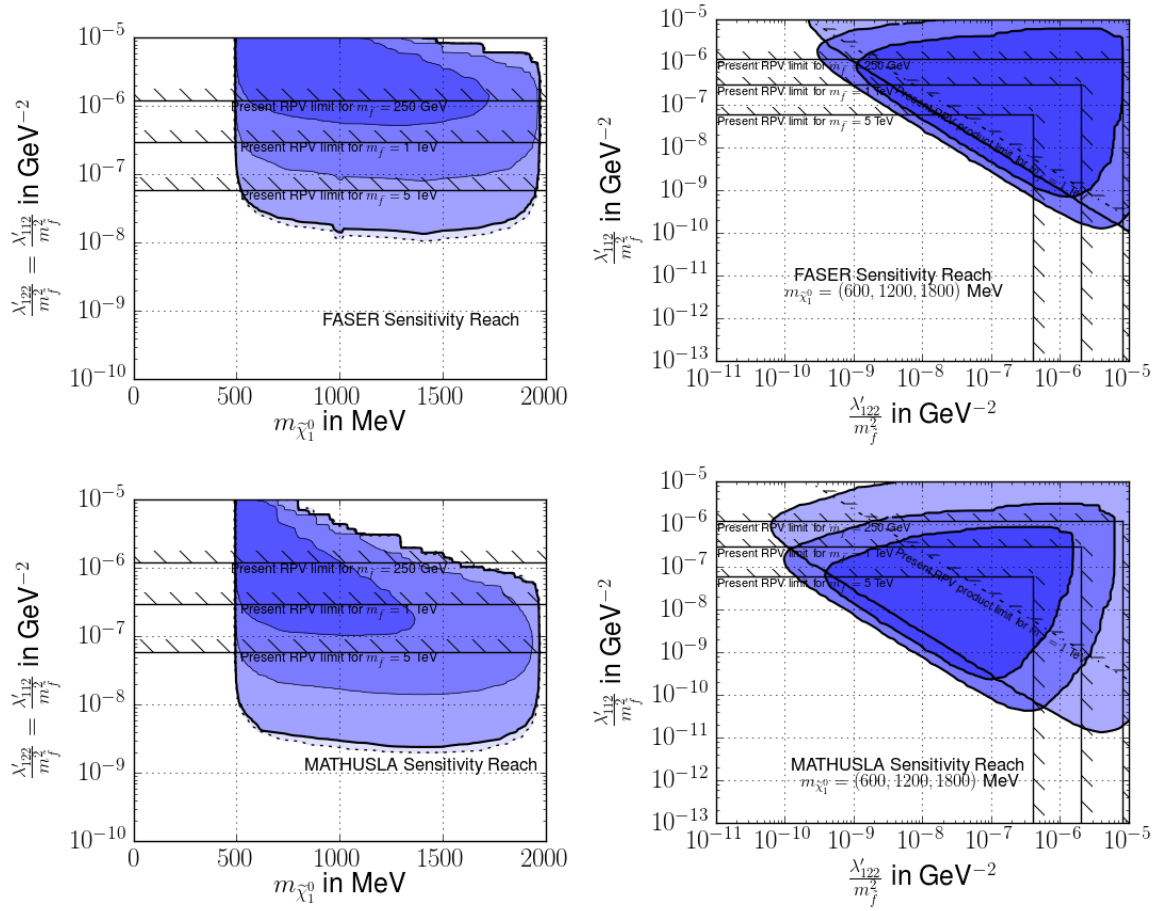

Figure 3.7: Sensitivity estimate of FASER and MATHUSLA for Benchmark Scenario 1. The format is the same as in Fig. 3.6

We now present our results. In Figs. 3.6 and 3.7 we show model-dependent sensitivity estimates for the four detectors: AL3X, CODEX-b, FASER and MATHUSLA. In the left column, plots are presented in the plane $m_{\tilde{\chi}_1^0}$ vs. $(\lambda'_P/m^2_{\tilde{f}} = \lambda'_D/m^2_{\tilde{f}})$. We have set $\lambda'_D = \lambda'_P$, and vary their values and the mass of $\tilde{\chi}_1^0$. In order to see how the number of neutralino decay events change with varying mass and RpV couplings, we show the light blue, blue, and dark blue areas corresponding to the parameter space where respectively ≥ 3, $\geq 3 \times 10^3$ and $\geq 3 \times 10^6$ events are observed. The hashed solid lines denote the present RpV limits for a set of sfermion mass values, Eq. (1.10), translated to $\lambda'/\tilde{m}^2$. We show the product bound from Eq. (1.11) only in the AL3X plot for a 5 TeV sfermion mass , for illustration purpose. The bound on $\lambda'/\tilde{m}^2$ scales linearly with the sfermion mass, when taking the scaling of the bound on λ' into account.

The 3-event dashed contour isocurve is extended to the lighter shaded region, bounded by a dotted line; this is obtained when we assume that invisible decays of the neutralinos can be detected as well. Whether this will be possible is an outstanding experimental question. In any case, we observe that for this benchmark scenario this would only give a very small extension in the sensitivity reach.

The range of sensitivity in the neutralino mass $m_{\tilde{\chi}_1^0}$ is strictly determined by the kinematics of the

production and decay

$$(M_{K^\pm} + m_e) < m_{\tilde{\chi}_1^0} < (M_{D_s} - m_e)\,. \tag{3.28}$$

and is thus identical for the three experiments. The range in sensitivity in $\lambda'/\tilde{m}^2$ is determined by the experimental set-up. Comparing the results for the four detectors, we find that for this model CODEX-b and FASER reach similar values of $\lambda'/m_{\tilde{f}}^2$, while AL3X is more sensitive by a factor ~ 2 and MATHUSLA is more sensitive by a factor ~ 5. Furthermore, they can all extend well beyond existing low-energy limits on the R-parity violating couplings.

On the right in Figs. 3.6 and 3.7, we show plots in the plane $\lambda'_P/m_{\tilde{f}}^2$ vs. $\lambda'_D/m_{\tilde{f}}^2$ for three values of $m_{\tilde{\chi}_1^0}$: 600 MeV (light blue region), 1200 MeV (blue region), 1800 MeV (dark blue region). For these results, the requirement that $\lambda'_P = \lambda'_D$ is lifted, so we observe an interplay between the production and decay of $\tilde{\chi}_1^0$. We may compare each detector's sensitivity range in different parameters. For example, the $\lambda'_P/m_{\tilde{f}}^2$ reach of FASER is only weaker than that of MATHUSLA by a factor ~ 3, even though FASER is more than 25,000 times smaller than MATHUSLA. This arises because FASER exploits the advantage of receiving the light D-mesons (and the produced neutralinos) boosted in the very forward direction, where the differential production cross section is significantly higher. As for the reach in $\lambda'_D/m_{\tilde{f}}^2$, MATHUSLA and AL3X show the strongest potential. Here we include single coupling bounds as solid hashed lines for three different sfermion masses (250, 1000 and 5000 GeV) and now also the product bound as a dashed hashed line for a 1 TeV sfermion mass. Again all experiments are sensitive well beyond existing limits.

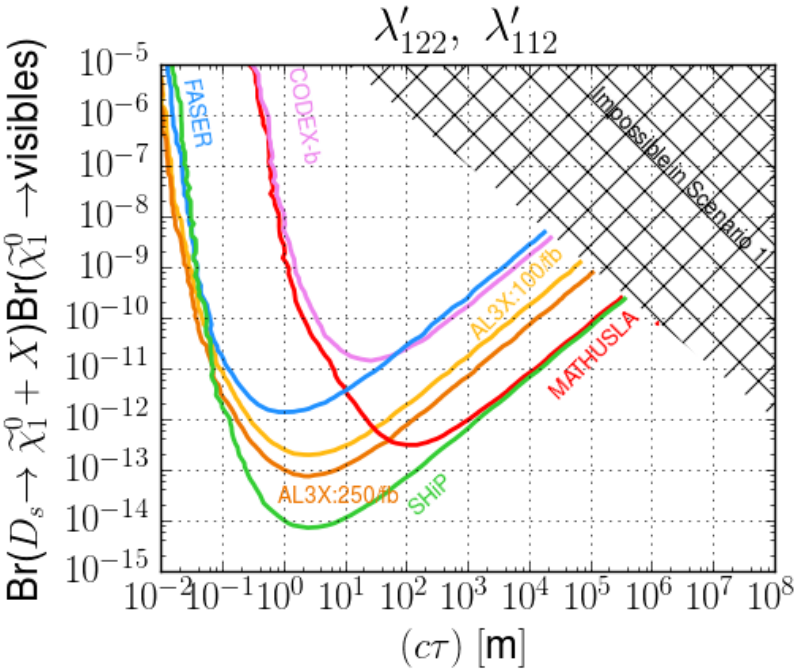

Figure 3.8: Model-independent sensitivity estimates for different experiments. We show the sensitivity reach as isocurves of 3 events of visible decays of neutralinos of mass 1200 MeV. For the axes, we choose the neutralino's unboosted decay length $c\tau$ and the relevant meson branching ratio times the relevant neutralino visible branching ratio. For scenario 1, regions with large $c\tau$ and large branching ratio are impossible to construct theoretically. $\lambda'_P = \lambda'_{122}$, $\lambda'_D = \lambda'_{112}$.

We next consider a model-independent description, where we interpret our results in terms of the physical observables, BR= $\mathrm{BR}_P \cdot \mathrm{BR}_D$, instead of the RpV-SUSY parameters. Here

$$\mathrm{BR}_P = \mathrm{BR}(D_s \to \mathrm{LLP} + e^{\pm}), \tag{3.29}$$

$$\mathrm{BR}_D = \mathrm{BR}(\mathrm{LLP} \to K^{(*)\pm} + e^{\mp}), \tag{3.30}$$

and we allow for any LLP. The results are shown in Fig. 3.8. The blue isocurve is for 3 events of visible decays inside the FASER decay chamber for the LLP mass value $m_{\mathrm{LLP}} = 1200$ MeV. The purple curve is for CODEX-b, the red for MATHUSLA and the yellow (orange) for AL3X:100(250)/fb. We do not show the curve for the other two mass value (600 and 1800 MeV) because they are almost the same as that for 1200 MeV. Remember that in Scenario 1, increasing λ'_P simultaneously increases Br(Meson $\to \tilde{\chi}_1^0 + X$) and decreases $c\tau$. For that reason there exists a region in this parameter plane which is theoretically impossible and we marked this as the hashed region in the upper right corner in Fig. 3.8. No such effect exists for Scenario 2. The $c\tau$ position of the valley of the isocurves, the point of maximal sensitivity, is determined by

$$\langle \beta\gamma \rangle c\tau \approx \langle L \rangle, \tag{3.31}$$

where $\langle \beta\gamma \rangle$ is the average boost of the neutralinos flying in the direction of the detector and $\langle L \rangle$ is the distance from the IP to the middle of the respective detector. We estimate $\langle \beta\gamma \rangle$ of the neutralinos that fly inside each detector by simulating 10,000 events in each case, and summarize the results for each Benchmark Scenario and detector in Table 3.2. The values for $\langle L \rangle$ are

$$\langle L \rangle = \begin{cases} 11.25 \text{ m} & \text{for AL3X,} \\ 30.0 \text{ m} & \text{for CODEX} - \text{b,} \\ 475 \text{ m} & \text{for FASER,} \\ 223 \text{ m} & \text{for MATHUSLA} \end{cases} \tag{3.32}$$

Using the values of Benchmark Scenario 1, we get for the most sensitive $c\tau$ value

$$(c\tau)_{\text{max. sensitivity}} = \begin{cases} 1.43 \text{ m} & \text{for AL3X,} \\ 18.3 \text{ m} & \text{for CODEX} - \text{b,} \\ 0.85 \text{ m} & \text{for FASER,} \\ 77 \text{ m} & \text{for MATHUSLA} \end{cases} \tag{3.33}$$

which agrees with Fig. 3.8.

The BR position of the valleys is determined by the luminosity of the experiment, the cross section of producing D_s-mesons, the pseudorapidity coverage, the volume of the detector and the product of the branching ratios. The BR reach of CODEX-b is roughly one order of magnitude larger than that of FASER. This is mainly due to the fact that LHCb has a one order of magnitude lower projected luminosity than that of ATLAS/CMS. Perhaps more importantly, in spite of the huge volume difference between MATHUSLA and CODEX-b/FASER, the BR reach in MATHUSLA is only one order of magnitude stronger than that in FASER. For large $c\tau$ values MATHUSLA performs far better than CODEX-b, but for shorter neutralino lifetimes the detectors perform equally well. The reason is that the distance traveled to MATHUSLA is about ten times larger than for CODEX-b, such that less neutralinos reach the former

Benchm. Sc.	$m_{\tilde{\chi}_1^0}$ (MeV)	$\langle\beta\gamma\rangle_{\texttt{AL3X}}$	$\langle\beta\gamma\rangle_{\texttt{CODEX-b}}$	$\langle\beta\gamma\rangle_{\texttt{FASER}}$	$\langle\beta\gamma\rangle_{\texttt{MATHUSLA}}$
1 (D_s)	1200	7.878	1.64	560	2.87
2 (B^0 & $\bar{B}^0$)	1000	19.57	4.07	793	7.32

Table 3.2: Summary of $\langle\beta\gamma\rangle$ values for each detector in all the Benchmark Scenarios. Inside the parenthesis in each column, the type of the mother meson of the neutralino is given.

detector for short-lived neutralinos. This leads to a similar sensitivity despite the larger integrated luminosity and the larger detector size of MATHUSLA. AL3X outperforms both FASER and CODEX-b, and can obtain far stronger results than MATHUSLA for models with $c\tau$ below roughly 20 m. Again, this can be explained by the different geometry: whilst AL3X is designed with a target-to-detector-distance of about 5 m close to the IP, MATHUSLA is planned as a surface experiment with a respective distance of more than 140 m. As scenario 1 relies on the abundant production of D-mesons, SHiP which works at a centre-of-mass energy of ≈ 27 GeV is significantly more sensitive. AL3X can only improve on the expected SHiP bound for scenarios with mean decay paths below 0.1 m, due to the proximity of the detector to IP2.

Note that Fig. 3.8 is very similar to the first plot of Fig. 1 in Ref. [204], the result of which was obtained in the context of a Type-I Seesaw model, where the right-handed neutrino is the LLP with a mass of 1 GeV produced from D-meson decays. This illustrates the model-independence of the results shown in the BR-$c\tau$-plane.

Benchmark Scenario 2

We now study one scenario where bottom mesons decay to a neutralino. Since the bottom mesons are much heavier than the charm mesons, the mass reach improves compared to the previous scenarios. In the present Benchmark Scenario 2, as before, we have $\lambda'_D = \lambda'_{112}$ giving both invisible and visible neutralino decays. For the neutralino production we have $\lambda'_P = \lambda'_{131}$ such that B^0 (and $\bar{B}^0$) decay to a neutralino. This is summarized in Table 3.1. Kinematically we can thus probe

$$(M_{K^\pm} + m_e) < m_{\tilde{\chi}_1^0} < (M_{B^0} - m_e)\,. \tag{3.34}$$

For this scenario we start with showing the model-dependent plots in the plane $\lambda'_P/m^2_{\tilde{f}}$ vs. $\lambda'_D/m^2_{\tilde{f}}$ in Figs. 3.9 and 3.10. Here, λ'_P does not produce any invisible final state from neutralino decays, see Table 3.1, which is why there is no lower bound on the sensitivity to $\lambda'_D/m^2_{\tilde{f}} = \lambda'_{112}/m^2_{\tilde{f}}$. In the previous scenario, CODEX-b shows similar sensitivity reach in $\lambda'_{P/D}/m^2_{\tilde{f}}$ to that of FASER, but now the former exceeds the latter, despite the fact that its projected luminosity is smaller by one order of magnitude. This is because the B-meson mass is more than twice the D-meson mass, and hence the produced B-mesons are not as much boosted in the very forward direction as the D-mesons. For the same reason, we also have a larger sensitive mass range than in the previous benchmark scenario. AL3X and MATHUSLA again has the most extensive sensitivity range.

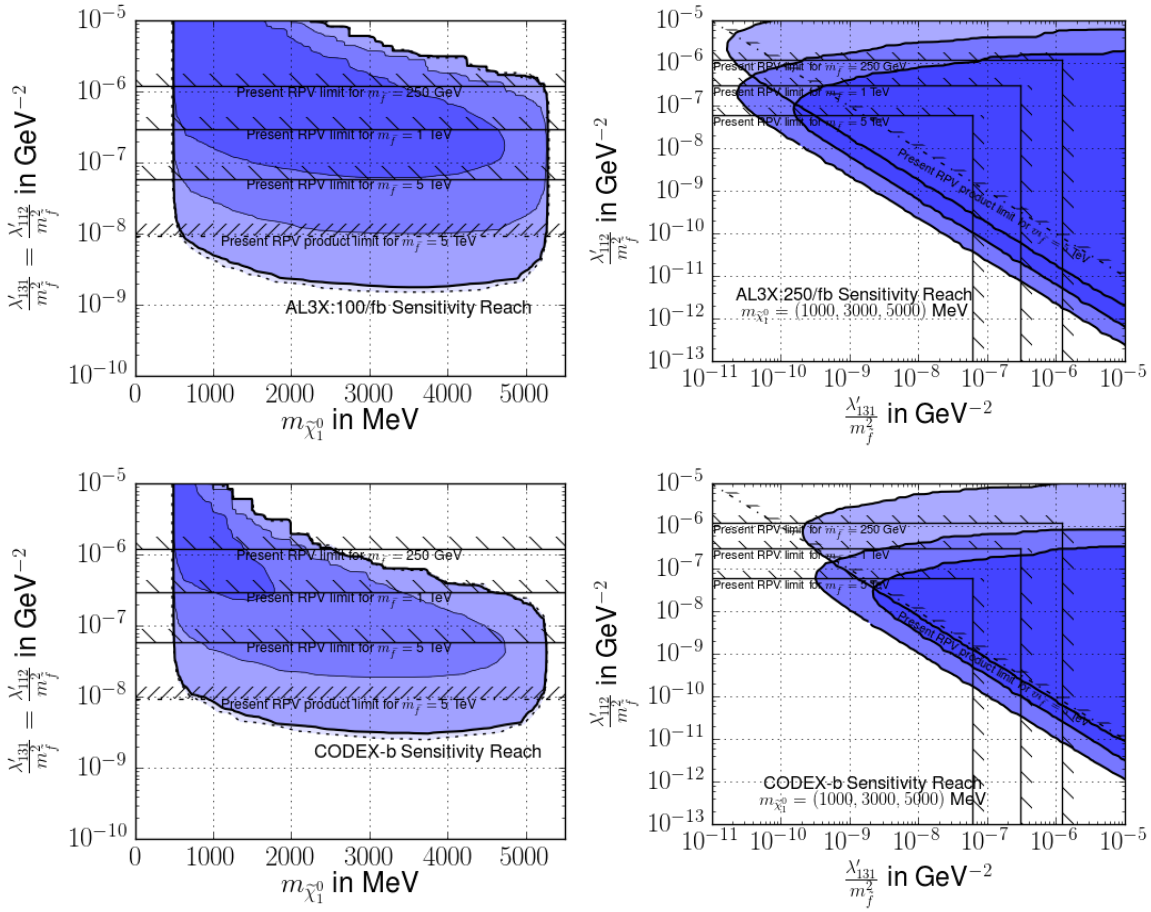

Figure 3.9: Model-dependent sensitivity estimate of AL3X and CODEX-b for Benchmark Scenario 2. The format is the same as in Fig. 3.6.

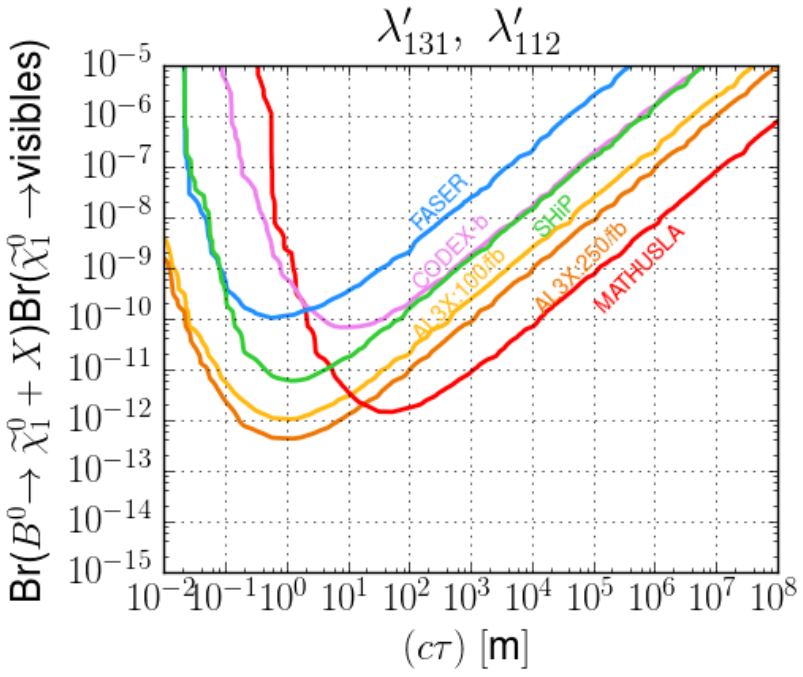

Figure 3.11: Model-independent sensitivity estimates for different experiments. The format is the same as that in Fig. 3.8. $\lambda'_P = \lambda'_{131}$, $\lambda'_D = \lambda'_{112}$.

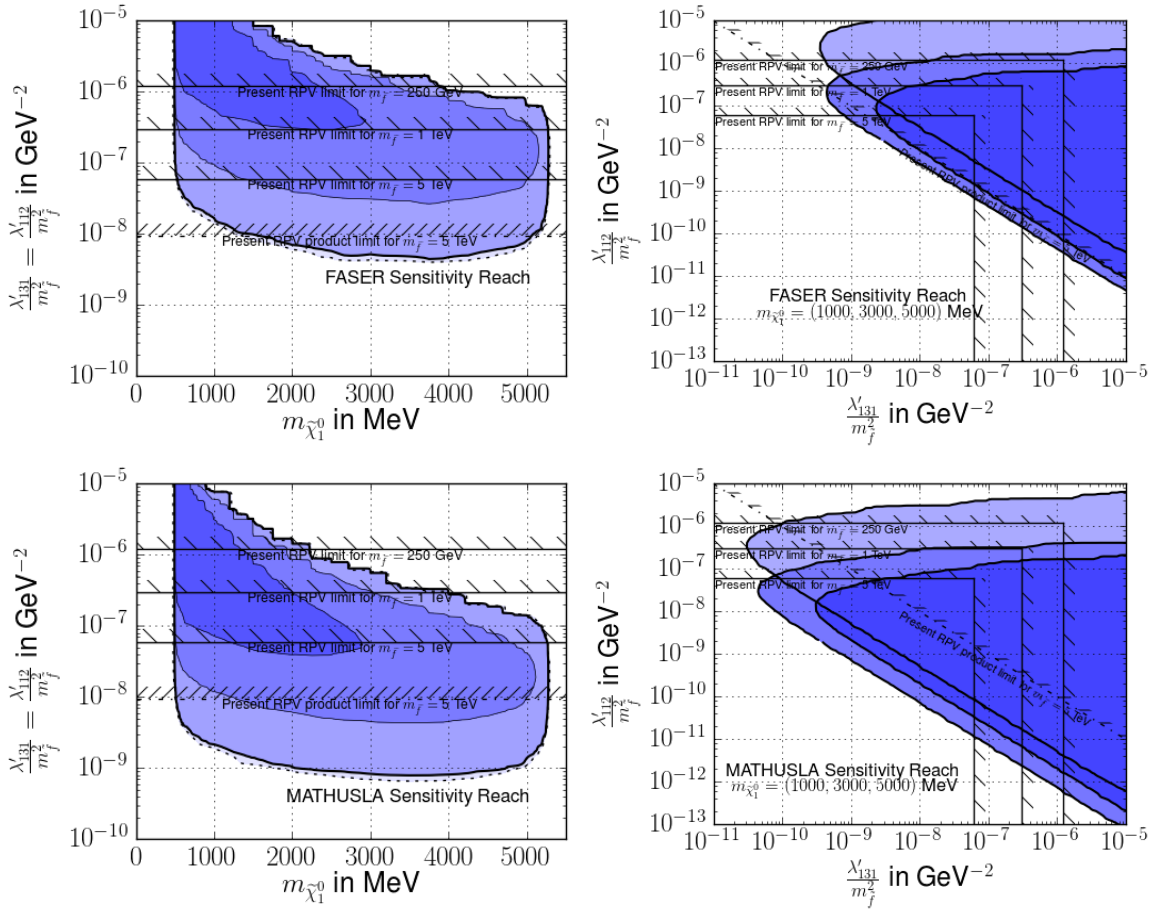

Figure 3.10: Model-dependent sensitivity estimate of FASER and MATHUSLA for Benchmark Scenario 2. The format is the same as in Fig. 3.6.

We proceed by showing in Fig. 3.11 the model-independet results, as in Benchmark Scenario 1, presented in the plane BR(Meson $\to \tilde{\chi}_1^0 + X$) $\times$ BR($\tilde{\chi}_1^0 \to$ charged final state) vs the proper decay length, $c\tau$, of the neutralino. We observe that AL3X:250/fb reaches smaller visible branching ratios than MATHUSLA by a factor ~ 4 and than SHiP by about one order of magnitude. FASER now has a similar reach in the visible branching ratio as CODEX-b. The positions of the $c\tau$ at the valley of different experiments can be explained in a similar way as in the previous benchmark scenario, *cf.* Table. 3.2.

Decay Branching Ratios of the $\tilde{\chi}_1^0$

After having presented results of the two benchmark scenarios in the previous subsections, we supplement our results by showing in Fig. 3.12 the decay branching ratios of the $\tilde{\chi}_1^0$ to visible, *i.e.* charged meson final states, as a function of $m_{\tilde{\chi}_1^0}$ in the kinematically allowed range for these scenarios. The curves can be well understood by considering the kinematic thresholds for the various neutralino

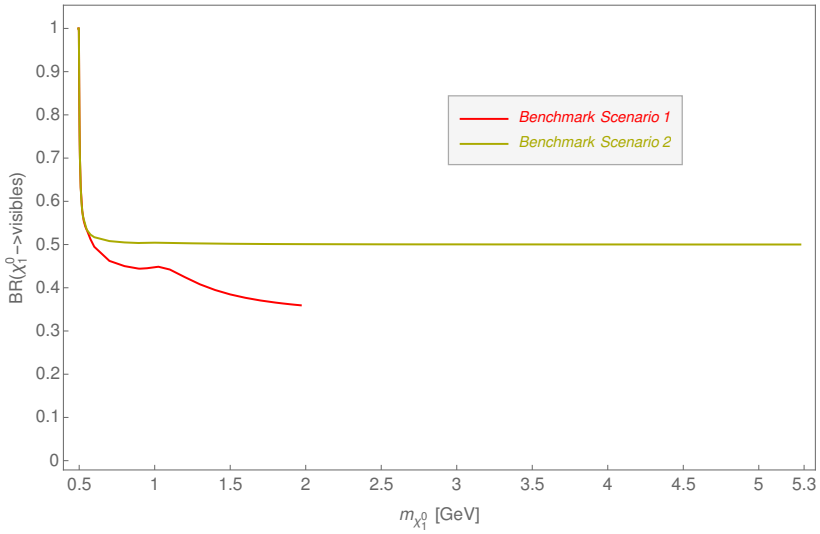

Figure 3.12: Branching ratios of $\tilde{\chi}_1^0$ to visible states in Benchmark Scenarios 1 & 2 as a function of $m_{\tilde{\chi}_1^0}$ [GeV], where we set $\lambda'_P = \lambda'_D$. For each curve, only the kinematically allowed range of $m_{\tilde{\chi}_1^0}$ is plotted.

decays. For Benchmark Scenarios 1 and 2 the first decay channel to open is to the charged kaon: $\tilde{\chi}_1^0 \to K^{\pm} e^{\mp}$. Thus the visible branching ratio starts at 1. It rapidly drops as the K^0-threshold is crossed. The asymptotic value of the branching ratios in Benchmark Scenarios 1 and 2 is simply determined by the number of charged or neutral decay channels. For example, in Benchmark Scenario 2 above all thresholds there are 4 visible final states and 8 invisible final states, giving a branching ratio to visible of 4/(4+4)=1/2. The bump in Benchmark Scenario 1 (red curve) is due to the extra threshold of the η-meson below the K^{+*} and K^{0*} masses. Note that it is the vector meson K^{0*} which is relevant for the neutralino decay, not the pseudoscalar [202].

3.3 Heavy Neutral Leptons

In this section we discuss the prospects of `AL3X`, `CODEX-b`, `FASER`, and `MATHUSLA` for detecting heavy neutral leptons (HNLs). The standard model predicts neutrinos to be massless, in contrast to the results of neutrino oscillation experiments. [8] The simplest extension of the SM, which can explain the experimental data, adds n fermionic singlets. Oscillation data requires $n \geq 2$. The Lagrangian of this model contains two new terms

$$\mathcal{L}^{\nu_R} = Y_\nu \bar{L} H^\dagger \nu_R + M_N \nu_R \nu_R \tag{3.35}$$

Here, we have suppressed generation indices. In general M_N is a complex symmetric (n,n) matrix, while Y_ν is a $(3,n)$ matrix. In the simple model considered here, without new interactions for the ν_R, one can perform a basis change and choose the entries of M_N to be diagonal, real and positive. The masses of the active neutrinos are small, if $(Y_\nu v) \cdot M_N^{-1} \ll 1$, this is the essence of the seesaw mechanism. Diagonalization of the mass matrix leads then to three light, active neutrinos and n nearly sterile mass eigenstates (or, HNLs), which we denote by N in the following.

[8] For the status of oscillation data, see for example the recent global fit [306].

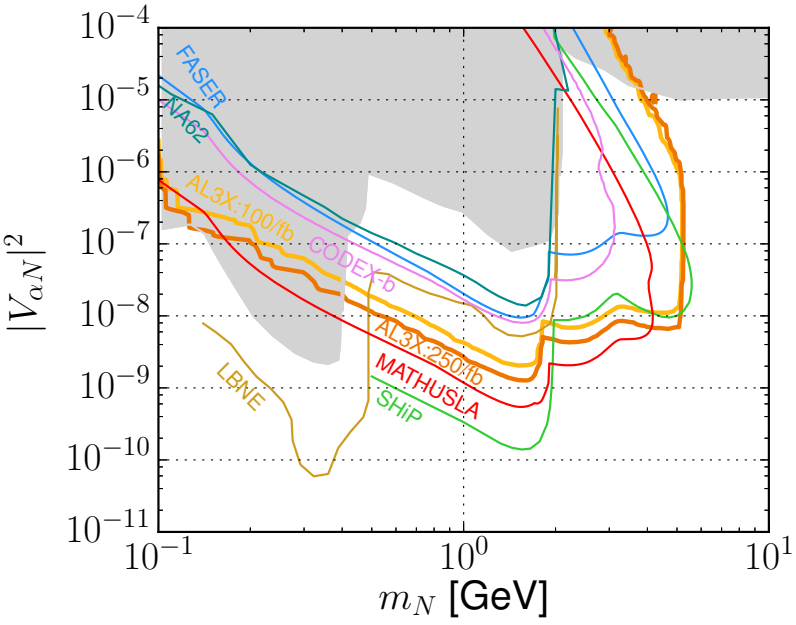

Figure 3.13: Estimates for the sensitivity of different experiments to HNLs in the plane mixing angle squared, $|V_{\alpha N}|^2$, versus mass of the HNL, m_N [GeV]. Here we perform Monte-Carlo simulation for `AL3X` only; we extract the corresponding results for `CODEX-b`, `FASER` and `MATHUSLA` from Ref. [204]. The references for the individual curves are given in the text.

The heavy sterile neutrino Charged (CC) and Neutral Current (NC) interactions are

$$\mathcal{L} = \frac{g}{\sqrt{2}} V_{\alpha j}\, \bar{l}_\alpha \gamma^\mu P_L N_j W^-_{L\mu} + \frac{g}{2\cos\theta_W} \sum_{\alpha,i,j} V^L_{\alpha i} V^*_{\alpha j} \overline{N_j} \gamma^\mu P_L \nu_i Z_\mu, \tag{3.36}$$

where $i = 1,2,3$ and $j = 1,..,n$ and α denotes the charged lepton generation. The left-handed sector neutrino mixing matrix V^L is measured in neutrino oscillations. $V_{\alpha j}$ describes the mixing between ordinary neutrinos and HNLs. Within the simple seesaw model, described by Eq. (3.35), one expects that $V_{\alpha j}$ is roughly of the order of $V_{\alpha j} \propto \sqrt{m_\nu / M_N}$, i.e. $|V_{\alpha j}|^2 \simeq 5 \times 10^{-11} (\frac{m_\nu}{0.05\ \text{eV}})(\frac{1\ \text{GeV}}{M_N})$. However, in extensions of this simple framework, for example the inverse seesaw [307], much larger values for the mixing can occur, despite the smallness of the observed neutrino masses. For this reason, for the sensitivity estimates of the different experiments we will take $|V_{\alpha j}|^2$ as a free parameter in our calculations. Note that the mixing between the HNLs and the active neutrinos controls both, production and decay of the HNLs.

Oscillation data shows two large mixing angles in the active neutrino sector [306]. Thus, one expects that the HNLs couple typically to more than one generation of charged leptons too, see Eq. (3.36). It is easy to fit all oscillation data with the seesaw mechanism, described by Eq. (3.35). However, the Yukawa matrices can be fixed by such a fit only up to an orthogonal rotation matrix containing three complex parameters [308], leaving $|V_{\alpha j}|$ essentially as free parameters.[9] In our sensitivity estimates

[9] For an extension of this Casas-Ibarra parametrization for the inverse seesaw case, see [309].

we will simply assume that only one HNL exists in the mass range to which the experiments are sensitive. We will also not distinguish between e and μ flavours, assuming simply that only one of the corresponding $|V_{\alpha N}|$ is non-zero. Since we are only interested in estimating sensitivity ranges, not in a full reconstruction of the seesaw parameters, this should be a reasonable approximation.

We now turn to the discussion of the results. Fig. 3.13 shows sensitivity estimates for the considered recent experimental proposals to HNLs. Here we perform the Monte-Carlo simulation exactly according to the procedure described in Sec. 3.1 only for the detector AL3X. For CODEX-b, FASER and MATHUSLA , we reproduce the isocurves from Ref. [204]. The difference between the two approaches would yield very little impact for this plot at the qualitative level. For AL3X we show two curves, one for 100/fb and one for 250/fb, corresponding to the two options discussed in Ref. [201]. The grey area in the background shows the parameter space currently excluded according to Ref. [310] by the searches from PS191 [311], JINR [312], CHARM [313], and DELPHI [281]. Fig. 3.13 shows that CODEX-b and FASER have quite similar sensitivities below $m_N \simeq 3.2$ GeV to HNL parameters, while MATHUSLA does better than both in most parts of the parameter space. AL3X is quite competitive for the search of HNLs, with a sensitivity better than FASER, CODEX-b or NA62, even for only 100/fb of statistics. In the mass range above $m_N \sim 2$ GeV, AL3X has a sensitivity that is better than the estimate for SHiP [314], and only slightly worse than MATHUSLA. FASER and CODEX-b are only worse than SHiP by approximately one order of magnitude. Below $m_N \sim 2$ GeV, SHiP gives the best sensitivity, with AL3X@250/fb only roughly a factor $(2-3)$ less sensitive than MATHUSLA which performs only slightly worse than SHiP.

3.4 Conclusions

In this chapter we have investigated the sensitivity of the proposed detectors AL3X, CODEX-b, FASER and MATHUSLA for detecting long-lived fermions in the context of the lightest neutralino of supersymmetry, and HNLs, also known as heavy sterile neutrinos. For the neutralino study, we consider two production mechanisms: pair-production from on-shell Z-boson decays via the (small) higgsino component of the neutralinos, and single production from D- or B-meson decays via a RpV $L \cdot Q\bar{D}$ coupling. In the study of neutralinos produced from a meson, we take two benchmark scenarios from Refs. [202, 203] for illustration of our results. Scenario 1 has the neutralino produced from a D_s-meson decay while scenario 2 from a B^0-meson decay. For the HNLs case, we present results where solely the mixing between $\nu_{e/\mu}$ and the HNL, N, is non-vanishing.

We present our results for detecting neutralinos pair-produced from Z-boson decays by showing two plots respectively for $\mathrm{BR}(Z \to 2\tilde{\chi}_1^0) = 10^{-3}$ at the experimental upper limit and for $\mathrm{BR}(Z \to 2\tilde{\chi}_1^0) = 10^{-5}$, switching on a single $L \cdot Q\bar{D}$ coupling: λ'_{112}, which induces neutralino decays to kaons and leptons. The plots are shown in the plane $\lambda'_{112}/m^2_{\tilde{f}}$ vs. $m_{\tilde{\chi}_1^0}$, *cf.* Fig. 3.5. We find the proposed detectors have a mass reach from ~ 1 GeV up to $\sim m_Z/2$. While MATHUSLA has the strongest reach in $\lambda'_{112}/m^2_{\tilde{f}}$, AL3X is only slightly worse by a factor ~ 2. Novel parameter space, which is orders of magnitude more sensitive than the present experimental limits on $\lambda'_{112}/m^2_{\tilde{f}}$, can be probed by all of these detectors.

We show three sets of plots for two benchmark scenarios for the light neutralinos singly produced from a charm or bottom meson, where two $L \cdot Q\bar{D}$ couplings are switched on: λ'_P and λ'_D, responsible for the production and the decay of the lightest neutralino, respectively. In the first set corresponding to the plots in the left column of Figs. 3.6, 3.7, 3.9 and 3.10 in the $\lambda'_P/m^2_{\tilde{f}} = \lambda'_D/m^2_{\tilde{f}}$ vs. $m_{\tilde{\chi}_1^0}$ plane,

we find for both scenarios, CODEX-b and FASER have a similar reach in $\lambda'/m^2_{\tilde{f}}$ while AL3X:250/fb and MATHUSLA are stronger by less than one order of magnitude. In the second set, the plots in the right column of Figs. 3.6, 3.7, 3.9 and 3.10, shown in the plane $\lambda'_P/m^2_{\tilde{f}}$ vs. $\lambda'_D/m^2_{\tilde{f}}$ for three representative values of $m_{\tilde{\chi}^0_1}$, we find that in scenario 1, CODEX-b and FASER have a similiar reach in both $\lambda'_P/m^2_{\tilde{f}}$ and $\lambda'_D/m^2_{\tilde{f}}$, and are worse than AL3X and MATHUSLA by approximately one order of magnitude. In the other scenario associated with a B^0-meson, again we observe a similar reach in both $\lambda'_P/m^2_{\tilde{f}}$ and $\lambda'_D/m^2_{\tilde{f}}$ from CODEX-b and FASER, while AL3X:250/fb and MATHUSLA show comparable performance. In particular, AL3X is more sensitive than SHiP by about a factor of 5 in both axes. In the final set of plots, Figs. 3.8 and 3.11, we present results in the plane Br(meson $\to \tilde{\chi}^0_1$)·Br($\tilde{\chi}^0_1 \to$ visibles) vs. $c\tau$, the proper decay length of $\tilde{\chi}^0_1$, and compare the different experiments. In Scenario 1, SHiP shows the strongest sensitivity in the product of branching ratios, covering all the sensitive areas of the other proposed detectors, while in Scenario 2 AL3X supersedes the whole sensitivity region of SHiP, and complements MATHUSLA in different $c\tau$ regimes. At the end, we also show an illustrative plot in Fig. 3.12, depicting the visible branching ratio of the lightest neutralino in the two benchmark scenarios considered, as a function of the neutralino mass.

As for our HNL results, we present a plot in the plane of mixing angle squared, $|V_{\alpha N}|^2$, vs. mass, m_N, where $\alpha = e, \mu$, *cf.* Fig. 3.13. We consider AL3X with 100/fb or 250/fb integrated luminosity, and show theoretical projections for all four detectors. We find that AL3X reaches smaller mixing angles than both FASER and CODEX-b in its whole mass reach, but is weaker than MATHUSLA by a factor ~ 3 for masses below ~ 4 GeV. Compared to SHiP, AL3X and MATHUSLA perform worse in mixing angle reach for m_N below the D-meson threshold, ~ 2 GeV, but better than SHiP for larger mass values.

In summary, we conclude that different experiments can complement each other in the parameter space of the different models considered here. In these studies, it seems having the three experiments, AL3X, SHiP and MATHUSLA can cover and extend the parameter space that could be covered by other detectors such as CODEX-b and FASER. Of course, it might be interesting to study also other models for these proposed detectors and to make comparisons. Finally, we stress that our sensitivity estimates are based on the assumption of essentially background-free experimental searches. Any unforeseen background could seriously affect these conclusions.

CHAPTER 4

Conclusions and Outlook

Ever since the discovery of the Higgs boson in 2012 completing the mass spectrum of the Standard Model, particle physics has been confronted with the question of pursuing its development without a clear guiding principle. The different theoretical and observational issues faced with the SM clearly imply the existence of new physics beyond the SM. This forces us to understand the SM merely as a low-energy effective field theory embedded in a more fundamental description, which in turn leads to the hierarchy problem. Solving the latter hence became one of the main requirements demanded of NP models, and several categories of theoretical constructions of BSM physics were proposed to serve this very purpose: a new symmetry, extra dimensions, etc. One particular concept is the supersymmetry which has stood as one of the most promising guiding principles in view of extending the SM. In these models, the quadratic sensitivity of the mass of the Higgs boson with respect to NP scales is put under control by the symmetry, thus solving the hierarchy problem in an elegant manner. Furthermore, unification of gauge couplings at a GUT scale of $\sim 10^{16}$ GeV is realized. R-parity appears as a natural ingredient of such models, as a means to forbid the violation of the baryon and the lepton numbers, and predicts the stability of the lightest R_p-odd particle, hence a possible candidate for cold DM. However, R_p is insufficient to protect the Lagrangian from higher dimensional terms, as produced by SUSY GUTs, that would induce proton decay. Thus, an equally viable alternative at the electroweak-SUSY scale consists in imposing directly the lepton or the baryon symmetry in the Lagrangian instead of R_p. New scenarios appear as the witnesses of a distinctive phenomenology in these models. Signals of decays mediated by RpV couplings are actively searched for at high-energy colliders, while indirect constraints also emerge from low-energy observables, in particular, in the presence of new sources of flavor violation. In the RpV-SUSY scenario, the LSP is no longer a stable DM candidate, as it would decay via a RpV coupling to SM particles. It would be still possible to accommodate the DM interpretation, provided one of the particles is sufficiently long-lived. In this thesis, we presented our work confronting the R-parity-violating MSSM with flavor observables based on updated experimental measurements in the neutral meson systems, and with projected searches at the LHC, based on displaced vertices.

In Chapter. 1, we recalled the basic ingredients of the SM, its limitations, a few promising avenues for BSM model building, as well as the motivations underlying the MSSM, R-parity and R-parity violation. The hierarchy problem persists as a central guideline for envisioning NP extensions of the SM. The elegant solution employing supersymmetry holds whether R_p is broken or not. Other benefits of these models include the prediction of the Higgs boson mass in the correct range and the

convergence of the SM gauge couplings at high energy pointing towards one-step unification. We then discussed the parameters and the spectrum of the RpV-MSSM, insisting on the extensive mixing effects that potentially arise. The last section of this chapter is devoted to a discussion of several phenomenologically relevant issues of RpV-SUSY in collider physics. This short review explores two directions: indirect bounds from low-energy observables involving only SM external states, and direct constraints from collider searches.

In Chapter. 2, we focused on testing the RpV-MSSM in the neutral meson systems with the CP-conserving quark-flavor-violating observables ΔM_K, ΔM_d and ΔM_s. We started with a discussion of the current experimental status of these observables along with a brief introduction to the principle and techniques involved in the experimental measurements. We then recalled the theoretical EFT framework in which these observables are usually evaluated, which allows to re-sum logarithms between high- and low-energy scales: flavor-violating effects are encoded within dim-6 operators whose Wilson coefficients collect high-energy contributions from the SM and beyond. The evaluation of the low-energy operators is a complex problem of hadronic physics that is addressed by lattice and effective descriptions. We restricted ourselves to considering the different types of Feynman diagrams at one-loop order which contributes to the Wilson coefficients at the matching scale. In the RpV-MSSM, contributions appear at tree-level through an sneutrino exchange. At one-loop level, box diagrams had already been partial explored in the literature. We completed this analysis, but also added contributions from self-energy and penguin diagrams which had been overlooked, even though consistency of the one-loop evaluation requires them in any renormalization scheme that is not on-shell. We also considered the field mixings to their full extent and collected the analytic expressions of the Wilson coefficients in Appendix A. For numerical investigation, we applied the computer tools `SARAH`, `SPheno` and `Flavio`. We considered various benchmark scenarios and presented multiple $n\,\sigma$ (n=1,2,3) boundaries in the RpV parameter space, after taking into account experimental results, SM predictions, and the uncertainties from SM and NP predictions. A list of the updated bounds on various RpV coupling products was provided, too. Finally, we studied the interplay between different sources of flavor violation, R-parity violationg or conserving that could interfere constructively or destructively. Such scenarios illustrate the complexities of combining the flavor-violating contributions in a full model.

In Chapter. 3, we presented a search strategy to investigate displaced vertex signatures at future experiments at the LHC. There, most of past searches focused on promptly decaying new particles. However, another regime involves longer lifetime. In recent years there have been several LLP-search proposals for new detectors at the LHC, that would exploit the large volume of data available ($3/ab$) at the High-luminosity LHC (after 15-20 years of data collection). Among these experiments, we considered `CODEX-b`, `FASER`, `MATHUSLA` and `AL3X`. By using Monte-Carlo simulation tools, we were able to estimate the sensitivity reach of these detectors for BSM theories. In this thesis, we considered two models: RpV-MSSM and heavy neutral leptons, where the LLPs are respectively the lightest neutralino and the HNL itself. We started with a detailed description of the simulation procedure for discovering LLPs in these detectors, and then described the geometries of each detector along with the projected integrated luminosity at the corresponding interaction point. In the RpV-MSSM scenario, we assumed that the lightest neutralino was the LSP, which would become long-lived and decay via a RpV coupling. We considered here two possible mechanisms for producing the light (O(GeV)) neutralinos: pair production from Z-boson decays via the Higgsino components of the neutralinos, and single production from charm and bottom mesons via a RpV coupling. We presented our results either in the parameter space of the model, or in a model-independent manner. We concluded this

chapter by discussing the sensitivity reach in the HNL model. The HNLs are hypothesized heavy states that would mix with active neutrinos. In this work, we considered only the HNLs produced from rare charm and bottom mesons decays, and hence HNL masses in the O(GeV) range. We presented a plot in the plane of mixing squared vs. the HNL mass, and compared the 3-event isocurves of the various experiments. In the end, we concluded that these future detectors could complement each other in the parameter space of the models that we studied, and also stressed that these results were all based on the assumption of zero background events, as the appearance of the latter could seriously distort these conclusions.

The RpV-MSSM stands as one of the viable and promising possibilities of extending the SM and the R_p-conserving MSSM. In the aftermath of the Higgs discovery and in the absence of solid NP signatures, a challenging question consists in evaluating how much of the popular models is already constrained and how robustly these limits hold when one considers effects beyond the standard scenarios. In this thesis, we have presented our work in a direction consistent with these guidelines, exploiting flavor observables and displaced vertices to illustrate this goal. Improved precision in experimental measurements, higher intensity and energies of colliders, should allow discovery of new fundamental particles and/or exclusion of larger area in the parameter space of various BSM models.

Bibliography

[1] D. J. Gross and F. Wilczek, *Ultraviolet Behavior of Nonabelian Gauge Theories*, Phys. Rev. Lett. **30** (1973) 1343, [,271(1973)] (cit. on p. 1).

[2] H. D. Politzer, *Reliable Perturbative Results for Strong Interactions?* Phys. Rev. Lett. **30** (1973) 1346, [,274(1973)] (cit. on p. 1).

[3] H. Fritzsch, M. Gell-Mann, and H. Leutwyler, *Advantages of the Color Octet Gluon Picture*, Phys. Lett. **47B** (1973) 365 (cit. on p. 1).

[4] A. Salam and J. C. Ward, *Electromagnetic and weak interactions*, Phys. Lett. **13** (1964) 168 (cit. on p. 1).

[5] S. Weinberg, *A Model of Leptons*, Phys. Rev. Lett. **19** (1967) 1264 (cit. on p. 1).

[6] S. L. Glashow, *Partial Symmetries of Weak Interactions*, Nucl. Phys. **22** (1961) 579 (cit. on p. 1).

[7] P. W. Higgs, *Broken Symmetries and the Masses of Gauge Bosons*, Phys. Rev. Lett. **13** (1964) 508, [,160(1964)] (cit. on p. 1).

[8] F. Englert and R. Brout, *Broken Symmetry and the Mass of Gauge Vector Mesons*, Phys. Rev. Lett. **13** (1964) 321, [,157(1964)] (cit. on p. 1).

[9] G. Arnison et al., *Experimental Observation of Isolated Large Transverse Energy Electrons with Associated Missing Energy at s**(1/2) = 540-GeV*, Phys. Lett. **B122** (1983) 103, [,611(1983)] (cit. on p. 1).

[10] G. Arnison et al., *Experimental Observation of Lepton Pairs of Invariant Mass Around 95-GeV/c**2 at the CERN SPS Collider*, Phys. Lett. **B126** (1983) 398, [,7.55(1983)] (cit. on p. 1).

[11] M. Banner et al., *Observation of Single Isolated Electrons of High Transverse Momentum in Events with Missing Transverse Energy at the CERN anti-p p Collider*, Phys. Lett. **B122** (1983) 476, [,7.45(1983)] (cit. on p. 1).

[12] P. Bagnaia et al., *Evidence for Z0 —> e+ e- at the CERN anti-p p Collider*, Phys. Lett. **B129** (1983) 130, [,7.69(1983)] (cit. on p. 1).

[13] R. Brandelik et al., *Evidence for Planar Events in e+ e- Annihilation at High-Energies*, Phys. Lett. **86B** (1979) 243 (cit. on p. 1).

[14] D. P. Barber et al., *Discovery of Three Jet Events and a Test of Quantum Chromodynamics at PETRA Energies*, Phys. Rev. Lett. **43** (1979) 830 (cit. on p. 1).

[15] C. Berger et al., *Evidence for Gluon Bremsstrahlung in e+ e- Annihilations at High-Energies*, Phys. Lett. **86B** (1979) 418 (cit. on p. 1).

[16] W. Bartel et al., *Observation of Planar Three Jet Events in e+ e- Annihilation and Evidence for Gluon Bremsstrahlung*, Phys. Lett. **91B** (1980) 142 (cit. on p. 1).

[17] G. Aad et al., *Observation of a new particle in the search for the Standard Model Higgs boson with the ATLAS detector at the LHC*, Phys. Lett. **B716** (2012) 1, arXiv: 1207.7214 [hep-ex] (cit. on pp. 1, 2).

[18] S. Chatrchyan et al., *Observation of a new boson at a mass of 125 GeV with the CMS experiment at the LHC*, Phys. Lett. **B716** (2012) 30, arXiv: 1207.7235 [hep-ex] (cit. on pp. 1, 2).

[19] J. J. Aubert et al., *Experimental Observation of a Heavy Particle J*, Phys. Rev. Lett. **33** (1974) 1404 (cit. on p. 1).

[20] J. E. Augustin et al., *Discovery of a Narrow Resonance in e^+e^- Annihilation*, Phys. Rev. Lett. **33** (1974) 1406, [Adv. Exp. Phys.5,141(1976)] (cit. on p. 1).

[21] S. Abachi et al., *Search for high mass top quark production in $p\bar{p}$ collisions at $\sqrt{s} = 1.8$ TeV*, Phys. Rev. Lett. **74** (1995) 2422, arXiv: hep-ex/9411001 [hep-ex] (cit. on p. 1).

[22] F. Abe et al., *Observation of top quark production in $\bar{p}p$ collisions*, Phys. Rev. Lett. **74** (1995) 2626, arXiv: hep-ex/9503002 [hep-ex] (cit. on p. 1).

[23] Q. R. Ahmad et al., *Direct evidence for neutrino flavor transformation from neutral current interactions in the Sudbury Neutrino Observatory*, Phys. Rev. Lett. **89** (2002) 011301, arXiv: nucl-ex/0204008 [nucl-ex] (cit. on p. 2).

[24] Y. Fukuda et al., *Evidence for oscillation of atmospheric neutrinos*, Phys. Rev. Lett. **81** (1998) 1562, arXiv: hep-ex/9807003 [hep-ex] (cit. on p. 2).

[25] P. Minkowski, *$\mu \to e\gamma$ at a Rate of One Out of 10^9 Muon Decays?* Phys. Lett. **67B** (1977) 421 (cit. on p. 2).

[26] M. Gell-Mann, P. Ramond, and R. Slansky, *Complex Spinors and Unified Theories*, Conf. Proc. **C790927** (1979) 315, arXiv: 1306.4669 [hep-th] (cit. on p. 2).

[27] R. N. Mohapatra and G. Senjanovic, *Neutrino Mass and Spontaneous Parity Nonconservation*, Phys. Rev. Lett. **44** (1980) 912, [,231(1979)] (cit. on p. 2).

[28] T. Yanagida, *Horizontal Symmetry and Masses of Neutrinos*, Prog. Theor. Phys. **64** (1980) 1103 (cit. on p. 2).

[29] J. Schechter and J. W. F. Valle, *Neutrino Masses in SU(2) x U(1) Theories*, Phys. Rev. **D22** (1980) 2227 (cit. on p. 2).

[30] D. E. Morrissey and M. J. Ramsey-Musolf, *Electroweak baryogenesis*, New J. Phys. **14** (2012) 125003, arXiv: 1206.2942 [hep-ph] (cit. on p. 2).

[31] J. M. Cline, "Baryogenesis," *Les Houches Summer School - Session 86: Particle Physics and Cosmology: The Fabric of Spacetime Les Houches, France, July 31-August 25, 2006*, 2006, arXiv: hep-ph/0609145 [hep-ph] (cit. on p. 2).

[32] M. Dine and A. Kusenko, *The Origin of the matter - antimatter asymmetry*, Rev. Mod. Phys. **76** (2003) 1, arXiv: hep-ph/0303065 [hep-ph] (cit. on p. 2).

[33] M. Trodden, *Electroweak baryogenesis*, Rev. Mod. Phys. **71** (1999) 1463, arXiv: hep-ph/9803479 [hep-ph] (cit. on p. 2).

[34] P. Huet and E. Sather, *Electroweak baryogenesis and standard model CP violation*, Phys. Rev. **D51** (1995) 379, arXiv: hep-ph/9404302 [hep-ph] (cit. on p. 2).

[35] A. D. Sakharov, *Violation of CP Invariance, C asymmetry, and baryon asymmetry of the universe*, Pisma Zh. Eksp. Teor. Fiz. **5** (1967) 32, [Usp. Fiz. Nauk161,no.5,61(1991)] (cit. on p. 2).

[36] M. B. Gavela et al., *Standard model CP violation and baryon asymmetry*, Mod. Phys. Lett. **A9** (1994) 795, arXiv: hep-ph/9312215 [hep-ph] (cit. on p. 2).

[37] M. B. Gavela et al., *Standard model CP violation and baryon asymmetry. Part 2: Finite temperature*, Nucl. Phys. **B430** (1994) 382, arXiv: hep-ph/9406289 [hep-ph] (cit. on p. 2).

[38] V. C. Rubin, N. Thonnard, and W. K. Ford Jr., *Rotational properties of 21 SC galaxies with a large range of luminosities and radii, from NGC 4605 /R = 4kpc/ to UGC 2885 /R = 122 kpc/*, Astrophys. J. **238** (1980) 471 (cit. on p. 2).

[39] F. Zwicky, *Die Rotverschiebung von extragalaktischen Nebeln*, Helv. Phys. Acta **6** (1933) 110, [Gen. Rel. Grav.41,207(2009)] (cit. on p. 2).

[40] W. Hu and S. Dodelson, *Cosmic microwave background anisotropies*, Ann. Rev. Astron. Astrophys. **40** (2002) 171, arXiv: astro-ph/0110414 [astro-ph] (cit. on p. 2).

[41] P. A. R. Ade et al., *Planck 2015 results. XIII. Cosmological parameters*, Astron. Astrophys. **594** (2016) A13, arXiv: 1502.01589 [astro-ph.CO] (cit. on p. 2).

[42] P. A. R. Ade et al., *Planck 2013 results. XVI. Cosmological parameters*, Astron. Astrophys. **571** (2014) A16, arXiv: 1303.5076 [astro-ph.CO] (cit. on p. 2).

[43] M. Markevitch et al., *Direct constraints on the dark matter self-interaction cross-section from the merging galaxy cluster 1E0657-56*, Astrophys. J. **606** (2004) 819, arXiv: astro-ph/0309303 [astro-ph] (cit. on p. 2).

[44] D. Clowe, A. Gonzalez, and M. Markevitch, *Weak lensing mass reconstruction of the interacting cluster 1E0657-558: Direct evidence for the existence of dark matter*, Astrophys. J. **604** (2004) 596, arXiv: astro-ph/0312273 [astro-ph] (cit. on p. 2).

[45] R. Massey et al., *The behaviour of dark matter associated with four bright cluster galaxies in the 10 kpc core of Abell 3827*, Mon. Not. Roy. Astron. Soc. **449** (2015) 3393, arXiv: 1504.03388 [astro-ph.CO] (cit. on p. 2).

[46] F. Kahlhoefer et al., *On the interpretation of dark matter self-interactions in Abell 3827*, Mon. Not. Roy. Astron. Soc. **452** (2015) L54, arXiv: 1504.06576 [astro-ph.CO] (cit. on p. 2).

[47] Y. B. Zel'dovich, *Magnetic Model of the Universe*, Soviet Journal of Experimental and Theoretical Physics **21** (1965) 656 (cit. on p. 2).

[48] Y. B. Zel'dovich, L. B. Okun', and S. B. Pikel'ner, *QUARKS: ASTROPHYSICAL AND PHYSICOCHEMICAL ASPECTS*, Soviet Physics Uspekhi **8** (1966) 702, URL: https://doi.org/10.1070%2Fpu1966v008n05abeh003030 (cit. on p. 2).

[49] H.-Y. Chiu, *Symmetry between particle and anti-particle populations in the universe*, Phys. Rev. Lett. **17** (1966) 712 (cit. on p. 2).

[50] B. W. Lee and S. Weinberg, *Cosmological Lower Bound on Heavy Neutrino Masses*, Phys. Rev. Lett. **39** (1977) 165, [,183(1977)] (cit. on p. 2).

[51] G. Steigman, *Cosmology Confronts Particle Physics*, Ann. Rev. Nucl. Part. Sci. **29** (1979) 313 (cit. on p. 2).

[52] R. J. Crewther et al., *Chiral Estimate of the Electric Dipole Moment of the Neutron in Quantum Chromodynamics*, Phys. Lett. **88B** (1979) 123, [Erratum: Phys. Lett.91B,487(1980)] (cit. on p. 2).

[53] C. A. Baker et al., *An Improved experimental limit on the electric dipole moment of the neutron*, Phys. Rev. Lett. **97** (2006) 131801, arXiv: hep-ex/0602020 [hep-ex] (cit. on p. 2).

[54] F. Wilczek, *Problem of Strong P and T Invariance in the Presence of Instantons*, Phys. Rev. Lett. **40** (1978) 279 (cit. on p. 2).

[55] S. Weinberg, *A New Light Boson?* Phys. Rev. Lett. **40** (1978) 223 (cit. on p. 2).

[56] R. D. Peccei and H. R. Quinn, *CP Conservation in the Presence of Instantons*, Phys. Rev. Lett. **38** (1977) 1440, [,328(1977)] (cit. on p. 2).

[57] R. D. Peccei and H. R. Quinn, *Constraints Imposed by CP Conservation in the Presence of Instantons*, Phys. Rev. **D16** (1977) 1791 (cit. on p. 2).

[58] *A Combination of preliminary electroweak measurements and constraints on the standard model*, (2004), arXiv: hep-ex/0412015 [hep-ex] (cit. on p. 3).

[59] http://lepewwg.web.cern.ch/LEPEWWG (cit. on p. 3).

[60] G. 't Hooft, *Naturalness, chiral symmetry, and spontaneous chiral symmetry breaking*, NATO Sci. Ser. B **59** (1980) 135 (cit. on p. 3).

[61] Y. A. Golfand and E. P. Likhtman, *Extension of the Algebra of Poincare Group Generators and Violation of p Invariance*, JETP Lett. **13** (1971) 323, [Pisma Zh. Eksp. Teor. Fiz.13,452(1971)] (cit. on p. 3).

[62] D. V. Volkov and V. P. Akulov, *Is the Neutrino a Goldstone Particle?* Phys. Lett. **46B** (1973) 109 (cit. on p. 3).

[63] J. Wess and B. Zumino, *A Lagrangian Model Invariant Under Supergauge Transformations*, Phys. Lett. **49B** (1974) 52 (cit. on p. 3).

[64] J. Wess and B. Zumino, *Supergauge Transformations in Four-Dimensions*, Nucl. Phys. **B70** (1974) 39, [,24(1974)] (cit. on p. 3).

[65] S. Dimopoulos and J. Preskill, *Massless Composites With Massive Constituents*, Nucl. Phys. **B199** (1982) 206 (cit. on p. 3).

[66] D. B. Kaplan, H. Georgi, and S. Dimopoulos, *Composite Higgs Scalars*, Phys. Lett. **136B** (1984) 187 (cit. on p. 3).

[67] D. B. Kaplan and H. Georgi, *SU(2) x U(1) Breaking by Vacuum Misalignment*, Phys. Lett. **136B** (1984) 183 (cit. on p. 3).

[68] H. Georgi and D. B. Kaplan, *Composite Higgs and Custodial SU(2)*, Phys. Lett. **145B** (1984) 216 (cit. on p. 3).

[69] H. Georgi, D. B. Kaplan, and P. Galison, *Calculation of the Composite Higgs Mass*, Phys. Lett. **143B** (1984) 152 (cit. on p. 3).

[70] M. J. Dugan, H. Georgi, and D. B. Kaplan, *Anatomy of a Composite Higgs Model*, Nucl. Phys. **B254** (1985) 299 (cit. on p. 3).

[71] T. Banks, *CONSTRAINTS ON SU(2) x U(1) BREAKING BY VACUUM MISALIGNMENT*, Nucl. Phys. **B243** (1984) 125 (cit. on p. 3).

[72] N. Arkani-Hamed, S. Dimopoulos, and G. R. Dvali, *The Hierarchy problem and new dimensions at a millimeter*, Phys. Lett. **B429** (1998) 263, arXiv: hep-ph/9803315 [hep-ph] (cit. on p. 3).

[73] T. Appelquist, H.-C. Cheng, and B. A. Dobrescu, *Bounds on universal extra dimensions*, Phys. Rev. **D64** (2001) 035002, arXiv: hep-ph/0012100 [hep-ph] (cit. on p. 3).

[74] L. Randall and R. Sundrum, *A Large mass hierarchy from a small extra dimension*, Phys. Rev. Lett. **83** (1999) 3370, arXiv: hep-ph/9905221 [hep-ph] (cit. on pp. 3, 4).

[75] G. F. Giudice and M. McCullough, *A Clockwork Theory*, JHEP **02** (2017) 036, arXiv: 1610.07962 [hep-ph] (cit. on p. 3).

[76] P. W. Graham, D. E. Kaplan, and S. Rajendran, *Cosmological Relaxation of the Electroweak Scale*, Phys. Rev. Lett. **115** (2015) 221801, arXiv: 1504.07551 [hep-ph] (cit. on p. 3).

[77] H. P. Nilles, *Supersymmetry, Supergravity and Particle Physics*, Phys. Rept. **110** (1984) 1 (cit. on pp. 3, 27).

[78] H. E. Haber and G. L. Kane, *The Search for Supersymmetry: Probing Physics Beyond the Standard Model*, Phys. Rept. **117** (1985) 75 (cit. on p. 3).

[79] E. Gildener, *Gauge Symmetry Hierarchies*, Phys. Rev. **D14** (1976) 1667 (cit. on p. 3).

[80] E. Witten, *Dynamical Breaking of Supersymmetry*, Nucl. Phys. **B188** (1981) 513 (cit. on p. 3).

[81] H. P. Nilles, *Dynamically Broken Supergravity and the Hierarchy Problem*, Phys. Lett. **115B** (1982) 193 (cit. on p. 3).

[82] M. J. G. Veltman, *The Infrared - Ultraviolet Connection*, Acta Phys. Polon. **B12** (1981) 437 (cit. on p. 3).

[83] M. Aaboud et al., *Search for electroweak production of supersymmetric states in scenarios with compressed mass spectra at* $\sqrt{s} = 13$ *TeV with the ATLAS detector*, (2017), arXiv: 1712.08119 [hep-ex] (cit. on pp. 4, 45).

[84] A. H. Chamseddine, R. L. Arnowitt, and P. Nath, *Locally Supersymmetric Grand Unification*, Phys. Rev. Lett. **49** (1982) 970 (cit. on p. 4).

[85] L. J. Hall, J. D. Lykken, and S. Weinberg,
Supergravity as the Messenger of Supersymmetry Breaking, Phys. Rev. **D27** (1983) 2359 (cit. on p. 4).

[86] R. Barbieri, S. Ferrara, and C. A. Savoy,
Gauge Models with Spontaneously Broken Local Supersymmetry,
Phys. Lett. **119B** (1982) 343 (cit. on p. 4).

[87] M. Dine and W. Fischler,
A Phenomenological Model of Particle Physics Based on Supersymmetry,
Phys. Lett. **110B** (1982) 227 (cit. on p. 4).

[88] C. R. Nappi and B. A. Ovrut, *Supersymmetric Extension of the SU(3) x SU(2) x U(1) Model*,
Phys. Lett. **113B** (1982) 175 (cit. on p. 4).

[89] L. Alvarez-Gaume, M. Claudson, and M. B. Wise, *Low-Energy Supersymmetry*,
Nucl. Phys. **B207** (1982) 96 (cit. on p. 4).

[90] M. Dine and A. E. Nelson, *Dynamical supersymmetry breaking at low-energies*,
Phys. Rev. **D48** (1993) 1277, arXiv: hep-ph/9303230 [hep-ph] (cit. on p. 4).

[91] M. Dine, A. E. Nelson, and Y. Shirman,
Low-energy dynamical supersymmetry breaking simplified, Phys. Rev. **D51** (1995) 1362,
arXiv: hep-ph/9408384 [hep-ph] (cit. on p. 4).

[92] M. Dine et al., *New tools for low-energy dynamical supersymmetry breaking*,
Phys. Rev. **D53** (1996) 2658, arXiv: hep-ph/9507378 [hep-ph] (cit. on p. 4).

[93] V. A. Rubakov and M. E. Shaposhnikov, *Do We Live Inside a Domain Wall?*
Phys. Lett. **125B** (1983) 136 (cit. on p. 4).

[94] V. A. Rubakov and M. E. Shaposhnikov,
Extra Space-Time Dimensions: Towards a Solution to the Cosmological Constant Problem,
Phys. Lett. **125B** (1983) 139 (cit. on p. 4).

[95] L. Randall and R. Sundrum, *An Alternative to compactification*,
Phys. Rev. Lett. **83** (1999) 4690, arXiv: hep-th/9906064 [hep-th] (cit. on p. 4).

[96] L. Randall and R. Sundrum, *Out of this world supersymmetry breaking*,
Nucl. Phys. **B557** (1999) 79, arXiv: hep-th/9810155 [hep-th] (cit. on p. 4).

[97] G. F. Giudice et al., *Gaugino mass without singlets*, JHEP **12** (1998) 027,
arXiv: hep-ph/9810442 [hep-ph] (cit. on p. 4).

[98] H. E. Haber, "Introductory low-energy supersymmetry,"
Proceedings, Theoretical Advanced Study Institute (TASI 92): From Black Holes and Strings to Particles: Boulder, USA, June 1-26, 1992, 1993 589, arXiv: hep-ph/9306207 [hep-ph]
(cit. on p. 5).

[99] G. Degrassi et al., *Towards high precision predictions for the MSSM Higgs sector*,
Eur. Phys. J. **C28** (2003) 133, arXiv: hep-ph/0212020 [hep-ph] (cit. on p. 6).

[100] S. P. Martin, *A Supersymmetry primer*,
(1997) 1, [Adv. Ser. Direct. High Energy Phys.18,1(1998)],
arXiv: hep-ph/9709356 [hep-ph] (cit. on p. 6).

[101] G. R. Farrar and P. Fayet, *Phenomenology of the Production, Decay, and Detection of New Hadronic States Associated with Supersymmetry*, Phys. Lett. **76B** (1978) 575 (cit. on p. 6).

[102] G. Jungman, M. Kamionkowski, and K. Griest, *Supersymmetric dark matter*, Phys. Rept. **267** (1996) 195, arXiv: hep-ph/9506380 [hep-ph] (cit. on p. 6).

[103] S. Weinberg, *Supersymmetry at Ordinary Energies. 1. Masses and Conservation Laws*, Phys. Rev. **D26** (1982) 287 (cit. on p. 7).

[104] H. K. Dreiner, C. Luhn, and M. Thormeier, *What is the discrete gauge symmetry of the MSSM?* Phys. Rev. **D73** (2006) 075007, arXiv: hep-ph/0512163 [hep-ph] (cit. on pp. 7, 8, 44).

[105] H. K. Dreiner et al., *Proton Hexality from an Anomalous Flavor U(1) and Neutrino Masses: Linking to the String Scale*, Nucl. Phys. **B795** (2008) 172, arXiv: 0708.0989 [hep-ph] (cit. on pp. 7, 8).

[106] L. E. Ibanez and G. G. Ross, *Discrete gauge symmetries and the origin of baryon and lepton number conservation in supersymmetric versions of the standard model*, Nucl. Phys. **B368** (1992) 3 (cit. on p. 7).

[107] H. K. Dreiner, *An Introduction to explicit R-parity violation*, (1997), [Adv. Ser. Direct. High Energy Phys.21,565(2010)], arXiv: hep-ph/9707435 [hep-ph] (cit. on p. 7).

[108] R. Barbier et al., *R-parity violating supersymmetry*, Phys. Rept. **420** (2005) 1, arXiv: hep-ph/0406039 [hep-ph] (cit. on pp. 7–9).

[109] S. Strandberg, *Searches for SUSY*, https://indico.cern.ch/event/686555/contributions/3028076/attachments/1683895/2706865/SUSYPlenaryICHEP2018.pdf, 2018 (cit. on p. 7).

[110] https://twiki.cern.ch/AtlasPublic/SupersymmetryPublicResults (cit. on p. 7).

[111] https://twiki.cern.ch/CMSPublic/PhysicsResultsSUS (cit. on p. 7).

[112] https://twiki.cern.ch/AtlasPublic/ExoticsPublicResults (cit. on p. 7).

[113] https://twiki.cern.ch/CMSPublic/PhysicsResultsEXO (cit. on p. 7).

[114] M. Aaboud et al., *Search for electroweak production of supersymmetric particles in final states with two or three leptons at* $\sqrt{s} = 13$ *TeV with the ATLAS detector*, (2018), arXiv: 1803.02762 [hep-ex] (cit. on p. 7).

[115] A. H. Chamseddine and H. K. Dreiner, *Anomaly free gauged R symmetry in local supersymmetry*, Nucl. Phys. **B458** (1996) 65, arXiv: hep-ph/9504337 [hep-ph] (cit. on p. 8).

[116] H. K. Dreiner, T. Opferkuch, and C. Luhn, *Froggatt-Nielsen models with a residual* $\mathbb{Z}_4^R$ *symmetry*, Phys. Rev. **D88** (2013) 115005, arXiv: 1308.0332 [hep-ph] (cit. on p. 8).

[117] M. Hanussek and J. S. Kim, *Testing neutrino masses in the R-parity violating minimal supersymmetric standard model with LHC results*, Phys. Rev. **D85** (2012) 115021, arXiv: 1205.0019 [hep-ph] (cit. on p. 8).

[118] D. Dercks et al., *R-Parity Violation at the LHC*, Eur. Phys. J. **C77** (2017) 856, arXiv: 1706.09418 [hep-ph] (cit. on pp. 8, 44).

[119] J.-H. Jang, J. K. Kim, and J. S. Lee, *Constraints on the R-parity and lepton flavor violating couplings from B0 decays to two charged leptons*, Phys. Rev. **D55** (1997) 7296, arXiv: hep-ph/9701283 [hep-ph] (cit. on pp. 9, 11).

[120] K.-m. Cheung and O. C. W. Kong, *Muon → e gamma from supersymmetry without R-parity*, Phys. Rev. **D64** (2001) 095007, arXiv: hep-ph/0101347 [hep-ph] (cit. on pp. 9, 11).

[121] A. Vicente, *Charged lepton flavor violation beyond minimal supersymmetry*, Nucl. Phys. Proc. Suppl. **248-250** (2014) 20, arXiv: 1310.8162 [hep-ph] (cit. on pp. 9, 11).

[122] D. F. Carvalho, M. E. Gomez, and J. C. Romao, *Charged lepton flavor violation in supersymmetry with bilinear R-parity violation*, Phys. Rev. **D65** (2002) 093013, arXiv: hep-ph/0202054 [hep-ph] (cit. on pp. 9, 11).

[123] M. Endo, K. Hamaguchi, and S. Iwamoto, *Lepton Flavor Violation and Cosmological Constraints on R-parity Violation*, JCAP **1002** (2010) 032, arXiv: 0912.0585 [hep-ph] (cit. on pp. 9, 11).

[124] K. Choi, E. J. Chun, and K. Hwang, *Lepton flavor violation and bilinear R-parity violation*, Phys. Lett. **B488** (2000) 145, arXiv: hep-ph/0005262 [hep-ph] (cit. on pp. 9, 11).

[125] A. de Gouvea, S. Lola, and K. Tobe, *Lepton flavor violation in supersymmetric models with trilinear R-parity violation*, Phys. Rev. **D63** (2001) 035004, arXiv: hep-ph/0008085 [hep-ph] (cit. on pp. 9, 11).

[126] A. Vicente, *Lepton flavor violation beyond the MSSM*, Adv. High Energy Phys. **2015** (2015) 686572, arXiv: 1503.08622 [hep-ph] (cit. on pp. 9, 11).

[127] A. Gemintern et al., *Lepton flavor violating decays L → l gamma gamma as a new probe of supersymmetry with broken R parity*, Phys. Rev. **D67** (2003) 115012, arXiv: hep-ph/0302186 [hep-ph] (cit. on pp. 9, 11).

[128] C.-Y. Chen and O. C. W. Kong, *Leptonic Radiative Decay in Supersymmetry without R parity*, Phys. Rev. **D79** (2009) 115013, arXiv: 0901.3371 [hep-ph] (cit. on pp. 9, 11).

[129] Y. Cheng and O. C. W. Kong, "Leptonic Flavor Violating Higgs to mu + tau Decay in Supersymmetry without R Parity," *20th International Conference on Supersymmetry and Unification of Fundamental Interactions (SUSY 2012) Beijing, China, August 13-17, 2012*, 2012, arXiv: 1211.0365 [hep-ph], URL: https://inspirehep.net/record/1198031/files/arXiv:1211.0365.pdf (cit. on pp. 9, 11).

[130] A. Arhrib, Y. Cheng, and O. C. W. Kong, *Comprehensive analysis on lepton flavor violating Higgs boson to $\mu^{\mp}\tau^{\pm}$ decay in supersymmetry without R parity*, Phys. Rev. **D87** (2013) 015025, arXiv: 1210.8241 [hep-ph] (cit. on pp. 9, 11).

[131] A. Arhrib, Y. Cheng, and O. C. W. Kong, *Higgs to mu+tau Decay in Supersymmetry without R-parity*, EPL **101** (2013) 31003, arXiv: 1208.4669 [hep-ph] (cit. on pp. 9, 11).

[132] J. Cao, L. Wu, and J. M. Yang,
Lepton flavor-changing processes in R-parity violating MSSM: Z → l(i) anti-l(j) and gamma gamma → l(i) anti-l(j) under new bounds from l(i) → l(j) gamma,
Nucl. Phys. **B829** (2010) 370, arXiv: 0908.4556 [hep-ph] (cit. on pp. 9, 11).

[133] M. Gomez and D. F. Carvalho, "Lepton flavor violation in SUSY with and without R parity,"
Proceedings, Corfu Summer Institute on Elementary Particle Physics (Corfu 2001): Corfu, Greece, August 31-September 20, 2001, 2001, arXiv: hep-ph/0204133 [hep-ph]
(cit. on pp. 9, 11).

[134] H. K. Dreiner, M. Kramer, and B. O'Leary, *Bounds on R-parity violating supersymmetric couplings from leptonic and semi-leptonic meson decays*, Phys. Rev. **D75** (2007) 114016,
arXiv: hep-ph/0612278 [hep-ph] (cit. on pp. 9, 11).

[135] H. K. Dreiner et al.,
New bounds on trilinear R-parity violation from lepton flavor violating observables,
Phys. Rev. **D86** (2012) 015003, arXiv: 1204.5925 [hep-ph] (cit. on pp. 9, 11).

[136] W.-j. Li, Y.-d. Yang, and X.-d. Zhang,
$\tau^- \to \mu^-\pi^0(\eta,\eta')$ *decays in new physics scenarios beyond the standard model*,
Phys. Rev. **D73** (2006) 073005, arXiv: hep-ph/0511273 [hep-ph] (cit. on pp. 9, 11).

[137] W. Li et al., *RPV SUSY effects in* $\tau^- \to e^-(\mu^-)K\bar{K}$ *Decays*,
Int. J. Mod. Phys. **A29** (2014) 1450063, arXiv: 1312.2231 [hep-ph] (cit. on pp. 9, 11).

[138] G.-C. Cho and H. Matsuo, *Constraints on R-parity violating interactions in supersymmetric standard model from leptonic decays of* D_s *and* B^+ *mesons*, Phys. Lett. **B703** (2011) 318,
arXiv: 1107.3004 [hep-ph] (cit. on pp. 9, 11).

[139] R. Bose, *Rare tau Decays in R-parity Violating Supersymmetry*, J. Phys. **G38** (2011) 065003,
arXiv: 1012.1736 [hep-ph] (cit. on pp. 9, 11).

[140] Y. Grossman and H. E. Haber,
(S)neutrino properties in R-parity violating supersymmetry. 1. CP conserving phenomena,
Phys. Rev. **D59** (1999) 093008, arXiv: hep-ph/9810536 [hep-ph] (cit. on pp. 9, 11).

[141] H. K. Dreiner et al., *Neutrino masses and mixings in the baryon triality constrained minimal supersymmetric standard model*, Phys. Rev. **D84** (2011) 113005,
arXiv: 1106.4338 [hep-ph] (cit. on pp. 9, 11).

[142] H. K. Dreiner, J. Soo Kim, and M. Thormeier,
A Simple baryon triality model for neutrino masses, (2007), arXiv: 0711.4315 [hep-ph]
(cit. on pp. 9, 11).

[143] M. Hirsch et al., *Neutrino masses and mixings from supersymmetry with bilinear R parity violation: A Theory for solar and atmospheric neutrino oscillations*,
Phys. Rev. **D62** (2000) 113008, [Erratum: Phys. Rev.D65,119901(2002)],
arXiv: hep-ph/0004115 [hep-ph] (cit. on pp. 9, 11).

[144] C. Arbeláez et al., *QCD-improved limits from neutrinoless double beta decay*,
Phys. Rev. **D96** (2017) 015010, arXiv: 1611.06095 [hep-ph] (cit. on p. 9).

[145] S. Eidelman et al., *Review of particle physics. Particle Data Group*, Phys. Lett. **B592** (2004) 1
(cit. on p. 9).

[146] D. Choudhury and P. Roy,
New constraints on lepton nonconserving R-parity violating couplings,
Phys. Lett. **B378** (1996) 153, arXiv: hep-ph/9603363 [hep-ph] (cit. on pp. 9, 11).

[147] H. K. Dreiner, G. Polesello, and M. Thormeier,
Bounds on broken R parity from leptonic meson decays, Phys. Rev. **D65** (2002) 115006,
arXiv: hep-ph/0112228 [hep-ph] (cit. on pp. 9, 11).

[148] J. P. Saha and A. Kundu, *Constraints on R parity violating supersymmetry from leptonic and semileptonic tau, B(d) and B(s) decays*, Phys. Rev. **D66** (2002) 054021,
arXiv: hep-ph/0205046 [hep-ph] (cit. on p. 9).

[149] Y. Grossman, Z. Ligeti, and E. Nardi,
B —> tau+ tau- (X) decays: First constraints and phenomenological implications,
Phys. Rev. **D55** (1997) 2768, arXiv: hep-ph/9607473 [hep-ph] (cit. on p. 9).

[150] S. Baek and Y. G. Kim,
Constraints on the R-parity violating couplings from B+- —> lepton+- neutrino decays,
Phys. Rev. **D60** (1999) 077701, arXiv: hep-ph/9906385 [hep-ph] (cit. on p. 9).

[151] Y. Grossman, Z. Ligeti, and E. Nardi,
New limit on inclusive $B \to X_s$ anti-neutrino neutrino decay and constraints on new physics,
Nucl. Phys. **B465** (1996) 369, [Erratum: Nucl. Phys.B480,753(1996)],
arXiv: hep-ph/9510378 [hep-ph] (cit. on p. 9).

[152] A. Deandrea, J. Welzel, and M. Oertel, *K —> pi nu anti-nu from standard to new physics*,
JHEP **10** (2004) 038, arXiv: hep-ph/0407216 [hep-ph] (cit. on p. 9).

[153] J.-H. Jang, Y. G. Kim, and J. S. Lee, *B —> X(s) l(i) + l(j) - decays with R-parity violation*,
Phys. Rev. **D58** (1998) 035006, arXiv: hep-ph/9711504 [hep-ph] (cit. on p. 9).

[154] C. E. Carlson, P. Roy, and M. Sher, *New bounds on R-parity violating couplings*,
Phys. Lett. **B357** (1995) 99, arXiv: hep-ph/9506328 [hep-ph] (cit. on p. 9).

[155] D. Chakraverty and D. Choudhury, *B physics constraints on baryon number violating couplings: Grand unification or R-parity violation*, Phys. Rev. **D63** (2001) 112002,
arXiv: hep-ph/0012309 [hep-ph] (cit. on p. 9).

[156] S. Bar-Shalom, G. Eilam, and Y.-D. Yang,
B —> phi pi and B0 —> phi phi in the standard model and new bounds on R parity violation,
Phys. Rev. **D67** (2003) 014007, arXiv: hep-ph/0201244 [hep-ph] (cit. on p. 9).

[157] K. Agashe and M. Graesser,
R-parity violation in flavor changing neutral current processes and top quark decays,
Phys. Rev. **D54** (1996) 4445, arXiv: hep-ph/9510439 [hep-ph] (cit. on pp. 9, 11, 14).

[158] B. de Carlos and P. L. White, *R-parity violation and quark flavor violation*,
Phys. Rev. **D55** (1997) 4222, arXiv: hep-ph/9609443 [hep-ph]
(cit. on pp. 9, 11, 15, 16, 27).

[159] G. Bhattacharyya and A. Raychaudhuri,
New constraints on R-parity violation from K and B systems, Phys. Rev. **D57** (1998) 3837,
arXiv: hep-ph/9712245 [hep-ph] (cit. on pp. 9, 11, 16, 24, 27).

[160] J. P. Saha and A. Kundu, *Reevaluating bounds on flavor changing neutral current parameters in R parity conserving and R parity violating supersymmetry from B0 anti-B0 mixing*, Phys. Rev. **D69** (2004) 016004, arXiv: hep-ph/0307259 [hep-ph] (cit. on pp. 9, 11, 24, 27, 32).

[161] A. Kundu and J. P. Saha, *Constraints on R-parity violating supersymmetry from neutral meson mixing*, Phys. Rev. **D70** (2004) 096002, arXiv: hep-ph/0403154 [hep-ph] (cit. on pp. 9, 11).

[162] S. Nandi and J. P. Saha, $B_s - \bar{B}_s$ *mixing, B decays and R-parity violating supersymmetry*, Phys. Rev. **D74** (2006) 095007, arXiv: hep-ph/0608341 [hep-ph] (cit. on pp. 9, 11).

[163] R.-M. Wang et al., *Probe the R-parity violating supersymmetry effects in the* $B_s^0 - \bar{B}_s^0$ *mixing*, HEPNP **31** (2007) 332, arXiv: hep-ph/0609276 [hep-ph] (cit. on pp. 9, 11).

[164] R.-M. Wang et al., *Reevaluating R-parity Violating Supersymmetry Effects in* $B_s^0 - \bar{B}_s^0$ *Mixing*, JHEP **12** (2010) 034, arXiv: 1007.2944 [hep-ph] (cit. on pp. 9, 11, 21, 24, 27).

[165] F. Domingo et al., *Updating Bounds on R-Parity Violating Supersymmetry from Meson Oscillation Data*, JHEP **02** (2019) 066, arXiv: 1810.08228 [hep-ph] (cit. on pp. 9, 11, 45).

[166] R. Aaij et al., *Test of lepton universality using* $B^+ \to K^+\ell^+\ell^-$ *decays*, Phys. Rev. Lett. **113** (2014) 151601, arXiv: 1406.6482 [hep-ex] (cit. on p. 9).

[167] R. Aaij et al., *Test of lepton universality with* $B^0 \to K^{*0}\ell^+\ell^-$ *decays*, JHEP **08** (2017) 055, arXiv: 1705.05802 [hep-ex] (cit. on p. 9).

[168] J. P. Lees et al., *Evidence for an excess of* $\bar{B} \to D^{(*)}\tau^-\bar{\nu}_\tau$ *decays*, Phys. Rev. Lett. **109** (2012) 101802, arXiv: 1205.5442 [hep-ex] (cit. on p. 9).

[169] J. P. Lees et al., *Measurement of an Excess of* $\bar{B} \to D^{(*)}\tau^-\bar{\nu}_\tau$ *Decays and Implications for Charged Higgs Bosons*, Phys. Rev. **D88** (2013) 072012, arXiv: 1303.0571 [hep-ex] (cit. on p. 9).

[170] M. Huschle et al., *Measurement of the branching ratio of* $\bar{B} \to D^{(*)}\tau^-\bar{\nu}_\tau$ *relative to* $\bar{B} \to D^{(*)}\ell^-\bar{\nu}_\ell$ *decays with hadronic tagging at Belle*, Phys. Rev. **D92** (2015) 072014, arXiv: 1507.03233 [hep-ex] (cit. on p. 9).

[171] Y. Sato et al., *Measurement of the branching ratio of* $\bar{B}^0 \to D^{*+}\tau^-\bar{\nu}_\tau$ *relative to* $\bar{B}^0 \to D^{*+}\ell^-\bar{\nu}_\ell$ *decays with a semileptonic tagging method*, Phys. Rev. **D94** (2016) 072007, arXiv: 1607.07923 [hep-ex] (cit. on p. 9).

[172] R. Aaij et al., *Measurement of the ratio of branching fractions* $\mathcal{B}(\bar{B}^0 \to D^{*+}\tau^-\bar{\nu}_\tau)/\mathcal{B}(\bar{B}^0 \to D^{*+}\mu^-\bar{\nu}_\mu)$, Phys. Rev. Lett. **115** (2015) 111803, [Erratum: Phys. Rev. Lett.115,no.15,159901(2015)], arXiv: 1506.08614 [hep-ex] (cit. on p. 9).

[173] S. Hirose et al., *Measurement of the* τ *lepton polarization and* $R(D^*)$ *in the decay* $\bar{B} \to D^*\tau^-\bar{\nu}_\tau$, Phys. Rev. Lett. **118** (2017) 211801, arXiv: 1612.00529 [hep-ex] (cit. on p. 9).

[174] S. Hirose et al., *Measurement of the* τ *lepton polarization and* $R(D^*)$ *in the decay* $\bar{B} \to D^*\tau^-\bar{\nu}_\tau$ *with one-prong hadronic* τ *decays at Belle*, Phys. Rev. **D97** (2018) 012004, arXiv: 1709.00129 [hep-ex] (cit. on p. 9).

[175] R. Aaij et al., *Measurement of the ratio of the $B^0 \to D^{*-}\tau^+\nu_\tau$ and $B^0 \to D^{*-}\mu^+\nu_\mu$ branching fractions using three-prong τ-lepton decays*, Phys. Rev. Lett. **120** (2018) 171802, arXiv: 1708.08856 [hep-ex] (cit. on p. 9).

[176] R. Aaij et al., *Test of Lepton Flavor Universality by the measurement of the $B^0 \to D^{*-}\tau^+\nu_\tau$ branching fraction using three-prong τ decays*, Phys. Rev. **D97** (2018) 072013, arXiv: 1711.02505 [hep-ex] (cit. on p. 9).

[177] Q.-Y. Hu et al., *R-parity violating solutions to the $R_{D^{(*)}}$ anomaly and their GUT-scale unifications*, Phys. Rev. **D99** (2019) 015008, arXiv: 1808.01419 [hep-ph] (cit. on p. 9).

[178] N. G. Deshpande and X.-G. He, *Consequences of R-parity violating interactions for anomalies in $\bar{B} \to D^{(*)}\tau\bar{\nu}$ and $b \to s\mu^+\mu^-$*, Eur. Phys. J. **C77** (2017) 134, arXiv: 1608.04817 [hep-ph] (cit. on p. 9).

[179] W. Huang and Y.-L. Tang, *Flavor anomalies at the LHC and the R-parity violating supersymmetric model extended with vectorlike particles*, Phys. Rev. **D92** (2015) 094015, arXiv: 1509.08599 [hep-ph] (cit. on p. 9).

[180] D. Das et al., *Scrutinizing R-parity violating interactions in light of $R_{K^{(*)}}$ data*, Phys. Rev. **D96** (2017) 095033, arXiv: 1705.09188 [hep-ph] (cit. on p. 9).

[181] J. E. Kim, B. Kyae, and H. M. Lee, *Effective supersymmetric theory and (g-2)(muon with R-parity violation*, Phys. Lett. **B520** (2001) 298, arXiv: hep-ph/0103054 [hep-ph] (cit. on p. 9).

[182] R. Adhikari and G. Rajasekaran, *Anomalous magnetic moment of muon and L violating supersymmetric models*, (2001), arXiv: hep-ph/0107279 [hep-ph] (cit. on p. 9).

[183] F. Vissani, *(B+L) conserving nucleon decays in supersymmetric models*, Phys. Rev. **D52** (1995) 4245, arXiv: hep-ph/9503227 [hep-ph] (cit. on p. 9).

[184] A. Y. Smirnov and F. Vissani, *Upper bound on all products of R-parity violating couplings lambda-prime and lambda-prime-prime from proton decay*, Phys. Lett. **B380** (1996) 317, arXiv: hep-ph/9601387 [hep-ph] (cit. on p. 9).

[185] H. N. Long and P. B. Pal, *Nucleon instability in a supersymmetric SU(3) C x SU(3)-L x U(1) model*, Mod. Phys. Lett. **A13** (1998) 2355, arXiv: hep-ph/9711455 [hep-ph] (cit. on p. 9).

[186] G. Bhattacharyya and P. B. Pal, *Upper bounds on all R-parity violating lambda lambda-prime-prime combinations from proton stability*, Phys. Rev. **D59** (1999) 097701, arXiv: hep-ph/9809493 [hep-ph] (cit. on p. 9).

[187] G. Bhattacharyya and P. B. Pal, *New constraints on R-parity violation from proton stability*, Phys. Lett. **B439** (1998) 81, arXiv: hep-ph/9806214 [hep-ph] (cit. on p. 9).

[188] D. Chang and W.-Y. Keung, *New limits on R-parity breakings in supersymmetric standard models*, Phys. Lett. **B389** (1996) 294, arXiv: hep-ph/9608313 [hep-ph] (cit. on p. 9).

[189] J. L. Goity and M. Sher, *Bounds on $\Delta B = 1$ couplings in the supersymmetric standard model*, Phys. Lett. **B346** (1995) 69, [Erratum: Phys. Lett.B385,500(1996)], arXiv: hep-ph/9412208 [hep-ph] (cit. on p. 9).

[190] B. C. Allanach, A. Dedes, and H. K. Dreiner, *Bounds on R-parity violating couplings at the weak scale and at the GUT scale*, Phys. Rev. **D60** (1999) 075014, arXiv: hep-ph/9906209 [hep-ph] (cit. on pp. 9, 21, 45).

[191] V. D. Barger, G. F. Giudice, and T. Han, *Some New Aspects of Supersymmetry R-Parity Violating Interactions*, Phys. Rev. **D40** (1989) 2987 (cit. on p. 9).

[192] G. Bhattacharyya, "A Brief review of R-parity violating couplings," *Beyond the desert 1997: Accelerator and non-accelerator approaches. Proceedings, 1st International Conference on Particle Physics beyond the Standard Model, Tegernsee, Ringberg Castle, Germany, June 8-14, 1997*, 1997 194, arXiv: hep-ph/9709395 [hep-ph] (cit. on p. 9).

[193] Y. Kao and T. Takeuchi, *Single-Coupling Bounds on R-parity violating Supersymmetry, an update*, (2009), arXiv: 0910.4980 [hep-ph] (cit. on pp. 9, 45–47).

[194] V. D. Barger, W. Y. Keung, and R. J. N. Phillips, *Possible sneutrino pair signatures with R-parity breaking*, Phys. Lett. **B364** (1995) 27, [Erratum: Phys. Lett.B381,486(1996)], arXiv: hep-ph/9507426 [hep-ph] (cit. on p. 10).

[195] T. Kon, T. Kobayashi, and S. Kitamura, *Signatures of scalar top with R-parity breaking coupling at HERA*, Phys. Lett. **B333** (1994) 263, arXiv: hep-ph/9403288 [hep-ph] (cit. on p. 10).

[196] E. A. Baltz and P. Gondolo, *Neutralino decay rates with explicit R-parity violation*, Phys. Rev. **D57** (1998) 2969, arXiv: hep-ph/9709445 [hep-ph] (cit. on p. 10).

[197] R. Barate et al., *Search for supersymmetry with a dominant R-parity violating L L anti-E coupling in e+ e- collisions at center-of-mass energies of 130-GeV to 172-GeV*, Eur. Phys. J. **C4** (1998) 433, arXiv: hep-ex/9712013 [hep-ex] (cit. on p. 10).

[198] J. P. Chou, D. Curtin, and H. J. Lubatti, *New Detectors to Explore the Lifetime Frontier*, Phys. Lett. **B767** (2017) 29, arXiv: 1606.06298 [hep-ph] (cit. on pp. 10, 37–39, 43).

[199] V. V. Gligorov et al., *Searching for Long-lived Particles: A Compact Detector for Exotics at LHCb*, (2017), arXiv: 1708.09395 [hep-ph] (cit. on pp. 10, 37–39, 41).

[200] J. Feng et al., *FASER: ForwArd Search ExpeRiment at the LHC*, (2017), arXiv: 1708.09389 [hep-ph] (cit. on pp. 10, 37–39, 42).

[201] V. V. Gligorov et al., *Leveraging the ALICE/L3 cavern for long-lived exotics*, (2018), arXiv: 1810.03636 [hep-ph] (cit. on pp. 10, 37, 39–41, 59).

[202] J. de Vries, H. K. Dreiner, and D. Schmeier,
R-Parity Violation and Light Neutralinos at SHiP and the LHC,
Phys. Rev. **D94** (2016) 035006, arXiv: 1511.07436 [hep-ph]
(cit. on pp. 10, 37, 38, 40, 44, 46, 48, 49, 57, 59).

[203] D. Dercks et al.,
R-parity Violation and Light Neutralinos at CODEX-b, FASER, and MATHUSLA, (2018),
arXiv: 1810.03617 [hep-ph] (cit. on pp. 10, 37, 59).

[204] J. C. Helo, M. Hirsch, and Z. S. Wang, *Heavy neutral fermions at the high-luminosity LHC*,
JHEP **07** (2018) 056, arXiv: 1803.02212 [hep-ph]
(cit. on pp. 10, 37, 39, 46, 47, 54, 58, 59).

[205] D. Dercks et al., *Long-Lived Fermions at AL3X*, (2018), arXiv: 1811.01995 [hep-ph]
(cit. on pp. 10, 37).

[206] W. Porod, *SPheno, a program for calculating supersymmetric spectra, SUSY particle decays and SUSY particle production at e+ e- colliders*, Comput. Phys. Commun. **153** (2003) 275,
arXiv: hep-ph/0301101 [hep-ph] (cit. on pp. 11, 17, 40, 45).

[207] W. Porod and F. Staub,
SPheno 3.1: Extensions including flavour, CP-phases and models beyond the MSSM,
Comput. Phys. Commun. **183** (2012) 2458, arXiv: 1104.1573 [hep-ph]
(cit. on pp. 11, 17, 40, 45).

[208] F. Staub and W. Porod,
Improved predictions for intermediate and heavy Supersymmetry in the MSSM and beyond,
Eur. Phys. J. **C77** (2017) 338, arXiv: 1703.03267 [hep-ph] (cit. on pp. 11, 17, 45).

[209] F. Staub, *SARAH*, (2008), arXiv: 0806.0538 [hep-ph] (cit. on pp. 11, 17, 45).

[210] F. Staub, *From Superpotential to Model Files for FeynArts and CalcHep/CompHep*,
Comput. Phys. Commun. **181** (2010) 1077, arXiv: 0909.2863 [hep-ph]
(cit. on pp. 11, 17, 45).

[211] F. Staub, *Automatic Calculation of supersymmetric Renormalization Group Equations and Self Energies*, Comput. Phys. Commun. **182** (2011) 808, arXiv: 1002.0840 [hep-ph]
(cit. on pp. 11, 17, 45).

[212] F. Staub, *SARAH 3.2: Dirac Gauginos, UFO output, and more*,
Comput. Phys. Commun. **184** (2013) 1792, arXiv: 1207.0906 [hep-ph]
(cit. on pp. 11, 17, 45).

[213] F. Staub, *SARAH 4 : A tool for (not only SUSY) model builders*,
Comput. Phys. Commun. **185** (2014) 1773, arXiv: 1309.7223 [hep-ph]
(cit. on pp. 11, 17, 45).

[214] F. Staub, *Exploring new models in all detail with SARAH*,
Adv. High Energy Phys. **2015** (2015) 840780, arXiv: 1503.04200 [hep-ph]
(cit. on pp. 11, 17, 45).

[215] W. Porod, F. Staub, and A. Vicente, *A Flavor Kit for BSM models*,
Eur. Phys. J. **C74** (2014) 2992, arXiv: 1405.1434 [hep-ph] (cit. on pp. 11, 17).

[216] D. Straub et al., *flav-io/flavio v0.23*, 2017,
URL: https://doi.org/10.5281/zenodo.897989 (cit. on pp. 11, 17).

[217] H. K. Dreiner, K. Nickel, and F. Staub,
$B^0_{s,d} \to \mu\overline{\mu}$ *and* $B \to X_s\gamma$ *in the R-parity violating MSSM*, Phys. Rev. **D88** (2013) 115001,
arXiv: 1309.1735 [hep-ph] (cit. on p. 11).

[218] W. Altmannshofer, A. J. Buras, and D. Guadagnoli,
The MFV limit of the MSSM for low tan(beta): Meson mixings revisited, JHEP **11** (2007) 065,
arXiv: hep-ph/0703200 [hep-ph] (cit. on pp. 11, 15).

[219] F. Gabbiani et al., *A Complete analysis of FCNC and CP constraints in general SUSY extensions of the standard model*, Nucl. Phys. **B477** (1996) 321,
arXiv: hep-ph/9604387 [hep-ph] (cit. on p. 11).

[220] R. Aaij et al., *A new algorithm for identifying the flavour of* B^0_s *mesons at LHCb*,
JINST **11** (2016) P05010, arXiv: 1602.07252 [hep-ex] (cit. on p. 12).

[221] R. Aaij et al.,
New algorithms for identifying the flavour of B^0 *mesons using pions and protons*,
Eur. Phys. J. **C77** (2017) 238, arXiv: 1610.06019 [hep-ex] (cit. on p. 12).

[222] R. Aaij et al., *Opposite-side flavour tagging of B mesons at the LHCb experiment*,
Eur. Phys. J. **C72** (2012) 2022, arXiv: 1202.4979 [hep-ex] (cit. on p. 12).

[223] R. Aaij et al., *B flavour tagging using charm decays at the LHCb experiment*,
JINST **10** (2015) P10005, arXiv: 1507.07892 [hep-ex] (cit. on p. 12).

[224] Y. Amhis et al., *Averages of b-hadron, c-hadron, and* τ*-lepton properties as of summer 2016*,
Eur. Phys. J. **C77** (2017) 895, arXiv: 1612.07233 [hep-ex] (cit. on p. 12).

[225] A. Lenz et al., *Anatomy of New Physics in* $B - \bar{B}$ *mixing*, Phys. Rev. **D83** (2011) 036004,
arXiv: 1008.1593 [hep-ph] (cit. on pp. 12, 18).

[226] A. Lenz and U. Nierste,
"Numerical Updates of Lifetimes and Mixing Parameters of B Mesons,"
CKM unitarity triangle. Proceedings, 6th International Workshop, CKM 2010, Warwick, UK, September 6-10, 2010, 2011, arXiv: 1102.4274 [hep-ph] (cit. on pp. 12, 18).

[227] M. Artuso, G. Borissov, and A. Lenz, *CP violation in the* B^0_s *system*,
Rev. Mod. Phys. **88** (2016) 045002, arXiv: 1511.09466 [hep-ph] (cit. on pp. 12, 18).

[228] L. Di Luzio, M. Kirk, and A. Lenz,
Updated B_s*-mixing constraints on new physics models for* $b \to s\ell^+\ell^-$ *anomalies*,
Phys. Rev. **D97** (2018) 095035, arXiv: 1712.06572 [hep-ph] (cit. on p. 12).

[229] A. Bazavov et al.,
$B^0_{(s)}$*-mixing matrix elements from lattice QCD for the Standard Model and beyond*,
Phys. Rev. **D93** (2016) 113016, arXiv: 1602.03560 [hep-lat] (cit. on pp. 12, 17, 18).

[230] C. Patrignani et al., *Review of Particle Physics*, Chin. Phys. **C40** (2016) 100001
(cit. on pp. 12, 17).

[231] J. Bijnens, J. M. Gerard, and G. Klein, *The K(L) - K(S) mass difference*,
Phys. Lett. **B257** (1991) 191 (cit. on p. 13).

[232] Z. Bai et al., *$K_L - K_S$ Mass Difference from Lattice QCD*, Phys. Rev. Lett. **113** (2014) 112003, arXiv: 1406.0916 [hep-lat] (cit. on p. 13).

[233] A. J. Buras and J. Girrbach, *Stringent tests of constrained Minimal Flavor Violation through ΔF =2 transitions*, Eur. Phys. J. **C73** (2013) 2560, arXiv: 1304.6835 [hep-ph] (cit. on pp. 13, 18).

[234] J. Brod and M. Gorbahn, *Next-to-Next-to-Leading-Order Charm-Quark Contribution to the CP Violation Parameter ϵ_K and ΔM_K*, Phys. Rev. Lett. **108** (2012) 121801, arXiv: 1108.2036 [hep-ph] (cit. on pp. 13, 17, 18).

[235] G. Buchalla, A. J. Buras, and M. E. Lautenbacher, *Weak decays beyond leading logarithms*, Rev. Mod. Phys. **68** (1996) 1125, arXiv: hep-ph/9512380 [hep-ph] (cit. on p. 13).

[236] A. J. Buras, S. Jager, and J. Urban, *Master formulae for Delta F=2 NLO QCD factors in the standard model and beyond*, Nucl. Phys. **B605** (2001) 600, arXiv: hep-ph/0102316 [hep-ph] (cit. on pp. 13, 17).

[237] K. Fujikawa, B. W. Lee, and A. I. Sanda, *Generalized Renormalizable Gauge Formulation of Spontaneously Broken Gauge Theories*, Phys. Rev. **D6** (1972) 2923 (cit. on p. 14).

[238] W. Siegel, *Supersymmetric dimensional regularization via dimensional reduction*, Physics Letters B **84** (1979) 193, ISSN: 0370-2693, URL: http://www.sciencedirect.com/science/article/pii/037026937990282X (cit. on p. 14).

[239] D. M. Capper, D. R. T. Jones, and P. van Nieuwenhuizen, *Regularization by Dimensional Reduction of Supersymmetric and Nonsupersymmetric Gauge Theories*, Nucl. Phys. **B167** (1980) 479 (cit. on p. 14).

[240] H. K. Dreiner and M. Thormeier, *Supersymmetric Froggatt-Nielsen models with baryon and lepton number violation*, Phys. Rev. **D69** (2004) 053002, arXiv: hep-ph/0305270 [hep-ph] (cit. on p. 14).

[241] B. C. Allanach, A. Dedes, and H. K. Dreiner, *R parity violating minimal supergravity model*, Phys. Rev. **D69** (2004) 115002, [Erratum: Phys. Rev.D72,079902(2005)], arXiv: hep-ph/0309196 [hep-ph] (cit. on pp. 14, 30).

[242] H. K. Dreiner, H. E. Haber, and S. P. Martin, *Two-component spinor techniques and Feynman rules for quantum field theory and supersymmetry*, Phys. Rept. **494** (2010) 1, arXiv: 0812.1594 [hep-ph] (cit. on p. 14).

[243] S. P. Martin, *Two loop scalar self energies in a general renormalizable theory at leading order in gauge couplings*, Phys. Rev. **D70** (2004) 016005, arXiv: hep-ph/0312092 [hep-ph] (cit. on p. 16).

[244] M. Goodsell, K. Nickel, and F. Staub, *Generic two-loop Higgs mass calculation from a diagrammatic approach*, Eur. Phys. J. **C75** (2015) 290, arXiv: 1503.03098 [hep-ph] (cit. on p. 17).

[245] T. Hahn and M. Perez-Victoria,
Automatized one loop calculations in four-dimensions and D-dimensions,
Comput. Phys. Commun. **118** (1999) 153, arXiv: hep-ph/9807565 [hep-ph]
(cit. on p. 17).

[246] T. Hahn, *Generating Feynman diagrams and amplitudes with FeynArts 3*,
Comput. Phys. Commun. **140** (2001) 418, arXiv: hep-ph/0012260 [hep-ph]
(cit. on p. 17).

[247] B. Chokoufe Nejad et al., *FormCalc 8: Better Algebra and Vectorization*,
J. Phys. Conf. Ser. **523** (2014) 012050, arXiv: 1310.0274 [hep-ph] (cit. on p. 17).

[248] F. Mahmoudi et al., *Flavour Les Houches Accord: Interfacing Flavour related Codes*,
Comput. Phys. Commun. **183** (2012) 285, arXiv: 1008.0762 [hep-ph] (cit. on p. 17).

[249] J. Brod and M. Gorbahn,
ε_K *at Next-to-Next-to-Leading Order: The Charm-Top-Quark Contribution*,
Phys. Rev. **D82** (2010) 094026, arXiv: 1007.0684 [hep-ph] (cit. on pp. 17, 18).

[250] N. Carrasco et al., $\Delta S = 2$ *and* $\Delta C = 2$ *bag parameters in the standard model and beyond from* N_f*=2+1+1 twisted-mass lattice QCD*, Phys. Rev. **D92** (2015) 034516,
arXiv: 1505.06639 [hep-lat] (cit. on pp. 17, 18).

[251] R. J. Dowdall et al., *B-Meson Decay Constants from Improved Lattice Nonrelativistic QCD with Physical u, d, s, and c Quarks*, Phys. Rev. Lett. **110** (2013) 222003,
arXiv: 1302.2644 [hep-lat] (cit. on p. 17).

[252] A. J. Buras, M. Jamin, and P. H. Weisz, *Leading and Next-to-leading QCD Corrections to* ϵ *Parameter and* $B^0 - \bar{B}^0$ *Mixing in the Presence of a Heavy Top Quark*,
Nucl. Phys. **B347** (1990) 491 (cit. on p. 18).

[253] G. D'Ambrosio et al., *Minimal flavor violation: An Effective field theory approach*,
Nucl. Phys. **B645** (2002) 155, arXiv: hep-ph/0207036 [hep-ph] (cit. on p. 19).

[254] J. E. Camargo-Molina et al., **Vevacious***: A Tool For Finding The Global Minima Of One-Loop Effective Potentials With Many Scalars*, Eur. Phys. J. **C73** (2013) 2588,
arXiv: 1307.1477 [hep-ph] (cit. on p. 20).

[255] C. L. Wainwright, *CosmoTransitions: Computing Cosmological Phase Transition Temperatures and Bubble Profiles with Multiple Fields*,
Comput. Phys. Commun. **183** (2012) 2006, arXiv: 1109.4189 [hep-ph] (cit. on p. 20).

[256] B. C. Allanach, A. Dedes, and H. K. Dreiner, *Two loop supersymmetric renormalization group equations including R-parity violation and aspects of unification*,
Phys. Rev. **D60** (1999) 056002, [Erratum: Phys. Rev.D86,039906(2012)],
arXiv: hep-ph/9902251 [hep-ph] (cit. on pp. 30, 32).

[257] R. Essig et al., "Working Group Report: New Light Weakly Coupled Particles,"
Proceedings, 2013 Community Summer Study on the Future of U.S. Particle Physics: Snowmass on the Mississippi (CSS2013): Minneapolis, MN, USA, July 29-August 6, 2013,
2013, arXiv: 1311.0029 [hep-ph], URL: http://www.slac.stanford.edu/econf/C1307292/docs/IntensityFrontier/NewLight-17.pdf (cit. on p. 37).

[258] S. Alekhin et al.,
A facility to Search for Hidden Particles at the CERN SPS: the SHiP physics case,
Rept. Prog. Phys. **79** (2016) 124201, arXiv: 1504.04855 [hep-ph] (cit. on pp. 37, 38).

[259] C. Adams et al.,
The Long-Baseline Neutrino Experiment: Exploring Fundamental Symmetries of the Universe,
(2013), arXiv: 1307.7335 [hep-ex] (cit. on p. 37).

[260] E. Cortina Gil et al., *The Beam and detector of the NA62 experiment at CERN*,
JINST **12** (2017) P05025, arXiv: 1703.08501 [physics.ins-det] (cit. on p. 37).

[261] S. Chatrchyan et al.,
Search in leptonic channels for heavy resonances decaying to long-lived neutral particles,
JHEP **02** (2013) 085, arXiv: 1211.2472 [hep-ex] (cit. on p. 37).

[262] G. Aad et al., *Search for a light Higgs boson decaying to long-lived weakly-interacting particles in proton-proton collisions at $\sqrt{s} = 7$ TeV with the ATLAS detector*,
Phys. Rev. Lett. **108** (2012) 251801, arXiv: 1203.1303 [hep-ex] (cit. on p. 37).

[263] P. Ilten et al., *Dark photons from charm mesons at LHCb*, Phys. Rev. **D92** (2015) 115017,
arXiv: 1509.06765 [hep-ph] (cit. on p. 37).

[264] CERN, *The High-Luminosity LHC*,
CERN document server http://cds.cern.ch/record/2114693 (2015) (cit. on p. 37).

[265] R. Aaij et al., *Expression of Interest for a Phase-II LHCb Upgrade: Opportunities in flavour physics, and beyond, in the HL-LHC era*, tech. rep. CERN-LHCC-2017-003, CERN, 2017,
URL: http://cds.cern.ch/record/2244311 (cit. on p. 37).

[266] J. L. Feng et al., *Dark Higgs Bosons at FASER*, (2017), arXiv: 1710.09387 [hep-ph]
(cit. on pp. 38, 42).

[267] F. Kling and S. Trojanowski, *Heavy Neutral Leptons at FASER*, (2018),
arXiv: 1801.08947 [hep-ph] (cit. on pp. 38, 42).

[268] J. L. Feng et al., *ALPs at FASER: The LHC as a Photon Beam Dump*, (2018),
arXiv: 1806.02348 [hep-ph] (cit. on pp. 38, 42).

[269] J. A. Evans, *Detecting Hidden Particles with MATHUSLA*, Phys. Rev. **D97** (2018) 055046,
arXiv: 1708.08503 [hep-ph] (cit. on p. 38).

[270] D. Curtin and M. E. Peskin,
Analysis of Long Lived Particle Decays with the MATHUSLA Detector,
Phys. Rev. **D97** (2018) 015006, arXiv: 1705.06327 [hep-ph] (cit. on p. 38).

[271] D. Curtin, K. R. Dienes, and B. Thomas,
Dynamical Dark Matter, MATHUSLA, and the Lifetime Frontier, (2018),
arXiv: 1809.11021 [hep-ph] (cit. on p. 38).

[272] D. Curtin et al., *Long-Lived Particles at the Energy Frontier: The MATHUSLA Physics Case*,
(2018), arXiv: 1806.07396 [hep-ph] (cit. on pp. 38, 41).

[273] A. Berlin and F. Kling, *Inelastic Dark Matter at the LHC Lifetime Frontier: ATLAS, CMS, LHCb, CODEX-b, FASER, and MATHUSLA*, (2018), arXiv: 1810.01879 [hep-ph]
(cit. on p. 38).

[274] D. Choudhury et al., *A Supersymmetric solution to the KARMEN time anomaly*, Phys. Rev. **D61** (2000) 095009, arXiv: hep-ph/9911365 [hep-ph] (cit. on pp. 38, 39, 44, 48).

[275] H. K. Dreiner et al., *Supernovae and light neutralinos: SN1987A bounds on supersymmetry revisited*, Phys. Rev. **D68** (2003) 055004, arXiv: hep-ph/0304289 [hep-ph] (cit. on pp. 38, 39).

[276] H. K. Dreiner, O. Kittel, and U. Langenfeld, *Discovery potential of radiative neutralino production at the ILC*, Phys. Rev. **D74** (2006) 115010, arXiv: hep-ph/0610020 [hep-ph] (cit. on p. 38).

[277] H. K. Dreiner et al., *Mass Bounds on a Very Light Neutralino*, Eur. Phys. J. **C62** (2009) 547, arXiv: 0901.3485 [hep-ph] (cit. on pp. 38, 44, 47, 48).

[278] A. Atre et al., *The Search for Heavy Majorana Neutrinos*, JHEP **05** (2009) 030, arXiv: 0901.3589 [hep-ph] (cit. on pp. 38, 40).

[279] G. Aad et al., *Search for heavy Majorana neutrinos with the ATLAS detector in pp collisions at $\sqrt{s}$ = 8 TeV*, JHEP **07** (2015) 162, arXiv: 1506.06020 [hep-ex] (cit. on p. 38).

[280] A. M. Sirunyan et al., *Search for heavy neutral leptons in events with three charged leptons in proton-proton collisions at $\sqrt{s}$ = 13 TeV*, (2018), arXiv: 1802.02965 [hep-ex] (cit. on p. 38).

[281] P. Abreu et al., *Search for neutral heavy leptons produced in Z decays*, Z. Phys. **C74** (1997) 57, [Erratum: Z. Phys.C75,580(1997)] (cit. on pp. 38, 59).

[282] J. C. Helo, M. Hirsch, and S. Kovalenko, *Heavy neutrino searches at the LHC with displaced vertices*, Phys. Rev. **D89** (2014) 073005, [Erratum: Phys. Rev.D93,no.9,099902(2016)], arXiv: 1312.2900 [hep-ph] (cit. on p. 38).

[283] A. M. Sirunyan et al., *Search for new long-lived particles at $\sqrt{s}$ = 13 TeV*, (2017), arXiv: 1711.09120 [hep-ex] (cit. on p. 38).

[284] G. Cottin, J. C. Helo, and M. Hirsch, *Searches for light sterile neutrinos with multitrack displaced vertices*, (2018), arXiv: 1801.02734 [hep-ph] (cit. on p. 38).

[285] D. Gorbunov and I. Timiryasov, *Decaying light particles in the SHiP experiment. II. Signal rate estimates for light neutralinos*, Phys. Rev. **D92** (2015) 075015, arXiv: 1508.01780 [hep-ph] (cit. on p. 38).

[286] R. Aaij et al., *Measurements of prompt charm production cross-sections in pp collisions at $\sqrt{s}$ = 13 TeV*, JHEP **03** (2016) 159, [Erratum: JHEP05,074(2017)], arXiv: 1510.01707 [hep-ex] (cit. on p. 39).

[287] R. Aaij et al., *Measurement of the b-quark production cross-section in 7 and 13 TeV pp collisions*, Phys. Rev. Lett. **118** (2017) 052002, [Erratum: Phys. Rev. Lett.119,no.16,169901(2017)], arXiv: 1612.05140 [hep-ex] (cit. on p. 39).

[288] G. Aad et al., *Measurement of $W^{\pm}$ and Z-boson production cross sections in pp collisions at $\sqrt{s}$ = 13 TeV with the ATLAS detector*, Phys. Lett. **B759** (2016) 601, arXiv: 1603.09222 [hep-ex] (cit. on p. 39).

[289] M. Tanabashi et al., *Review of Particle Physics*, Phys. Rev. **D98** (2018) 030001 (cit. on p. 39).

[290] T. Sjostrand, S. Mrenna, and P. Z. Skands, *PYTHIA 6.4 Physics and Manual*, JHEP **05** (2006) 026, arXiv: hep-ph/0603175 [hep-ph] (cit. on p. 40).

[291] T. Sjöstrand et al., *An Introduction to PYTHIA 8.2*, Comput. Phys. Commun. **191** (2015) 159, arXiv: 1410.3012 [hep-ph] (cit. on p. 40).

[292] M. Cacciari, M. Greco, and P. Nason, *The P(T) spectrum in heavy flavor hadroproduction*, JHEP **05** (1998) 007, arXiv: hep-ph/9803400 [hep-ph] (cit. on p. 40).

[293] M. Cacciari, S. Frixione, and P. Nason, *The p(T) spectrum in heavy flavor photoproduction*, JHEP **03** (2001) 006, arXiv: hep-ph/0102134 [hep-ph] (cit. on p. 40).

[294] M. Cacciari et al., *Theoretical predictions for charm and bottom production at the LHC*, JHEP **10** (2012) 137, arXiv: 1205.6344 [hep-ph] (cit. on p. 40).

[295] M. Cacciari, M. L. Mangano, and P. Nason, *Gluon PDF constraints from the ratio of forward heavy-quark production at the LHC at $\sqrt{S}$ = 7 and 13 TeV*, Eur. Phys. J. **C75** (2015) 610, arXiv: 1507.06197 [hep-ph] (cit. on p. 40).

[296] C. Patrignani et al., *Review of Particle Physics*, Chin. Phys. **C40** (2016) 100001 (cit. on pp. 44, 45).

[297] H. K. Dreiner, M. Hanussek, and C. Luhn, *What is the discrete gauge symmetry of the R-parity violating MSSM?* Phys. Rev. **D86** (2012) 055012, arXiv: 1206.6305 [hep-ph] (cit. on p. 44).

[298] H. K. Dreiner et al., *Baryon triality and neutrino masses from an anomalous flavor U(1)*, Nucl. Phys. **B774** (2007) 127, arXiv: hep-ph/0610026 [hep-ph] (cit. on p. 44).

[299] F. de Campos et al., *Probing bilinear R-parity violating supergravity at the LHC*, JHEP **05** (2008) 048, arXiv: 0712.2156 [hep-ph] (cit. on p. 44).

[300] K. Desch et al., *Stau as the Lightest Supersymmetric Particle in R-Parity Violating SUSY Models: Discovery Potential with Early LHC Data*, Phys. Rev. **D83** (2011) 015013, arXiv: 1008.1580 [hep-ph] (cit. on p. 44).

[301] A. Dedes, H. K. Dreiner, and P. Richardson, *Attempts at explaining the NuTeV observation of dimuon events*, Phys. Rev. **D65** (2001) 015001, arXiv: hep-ph/0106199 [hep-ph] (cit. on pp. 44, 48).

[302] H. K. Dreiner et al., *Rare meson decays into very light neutralinos*, Phys. Rev. **D80** (2009) 035018, arXiv: 0905.2051 [hep-ph] (cit. on p. 45).

[303] A. Bartl, W. Majerotto, and N. Oshimo, *On the Production of Neutralinos at the Z and W and Their Decay Into Higgs Bosons*, Phys. Lett. **B216** (1989) 233 (cit. on p. 45).

[304] G. Aad et al., *Search for invisible decays of a Higgs boson using vector-boson fusion in pp collisions at $\sqrt{s}$ = 8 TeV with the ATLAS detector*, JHEP **01** (2016) 172, arXiv: 1508.07869 [hep-ex] (cit. on p. 45).

[305] M. Aaboud et al.,
Search for an invisibly decaying Higgs boson or dark matter candidates produced in association with a Z boson in pp collisions at $\sqrt{s}$ = 13 TeV with the ATLAS detector,
Phys. Lett. **B776** (2018) 318, arXiv: 1708.09624 [hep-ex] (cit. on p. 45).

[306] P. F. de Salas et al., *Status of neutrino oscillations 2017*, (2017),
arXiv: 1708.01186 [hep-ph] (cit. on pp. 57, 58).

[307] R. Mohapatra and J. Valle,
Neutrino Mass and Baryon Number Nonconservation in Superstring Models,
Phys. Rev. **D34** (1986) 1642 (cit. on p. 58).

[308] J. A. Casas and A. Ibarra, *Oscillating neutrinos and muon —> e, gamma*,
Nucl. Phys. **B618** (2001) 171, arXiv: hep-ph/0103065 [hep-ph] (cit. on p. 58).

[309] G. Anamiati, M. Hirsch, and E. Nardi, *Quasi-Dirac neutrinos at the LHC*,
JHEP **10** (2016) 010, arXiv: 1607.05641 [hep-ph] (cit. on p. 58).

[310] F. F. Deppisch, P. S. Bhupal Dev, and A. Pilaftsis, *Neutrinos and Collider Physics*,
New J. Phys. **17** (2015) 075019, arXiv: 1502.06541 [hep-ph] (cit. on p. 59).

[311] G. Bernardi et al., *FURTHER LIMITS ON HEAVY NEUTRINO COUPLINGS*,
Phys. Lett. **B203** (1988) 332 (cit. on p. 59).

[312] S. A. Baranov et al., *Search for heavy neutrinos at the IHEP-JINR neutrino detector*,
Phys. Lett. **B302** (1993) 336 (cit. on p. 59).

[313] F. Bergsma et al.,
A Search for Decays of Heavy Neutrinos in the Mass Range 0.5-GeV to 2.8-GeV,
Phys. Lett. **166B** (1986) 473 (cit. on p. 59).

[314] K. Bondarenko et al., *Phenomenology of GeV-scale Heavy Neutral Leptons*, (2018),
arXiv: 1805.08567 [hep-ph] (cit. on p. 59).

[315] A. Abada et al.,
Lepton flavor violation in low-scale seesaw models: SUSY and non-SUSY contributions,
JHEP **11** (2014) 048, arXiv: 1408.0138 [hep-ph] (cit. on p. 95).

APPENDIX A

Analytic Expressions of Wilson Coefficients for RpV contributions to meson oscillation

A.1 Notations

A.1.1 Mixing matrices

- The squark mass matrices mix left- and right-handed components. We define the mass-eigenstates in terms of a unitary rotation of the gauge/flavor-eigenstates:

$$\begin{cases} U_\alpha = X^{U_L}_{\alpha f}\, U^f_L + X^{U_R}_{\alpha f}\, \bar{U}^{f\,*}_R \\ D_\alpha = X^{D_L}_{\alpha f}\, D^f_L + X^{D_R}_{\alpha f}\, \bar{D}^{f\,*}_R \end{cases} \tag{A.1}$$

  Here, U_α (resp. D_α) represents the scalar-up (resp. sdown) mass state with mass m_{U_α} (resp. m_{D_α}). Summation over the generation index f is implicit.

- R-parity violation leads to a mixing of charged-Higgs and slepton fields. We define the mass-eigenstates $H^\pm_\alpha$ with mass m_{H_α} as:

$$H^-_\alpha = X^C_{\alpha u}\, H^-_u + X^C_{\alpha d}\, H^-_d + X^C_{\alpha E^f_L}\, E^f_L + X^C_{\alpha E^f_R}\, \bar{E}^{f\,*}_R\,. \tag{A.2}$$

- Similarly, the neutral Higgs mass-states involve both the doublet-Higgs, $H^0_u = v_u + \frac{h^0_u + \imath\, a^0_u}{\sqrt{2}}$ and $H^0_d = v_d + \frac{h^0_d + \imath\, a^0_d}{\sqrt{2}}$, and the sneutrino fields, $N^f_L = \frac{h^0_{N_f} + \imath\, a^0_{N_f}}{\sqrt{2}}$; in the CP-violating case, CP-even and CP-odd components mix as well.

$$S_\alpha = X^R_{\alpha u}\, h^0_u + X^R_{\alpha d}\, h^0_d + X^R_{\alpha N_f}\, h^0_{N_f} + X^I_{\alpha u}\, a^0_u + X^I_{\alpha d}\, a^0_d + X^I_{\alpha N_f}\, a^0_{N_f}\,. \tag{A.3}$$

  S_α denotes the mass-eigenstate associated with the mass m_{S_α}.

- The charged winos $\tilde{w}^+$, $\tilde{w}^-$, higgsinos $\tilde{h}^+_u$, $\tilde{h}^-_d$ and lepton fields e^f_L, $\bar{e}^f_R$ define the chargino sector.

For the mass $m_{\chi_k^\pm}$, the associated eignstate is given by:

$$\begin{cases} \chi_k^+ = V_{kw}\,\tilde{w}^+ + V_{ku}\,\tilde{h}_u^+ + V_{ke_f}\,\bar{e}_R^f\,, \\ \chi_k^- = U_{kw}\,\tilde{w}^- + U_{kd}\,\tilde{h}_d^- + U_{ke_f}\,e_L^f\,. \end{cases} \tag{A.4}$$

- The violation of R-parity also mixes neutrino and neutralino states. The eigenstate with mass $m_{\chi_k^0}$ reads:

$$\chi_k^0 = N_{kb}\,\tilde{b}^0 + N_{kw}\,\tilde{w}^0 + N_{ku}\,\tilde{h}_u^0 + N_{kd}\,\tilde{h}_d^0 + N_{k\nu_f}\,\nu_L^f\,. \tag{A.5}$$

A.1.2 Feynman rules

Here, we list the various couplings that are relevant in our calculation. The combinatorial factors appearing in the lagrangian density in the case of identical coupling particles have been explicitly factored out, e.g. $\mathcal{L} \ni -\frac{g^{S_\alpha ZZ}}{2} S_\alpha ZZ$.

- Neutral-Higgs-sneutrinos / down quarks:

$$g_L^{S_\alpha d_k d_i} = -\frac{1}{\sqrt{2}}\left[Y_d^i \delta_{ki}(X_{\alpha d}^R + \imath X_{\alpha d}^I) + \lambda'_{fik}(X_{\alpha N_L^f}^R + \imath X_{\alpha N_L^f}^I)\right] = (g_R^{S_\alpha d_i d_k})^* \tag{A.6}$$

- Charged-Higgs-sleptons / quarks:

$$g_L^{H_\alpha u_k d_i} = -Y_u^k V_{ki}^{CKM} X_{\alpha u}^C\,; \quad g_R^{H_\alpha u_k d_i} = -Y_d^i V_{ki}^{CKM} X_{\alpha d}^C - \lambda'^*_{fli} V_{kl}^{CKM} X_{\alpha E_L^f}^C \tag{A.7}$$

- sdowns / neutralino-neutrinos / down quarks:

$$\begin{aligned} g_L^{D_\alpha \chi_k d_i} &= -\frac{1}{\sqrt{2}}\left(\frac{g'}{3} N_{k\tilde{b}}^* - g N_{k\tilde{w}}^*\right) X_{\alpha i}^{D_L} - Y_d^i N_{kd}^* X_{\alpha i}^{D_R} - \lambda'_{fi\beta} N_{k\nu_f}^* X_{\alpha\beta}^{D_R} \\ g_R^{D_\alpha \chi_k d_i} &= -\frac{\sqrt{2}}{3} g' N_{k\tilde{b}} X_{\alpha i}^{D_R} - Y_d^i N_{kd} X_{\alpha i}^{D_L} - \lambda'^*_{f\beta i} N_{k\nu_f} X_{\alpha\beta}^{D_L} \end{aligned} \tag{A.8}$$

- sdowns / gluinos / down quarks (T^A are the colour Gell-Mann matrices):

$$g_L^{D_\alpha^a \tilde{g}^A d_i^b} = -\sqrt{2} g_s e^{-\imath\phi_{M_3}/2} X_{\alpha i}^{D_L} T_{ab}^A \quad ; \quad g_R^{D_\alpha^a \tilde{g}^A d_i^b} = \sqrt{2} g_s e^{\imath\phi_{M_3}/2} X_{\alpha i}^{D_R} T_{ab}^A \tag{A.9}$$

- scalar-ups / chargino-leptons / down quarks:

$$\begin{aligned} g_L^{U_\alpha \chi_k d_i} &= V_{\beta i}^{CKM}\left[Y_u^\beta V_{ku}^* X_{\alpha\beta}^{U_R} - g V_{k\tilde{w}}^* X_{\alpha\beta}^{U_L}\right] \\ g_R^{U_\alpha \chi_k d_i} &= V_{\beta f}^{CKM}\left[Y_d^i \delta_{if} U_{kd} X_{\alpha\beta}^{U_L} + \lambda'^*_{lfi} U_{ke_l} X_{\alpha\beta}^{U_L}\right] \end{aligned} \tag{A.10}$$

- scalar-ups / down quarks (a, b, c: colour-indices):

$$g_L^{U_\alpha^a d_k^b d_i^c} = 0 \quad ; \quad g_R^{U_\alpha^a d_k^b d_i^c} = \varepsilon_{abc} \lambda''^*_{fki} X_{\alpha f}^{U_R} \tag{A.11}$$

- sdowns / up / down quarks (a, b, c: colour-indices):

$$g_L^{D_\alpha^a u_k^b d_i^c} = 0 \quad ; \quad g_R^{D_\alpha^a u_k^b d_i^c} = \varepsilon_{bac} \lambda''^*_{kfi} X^{D_R}_{\alpha f} \tag{A.12}$$

- W / up / down quarks:

$$g_L^{W u_k d_i} = \frac{g}{\sqrt{2}} V_{ki}^{CKM} \quad ; \quad g_R^{W u_k d_i} = 0 \tag{A.13}$$

- Z / down quarks:

$$g_L^{Z d_k d_i} = \frac{\sqrt{g'^2 + g^2}}{2} \left(-1 + \frac{2}{3} s_W^2 \right) \delta_{ik} \quad ; \quad g_R^{Z d_k d_i} = \frac{\sqrt{g'^2 + g^2}}{3} s_W^2 \delta_{ik} \tag{A.14}$$

- Neutral-Higgs-sneutrinos / up quarks:

$$g_L^{S_\alpha u_j u_k} = -\frac{Y_u^j}{\sqrt{2}} \delta_{jk} \left(X^R_{\alpha u} + \imath X^I_{\alpha u} \right) = \left(g_R^{S_\alpha u_k u_j} \right)^* \tag{A.15}$$

- Neutral-Higgs-sneutrinos / charginos-leptons:

$$\begin{aligned} g_L^{S_\alpha \chi_j^+ \chi_k^-} = -\frac{1}{\sqrt{2}} \Big\{ & Y_e^f \left[\left(X^R_{\alpha d} + \imath X^I_{\alpha d} \right) V^*_{j e_f} U^*_{k e_f} - \left(X^R_{\alpha \tilde{N}_f} + \imath X^I_{\alpha \tilde{N}_f} \right) V^*_{j e_f} U^*_{k d} \right] \\ & + g \left[\left(X^R_{\alpha u} - \imath X^I_{\alpha u} \right) V^*_{j u} U^*_{k w} + \left(X^R_{\alpha d} - \imath X^I_{\alpha d} \right) V^*_{j w} U^*_{k d} + \left(X^R_{\alpha \tilde{N}_f} - \imath X^I_{\alpha \tilde{N}_f} \right) V^*_{j w} U^*_{k e_f} \right] \\ & + \lambda_{f m n} \left(X^R_{\alpha \tilde{N}_f} + \imath X^I_{\alpha \tilde{N}_f} \right) V^*_{j e_n} U^*_{k e_m} \Big\} = \left(g_R^{S_\alpha \chi_k^+ \chi_j^-} \right)^* \end{aligned} \tag{A.16}$$

- Neutral-Higgs-sneutrinos / neutrino-neutralinos:

$$\begin{aligned} g_L^{S_\alpha \chi_j^0 \chi_k^0} = -\frac{g'}{2} \Big[& \left(X^R_{\alpha u} - \imath X^I_{\alpha u} \right) \left(N^*_{j u} N^*_{k b} + N^*_{j b} N^*_{k u} \right) - \left(X^R_{\alpha d} - \imath X^I_{\alpha d} \right) \left(N^*_{j d} N^*_{k b} + N^*_{k d} N^*_{j b} \right) \\ & - \left(X^R_{\alpha \tilde{N}_f} - \imath X^I_{\alpha \tilde{N}_f} \right) \left(N^*_{j \nu_f} N^*_{k b} + N^*_{k \nu_f} N^*_{j b} \right) \Big] \\ + \frac{g}{2} \Big[& \left(X^R_{\alpha u} - \imath X^I_{\alpha u} \right) \left(N^*_{j u} N^*_{k w} + N^*_{j w} N^*_{k u} \right) - \left(X^R_{\alpha d} - \imath X^I_{\alpha d} \right) \left(N^*_{j d} N^*_{k w} + N^*_{k d} N^*_{j w} \right) \\ & - \left(X^R_{\alpha \tilde{N}_f} - \imath X^I_{\alpha \tilde{N}_f} \right) \left(N^*_{j \nu_f} N^*_{k w} + N^*_{k \nu_f} N^*_{j w} \right) \Big] = \left(g_R^{S_\alpha \chi_k^0 \chi_j^0} \right)^* \end{aligned} \tag{A.17}$$

- Neutral-Higgs-sneutrinos / W's:

$$g^{S_\alpha W W} = \frac{g^2}{\sqrt{2}} \left(v_u X^R_{\alpha u} + v_d X^R_{\alpha d} \right) \tag{A.18}$$

- Neutral-Higgs-sneutrinos / Z's:

$$g^{S_\alpha ZZ} = \frac{g'^2 + g^2}{\sqrt{2}} \left(v_u X^R_{\alpha u} + v_d X^R_{\alpha d} \right) \tag{A.19}$$

- Neutral-Higgs-sneutrinos / W-ghosts $g^\pm_W$'s:

$$g^{S_\alpha g_W g_W} = -\frac{g^2}{2\sqrt{2}} \left[v_u (X^R_{\alpha u} + \imath X^I_{\alpha u}) + v_d (X^R_{\alpha d} - \imath X^I_{\alpha d}) \right] \tag{A.20}$$

- Neutral-Higgs-sneutrinos / Z-ghosts g_Z's:

$$g^{S_\alpha g_Z g_Z} = -\frac{g'^2 + g^2}{2\sqrt{2}} \left[v_u X^R_{\alpha u} + v_d X^R_{\alpha d} \right] \tag{A.21}$$

- Neutral-Higgs-sneutrinos / W / Charged-Higgs-sleptons:

$$g^{S_\alpha W H_k} = \frac{g}{2} \left[(X^R_{\alpha d} - \imath X^I_{\alpha d}) X^{C\,*}_{kd} - (X^R_{\alpha u} + \imath X^I_{\alpha u}) X^{C\,*}_{ku} + (X^R_{\alpha \tilde{N}_f} - \imath X^I_{\alpha \tilde{N}_f}) X^{C\,*}_{k \tilde{E}^f_L} \right] \tag{A.22}$$

- Neutral-Higgs-sneutrinos / Z / Neutral-Higgs-sneutrinos:

$$g^{S_\alpha Z S_k} = \imath \frac{\sqrt{g'^2 + g^2}}{2} \left[X^R_{\alpha d} X^I_{kd} - X^I_{\alpha d} X^R_{kd} - X^R_{\alpha u} X^I_{ku} + X^I_{\alpha u} X^R_{ku} + X^R_{\alpha \tilde{N}_f} X^I_{k \tilde{N}_f} - X^I_{\alpha \tilde{N}_f} X^R_{k \tilde{N}_f} \right] \tag{A.23}$$

- Neutral-Higgs-sneutrinos / scalar-ups:

$$\begin{aligned} g^{\tilde{U}_k \tilde{U}_l S_\alpha} = & -\sqrt{2} \left[Y^{f\,2}_u v_u X^R_{\alpha u} + \frac{1}{4} \left(\frac{g'^2}{3} - g^2 \right) (v_u X^R_{\alpha u} - v_d X^R_{\alpha d}) \right] X^{\tilde{U}_f}_{kL} X^{\tilde{U}_f\,*}_{lL} \\ & - \sqrt{2} \left[Y^{f\,2}_u v_u X^R_{\alpha u} - \frac{g'^2}{3} (v_u X^R_{\alpha u} - v_d X^R_{\alpha d}) \right] X^{\tilde{U}_f}_{kR} X^{\tilde{U}_f\,*}_{lR} \\ & - \frac{1}{\sqrt{2}} \left[A^{ff'}_u (X^R_{\alpha u} + \imath X^I_{\alpha u}) - \mu^* Y^f_u \delta_{ff'} (X^R_{\alpha d} - \imath X^I_{\alpha d}) \right] X^{\tilde{U}_{f'}}_{kR} X^{\tilde{U}_f\,*}_{lL} \\ & - \frac{1}{\sqrt{2}} \left[A^{ff'\,*}_u (X^R_{\alpha u} - \imath X^I_{\alpha u}) - \mu Y^f_u \delta_{ff'} (X^R_{\alpha d} + \imath X^I_{\alpha d}) \right] X^{\tilde{U}_f}_{kL} X^{\tilde{U}_{f'}\,*}_{lR} \end{aligned} \tag{A.24}$$

- Neutral-Higgs-sneutrinos / sdowns:

$$
\begin{aligned}
g^{\tilde{D}_k \tilde{D}_l S_\alpha} = &-\sqrt{2}\left[Y_d^{f\,2} v_d X^R_{\alpha d} + \frac{1}{4}\left(\frac{g'^2}{3} + g^2\right)(v_u X^R_{\alpha u} - v_d X^R_{\alpha d})\right] X^{\tilde{D}_f}_{kL} X^{\tilde{D}_f\,*}_{lL} \\
&- \frac{v_d}{\sqrt{2}}\left[Y_d^f \lambda'^*_{ghf}(X^R_{\alpha \tilde{N}_g} - \imath X^I_{\alpha \tilde{N}_g}) + Y_d^h \lambda'_{gfh}(X^R_{\alpha \tilde{N}_g} + \imath X^I_{\alpha \tilde{N}_g})\right] X^{\tilde{D}_h}_{kL} X^{\tilde{D}_f\,*}_{lL} \\
&- \sqrt{2}\left[Y_d^{f\,2} v_d X^R_{\alpha d} + \frac{g'^2}{6}(v_u X^R_{\alpha u} - v_d X^R_{\alpha d})\right] X^{\tilde{D}_f}_{kR} X^{\tilde{D}_f\,*}_{lR} \\
&- \frac{v_d}{\sqrt{2}}\left[Y_d^f \lambda'^*_{gfh}(X^R_{\alpha \tilde{N}_g} - \imath X^I_{\alpha \tilde{N}_g}) + Y_d^h \lambda'_{ghf}(X^R_{\alpha \tilde{N}_g} + \imath X^I_{\alpha \tilde{N}_g})\right] X^{\tilde{D}_f}_{kR} X^{\tilde{D}_h\,*}_{lR} \\
&- \frac{1}{\sqrt{2}}\left[A_d^{ff'}(X^R_{\alpha d} + \imath X^I_{\alpha d}) - \mu^* Y_d^f \delta_{ff'}(X^R_{\alpha u} - \imath X^I_{\alpha u}) + A'_{gff'}(X^R_{\alpha \tilde{N}_g} + \imath X^I_{\alpha \tilde{N}_g})\right] X^{\tilde{D}_{f'}}_{kR} X^{\tilde{D}_f\,*}_{lL} \\
&- \frac{1}{\sqrt{2}}\left[A_d^{ff'\,*}(X^R_{\alpha d} - \imath X^I_{\alpha d}) - \mu Y_d^f \delta_{ff'}(X^R_{\alpha u} + \imath X^I_{\alpha u}) + A'^*_{gff'}(X^R_{\alpha \tilde{N}_g} - \imath X^I_{\alpha \tilde{N}_g})\right] X^{\tilde{D}_f}_{kL} X^{\tilde{D}_{f'}\,*}_{lR}
\end{aligned}
\tag{A.25}
$$

- Neutral-Higgs-sneutrinos / Charged Higgs-sleptons

$$
\begin{aligned}
g^{H_k H_l S_\alpha} = -\sqrt{2}\Bigg\{ & \left[Y_e^{f\,2} v_d X^R_{\alpha d} + \frac{1}{4}\left(-g'^2 + g^2\right)(v_u X^R_{\alpha u} - v_d X^R_{\alpha d}) \right] \delta_{ff'} \\
& - \frac{v_d}{2}\left[Y_e^{f'} \lambda^*_{fgf'} (X^R_{\alpha \tilde{N}_g} - \imath X^I_{\alpha \tilde{N}_g}) + Y_e^{f} \lambda_{f'gf} (X^R_{\alpha \tilde{N}_g} + \imath X^I_{\alpha \tilde{N}_g}) \right] \Bigg\} X^C_{k\tilde{E}^f_L} X^{C\,*}_{l\tilde{E}^{f'}_L} \\
& - \sqrt{2}\Bigg\{ \left[Y_e^{f\,2} v_d X^R_{\alpha d} + \frac{g'^2}{2}(v_u X^R_{\alpha u} - v_d X^R_{\alpha d}) \right] \delta_{ff'} \\
& - \frac{v_d}{2}\left[Y_e^{f} \lambda^*_{fgf'} (X^R_{\alpha \tilde{N}_g} - \imath X^I_{\alpha \tilde{N}_g}) + Y_e^{f'} \lambda_{f'gf} (X^R_{\alpha \tilde{N}_g} + \imath X^I_{\alpha \tilde{N}_g}) \right] \Bigg\} X^C_{k\tilde{E}^f_R} X^{C\,*}_{l\tilde{E}^{f'}_R} \\
& - \frac{1}{\sqrt{2}}\left[A_e^{f'f} (X^R_{\alpha d} + \imath X^I_{\alpha d}) - \mu^* Y_e^f \delta_{ff'} (X^R_{\alpha u} - \imath X^I_{\alpha u}) + A_{gf'f} (X^R_{\alpha \tilde{N}_g} + \imath X^I_{\alpha \tilde{N}_g}) \right] X^C_{k\tilde{E}^f_R} X^{C\,*}_{l\tilde{E}^{f'}_L} \\
& - \frac{1}{\sqrt{2}}\left[A_e^{ff'\,*} (X^R_{\alpha d} - \imath X^I_{\alpha d}) - \mu Y_e^f \delta_{ff'} (X^R_{\alpha u} + \imath X^I_{\alpha u}) + A^*_{gff'} (X^R_{\alpha \tilde{N}_g} - \imath X^I_{\alpha \tilde{N}_g}) \right] X^C_{k\tilde{E}^f_L} X^{C\,*}_{l\tilde{E}^{f'}_R} \\
& - \frac{1}{2\sqrt{2}}\left[g'^2 (v_u X^R_{\alpha u} - v_d X^R_{\alpha d}) + g^2 (v_u X^R_{\alpha u} + v_d X^R_{\alpha d}) \right] X^C_{ku} X^{C\,*}_{lu} \\
& - \frac{1}{2\sqrt{2}}\left[g'^2 (v_d X^R_{\alpha d} - v_u X^R_{\alpha u}) + g^2 (v_u X^R_{\alpha u} + v_d X^R_{\alpha d}) \right] X^C_{kd} X^{C\,*}_{ld} \\
& - \frac{g^2}{2\sqrt{2}}\left[v_u (X^R_{\alpha d} - \imath X^I_{\alpha d}) + v_d (X^R_{\alpha u} - \imath X^I_{\alpha u}) \right] X^C_{ku} X^{C\,*}_{ld} \\
& - \frac{g^2}{2\sqrt{2}}\left[v_u (X^R_{\alpha d} + \imath X^I_{\alpha d}) + v_d (X^R_{\alpha u} + \imath X^I_{\alpha u}) \right] X^C_{kd} X^{C\,*}_{lu} \\
& + \frac{1}{\sqrt{2}}\left[A_e^{ff'} (X^R_{\alpha \tilde{N}_f} + \imath X^I_{\alpha \tilde{N}_f}) X^C_{k\tilde{E}^{f'}_R} X^{C\,*}_{ld} + A_e^{ff'\,*} (X^R_{\alpha \tilde{N}_f} - \imath X^I_{\alpha \tilde{N}_f}) X^C_{kd} X^{C\,*}_{l\tilde{E}^{f'}_R} \right] \\
& + \frac{Y_e^{f\,2} v_d}{\sqrt{2}}\left[(X^R_{\alpha \tilde{N}_f} - \imath X^I_{\alpha \tilde{N}_f}) X^C_{kd} X^{C\,*}_{l\tilde{E}^f_L} + (X^R_{\alpha \tilde{N}_f} + \imath X^I_{\alpha \tilde{N}_f}) X^C_{k\tilde{E}^f_L} X^{C\,*}_{ld} \right] \\
& + \frac{Y_e^f}{\sqrt{2}}\left[\mu^* (X^R_{\alpha \tilde{N}_f} + \imath X^I_{\alpha \tilde{N}_f}) X^C_{k\tilde{E}^f_R} X^{C\,*}_{lu} + \mu (X^R_{\alpha \tilde{N}_f} - \imath X^I_{\alpha \tilde{N}_f}) X^C_{ku} X^{C\,*}_{l\tilde{E}^f_R} \right] \\
& - \frac{g^2}{2\sqrt{2}}\left[(X^R_{\alpha \tilde{N}_f} + \imath X^I_{\alpha \tilde{N}_f}) X^C_{k\tilde{E}^f_L} (v_u X^{C\,*}_{lu} + v_d X^{C\,*}_{ld}) + (X^R_{\alpha \tilde{N}_f} - \imath X^I_{\alpha \tilde{N}_f}) (v_u X^C_{ku} + v_d X^C_{kd}) X^{C\,*}_{l\tilde{E}^f_L} \right]
\end{aligned}
\tag{A.26}
$$

- Cubic Neutral-Higgs-sneutrinos:

$$
\begin{aligned}
g^{S_\alpha S_\beta S_\gamma} = \frac{g'^2 + g^2}{4\sqrt{2}} \Bigg[& v_u \left(\Pi^{S\,uuu}_{\alpha\beta\gamma} + \Pi^{A\,uuu}_{\alpha\beta\gamma} - \Pi^{S\,udd}_{\alpha\beta\gamma} - \Pi^{A\,udd}_{\alpha\beta\gamma} - \Pi^{S\,u\tilde{N}_f\tilde{N}_f}_{\alpha\beta\gamma} - \Pi^{A\,u\tilde{N}_f\tilde{N}_f}_{\alpha\beta\gamma} \right) \\
& + v_d \left(\Pi^{S\,ddd}_{\alpha\beta\gamma} + \Pi^{A\,ddd}_{\alpha\beta\gamma} - \Pi^{S\,duu}_{\alpha\beta\gamma} - \Pi^{A\,duu}_{\alpha\beta\gamma} - \Pi^{S\,d\tilde{N}_f\tilde{N}_f}_{\alpha\beta\gamma} - \Pi^{A\,d\tilde{N}_f\tilde{N}_f}_{\alpha\beta\gamma} \right) \Bigg]
\end{aligned}
\tag{A.27}
$$

where:

$$
\begin{aligned}
\Pi^{S\,abc}_{\alpha\beta\gamma} =& X^R_{\alpha a} X^R_{\beta b} X^R_{\gamma c} + X^R_{\alpha b} X^R_{\beta c} X^R_{\gamma a} + X^R_{\alpha c} X^R_{\beta a} X^R_{\gamma b} + X^R_{\alpha a} X^R_{\beta c} X^R_{\gamma b} + X^R_{\alpha c} X^R_{\beta b} X^R_{\gamma a} + X^R_{\alpha b} X^R_{\beta a} X^R_{\gamma c} \\
\Pi^{A\,abc}_{\alpha\beta\gamma} =& X^R_{\alpha a} \left(X^I_{\beta b} X^I_{\gamma c} + X^I_{\beta c} X^I_{\gamma b} \right) + X^R_{\beta a} \left(X^I_{\alpha b} X^I_{\gamma c} + X^I_{\alpha c} X^I_{\gamma b} \right) + X^R_{\gamma a} \left(X^I_{\alpha b} X^I_{\beta c} + X^I_{\alpha c} X^I_{\beta b} \right)
\end{aligned}
$$

- Neutral-Higgs-sneutrinos / W quartic:

$$g^{WWS_\alpha S_\beta} = \frac{g^2}{2}\left[X^R_{\alpha u}X^R_{\beta u} + X^I_{\alpha u}X^I_{\beta u} + X^R_{\alpha d}X^R_{\beta d} + X^I_{\alpha d}X^I_{\beta d} + X^R_{\alpha \tilde{N}_f}X^R_{\beta \tilde{N}_f} + X^I_{\alpha \tilde{N}_f}X^I_{\beta \tilde{N}_f}\right] \tag{A.28}$$

- Neutral-Higgs-sneutrinos / Z quartic:

$$g^{ZZS_\alpha S_\beta} = \frac{g'^2 + g^2}{2}\left[X^R_{\alpha u}X^R_{\beta u} + X^I_{\alpha u}X^I_{\beta u} + X^R_{\alpha d}X^R_{\beta d} + X^I_{\alpha d}X^I_{\beta d} + X^R_{\alpha \tilde{N}_f}X^R_{\beta \tilde{N}_f} + X^I_{\alpha \tilde{N}_f}X^I_{\beta \tilde{N}_f}\right] \tag{A.29}$$

- Neutral-Higgs-sneutrinos / scalar-ups quartic:

$$\begin{aligned} g^{\tilde{U}_k \tilde{U}_l S_\alpha S_\beta} = & -Y_u^{f\,2}\left(X^R_{\alpha u}X^R_{\beta u} + X^I_{\alpha u}X^I_{\beta u}\right)\left(X^{\tilde{U}_f}_{kL}X^{\tilde{U}_f\,*}_{lL} + X^{\tilde{U}_f}_{kR}X^{\tilde{U}_f\,*}_{lR}\right) \\ & - \left[\frac{1}{4}\left(\frac{g'^2}{3} - g^2\right)X^{\tilde{U}_f}_{kL}X^{\tilde{U}_f\,*}_{lL} - \frac{g'^2}{3}X^{\tilde{U}_f}_{kR}X^{\tilde{U}_f\,*}_{lR}\right] \\ & \times\left(X^R_{\alpha u}X^R_{\beta u} + X^I_{\alpha u}X^I_{\beta u} - X^R_{\alpha d}X^R_{\beta d} - X^I_{\alpha d}X^I_{\beta d} - X^R_{\alpha \tilde{N}_{f'}}X^R_{\beta \tilde{N}_{f'}} - X^I_{\alpha \tilde{N}_{f'}}X^I_{\beta \tilde{N}_{f'}}\right) \end{aligned} \tag{A.30}$$

- Neutral-Higgs-sneutrinos / sdowns quartic:

$$\begin{aligned} g^{\tilde{D}_k \tilde{D}_l S_\alpha S_\beta} = & -Y_d^{f\,2}\left(X^R_{\alpha d}X^R_{\beta d} + X^I_{\alpha d}X^I_{\beta d}\right)\left(X^{\tilde{D}_f}_{kL}X^{\tilde{D}_f\,*}_{lL} + X^{\tilde{D}_f}_{kR}X^{\tilde{D}_f\,*}_{lR}\right) \\ & - \left[\frac{1}{4}\left(\frac{g'^2}{3} + g^2\right)X^{\tilde{D}_f}_{kL}X^{\tilde{D}_f\,*}_{lL} + \frac{g'^2}{6}X^{\tilde{D}_f}_{kR}X^{\tilde{D}_f\,*}_{lR}\right] \\ & \times\left(X^R_{\alpha u}X^R_{\beta u} + X^I_{\alpha u}X^I_{\beta u} - X^R_{\alpha d}X^R_{\beta d} - X^I_{\alpha d}X^I_{\beta d} - X^R_{\alpha \tilde{N}_{f'}}X^R_{\beta \tilde{N}_{f'}} - X^I_{\alpha \tilde{N}_{f'}}X^I_{\beta \tilde{N}_{f'}}\right) \\ & - \frac{Y_d^f}{2}\left(\lambda'^*_{ghf}X^{\tilde{D}_h}_{kL}X^{\tilde{D}_f\,*}_{lL} + \lambda'^*_{gfh}X^{\tilde{D}_f}_{kR}X^{\tilde{D}_h\,*}_{lR}\right)\left[(X^R_{\alpha d} + \imath X^I_{\alpha d})(X^R_{\beta \tilde{N}_g} - \imath X^I_{\beta \tilde{N}_g}) + (\alpha \leftrightarrow \beta)\right] \\ & - \frac{Y_d^f}{2}\left(\lambda'_{ghf}X^{\tilde{D}_f}_{kL}X^{\tilde{D}_h\,*}_{lL} + \lambda'_{gfh}X^{\tilde{D}_h}_{kR}X^{\tilde{D}_f\,*}_{lR}\right)\left[(X^R_{\alpha d} - \imath X^I_{\alpha d})(X^R_{\beta \tilde{N}_g} + \imath X^I_{\beta \tilde{N}_g}) + (\alpha \leftrightarrow \beta)\right] \\ & -\frac{1}{2}\left(\lambda'_{ghf}\lambda'^*_{mnf}X^{\tilde{D}_n}_{kL}X^{\tilde{D}_h\,*}_{lL} + \lambda'_{gfh}\lambda'^*_{mfn}X^{\tilde{D}_h}_{kR}X^{\tilde{D}_n\,*}_{lR}\right)\left[(X^R_{\alpha \tilde{N}_g} + \imath X^I_{\alpha \tilde{N}_g})(X^R_{\beta \tilde{N}_m} - \imath X^I_{\beta \tilde{N}_m}) + (\alpha \leftrightarrow \beta)\right] \end{aligned} \tag{A.31}$$

- Neutral-Higgs-sneutrinos / Charged Higgs-sleptons quartic:

$$\begin{aligned}\mathcal{L} \ni & -Y_e^{f\,2}\left[|H_d^0|^2\left(|E_L^f|^2+|E_R^{c\,f}|^2\right)+|N_L^f|^2H_d^+H_d^- - H_d^0N_L^{f\,*}H_d^+E_L^f - H_d^{0*}N_L^fE_L^{f\,*}H_d^-\right]\\ & -\lambda_{jki}\lambda^*_{mni}N_L^jN_L^{m\,*}E_L^{n\,*}E_L^k-\lambda_{ijk}\lambda^*_{imn}N_L^jN_L^{m\,*}E_R^{c\,k}E_R^{c\,n\,*}-Y_e^fY_e^{f'}N_L^fN_L^{f'\,*}E_R^{c\,f}E_R^{c\,f'\,*}\\ & +Y_e^f\left[\lambda^*_{fij}H_d^0N_L^{i\,*}E_R^{c\,f}E_R^{c\,j\,*}+\lambda^*_{ijf}H_d^0N_L^{j\,*}E_L^{i\,*}E_L^f+\lambda^*_{ijf}N_L^fN_L^{i\,*}E_L^{j\,*}H_d^-+cc\right]\\ & -\frac{g'^2}{4}\left[|H_u^0|^2-|H_d^0|^2-|N_L^f|^2\right]\left[H_u^+H_u^- - H_d^+H_d^- - |E_L^{f'}|^2+2|E_R^{c\,f'}|^2\right]\\ & -\frac{g^2}{4}\left[\left(|H_u^0|^2+|H_d^0|^2+|N_L^f|^2\right)H_u^+H_u^- + \left(|H_d^0|^2+|H_u^0|^2-|N_L^f|^2\right)H_d^+H_d^-\right.\\ & +2N_L^fN_L^{f'\,*}E_L^{f\,*}E_L^{f'}+\left(|H_u^0|^2-|H_d^0|^2-|N_L^f|^2\right)|E_L^f|^2+2H_u^{0\,*}H_d^{0\,*}H_u^+H_d^-+2H_u^0H_d^0H_d^+H_u^-\\ & \left.+2N_L^{f\,*}H_u^{0\,*}H_u^+E_L^f+2N_L^fH_u^0E_L^{f\,*}H_u^-+2N_L^{f\,*}H_d^0H_d^+E_L^f+2N_L^fH_d^{0\,*}E_L^{f\,*}H_d^-\right] \quad \text{(A.32)}\end{aligned}$$

The coupling $g^{H_kH_lS_\alpha S_\beta}$ is obtained through the replacements $H_u^+ \to X_{ku}^C$, $H_d^+ \to X_{kd}^C$, $E_L^{f\,*} \to X^C_{k\tilde{E}_L^f}$, $E_R^{c\,f} \to X^C_{k\tilde{E}_R^f}$, $H_u^- \to X_{lu}^{C\,*}$, $H_d^- \to X_{ld}^{C\,*}$, $E_L^f \to X^{C\,*}_{l\tilde{E}_L^f}$, $E_R^{c\,f\,*} \to X^{C\,*}_{l\tilde{E}_R^f}$, $H_u^0 \to X^R_{.u}+\imath X^I_{.u}$, $H_d^0 \to X^R_{.d}+\imath X^I_{.d}$, and $N_L^f \to X^R_{.\tilde{N}_f}+\imath X^I_{.\tilde{N}_f}$ ($. = \alpha,\ \beta$ indifferently, such that the coupling is symmetric over the exchange $\alpha \leftrightarrow \beta$ in the end).

- Neutral-Higgs-sneutrinos quartic:

$$\begin{aligned}g^{S_\alpha S_\beta S_\gamma S_\delta} = \frac{g'^2+g^2}{32}\Big[& \Pi^{S\,uuuu}_{\alpha\beta\gamma\delta}+\Pi^{S\,dddd}_{\alpha\beta\gamma\delta}-2\Pi^{S\,uudd}_{\alpha\beta\gamma\delta}-2\Pi^{S\,uu\tilde{N}_f\tilde{N}_f}_{\alpha\beta\gamma\delta}+2\Pi^{S\,dd\tilde{N}_f\tilde{N}_f}_{\alpha\beta\gamma\delta}\\ & +\Pi^{S\,\tilde{N}_f\tilde{N}_f\tilde{N}_{f'}\tilde{N}_{f'}}_{\alpha\beta\gamma\delta}+\Pi^{P\,uuuu}_{\alpha\beta\gamma\delta}+\Pi^{P\,dddd}_{\alpha\beta\gamma\delta}-2\Pi^{P\,uudd}_{\alpha\beta\gamma\delta}-2\Pi^{P\,uu\tilde{N}_f\tilde{N}_f}_{\alpha\beta\gamma\delta}+2\Pi^{P\,dd\tilde{N}_f\tilde{N}_f}_{\alpha\beta\gamma\delta}\\ & +\Pi^{P\,\tilde{N}_f\tilde{N}_f\tilde{N}_{f'}\tilde{N}_{f'}}_{\alpha\beta\gamma\delta}+2\Pi^{S\,uu\,P\,uu}_{\alpha\beta\gamma\delta}+2\Pi^{S\,dd\,P\,dd}_{\alpha\beta\gamma\delta}-2\Pi^{S\,uu\,P\,dd}_{\alpha\beta\gamma\delta}-2\Pi^{S\,dd\,P\,uu}_{\alpha\beta\gamma\delta}\\ & -2\Pi^{S\,uu\,P\,\tilde{N}_f\tilde{N}_f}_{\alpha\beta\gamma\delta}-2\Pi^{S\,\tilde{N}_f\tilde{N}_f\,P\,uu}_{\alpha\beta\gamma\delta}+2\Pi^{S\,dd\,P\,\tilde{N}_f\tilde{N}_f}_{\alpha\beta\gamma\delta}+2\Pi^{S\,\tilde{N}_f\tilde{N}_f\,P\,dd}_{\alpha\beta\gamma\delta}+2\Pi^{S\,\tilde{N}_f\tilde{N}_f\,P\,\tilde{N}_{f'}\tilde{N}_{f'}}_{\alpha\beta\gamma\delta}\Big]\end{aligned} \quad \text{(A.33)}$$

where:

$$\Pi^{S\,abcd}_{ijkl} = \sum_{\sigma\in S_4} X^R_{\sigma(i)a}X^R_{\sigma(j)b}X^R_{\sigma(k)c}X^R_{\sigma(l)d} \quad ; \quad \Pi^{P\,abcd}_{ijkl} = \sum_{\sigma\in S_4} X^I_{\sigma(i)a}X^I_{\sigma(j)b}X^I_{\sigma(k)c}X^I_{\sigma(l)d}$$

$$\Pi^{S\,ab\,P\,cd}_{ijkl} = \sum_{\sigma\in S_4} X^R_{\sigma(i)a}X^R_{\sigma(j)b}X^I_{\sigma(k)c}X^I_{\sigma(l)d}$$

A.1.3 Loop-functions

The loop functions relevant for our computations are

- $A_0(m) = -16\pi^2\imath\int\frac{d^Dk}{(2\pi)^D}\frac{1}{k^2-m^2}$.

- $B_0(p,m_1,m_2) = -16\pi^2\imath \int \frac{d^Dk}{(2\pi)^D} \frac{1}{[k^2-m_1^2][(k+p)^2-m_2^2]}$.
- $p^\mu B_1(p,m_1,m_2) = -16\pi^2\imath \int \frac{d^Dk}{(2\pi)^D} \frac{k^\mu}{[k^2-m_1^2][(k+p)^2-m_2^2]}$.
- $\left[g^{\mu\nu}B_{22} + p^\mu p^\nu B_{21}\right](p,m_1,m_2) = -16\pi^2\imath \int \frac{d^Dk}{(2\pi)^D} \frac{k^\mu k^\nu}{[k^2-m_1^2][(k+p)^2-m_2^2]}$.
- $C_0(p_1,p_2,m_1,m_2,m_3) = -16\pi^2\imath \int \frac{d^Dk}{(2\pi)^D} \frac{1}{[k^2-m_1^2][(k+p_1)^2-m_2^2][(k+p_1+p_2)^2-m_3^2]}$.
- $\left[p_1^\mu C_{11} + p_2^\mu C_{12}\right](p_1,p_2,m_1,m_2,m_3) = -16\pi^2\imath \int \frac{d^Dk}{(2\pi)^D} \frac{k^\mu}{[k^2-m_1^2][(k+p_1)^2-m_2^2][(k+p_1+p_2)^2-m_3^2]}$.
- $\left[g^{\mu\nu}C_{24} + p_1^\mu p_1^\nu C_{21} + p_2^\mu p_2^\nu C_{22} + (p_1^\mu p_2^\nu + p_2^\mu p_1^\nu)C_{23}\right](p_1,p_2,m_1,m_2,m_3) =$
  $-16\pi^2\imath \int \frac{d^Dk}{(2\pi)^D} \frac{k^\mu k^\nu}{[k^2-m_1^2][(k+p_1)^2-m_2^2][(k+p_1+p_2)^2-m_3^2]}$.
- $D_0(m_1,m_2,m_3,m_4) = -16\pi^2\imath \int \frac{d^Dk}{(2\pi)^D} \frac{1}{[k^2-m_1^2][k^2-m_2^2][k^2-m_3^2][k^2-m_4^2]}$.
- $D_2(m_1,m_2,m_3,m_4) = -16\pi^2\imath \int \frac{d^Dk}{(2\pi)^D} \frac{k^2}{[k^2-m_1^2][k^2-m_2^2][k^2-m_3^2][k^2-m_4^2]}$.

Explicit expressions for these functions in the limit of vanishing external momenta can *e.g.* be found in Ref. [315].

A.2 Tree level contributions

The tree-level contribution to the $d_i\bar{d}_j \to d_j\bar{d}_i$ amplitudes corresponds to the topology of Fig.2.1(a) and is mediated by a sneutrino internal line. It generates the following terms in the EFT:

$$\mathcal{L}_{\text{EFT}} \ni \frac{1}{2m_{S_\alpha}^2}\left[\left(g_L^{S_\alpha d_j d_i}\right)^2 O_2 + \left(g_R^{S_\alpha d_j d_i}\right)^2 \tilde{O}_2 + 2g_L^{S_\alpha d_j d_i} g_R^{S_\alpha d_j d_i} O_4\right] \tag{A.34}$$

where the couplings $g_{L,R}^{S_\alpha d_j d_i}$ are defined in Eq.(A.6). The sum over sneutrino/neutral-Higgs mixed states S_α with mass m_{S_α} is implicit. The operators O_2, $\tilde{O}_2$, etc, are defined in Eq.(2.4).

A.3 $d_i - d_j$ self-energy contributions

Loop corrections on the external d-fermion legs are determined by the LSZ reduction. Defining the matrix of renormalized $d_i - d_j$ self energies as: $\hat{\Sigma}^{ij}(\not{p}) = \hat{\Sigma}_L^{ij}(\not{p})P_L + \hat{\Sigma}_R^{ij}(\not{p})P_R = P_L\tilde{\Sigma}_L^{ij}(\not{p}) + P_R\tilde{\Sigma}_R^{ij}(\not{p})$,

we derive the contribution to the EFT:

$$
\begin{aligned}
\mathcal{L}_{\text{EFT}} \ni \frac{1}{2m^2_{S_\alpha}} \Bigg\{ & g_L^{S_\alpha d_j d_i} \Bigg[\frac{1}{2} g_L^{S_\alpha d_j d_i} \left(\left.\frac{d\hat{\Sigma}_L^{jj}}{d\not{p}}\right|_{\not{p}_{d_j}} + \left.\frac{d\hat{\Sigma}_L^{jj}}{d\not{p}}\right|_{\not{p}'_{d_j}} + \left.\frac{d\tilde{\Sigma}_L^{ii}}{d\not{p}}\right|_{\not{p}_{d_i}} + \left.\frac{d\tilde{\Sigma}_L^{ii}}{d\not{p}}\right|_{\not{p}'_{d_i}} \right) \\
& + \sum_{k\neq j} g_L^{S_\alpha d_k d_i} \left(\left.\frac{m_{d_k}\hat{\Sigma}_L^{jk} + \not{p}_{d_j}\hat{\Sigma}_R^{jk}}{m^2_{d_j} - m^2_{d_k}}\right|_{\not{p}_{d_j}} + \left.\frac{m_{d_k}\hat{\Sigma}_L^{jk} + \not{p}'_{d_j}\hat{\Sigma}_R^{jk}}{m^2_{d_j} - m^2_{d_k}}\right|_{\not{p}'_{d_j}} \right) \\
& + \sum_{k\neq i} g_L^{S_\alpha d_j d_k} \left(\left.\frac{m_{d_k}\tilde{\Sigma}_L^{ki} + \not{p}_{d_i}\tilde{\Sigma}_R^{ki}}{m^2_{d_i} - m^2_{d_k}}\right|_{\not{p}_{d_i}} + \left.\frac{m_{d_k}\tilde{\Sigma}_L^{ki} + \not{p}'_{d_i}\tilde{\Sigma}_R^{ki}}{m^2_{d_i} - m^2_{d_k}}\right|_{\not{p}'_{d_i}} \right) \Bigg] O_2 \\
& + g_R^{S_\alpha d_j d_i} \Bigg[\frac{1}{2} g_R^{S_\alpha d_j d_i} \left(\left.\frac{d\hat{\Sigma}_R^{jj}}{d\not{p}}\right|_{\not{p}_{d_j}} + \left.\frac{d\hat{\Sigma}_R^{jj}}{d\not{p}}\right|_{\not{p}'_{d_j}} + \left.\frac{d\tilde{\Sigma}_R^{ii}}{d\not{p}}\right|_{\not{p}_{d_i}} + \left.\frac{d\tilde{\Sigma}_R^{ii}}{d\not{p}}\right|_{\not{p}'_{d_i}} \right) \\
& + \sum_{k\neq j} g_R^{S_\alpha d_k d_i} \left(\left.\frac{m_{d_k}\hat{\Sigma}_R^{jk} + \not{p}_{d_j}\hat{\Sigma}_L^{jk}}{m^2_{d_j} - m^2_{d_k}}\right|_{\not{p}_{d_j}} + \left.\frac{m_{d_k}\hat{\Sigma}_R^{jk} + \not{p}'_{d_j}\hat{\Sigma}_L^{jk}}{m^2_{d_j} - m^2_{d_k}}\right|_{\not{p}'_{d_j}} \right) \\
& + \sum_{k\neq i} g_R^{S_\alpha d_j d_k} \left(\left.\frac{m_{d_k}\tilde{\Sigma}_R^{ki} + \not{p}_{d_i}\tilde{\Sigma}_L^{ki}}{m^2_{d_i} - m^2_{d_k}}\right|_{\not{p}_{d_i}} + \left.\frac{m_{d_k}\tilde{\Sigma}_R^{ki} + \not{p}'_{d_i}\tilde{\Sigma}_L^{ki}}{m^2_{d_i} - m^2_{d_k}}\right|_{\not{p}'_{d_i}} \right) \Bigg] \tilde{O}_2 \\
& + \Bigg(g_L^{S_\alpha d_j d_i} \Bigg[\frac{1}{2} g_R^{S_\alpha d_j d_i} \left(\left.\frac{d\hat{\Sigma}_R^{jj}}{d\not{p}}\right|_{\not{p}_{d_j}} + \left.\frac{d\hat{\Sigma}_R^{jj}}{d\not{p}}\right|_{\not{p}'_{d_j}} + \left.\frac{d\tilde{\Sigma}_R^{ii}}{d\not{p}}\right|_{\not{p}_{d_i}} + \left.\frac{d\tilde{\Sigma}_R^{ii}}{d\not{p}}\right|_{\not{p}'_{d_i}} \right) \\
& + \sum_{k\neq j} g_R^{S_\alpha d_k d_i} \left(\left.\frac{m_{d_k}\hat{\Sigma}_R^{jk} + \not{p}_{d_j}\hat{\Sigma}_L^{jk}}{m^2_{d_j} - m^2_{d_k}}\right|_{\not{p}_{d_j}} + \left.\frac{m_{d_k}\hat{\Sigma}_R^{jk} + \not{p}'_{d_j}\hat{\Sigma}_L^{jk}}{m^2_{d_j} - m^2_{d_k}}\right|_{\not{p}'_{d_j}} \right) \\
& + \sum_{k\neq i} g_R^{S_\alpha d_j d_k} \left(\left.\frac{m_{d_k}\tilde{\Sigma}_R^{ki} + \not{p}_{d_i}\tilde{\Sigma}_L^{ki}}{m^2_{d_i} - m^2_{d_k}}\right|_{\not{p}_{d_i}} + \left.\frac{m_{d_k}\tilde{\Sigma}_R^{ki} + \not{p}'_{d_i}\tilde{\Sigma}_L^{ki}}{m^2_{d_i} - m^2_{d_k}}\right|_{\not{p}'_{d_i}} \right) \Bigg] \\
& + g_R^{S_\alpha d_j d_i} \Bigg[\frac{1}{2} g_L^{S_\alpha d_j d_i} \left(\left.\frac{d\hat{\Sigma}_L^{jj}}{d\not{p}}\right|_{\not{p}_{d_j}} + \left.\frac{d\hat{\Sigma}_L^{jj}}{d\not{p}}\right|_{\not{p}'_{d_j}} + \left.\frac{d\tilde{\Sigma}_L^{ii}}{d\not{p}}\right|_{\not{p}_{d_i}} + \left.\frac{d\tilde{\Sigma}_L^{ii}}{d\not{p}}\right|_{\not{p}'_{d_i}} \right) \\
& + \sum_{k\neq j} g_L^{S_\alpha d_k d_i} \left(\left.\frac{m_{d_k}\hat{\Sigma}_L^{jk} + \not{p}_{d_j}\hat{\Sigma}_R^{jk}}{m^2_{d_j} - m^2_{d_k}}\right|_{\not{p}_{d_j}} + \left.\frac{m_{d_k}\hat{\Sigma}_L^{jk} + \not{p}'_{d_j}\hat{\Sigma}_R^{jk}}{m^2_{d_j} - m^2_{d_k}}\right|_{\not{p}'_{d_j}} \right) \\
& + \sum_{k\neq i} g_L^{S_\alpha d_j d_k} \left(\left.\frac{m_{d_k}\tilde{\Sigma}_L^{ki} + \not{p}_{d_i}\tilde{\Sigma}_R^{ki}}{m^2_{d_i} - m^2_{d_k}}\right|_{\not{p}_{d_i}} + \left.\frac{m_{d_k}\tilde{\Sigma}_L^{ki} + \not{p}'_{d_i}\tilde{\Sigma}_R^{ki}}{m^2_{d_i} - m^2_{d_k}}\right|_{\not{p}'_{d_i}} \right) \Bigg] \Bigg) O_4 \Bigg\}, \qquad \text{(A.35)}
\end{aligned}
$$

where the momenta $\not{p}_{d_j}$, $\not{p}'_{d_j}$, $\not{p}_{d_i}$ and $\not{p}'_{d_i}$ are evaluated at the values m_{d_j}, $-m_{d_j}$, m_{d_i} and $-m_{d_i}$. We list below the contributions to the self-energies.

A.3.1 Scalar/fermion loop

$$-\imath\Sigma^{S/f}_{d_j d_i}(\not{p}) = \frac{\imath}{16\pi^2}\left\{-\not{p}\left[g_L^{Sfd_j\,*} g_L^{Sfd_i} P_L + g_R^{Sfd_j\,*} g_R^{Sfd_i} P_R\right] B_1 + m_f\left[g_R^{Sfd_j\,*} g_L^{Sfd_i} P_L + g_L^{Sfd_j\,*} g_R^{Sfd_i} P_R\right] B_0\right\}$$
$$(-p, m_f, m_S) \quad \text{(A.36)}$$

The scalar/fermion pair (S/f) is summed over the following list of particles:

- Higgs-sneutrino/down: couplings from Eq.(A.6).
- Charged Higgs-slepton/up: couplings from Eq.(A.7).
- sdown/neutralino-neutrino: couplings from Eq.(A.8).
- sdown/gluino: couplings from Eq.(A.9); color-factor $C_2(3) = 4/3$.
- sup/chargino-lepton: couplings from Eq.(A.10).
- sup/down: couplings from Eq.(A.11); color factor: $\varepsilon_{abc}\varepsilon_{abd} = 2\delta_{cd}$.
- sdown/up: couplings from Eq.(A.12); color factor: $\varepsilon_{abc}\varepsilon_{abd} = 2\delta_{cd}$.

A.3.2 Vector/fermion loop

$$-\imath\Sigma^{V/f}_{d_j d_i}(p) = -\frac{\imath}{16\pi^2}\left\{(D-2)\not{p}\left[g_L^{Vfd_j\,*} g_L^{Vfd_i} P_L + g_R^{Vfd_j\,*} g_R^{Vfd_i} P_R\right] B_1 \right.$$
$$\left. + D m_f\left[g_R^{Vfd_j\,*} g_L^{Vfd_i} P_L + g_L^{Vfd_j\,*} g_R^{Vfd_i} P_R\right] B_0\right\}(-p, m_f, m_V) \quad \text{(A.37)}$$

The vector/fermion pair (S/f) is summed over the following list of particles:

- W/up: Eq.(A.13).
- Z/down: Eq.(A.14).

A.3.3 Counterterm

Defining the generic d-mass counterterm $\delta m_{d\,ji} = \delta m^L_{d\,ji} P_L + \delta m^R_{d\,ji} P_R$ as well as the d-wave-function counterterm $\delta Z_{d\,ji} = \delta Z^L_{d\,ji} P_L + \delta Z^R_{d\,ji} P_R$, we arrive at the following contribution:

$$-\imath\Sigma^{CT}_{d_j d_i}(p) = \imath\frac{\not{p}}{2}\left[\left(\delta Z^L_{d\,ji} + \delta Z^{L\,*}_{d\,ij}\right) P_L + \left(\delta Z^R_{d\,ji} + \delta Z^{R\,*}_{d\,ij}\right) P_R\right]$$
$$-\imath\left[\left(\delta m^L_{d\,ji} + \frac{1}{2}\left(m_{d_i}\delta Z^{R\,*}_{d\,ij} + m_{d_j}\delta Z^L_{d\,ji}\right)\right) P_L + \left(\delta m^R_{d\,ji} + \frac{1}{2}\left(m_{d_i}\delta Z^{L\,*}_{d\,ij} + m_{d_j}\delta Z^R_{d\,ji}\right)\right) P_R\right] \quad \text{(A.38)}$$

In principle, $\delta m^L_{d\,ji} = \left(\delta m^R_{d\,ij}\right)^* = \delta Y^L_{d\,ji} v_d + Y^i_d \delta_{ij} \delta v_d$.

A.4 Sneutrino-Higgs self-energies

We assume that the tadpoles (Higgs, gauge bosons) vanish, which supposes certain relations at the loop-level between vevs and tree-level parameters. Then, defining the renormalized neutral-scalar self-energy matrix $\hat{\Sigma}^S_{\alpha\beta}$, we derive the following contribution to the EFT:

$$\mathcal{L}_{\text{EFT}} \ni \frac{-1}{2m^2_{S_\alpha} m^2_{S_\beta}} \left[g_L^{S_\alpha d_j d_i} \hat{\Sigma}^S_{\alpha\beta} g_L^{S_\beta d_j d_i} \, O_2 + g_R^{S_\alpha d_j d_i} \hat{\Sigma}^S_{\alpha\beta} g_R^{S_\beta d_j d_i} \, \tilde{O}_2 + 2 g_L^{S_\alpha d_j d_i} \hat{\Sigma}^S_{\alpha\beta} g_R^{S_\beta d_j d_i} \, O_4 \right] . \tag{A.39}$$

The various contributions to the neutral-scalar self-energies are listed below.

A.4.1 Scalar A_0-loop

$$-\imath \Sigma^{S\,A_S}_{\alpha\beta} = -\frac{\imath}{16\pi^2} g^{\tilde{S}\tilde{S}S_\alpha S_\beta} A_0(m_{\tilde{S}}) \, . \tag{A.40}$$

This contribution is summed over the scalar $\tilde{S}$, taking value in the following list of particles:

- scalar-ups: couplings from Eq.(A.30). 3 colors contributing.
- sdowns: couplings from Eq.(A.31). 3 colors contributing.
- Charged Higgs-sleptons: couplings from Eq.(A.32).
- Higgs-sneutrinos: couplings from Eq.(A.33); symmetry-factor 1/2.

A.4.2 Vector A_0-loop

$$-\imath \Sigma^{S\,A_V}_{\alpha\beta} = \frac{\imath}{16\pi^2} g^{VVS_\alpha S_\beta} D \, A_0(m_V) \tag{A.41}$$

The vector V belongs to the following list of particles:

- W's: couplings from Eq.(A.28).
- Z's: couplings from Eq.(A.29); symmetry-factor 1/2.

A.4.3 Scalar B-loop

$$-\imath \Sigma^{S\,B_S}_{\alpha\beta} == \frac{\imath}{16\pi^2} g^{S_\delta S_\gamma S_\alpha} g^{S_\gamma S_\delta S_\beta} B_0(m_{S_\gamma}, m_{S_\delta}) \tag{A.42}$$

The scalar pair (S_γ, S_δ) is summed over the particles:

- scalar-ups: couplings from Eq.(A.24). 3 colors contributing.
- sdowns: couplings from Eq.(A.25). 3 colors contributing.
- Charged Higgs-sleptons: couplings from Eq.(A.26).
- Higgs-sneutrinos: couplings from Eq.(A.27).

A.4.4 Fermion B-loop

$$-\imath\Sigma^{S\,B_f}_{\alpha\beta} = \frac{-2\imath}{16\pi^2}\left\{\left[g_L^{S_\alpha \tilde{f} f} g_L^{S_\beta \tilde{f} f *} + g_R^{S_\alpha \tilde{f} f} g_R^{S_\beta \tilde{f} f *}\right] DB_{22} + \left[g_L^{S_\alpha \tilde{f} f} g_R^{S_\beta \tilde{f} f *} + g_R^{S_\alpha \tilde{f} f} g_L^{S_\beta \tilde{f} f *}\right] m_f m_{\tilde{f}} B_0\right\}(m_f, m_{\tilde{f}}) \tag{A.43}$$

List of particles for the fermion pair $(f, \tilde{f})$:

- ups: couplings of Eq.(A.15). 3 colors contributing.
- downs: couplings of Eq.(A.6). 3 colors contributing.
- charginos-leptons: couplings of Eq.(A.16).
- neutrino-neutralinos: couplings of Eq.(A.17); symmetry-factor $1/2$.

A.4.5 Vector B-loop

$$-\imath\Sigma^{S\,B_V}_{\alpha\beta} = \frac{\imath}{16\pi^2} g^{S_\alpha VV} g^{S_\beta VV} DB_0(m_V, m_V) \tag{A.44}$$

The vector V is summed over:

- W's: couplings of Eq.(A.18).
- Z's: couplings of Eq.(A.19); symmetry-factor $1/2$

A.4.6 Ghost B-loop

$$-\imath\Sigma^{S\,B_g}_{\alpha\beta} = -\frac{\imath}{16\pi^2} g^{S_\alpha gg} g^{S_\beta gg} B_0(m_g, m_g) \tag{A.45}$$

The contribution is summed over the ghost fields g:

- g_W's: couplings of Eq.(A.20).
- g_Z: couplings of Eq.(A.21).

A.4.7 Scalar/vector B-loop

$$-\imath\Sigma^{S\,B_{SV}}_{\alpha\beta} = \frac{\imath}{16\pi^2} g^{S_\alpha VS *} g^{S_\beta VS} DB_{22}(m_V, m_S) \tag{A.46}$$

List of particles for the scalar/vector pair (S/V):

- Charged Higgs-slepton / W: couplings of Eq.(A.22).
- Higgs - sneutrino / Z: couplings of Eq.(A.23).

A.4.8 Counterterms

Defining the neutral scalar mass and wave-function counterterms $\delta m^2_{\alpha\beta}$ and $\delta Z^S_{\alpha\beta}$:

$$-\imath\Sigma^{S\,CT}_{\alpha\beta} = -\imath\left[\delta m^2_{\alpha\beta} + \frac{1}{2}\delta Z^S_{\alpha\beta}\left(m^2_{S_\alpha} + m^2_{S_\beta}\right)\right] \tag{A.47}$$

A.5 Vertex corrections

The vertex corrections to the EFT are obtained as:

$$\mathcal{L}_{\text{EFT}} \ni \frac{1}{2m^2_{S_\alpha}}\left[g_L^{S_\alpha d_j d_i}\hat{V}_L^{S_\alpha d_j d_i}\,O_2 + g_R^{S_\alpha d_j d_i}\hat{V}_R^{S_\alpha d_j d_i}\,\tilde{O}_2 + \left(g_R^{S_\alpha d_j d_i}\hat{V}_L^{S_\alpha d_j d_i} + g_L^{S_\alpha d_j d_i}\hat{V}_R^{S_\alpha d_j d_i}\right)O_4\right] \tag{A.48}$$

where the $\bar{d}_j d_i$-neutral-Higgs renormalized vertex function $\hat{V}^{S_\alpha d_j d_i} = \hat{V}_L^{S_\alpha d_j d_i}P_L + \hat{V}_L^{S_\alpha d_j d_i}P_R$ receives the contributions listed below.

A.5.1 Scalar/fermion loop with cubic scalar coupling

$$-\imath\hat{V}^{S_\alpha d_j d_i}[Sff, S^3] = -\frac{\imath}{16\pi^2}g^{S_\alpha S_k S_l}\left[g_R^{S_l f d_j *}g_L^{S_k f d_i}P_L + g_L^{S_l f d_j *}g_R^{S_k f d_i}P_R\right]m_f C_0(m_f, m_{S_k}, m_{S_l}) \tag{A.49}$$

List of particles for the scalar/fermion triplet $(S_k, S_l/f)$:

- Higgs-sneutrino/down: couplings from Eqs.(A.6),(A.27).
- Charged Higgs-slepton/up: couplings from Eqs.(A.7),(A.26).
- sdown/neutralino-neutrino: couplings from Eqs.(A.8),(A.25).
- sdown/gluino: couplings from Eqs.(A.9),(A.25); color-factor $C_2(3) = 4/3$.
- sup/chargino-lepton: couplings from Eqs.(A.10),(A.24).
- sup/down: couplings from Eqs.(A.11),(A.24).
- sdown/up: couplings from Eqs.(A.12),(A.25).

A.5.2 Scalar/fermion loop without cubic scalar coupling

$$\begin{aligned}-\imath\hat{V}^{S_\alpha d_j d_i}[Sff] = -\frac{\imath}{16\pi^2}\Big\{&\left[g_R^{Sf_l d_j *}g_R^{S_\alpha f_l f_k}g_L^{Sf_k d_i}P_L + g_L^{Sf_l d_j *}g_L^{S_\alpha f_l f_k}g_R^{Sf_k d_i}P_R\right]D\,C_{24}\\ &+\left[g_R^{Sf_l d_j *}g_L^{S_\alpha f_l f_k}g_L^{Sf_k d_i}P_L + g_L^{Sf_l d_j *}g_R^{S_\alpha f_l f_k}g_R^{Sf_k d_i}P_R\right]m_{f_k}m_{f_l}C_0\Big\}(m_S, m_{f_k}, m_{f_l})\end{aligned} \tag{A.50}$$

List of particles for the scalar/fermion triplet $(S/f_k, f_l)$:

- Higgs-sneutrino/down: couplings from Eq.(A.6).

- Charged Higgs-slepton/up: couplings from Eqs.(A.7),(A.15).
- sdown/neutralino-neutrino: couplings from Eqs.(A.8),(A.17).
- sup/chargino-lepton: couplings from Eqs.(A.10),(A.16).
- sup/down: couplings from Eqs.(A.11),(A.6).
- sdown/up: couplings from Eqs.(A.12),(A.15).

A.5.3 Vector/fermion loop with scalar-vector coupling

$$-\imath\hat{V}^{S_\alpha d_j d_i}[SVV,Vff] = -\frac{\imath}{16\pi^2} g^{S_\alpha V_k V_l}\left[g_R^{V_l f d_j *} g_L^{V_k f d_i} P_L + g_L^{V_l f d_j *} g_R^{V_k f d_i} P_R\right] Dm_f\, C_0(m_f, m_{V_k}, m_{V_l}) \quad \text{(A.51)}$$

The vector/fermion triplet $(V_k, V_l/f)$ takes the following values:

- W/up: couplings from Eqs.(A.13),(A.18).
- Z/down: couplings from Eqs.(A.14),(A.19).

A.5.4 Vector/fermion loop with scalar-fermion coupling

$$\begin{aligned}-\imath\hat{V}^{S_\alpha d_j d_i}[SVV,Sff] = \frac{\imath}{16\pi^2}\Big\{&\left[g_R^{V f_l d_j *} g_L^{S_\alpha f_l f_k} g_L^{V f_k d_i} P_L + g_L^{V f_l d_j *} g_R^{S_\alpha f_l f_k} g_R^{V f_k d_i} P_R\right] D^2 C_{24} \\ &+ \left[g_R^{V f_l d_j *} g_R^{S_\alpha f_l f_k} g_L^{V f_k d_i} P_L + g_L^{V f_l d_j *} g_L^{S_\alpha f_l f_k} g_R^{V f_k d_i} P_R\right] Dm_{f_k} m_{f_l} C_0\Big\}(m_V, m_{f_k}, m_{f_l}) \quad \text{(A.52)}\end{aligned}$$

The vector/fermion triplet $(V/f_k, f_l)$ takes the following values:

- W/up: couplings from Eqs.(A.13),(A.15).
- Z/down: couplings from Eqs.(A.14),(A.6).

A.5.5 Vector/Scalar/fermion loops

$$\begin{aligned}-\imath\hat{V}^{S_\alpha d_j d_i}[VSf] = -\frac{\imath}{16\pi^2}\Big\{&g^{VSS_\alpha}\left[g_R^{S f d_j *} g_L^{V f d_i} P_L + g_L^{S f d_j *} g_R^{V f d_i} P_R\right] + g^{SVS_\alpha}\left[g_R^{V f d_j *} g_L^{S f d_i} P_L + g_L^{V f d_j *} g_R^{S f d_i} P_R\right]\Big\} \\ &\times D\, C_{24}(m_f, m_S, m_V) \quad \text{(A.53)}\end{aligned}$$

List of particles for the scalar/vector/fermion triplet $(S/V/f)$:

- charged-Higgs-slepton/W/up: couplings from Eqs.(A.13),(A.7),(A.22).
- neutral-Higgs-sneutrino/Z/down: couplings from Eqs.(A.14),(A.6),(A.23).

A.5.6 Counterterms

The counterterm contribution $-\imath\hat{V}^{S_\alpha d_j d_i}[CT]$ reads:

$$\begin{aligned}
&\imath\left\{-\frac{1}{\sqrt{2}}\left[\delta Y^L_{d\,ji}(X^R_{kd}+\imath X^I_{kd})+\delta\lambda'^L_{fij}(X^R_{k\tilde{N}_f}+\imath X^I_{k\tilde{N}_f})\right]+\frac{1}{2}\left[\delta Z^{R\,*}_{d\,jl}g_L^{S_\alpha d_l d_i}+\delta Z^L_{d\,il}g_L^{S_\alpha d_j d_l}+\delta Z^S_{k\alpha}g_L^{S_\alpha d_j d_i}\right]\right\}P_L\\
&+\imath\left\{-\frac{1}{\sqrt{2}}\left[\delta Y^R_{d\,ji}(X^R_{kd}-\imath X^I_{kd})+\delta\lambda'^R_{fji}(X^R_{k\tilde{N}_f}-\imath X^I_{k\tilde{N}_f})\right]+\frac{1}{2}\left[\delta Z^{L\,*}_{d\,jl}g_R^{S_\alpha d_l d_i}+\delta Z^R_{d\,il}g_R^{S_\alpha d_j d_l}+\delta Z^S_{k\alpha}g_R^{S_\alpha d_j d_i}\right]\right\}P_R
\end{aligned} \tag{A.54}$$

where $\delta Y^R_{d\,ji}=\left(\delta Y^L_{d\,ij}\right)^*$ is the counterterm to the Yukawa coupling and $\delta\lambda'^R_{fji}=\left(\delta\lambda'^L_{fji}\right)^*$ is the counterterm to the λ' coupling.

A.6 Box diagrams

Here, we collect the box-diagram contributions to the $d_i\bar{d}_j\to d_j\bar{d}_i$ amplitude. The results are listed according to the topologies of Fig.2.2.

A.6.1 Vector/fermion/vector/fermion "straight" box

Case $V_{\alpha,\beta}$ colour-singlets

$$\begin{aligned}
\mathcal{L}_{\text{EFT}}\ni\frac{1}{32\pi^2}\Big\{&g_L^{V_\alpha f_k d_j\,*}g_L^{V_\beta f_k d_i}g_L^{V_\beta f_l d_j\,*}g_L^{V_\alpha f_l d_i}\,D_2\,O_1+g_R^{V_\alpha f_k d_j\,*}g_R^{V_\beta f_k d_i}g_R^{V_\beta f_l d_j\,*}g_R^{V_\alpha f_l d_i}\,D_2\,\tilde{O}_1\\
&+16g_R^{V_\alpha f_k d_j\,*}g_L^{V_\beta f_k d_i}g_R^{V_\beta f_l d_j\,*}g_L^{V_\alpha f_l d_i}m_{f_k}m_{f_l}D_0\,O_2+16g_L^{V_\alpha f_k d_j\,*}g_R^{V_\beta f_k d_i}g_L^{V_\beta f_l d_j\,*}g_R^{V_\alpha f_l d_i}m_{f_k}m_{f_l}D_0\,\tilde{O}_2\\
&+16\left[g_R^{V_\alpha f_k d_j\,*}g_L^{V_\beta f_k d_i}g_L^{V_\beta f_l d_j\,*}g_R^{V_\alpha f_l d_i}+g_L^{V_\alpha f_k d_j\,*}g_R^{V_\beta f_k d_i}g_R^{V_\beta f_l d_j\,*}g_L^{V_\alpha f_l d_i}\right]m_{f_k}m_{f_l}D_0\,O_4\\
&-2\left[g_L^{V_\alpha f_k d_j\,*}g_L^{V_\beta f_k d_i}g_R^{V_\beta f_l d_j\,*}g_R^{V_\alpha f_l d_i}+g_R^{V_\alpha f_k d_j\,*}g_R^{V_\beta f_k d_i}g_L^{V_\beta f_l d_j\,*}g_L^{V_\alpha f_l d_i}\right]D_2\,O_5\Big\}(m_{S_\alpha},m_{f_k},m_{S_\beta},m_{f_l})
\end{aligned} \tag{A.55}$$

List of particles:

- W / up: couplings from Eq.(A.13).

A.6.2 Scalar/fermion/scalar/fermion "straight" box

Case 1: $S_{\alpha,\beta}$ colour-singlets

$$\begin{aligned}
\mathcal{L}_{\text{EFT}}\ni\frac{1}{32\pi^2}\Big\{&g_L^{S_\alpha f_k d_j\,*}g_L^{S_\beta f_k d_i}g_L^{S_\beta f_l d_j\,*}g_L^{S_\alpha f_l d_i}\frac{D_2}{4}\,O_1+g_R^{S_\alpha f_k d_j\,*}g_R^{S_\beta f_k d_i}g_R^{S_\beta f_l d_j\,*}g_R^{S_\alpha f_l d_i}\frac{D_2}{4}\,\tilde{O}_1\\
&+g_R^{S_\alpha f_k d_j\,*}g_L^{S_\beta f_k d_i}g_R^{S_\beta f_l d_j\,*}g_L^{S_\alpha f_l d_i}m_{f_k}m_{f_l}D_0\,O_2+g_L^{S_\alpha f_k d_j\,*}g_R^{S_\beta f_k d_i}g_L^{S_\beta f_l d_j\,*}g_R^{S_\alpha f_l d_i}m_{f_k}m_{f_l}D_0\,\tilde{O}_2\\
&+\left[g_R^{S_\alpha f_k d_j\,*}g_L^{S_\beta f_k d_i}g_L^{S_\beta f_l d_j\,*}g_R^{S_\alpha f_l d_i}+g_L^{S_\alpha f_k d_j\,*}g_R^{S_\beta f_k d_i}g_R^{S_\beta f_l d_j\,*}g_L^{S_\alpha f_l d_i}\right]m_{f_k}m_{f_l}D_0\,O_4\\
&-\left[g_L^{S_\alpha f_k d_j\,*}g_L^{S_\beta f_k d_i}g_R^{S_\beta f_l d_j\,*}g_R^{S_\alpha f_l d_i}+g_R^{S_\alpha f_k d_j\,*}g_R^{S_\beta f_k d_i}g_L^{S_\beta f_l d_j\,*}g_L^{S_\alpha f_l d_i}\right]\frac{D_2}{2}\,O_5\Big\}(m_{S_\alpha},m_{f_k},m_{S_\beta},m_{f_l})
\end{aligned} \tag{A.56}$$

List of particles:

- Higgs-sneutrino / down: couplings from Eq.(A.6).

- Charged Higgs-slepton / up: couplings from Eq.(A.7).

Case 2: $f_{k,l}$ colour-singlets

$$\begin{aligned}\mathcal{L}_{\text{EFT}} \ni \frac{1}{32\pi^2}\Big\{ & g_L^{S_\alpha f_k d_j *} g_L^{S_\beta f_k d_i} g_L^{S_\beta f_l d_j *} g_L^{S_\alpha f_l d_i} \frac{D_2}{4} O_1 + g_R^{S_\alpha f_k d_j *} g_R^{S_\beta f_k d_i} g_R^{S_\beta f_l d_j *} g_R^{S_\alpha f_l d_i} \frac{D_2}{4} \tilde{O}_1 \\ & + g_R^{S_\alpha f_k d_j *} g_L^{S_\beta f_k d_i} g_R^{S_\beta f_l d_j *} g_L^{S_\alpha f_l d_i} m_{f_k} m_{f_l} D_0 O_3 + g_L^{S_\alpha f_k d_j *} g_R^{S_\beta f_k d_i} g_L^{S_\beta f_l d_j *} g_R^{S_\alpha f_l d_i} m_{f_k} m_{f_l} D_0 \tilde{O}_3 \\ & - \left[g_L^{S_\alpha f_k d_j *} g_L^{S_\beta f_k d_i} g_R^{S_\beta f_l d_j *} g_R^{S_\alpha f_l d_i} + g_R^{S_\alpha f_k d_j *} g_R^{S_\beta f_k d_i} g_L^{S_\beta f_l d_j *} g_L^{S_\alpha f_l d_i} \right] \frac{D_2}{2} O_4 \\ & + \left[g_R^{S_\alpha f_k d_j *} g_L^{S_\beta f_k d_i} g_L^{S_\beta f_l d_j *} g_R^{S_\alpha f_l d_i} + g_L^{S_\alpha f_k d_j *} g_R^{S_\beta f_k d_i} g_R^{S_\beta f_l d_j *} g_L^{S_\alpha f_l d_i} \right] m_{f_k} m_{f_l} D_0 O_5 \Big\} (m_{S_\alpha}, m_{f_k}, m_{S_\beta}, m_{f_l}) \end{aligned} \tag{A.57}$$

List of particles:

- sdown / neutrino-neutralino: couplings from Eq.(A.8).
- sup / chargino-lepton: couplings from Eq.(A.10).

Case 3: all fields colour-triplets

$$\begin{aligned}\mathcal{L}_{\text{EFT}} \ni \frac{1}{32\pi^2}\Big\{ & g_L^{S_\alpha f_k d_j *} g_L^{S_\beta f_k d_i} g_L^{S_\beta f_l d_j *} g_L^{S_\alpha f_l d_i} \frac{D_2}{2} O_1 + g_R^{S_\alpha f_k d_j *} g_R^{S_\beta f_k d_i} g_R^{S_\beta f_l d_j *} g_R^{S_\alpha f_l d_i} \frac{D_2}{2} \tilde{O}_1 \\ & + g_R^{S_\alpha f_k d_j *} g_L^{S_\beta f_k d_i} g_R^{S_\beta f_l d_j *} g_L^{S_\alpha f_l d_i} m_{f_k} m_{f_l} D_0 (O_2 + O_3) + g_L^{S_\alpha f_k d_j *} g_R^{S_\beta f_k d_i} g_L^{S_\beta f_l d_j *} g_R^{S_\alpha f_l d_i} m_{f_k} m_{f_l} D_0 (\tilde{O}_2 + \tilde{O}_3) \\ & + (O_4 + O_5) \Bigg(\left[g_R^{S_\alpha f_k d_j *} g_L^{S_\beta f_k d_i} g_L^{S_\beta f_l d_j *} g_R^{S_\alpha f_l d_i} + g_L^{S_\alpha f_k d_j *} g_R^{S_\beta f_k d_i} g_R^{S_\beta f_l d_j *} g_L^{S_\alpha f_l d_i} \right] m_{f_k} m_{f_l} D_0 \\ & - \left[g_L^{S_\alpha f_k d_j *} g_L^{S_\beta f_k d_i} g_R^{S_\beta f_l d_j *} g_R^{S_\alpha f_l d_i} + g_R^{S_\alpha f_k d_j *} g_R^{S_\beta f_k d_i} g_L^{S_\beta f_l d_j *} g_L^{S_\alpha f_l d_i} \right] \frac{D_2}{2} \Bigg) \Big\} (m_{S_\alpha}, m_{f_k}, m_{S_\beta}, m_{f_l}) \end{aligned} \tag{A.58}$$

List of particles:

- sdown / up: couplings from Eq.(A.12).
- sup / down: couplings from Eq.(A.11).

Case 4: $f_{k,l}$ colour-octets

$$\begin{aligned}\mathcal{L}_{\text{EFT}} \ni \frac{1}{32\pi^2}\Big\{ & \frac{11}{18} g_L^{S_\alpha f_k d_j *} g_L^{S_\beta f_k d_i} g_L^{S_\beta f_l d_j *} g_L^{S_\alpha f_l d_i} \frac{D_2}{4} O_1 + \frac{11}{18} g_R^{S_\alpha f_k d_j *} g_R^{S_\beta f_k d_i} g_R^{S_\beta f_l d_j *} g_R^{S_\alpha f_l d_i} \frac{D_2}{4} \tilde{O}_1 \\ & + g_R^{S_\alpha f_k d_j *} g_L^{S_\beta f_k d_i} g_R^{S_\beta f_l d_j *} g_L^{S_\alpha f_l d_i} m_{f_k} m_{f_l} D_0 \left(\frac{7}{12} O_2 + \frac{1}{36} O_3 \right) + g_L^{S_\alpha f_k d_j *} g_R^{S_\beta f_k d_i} g_L^{S_\beta f_l d_j *} g_R^{S_\alpha f_l d_i} m_{f_k} m_{f_l} D_0 \left(\frac{7}{12} \tilde{O}_2 + \frac{1}{36} \tilde{O}_3 \right) \\ & + \left[g_R^{S_\alpha f_k d_j *} g_L^{S_\beta f_k d_i} g_L^{S_\beta f_l d_j *} g_R^{S_\alpha f_l d_i} + g_L^{S_\alpha f_k d_j *} g_R^{S_\beta f_k d_i} g_R^{S_\beta f_l d_j *} g_L^{S_\alpha f_l d_i} \right] m_{f_k} m_{f_l} D_0 \left(\frac{7}{12} O_4 + \frac{1}{36} O_5 \right) \\ & - \left[g_L^{S_\alpha f_k d_j *} g_L^{S_\beta f_k d_i} g_R^{S_\beta f_l d_j *} g_R^{S_\alpha f_l d_i} + g_R^{S_\alpha f_k d_j *} g_R^{S_\beta f_k d_i} g_L^{S_\beta f_l d_j *} g_L^{S_\alpha f_l d_i} \right] \frac{D_2}{4} \left(\frac{1}{18} O_4 + \frac{7}{6} O_5 \right) \Big\} (m_{S_\alpha}, m_{f_k}, m_{S_\beta}, m_{f_l}) \end{aligned} \tag{A.59}$$

List of particles:

- sdown / gluino: couplings from Eq.(A.9) (stripped from Gell-Mann matrix element).

Case 5: $f_{k,l}$ colour-octet+singlet

$$\begin{aligned}\mathcal{L}_{\text{EFT}} \ni \frac{1}{32\pi^2}\Bigg\{&\frac{1}{3}g_L^{S_\alpha f_k d_j *}g_L^{S_\beta f_k d_i}g_L^{S_\beta f_l d_j *}g_L^{S_\alpha f_l d_i}\frac{D_2}{4}O_1+\frac{1}{3}g_R^{S_\alpha f_k d_j *}g_R^{S_\beta f_k d_i}g_R^{S_\beta f_l d_j *}g_R^{S_\alpha f_l d_i}\frac{D_2}{4}\tilde{O}_1\\
&+g_R^{S_\alpha f_k d_j *}g_L^{S_\beta f_k d_i}g_R^{S_\beta f_l d_j *}g_L^{S_\alpha f_l d_i}m_{f_k}m_{f_l}D_0\frac{1}{2}\left(O_2-\frac{1}{3}O_3\right)+g_L^{S_\alpha f_k d_j *}g_R^{S_\beta f_k d_i}g_L^{S_\beta f_l d_j *}g_R^{S_\alpha f_l d_i}m_{f_k}m_{f_l}D_0\frac{1}{2}\left(\tilde{O}_2-\frac{1}{3}\tilde{O}_3\right)\\
&+\left[g_R^{S_\alpha f_k d_j *}g_L^{S_\beta f_k d_i}g_L^{S_\beta f_l d_j *}g_R^{S_\alpha f_l d_i}+g_L^{S_\alpha f_k d_j *}g_R^{S_\beta f_k d_i}g_R^{S_\beta f_l d_j *}g_L^{S_\alpha f_l d_i}\right]m_{f_k}m_{f_l}D_0\left(O_4-\frac{1}{3}O_5\right)\\
&+\left[g_L^{S_\alpha f_k d_j *}g_L^{S_\beta f_k d_i}g_R^{S_\beta f_l d_j *}g_R^{S_\alpha f_l d_i}+g_R^{S_\alpha f_k d_j *}g_R^{S_\beta f_k d_i}g_L^{S_\beta f_l d_j *}g_L^{S_\alpha f_l d_i}\right]\frac{D_2}{4}\left(\frac{1}{3}O_4-O_5\right)\Bigg\}(m_{S_\alpha},m_{f_k},m_{S_\beta},m_{f_l})\end{aligned} \tag{A.60}$$

List of particles:

- sdown / gluino / sdown / neutralino-neutrino: couplings from Eqs.(A.8),(A.9) (stripped from Gell-Mann matrix element); $\times 2$ (π-rotated diagram).

A.6.3 Scalar/fermion/scalar/fermion "scalar-cross" box

Case 1: $S_{\alpha,\beta}$ colour-singlets

$$\begin{aligned}\mathcal{L}_{\text{EFT}} \ni \frac{1}{32\pi^2}\Bigg\{&-g_L^{S_\alpha f_k d_j *}g_L^{S_\beta f_k d_i}g_L^{S_\alpha f_l d_j *}g_L^{S_\beta f_l d_i}\frac{D_2}{4}O_1-g_R^{S_\alpha f_k d_j *}g_R^{S_\beta f_k d_i}g_R^{S_\alpha f_l d_j *}g_R^{S_\beta f_l d_i}\frac{D_2}{4}\tilde{O}_1\\
&+g_R^{S_\alpha f_k d_j *}g_L^{S_\beta f_k d_i}g_R^{S_\alpha f_l d_j *}g_L^{S_\beta f_l d_i}m_{f_k}m_{f_l}D_0O_2+g_L^{S_\alpha f_k d_j *}g_R^{S_\beta f_k d_i}g_L^{S_\alpha f_l d_j *}g_R^{S_\beta f_l d_i}m_{f_k}m_{f_l}D_0\tilde{O}_2\\
&+\left[g_R^{S_\alpha f_k d_j *}g_L^{S_\beta f_k d_i}g_L^{S_\alpha f_l d_j *}g_R^{S_\beta f_l d_i}+g_L^{S_\alpha f_k d_j *}g_R^{S_\beta f_k d_i}g_R^{S_\alpha f_l d_j *}g_L^{S_\beta f_l d_i}\right]m_{f_k}m_{f_l}D_0O_4\\
&+\left[g_L^{S_\alpha f_k d_j *}g_L^{S_\beta f_k d_i}g_R^{S_\alpha f_l d_j *}g_R^{S_\beta f_l d_i}+g_R^{S_\alpha f_k d_j *}g_R^{S_\beta f_k d_i}g_L^{S_\alpha f_l d_j *}g_L^{S_\beta f_l d_i}\right]\frac{D_2}{2}O_5\Bigg\}(m_{S_\alpha},m_{f_k},m_{S_\beta},m_{f_l})\end{aligned} \tag{A.61}$$

List of particles:

- Higgs-sneutrino / down: couplings from Eq.(A.6).

Case 2: f_k colour-singlet

$$\begin{aligned}\mathcal{L}_{\text{EFT}} \ni \frac{1}{32\pi^2}\Bigg\{&g_R^{S_\alpha f_k d_j *}g_L^{S_\beta f_k d_i}g_R^{S_\alpha f_l d_j *}g_L^{S_\beta f_l d_i}m_{f_k}m_{f_l}D_0(O_2-O_3)+g_L^{S_\alpha f_k d_j *}g_R^{S_\beta f_k d_i}g_L^{S_\alpha f_l d_j *}g_R^{S_\beta f_l d_i}m_{f_k}m_{f_l}D_0(\tilde{O}_2-\tilde{O}_3)\\
&+(O_4-O_5)\Bigg(\left[g_R^{S_\alpha f_k d_j *}g_L^{S_\beta f_k d_i}g_L^{S_\alpha f_l d_j *}g_R^{S_\beta f_l d_i}+g_L^{S_\alpha f_k d_j *}g_R^{S_\beta f_k d_i}g_R^{S_\alpha f_l d_j *}g_L^{S_\beta f_l d_i}\right]m_{f_k}m_{f_l}D_0\\
&-\left[g_L^{S_\alpha f_k d_j *}g_L^{S_\beta f_k d_i}g_R^{S_\alpha f_l d_j *}g_R^{S_\beta f_l d_i}+g_R^{S_\alpha f_k d_j *}g_R^{S_\beta f_k d_i}g_L^{S_\alpha f_l d_j *}g_L^{S_\beta f_l d_i}\right]\frac{D_2}{2}\Bigg)\Bigg\}(m_{S_\alpha},m_{f_k},m_{S_\beta},m_{f_l})\end{aligned} \tag{A.62}$$

List of particles:

- sup / chargino-lepton / sup / down: couplings from Eqs.(A.10),(A.11).
- sdown / neutralino-neutrino / sdown / up: couplings from Eqs.(A.8),(A.12).

Case 3: f_k colour-triplet

$$\begin{aligned}\mathcal{L}_{\text{EFT}} \ni \frac{1}{32\pi^2}\Bigg\{&-g_L^{S_\alpha f_k d_j *} g_L^{S_\beta f_k d_i} g_L^{S_\alpha f_l d_j *} g_L^{S_\beta f_l d_i} \frac{D_2}{4} O_1 - g_R^{S_\alpha f_k d_j *} g_R^{S_\beta f_k d_i} g_R^{S_\alpha f_l d_j *} g_R^{S_\beta f_l d_i} \frac{D_2}{4} \tilde{O}_1 \\ &+ g_R^{S_\alpha f_k d_j *} g_L^{S_\beta f_k d_i} g_R^{S_\alpha f_l d_j *} g_L^{S_\beta f_l d_i} m_{f_k} m_{f_l} D_0 \frac{1}{6}(5O_2 + O_3) + g_L^{S_\alpha f_k d_j *} g_R^{S_\beta f_k d_i} g_L^{S_\alpha f_l d_j *} g_R^{S_\beta f_l d_i} m_{f_k} m_{f_l} D_0 \frac{1}{6}(5\tilde{O}_2 + \tilde{O}_3) \\ &+ \left[g_R^{S_\alpha f_k d_j *} g_L^{S_\beta f_k d_i} g_L^{S_\alpha f_l d_j *} g_R^{S_\beta f_l d_i} + g_L^{S_\alpha f_k d_j *} g_R^{S_\beta f_k d_i} g_R^{S_\alpha f_l d_j *} g_L^{S_\beta f_l d_i} \right] m_{f_k} m_{f_l} D_0 \frac{1}{6}(5O_4 + O_5) \\ &+ \left[g_L^{S_\alpha f_k d_j *} g_L^{S_\beta f_k d_i} g_R^{S_\alpha f_l d_j *} g_R^{S_\beta f_l d_i} + g_R^{S_\alpha f_k d_j *} g_R^{S_\beta f_k d_i} g_L^{S_\alpha f_l d_j *} g_L^{S_\beta f_l d_i} \right] \frac{D_2}{4} \frac{1}{3}(O_4 + 5O_5) \Bigg\} (m_{S_\alpha}, m_{f_k}, m_{S_\beta}, m_{f_l})\end{aligned} \tag{A.63}$$

List of particles:

- sdown / gluino / sdown / up: couplings from Eqs.(A.12),(A.9) (stripped from Gell-Mann matrix element); $\times 2$ (π-rotated diagram).

A.6.4 Scalar/fermion/scalar/fermion "fermion-cross" box

Case 1: f_k colour-singlet

$$\begin{aligned}\mathcal{L}_{\text{EFT}} \ni \frac{1}{32\pi^2}\Bigg\{&g_L^{S_\alpha f_k d_j *} g_L^{S_\beta f_k d_j *} g_L^{S_\alpha f_l d_i} g_L^{S_\beta f_l d_i} \frac{m_{f_k} m_{f_l}}{2} D_0 O_1 + g_R^{S_\alpha f_k d_j *} g_R^{S_\beta f_k d_j *} g_R^{S_\alpha f_l d_i} g_R^{S_\beta f_l d_i} \frac{m_{f_k} m_{f_l}}{2} D_0 \tilde{O}_1 \\ &- g_R^{S_\alpha f_k d_j *} g_R^{S_\beta f_k d_j *} g_L^{S_\alpha f_l d_i} g_L^{S_\beta f_l d_i} m_{f_k} m_{f_l} D_0 (O_2 + O_3) - g_L^{S_\alpha f_k d_j *} g_L^{S_\beta f_k d_j *} g_R^{S_\alpha f_l d_i} g_R^{S_\beta f_l d_i} m_{f_k} m_{f_l} D_0 (\tilde{O}_2 + \tilde{O}_3) \\ &- \left[g_L^{S_\alpha f_k d_j *} g_R^{S_\beta f_k d_j *} g_R^{S_\alpha f_l d_i} g_L^{S_\beta f_l d_i} + g_R^{S_\alpha f_k d_j *} g_L^{S_\beta f_k d_j *} g_L^{S_\alpha f_l d_i} g_R^{S_\beta f_l d_i} \right] \frac{D_2}{2} O_4 \\ &+ \left[g_R^{S_\alpha f_k d_j *} g_L^{S_\beta f_k d_j *} g_R^{S_\alpha f_l d_i} g_L^{S_\beta f_l d_i} + g_L^{S_\alpha f_k d_j *} g_R^{S_\beta f_k d_j *} g_L^{S_\alpha f_l d_i} g_R^{S_\beta f_l d_i} \right] \frac{D_2}{2} O_5 \Bigg\} (m_{S_\alpha}, m_{f_k}, m_{S_\beta}, m_{f_l})\end{aligned} \tag{A.64}$$

List of particles:

- sdown / neutrino-neutralino: couplings from Eq.(A.8).

Case 2: S_α colour-singlet

$$\begin{aligned}\mathcal{L}_{\text{EFT}} \ni \frac{1}{32\pi^2}\Bigg\{&-g_R^{S_\alpha f_k d_j *} g_R^{S_\beta f_k d_j *} g_L^{S_\alpha f_l d_i} g_L^{S_\beta f_l d_i} m_{f_k} m_{f_l} D_0 O_3 - g_L^{S_\alpha f_k d_j *} g_L^{S_\beta f_k d_j *} g_R^{S_\alpha f_l d_i} g_R^{S_\beta f_l d_i} m_{f_k} m_{f_l} D_0 \tilde{O}_3 \\ &- (O_4 - O_5) \Bigg(\left[g_R^{S_\alpha f_k d_j *} g_L^{S_\beta f_k d_j *} g_R^{S_\alpha f_l d_i} g_L^{S_\beta f_l d_i} + g_L^{S_\alpha f_k d_j *} g_R^{S_\beta f_k d_j *} g_L^{S_\alpha f_l d_i} g_R^{S_\beta f_l d_i} \right] \\ &+ \left[g_L^{S_\alpha f_k d_j *} g_R^{S_\beta f_k d_j *} g_R^{S_\alpha f_l d_i} g_L^{S_\beta f_l d_i} + g_R^{S_\alpha f_k d_j *} g_L^{S_\beta f_k d_j *} g_L^{S_\alpha f_l d_i} g_R^{S_\beta f_l d_i} \right] \Bigg) \frac{D_2}{2} \Bigg\} (m_{S_\alpha}, m_{f_k}, m_{S_\beta}, m_{f_l})\end{aligned} \tag{A.65}$$

List of particles:

- Charged Higgs-slepton / up / sdown / up: couplings from Eqs.(A.7),(A.12).
- Higgs-sneutrino / down / sup / down: couplings from Eqs.(A.6),(A.11).

Case 3: $f_{k,l}$ colour-octets

$$\begin{aligned}\mathcal{L}_{\text{EFT}} \ni \frac{1}{32\pi^2}\Bigg\{&\frac{1}{18}g_L^{S_\alpha f_k d_j *}g_L^{S_\beta f_k d_j *}g_L^{S_\alpha f_l d_i}g_L^{S_\beta f_l d_i}m_{f_k}m_{f_l}D_0\,O_1+\frac{1}{18}g_R^{S_\alpha f_k d_j *}g_R^{S_\beta f_k d_j *}g_R^{S_\alpha f_l d_i}g_R^{S_\beta f_l d_i}m_{f_k}m_{f_l}D_0\,\tilde{O}_1\\
&-\frac{1}{9}g_R^{S_\alpha f_k d_j *}g_R^{S_\beta f_k d_j *}g_L^{S_\alpha f_l d_i}g_L^{S_\beta f_l d_i}m_{f_k}m_{f_l}D_0(O_2+O_3)-\frac{1}{9}g_L^{S_\alpha f_k d_j *}g_L^{S_\beta f_k d_j *}g_R^{S_\alpha f_l d_i}g_R^{S_\beta f_l d_i}m_{f_k}m_{f_l}D_0(\tilde{O}_2+\tilde{O}_3)\\
&-\frac{1}{9}\left[g_R^{S_\alpha f_k d_j *}g_L^{S_\beta f_k d_j *}g_R^{S_\alpha f_l d_i}g_L^{S_\beta f_l d_i}+g_L^{S_\alpha f_k d_j *}g_R^{S_\beta f_k d_j *}g_L^{S_\alpha f_l d_i}g_R^{S_\beta f_l d_i}\right]\frac{D_2}{4}(5O_4-3O_5)\\
&-\frac{1}{9}\left[g_L^{S_\alpha f_k d_j *}g_R^{S_\beta f_k d_j *}g_R^{S_\alpha f_l d_i}g_L^{S_\beta f_l d_i}+g_R^{S_\alpha f_k d_j *}g_L^{S_\beta f_k d_j *}g_L^{S_\alpha f_l d_i}g_R^{S_\beta f_l d_i}\right]\frac{D_2}{4}(3O_4-5O_5)\Bigg\}(m_{S_\alpha},m_{f_k},m_{S_\beta},m_{f_l})\end{aligned} \tag{A.66}$$

List of particles:

- sdown / gluinos: couplings from Eq.(A.9) (stripped from Gell-Mann matrix element).

Case 4: $f_{k,l}$ colour-octet+singlet

$$\begin{aligned}\mathcal{L}_{\text{EFT}} \ni \frac{1}{32\pi^2}\Bigg\{&\frac{1}{6}g_L^{S_\alpha f_k d_j *}g_L^{S_\beta f_k d_j *}g_L^{S_\alpha f_l d_i}g_L^{S_\beta f_l d_i}m_{f_k}m_{f_l}D_0\,O_1+\frac{1}{6}g_R^{S_\alpha f_k d_j *}g_R^{S_\beta f_k d_j *}g_R^{S_\alpha f_l d_i}g_R^{S_\beta f_l d_i}m_{f_k}m_{f_l}D_0\,\tilde{O}_1\\
&-\frac{1}{3}g_R^{S_\alpha f_k d_j *}g_R^{S_\beta f_k d_j *}g_L^{S_\alpha f_l d_i}g_L^{S_\beta f_l d_i}m_{f_k}m_{f_l}D_0(O_2+O_3)-\frac{1}{3}g_L^{S_\alpha f_k d_j *}g_L^{S_\beta f_k d_j *}g_R^{S_\alpha f_l d_i}g_R^{S_\beta f_l d_i}m_{f_k}m_{f_l}D_0(\tilde{O}_2+\tilde{O}_3)\\
&+\frac{1}{3}\left[g_R^{S_\alpha f_k d_j *}g_L^{S_\beta f_k d_j *}g_R^{S_\alpha f_l d_i}g_L^{S_\beta f_l d_i}+g_L^{S_\alpha f_k d_j *}g_R^{S_\beta f_k d_j *}g_L^{S_\alpha f_l d_i}g_R^{S_\beta f_l d_i}\right]\frac{D_2}{4}(O_4-3O_5)\\
&+\frac{1}{3}\left[g_L^{S_\alpha f_k d_j *}g_R^{S_\beta f_k d_j *}g_R^{S_\alpha f_l d_i}g_L^{S_\beta f_l d_i}+g_R^{S_\alpha f_k d_j *}g_L^{S_\beta f_k d_j *}g_L^{S_\alpha f_l d_i}g_R^{S_\beta f_l d_i}\right]\frac{D_2}{4}(3O_4-O_5)\Bigg\}(m_{S_\alpha},m_{f_k},m_{S_\beta},m_{f_l})\end{aligned} \tag{A.67}$$

List of particles:

- sdown / gluino / sdown / neutralino-neutrino: couplings from Eqs.(A.8),(A.9) (stripped from Gell-Mann matrix element); + diagram with $\chi^0 \leftrightarrow \tilde{g}$.

A.6.5 Vector/fermion/scalar/fermion "straight" box

Case S colour-singlet

$$\begin{aligned}\mathcal{L}_{\text{EFT}} \ni \frac{1}{32\pi^2}\Bigg\{&-g_L^{V f_k d_j *}g_L^{S f_k d_i}g_L^{S f_l d_j *}g_L^{V f_l d_i}m_{f_k}m_{f_l}D_0\,O_1-g_R^{V f_k d_j *}g_R^{S f_k d_i}g_R^{S f_l d_j *}g_R^{V f_l d_i}m_{f_k}m_{f_l}D_0\,\tilde{O}_1\\
&-2g_R^{V f_k d_j *}g_L^{S f_k d_i}g_R^{S f_l d_j *}g_L^{V f_l d_i}D_2(O_2+O_3)-2g_L^{V f_k d_j *}g_R^{S f_k d_i}g_L^{S f_l d_j *}g_R^{V f_l d_i}D_2(\tilde{O}_2+\tilde{O}_3)\\
&-\left[g_L^{V f_k d_j *}g_R^{S f_k d_i}g_R^{S f_l d_j *}g_L^{V f_l d_i}+g_R^{V f_k d_j *}g_L^{S f_k d_i}g_L^{S f_l d_j *}g_R^{V f_l d_i}\right]D_2O_4\\
&+2\left[g_L^{V f_k d_j *}g_L^{S f_k d_i}g_R^{S f_l d_j *}g_R^{V f_l d_i}+g_R^{V f_k d_j *}g_R^{S f_k d_i}g_L^{S f_l d_j *}g_L^{V f_l d_i}\right]m_{f_k}m_{f_l}D_0\,O_5\Bigg\}(m_V,m_{f_k},m_S,m_{f_l})\end{aligned} \tag{A.68}$$

List of particles:

- Z / down / sneutrino-neutral Higgs /down: couplings from Eqs.(A.6),(A.14); ×2 (π-rotated diagram).
- W / up / charged Higgs-slepton / up: couplings from Eqs.(A.7),(A.13); ×2 (π-rotated diagram).

A.6.6 Vector/fermion/scalar/fermion "cross" boxes

Case S colour-singlet

$$\begin{aligned}\mathcal{L}_{\text{EFT}} \ni \frac{1}{32\pi^2}\Big\{&-\left(g_L^{Vf_k d_j *} g_L^{Sf_k d_i} g_L^{Vf_l d_j *} g_L^{Sf_l d_i} m_{f_k} m_{f_l} + g_L^{Sf_k d_j *} g_L^{Vf_k d_i} g_L^{Sf_l d_j *} g_L^{Vf_l d_i}\right) m_{f_k} m_{f_l} D_0 O_1 \\ &-\left(g_R^{Vf_k d_j *} g_R^{Sf_k d_i} g_R^{Vf_l d_j *} g_R^{Sf_l d_i} + g_R^{Sf_k d_j *} g_R^{Vf_k d_i} g_R^{Sf_l d_j *} g_R^{Vf_l d_i}\right) m_{f_k} m_{f_l} D_0 \tilde{O}_1 \\ &-2\left(g_R^{Vf_k d_j *} g_L^{Sf_k d_i} g_R^{Vf_l d_j *} g_L^{Sf_l d_i} + g_R^{Sf_k d_j *} g_L^{Vf_k d_i} g_R^{Sf_l d_j *} g_L^{Vf_l d_i}\right) D_2 O_3 \\ &-2\left(g_L^{Vf_k d_j *} g_R^{Sf_k d_i} g_L^{Vf_l d_j *} g_R^{Sf_l d_i} + g_L^{Sf_k d_j *} g_R^{Vf_k d_i} g_L^{Sf_l d_j *} g_R^{Vf_l d_i}\right) D_2 \tilde{O}_3 \\ &+\Big[g_L^{Vf_k d_j *} g_R^{Sf_k d_i} g_R^{Vf_l d_j *} g_L^{Sf_l d_i} + g_R^{Vf_k d_j *} g_L^{Sf_k d_i} g_L^{Vf_l d_j *} g_R^{Sf_l d_i} \\ &+g_L^{Sf_k d_j *} g_R^{Vf_k d_i} g_R^{Sf_l d_j *} g_L^{Vf_l d_i} + g_R^{Sf_k d_j *} g_L^{Vf_k d_i} g_L^{Sf_l d_j *} g_R^{Vf_l d_i}\Big] D_2 O_4 \\ &+2\Big[g_L^{Vf_k d_j *} g_L^{Sf_k d_i} g_R^{Vf_l d_j *} g_R^{Sf_l d_i} + g_R^{Vf_k d_j *} g_R^{Sf_k d_i} g_L^{Vf_l d_j *} g_L^{Sf_l d_i} \\ &+g_L^{Sf_k d_j *} g_L^{Vf_k d_i} g_R^{Sf_l d_j *} g_R^{Vf_l d_i} + g_R^{Sf_k d_j *} g_R^{Vf_k d_i} g_L^{Sf_l d_j *} g_L^{Vf_l d_i}\Big] m_{f_k} m_{f_l} D_0 O_5\Big\}(m_V, m_{f_k}, m_S, m_{f_l})\end{aligned} \tag{A.69}$$

List of particles:

- Z / down / sneutrino-neutral Higgs / down: couplings from Eqs.(A.6),(A.14).

A.6.7 Vector/fermion/scalar/fermion "fermion-cross" box

Case S colour-triplet

$$\begin{aligned}\mathcal{L}_{\text{EFT}} \ni \frac{1}{32\pi^2}\Big\{&g_R^{Vf_k d_j *} g_R^{Sf_k d_j *} g_L^{Sf_l d_i} g_L^{Vf_l d_i} \frac{D_2}{4}(O_2 - O_3) - g_L^{Vf_k d_j *} g_L^{Sf_k d_j *} g_R^{Sf_l d_i} g_R^{Vf_l d_i} \frac{D_2}{4}(\tilde{O}_2 - \tilde{O}_3) \\ &+2\left(g_L^{Vf_k d_j *} g_R^{Sf_k d_j *} + g_R^{Vf_k d_j *} g_L^{Sf_k d_j *}\right)\left(g_R^{Sf_l d_i} g_L^{Vf_l d_i} + g_L^{Sf_l d_i} g_R^{Vf_l d_i}\right) m_{f_k} m_{f_l} D_0 (O_4 - O_5)\Big\}(m_V, m_{f_k}, m_S, m_{f_l})\end{aligned} \tag{A.70}$$

List of particles:

- W / up / sdown / up: couplings from Eqs.(A.13),(A.12); $\times 2$ (π-rotated diagram).
- Z / down / sup / down: couplings from Eqs.(A.14),(A.11); vanishes from antisymmetry of λ''; $\times 2$ (π-rotated diagram).

List of Figures

List of Tables